Herstellung, Charakterisierung und Anwendungen von funktionalen Polymer/Bakterien Vliesstoff-Kompositen

DISSERTATION

zur Erlangung des akademischen Grades einer Doktorin/eines
Doktors der Naturwissenschaften (Dr. rer. nat.)
in der Bayreuther Graduiertenschule für Mathematik und Naturwissenschaften
(BayNAT)
der Universität Bayreuth

vorgelegt von

Steffen Reich
aus Göppingen
Bayreuth, 2018

Die vorliegende Arbeit wurde in der Zeit von (*07/2014)* bis (*12/2017)* in Bayreuth am Lehrstuhl Makromolekulare Chemie II unter Betreuung von Herrn Professor Dr. *Andreas Greiner* angefertigt.

Vollständiger Abdruck der von der Bayreuther Graduiertenschule für Mathematik und Naturwissenschaften (BayNAT) der Universität Bayreuth genehmigten Dissertation zur Erlangung des akademischen Grades einer Doktorin/ eines Doktors der Naturwissenschaften (Dr. rer. Nat.).

Dissertation eingereicht am:	14.02.2018
Zulassung durch das Leitungsgremium:	13.03.2018
Wissenschaftliches Kolloquium:	26.10.2018

Amtierender Direktor: Prof. Dr. Dirk Schüler

Prüfungsausschuss:

Prof. Dr. Andreas Greiner	(Gutachter)
Prof. Dr. Ruth Freitag	(Gutachterin)
JProf. Dr. Anna Schenk	(Vorsitz)
Prof. Dr. Peter Strohriegl	

Inhaltsverzeichnis

Zusammenfassung

Die vorliegende Dissertation beinhaltet die Entwicklung von Nanokomposit-Materialien unter Verwendung von Polymeren, Mikroorganismen und Metallnanostrukturen. Polymer/Bakterien-Kompositvliese eignen sich besonders für die Reinigung von Abwässern in Bezug auf die Rückgewinnung anorganischer Edelmetalle und die Produktion von Energie. Polymer/Metall-Kompositvliese sind in der Lage Strom zu leiten und gleichzeitig als Joule heater zu fungieren, während Polymer/Metall-Kompositschwämme durch eine gezielte Kompression leitfähige Perkolationspfade bilden und als Joule heater ihre Anwendung finden. Der kumulative Teil wurde in 5 ineinander aufbauende Kapitel aufgeteilt.

Polymer/*Micrococcus luteus* - Kompositvliese wurden durch Elektrospinnen einer Polyvinylalkohol *Micrococcus luteus* – Dispersion in Wasser zu Nanofasern verarbeitet und in einem weiteren Schritt mit Poly(*p*-xylylen) mit Hilfe der chemischen Gasphasenabscheidung zu wasserstabilen Kompositvliesen verarbeitet. Dieses Kompositvlies diente zur Rückgewinnung von Gold und konnte in den Kompositvliesen mittels Raserelektronenmikroskopie und einem energiedispersiven Röntgenanalysedetektor qualitativ und mit Hilfe von optischer Emmissionsspektrometrie mittels induktiv gekoppeltem Plasma quantitativ nachgewiesen werden. Diese Goldnanopartikel konnten erfolgreich an einem Katalysesystem, der hydrolytischen Oxidation von Dimethylphenylsilan mit Wasser, überprüft werden. Dieses System macht sich nicht nur der Bioremediation von Edelmetallen zu Nutze, sondern wird auch in der Energieproduktion aus Abwässer eingesetzt. Polymer/*Shewanella oneidensis MR-1* – Kompositvliese wurden durch Elektrospinnen einer Polyvinylalkohol *Shewanella oneidensis MR-1* – Dispersion in Wasser zu Nanofasern verarbeitet und in einem weiteren Schritt mit Poly (*p*-xylylen) mit Hilfe der chemischen Gasphasenabscheidung zu wasserstabilen Kompositvliesen verarbeitet. Das Kompositvlies wurde als Anodenmaterial in einer mikrobiellen Brennstoffzelle getestet. In diesem Fall wurden die Leistungssteigerungen von freien *Shewanella oneidensis MR-1*, natürlichen Biofilmen, und Kompositmaterialien verglichen, wobei das Kompositvlies eine deutliche Leistungsteigerung im Gegensatz zu den natürlichen Biofilmen aufgezeigt hat. Neben dem Elektrospinnen als Immobiliserungsmethode sind auch weitere Verfahren, wie dem Sprühtrocknen, bekannt. Polymer/Bakterien-Kapseln wurden durch das Sprühtrocknungsverfahren in großen Mengen hergestellt. Diverse Polymere, wie Polyvinylalkohol, Polyvinylpyrrolidon, Hydroxypropylcellulose und Gelatine, konnten erfolgreich zu Polymerkapseln verarbeitet werden. In diese Polymerkapseln wurden *Micrococcus luteus* und *Escherichia coli* bei 150 °C und 120 °C verkapselt und mittels Raman-Rasterkraft-Spektroskopie, Rasterelektronen-mikroskopie und Transmissionselektronen-

mikroskopie nachgewiesen. Die hergestellten Polymer/Bakterien-Kapseln konnten in ausgerichteten hydrophoben Polymernanofasern verarbeitet werden, die ihre spätere Anwendung in der Bioremediation, Katalyse oder als Anodenmaterial in einer mikrobiellen Brennstoffzelle finden können. Für die Herstellung von mikrobiellen Brennstoffzellen sind leitfähige Komposite essentiell, welche durch das Wet-laid Verfahren hergestellt werden konnten.

Polymer/Metall - Kompositvliese wurden durch das Wet-laid-Verfahren erfolgreich hergestellt. Für die Herstellung solcher Kompositvliese werden Kurzschnitt-faser - Dipsersionen und leitfähige Silbernanodrähte benötigt. Die Kurzschnittfaser-dispersionen werden erhalten, indem elektrogesponnene Polyacrylnitrilfasern und Poly (ε- caprolacton)-fasern in einem Blender zerkleinert werden. Polyacrylnitrilfasern dienen als Matrix während Poly(ε-caprolacton)-fasern als Binder eingesetzt werden, um die Matrix mit einander zu verkleben. Silbernanodrähte wurden als leitfähiges Additiv zugesetzt, um einen elektrischen Perkolationspfad in der Matrix zu gewährleisten. Die sukzessive Erhöhung der Silbernanodrahtmenge in der Matrix steigert ebenfalls die elektrische Leitfähigkeit und kann einen Wert von 750000 S/m annehmen. Das hergestellte Polymerkompositvlies kann anschließend als Elektrodenmaterial in einem Joule heater erfolgreich verwendet werden. Das Kompositvlies ist zudem porös, atmungsfähig, biegsam und faltbar, was zu einem weitreichenden Einsatzgebiet als Elektrodenmaterial führt. Diese Materialien sind in ihrer Funktion jedoch eingeschränkt, denn in diesem Fall werden leitfähige Komposite hergestellt, die entweder permanent leitfähig sind oder keine Leitfähigkeit aufweisen. Die Kombination aus Isolator und Leiter lässt sich durch die Herstellung dreidimensionaler Schwämme erhalten, die durch eine Kompression ihren Widerstand verändern. Polymer/Metall - Kompositschwämme wurden durch den Gefriertrocknungsprozess hergestellt. Hierfür kommen Kurzschnittfasern aus Polyimidfasern und Silbernanodrähten zum Einsatz. Zu dieser Dispersion wird Polyamidocarbonsäure, welches als Binder zum Einsatz kommt, gemischt, um die Stabilität zu gewährleisten. Die Silbernanodrähte dienen erneut als leitfähiges Additiv. Im Ausgangszustand besitzt der Kompositschwamm keine bis eine geringe Leitfähigkeit, während bei einer Kompression des Schwammes eine elektrische Leitfähigkeissteigerung erreicht wird. Der Kompositschwamm fungiert ebenfalls als Joule heater. Auch hier wird ein weitreichendes Einsatzgebiet als Elektrodenmaterial prognostiziert.

Summary

The present thesis includes the development of nanocomposite materials using polymers, microorganisms, and metal nanostructures. Polymer/bacteria composite nonwovens are especially suitable for the cleaning of sewage with regard to the recovery of inorganic precious metals and the production of energy. Polymer/metal composite nonwovens are able to conduct electricity and, at the same time, act as Joule heater, while polymer/metal/composite sponges form conductive percolation paths via directed compression and can be applied as Joule heater. The cumulative part is divided into five successive chapters.

Polymer/*Micrococcus luteus* composite nonwovens were processed to nanofibers in water by electrospinning of a poly(vinyl alcohol) *Micrococcus luteus*-dispersion. In a second step, they were processed to water-stable composite nonwovens with poly(p-xylylene) with the help of chemical vapor deposition. This composite nonwoven was used for the recovery of gold. Whereas its quality in the composite nonwovens was proven by scanning electron microscopy and an energy-dispersive X-ray analysis detector, its quantity was proven with the help of optical emission spectrometry via inductively linked plasma. These gold nanoparticles were successfully investigated at a catalysis system, the hydrolytic oxidation of dimethylphenylsilane with water. An equal system was used for energy production of encapsulated microorganism in polymer fibers. Polymer/*Shewanella oneidensis MR-1* composite nonwovens were processed to nanofibers by electrospinning of a poly(vinyl alcohol) *Shewanella oneidensis MR-1* dispersion in water and, in a second step, they were processed with poly(p-xylylene) to water-stable composite nonwovens by using chemical vapor deposition. The composite nonwoven was tested as anode material in a microbial fuel cell. In this case, the increases in efficiency of free *Shewanella oneidensis MR- 1*, natural biofilms, and composite materials were compared, whereas the composite nonwoven showed a considerable increase in efficiency compared to the natural biofilms. Additionaly, spray drying technique is known for encapsulation of microorganism in polymer formulations. Polymer/bacteria-capsules were manufactured in large quantities by spray-drying. Miscellaneous polymers such as poly(vinyl alcohol), poly(vinyl pyrrolidone), hydroxypropyl cellulose, and gelatin were successfully processed to polymer capsules. In these polymer capsules, *Micrococcus luteus* and *Escherichia coli* were encapsulated at 150°C and 120°C and were proven via Raman-scanning-force-spectroscopy, scanning electron microscopy, and transmission electron microscopy. The manufactured polymer/bacteria-capsules could be processed into aligned hydrophobic polymer nanofibers. Electrical conductivity is essential for materials in microbial fuel cells. For this purpose, electrically conductive composites were prepared with a wet-laid method.

Polymer/metal composite nonwovens were successfully manufactured by wet-laid processes. The manufacture of such composite nonwovens requires short cut fiber dispersions and conductive silver nanowires. Short cut fiber dispersions are obtained by cutting electrospun polyacrylonitrile fibers and poly(ε-caprolactone) fibers in a blender. Polyacrylonitrile fibers serve as matrix while poly(ε-caprolactone) fibers are used as binder in order to stick the matrix together. Silver nanowires were added as conductive additive in order to ensure an electric percolation path in the matrix. The gradual increase of the quantity of silver nanowires in the matrix also increases the electric conductivity and can reach a value of 750.000 S/m. Afterwards, the manufactured polymer composite nonwoven can be successfully used as electrode material in a Joule heater. In addition to that, the composite nonwoven is porous, breathable, flexible and foldable. This results in a wide range of applications as electrode material. This two dimensional system is permanent electrically conductive or insulating. Three dimensional systems have the advantage in induction of electrical conductivity by compression. Three dimensional Polymer/metal-composite sponges were manufactured by freeze-drying. For this purpose, short cut fibers from polyimide fibers and silver nanowires are used. Poly(amidocarboxylic acid), which serves as binder in order to ensure stability, is added to the polyimide fiber dispersion. This is necessary in order to achieve stability during compression. The silver nanowires serve again as conductive additive. In its initial state, the composite sponge shows no or low conductivity. However, during a compression of the sponge, its electrical conductivity increases. The composite sponge also serves as joule heater. In this case, a wide range of applications can also be anticipated.

Abkürzungsverzeichnis

EPS	extrazelluläre Polymerschleimschicht
UV	Ultraviolett
M.luteus	*Micrococcus luteus*
GC	Guanin Cytosin
DNA	Desoxyribonukleinsäure
Au	Gold
AuNP	Goldnanopartikel
S.oneidensis MR-1	*Shewanella oneidensis MR-1*
MtrC	Cytochrom
OmcA	Cytochrom
MtrB	Membranprotein
O_2	Sauerstoff
kV	Kilovolt
m	Meter
mg	Milligramm
g	Gramm
E.coli	*Escherichia coli*
PEO	Polyethylenoxid
PVA	Polyvinylalkohol
PCL	Poly(ε-caprolacton)
PVDF-HFP	Poly(vinylfluorid-co-hexafluorpropen)
PEG	Polyethylenglykol
CVD	chemische Gasphasenabscheidung
PPX	Poly(p-xylylen)
PAA	Polyacrylsäure
AgNW	Silbernanodrähte
AuNW	Goldnanodrähte
PdNW	Palladiumnanodrähte
AuNP	Goldnanopartikel
PdNP	Palladiumnanopartikel
PtNP	Platinnanopartikel
AgNP	Silbernanopartikel
C.glutamicum	*Corynebacterium glutamicum*

N.winogradskyi	*Nitrobacter winogradskyi*
S	Siemens
PVP	Polyvinylpyrrolidon
HPC	Hydroxypropylcellulose
PVAc	Polyvinylacetat
PVB	Polyvinylbutyral
PMMA	Polymethylmethacrylat
PS	Polystyrol
PAN	Polyacrylnitril
TPU	thermoplastisches Polyurethan
2D	zweidimensional
3D	dreidimensional
nm	Nanometer
µm	Mikrometer
CLSM	Konfokale Rasterfluoreszenzmikroskopie
BSE-Detektor	Rückstreu-Sekundärelektronen-Detektor
EDX-Analyse	Energiedispersive Rötgenanalyse
mW	Milliwatt
SEM	Rasterelektronenmikroskopie
TEM	Transmissionelektronenmikroskopie
AFM	Rasterkraftmikroskopie
CNT	Kohlenstoffnanoröhrchen
PLA	Polylactid
PANI	Polyanilin
PET	Polyethylenterephthalat
PEDOT	Poly(3,4-Ethylendioxythiophen)
PSS	Polystyrolsulfonat
MWNT	Multiwalled Nanoröhrchen
LED	Leuchtdiode
°	Grad
°C	Grad Celsius
vol%	Volumenprozent
IR	Infrarot
cm	Zentimeter

PI	Polyimid
%	Prozent
A	Ampere
s	Sekunde
GC	Gaschromatographie
MS	Massenspektrometrie
ICP	Induktiv gekoppeltes Plasma
OES	optische Emissionsspektrometrie
TGA	Thermogravimetrische Analyse

1 Einleitung

Die Kombination aus Bereichen der Chemie und der Biologie, genauer der Polymerchemie und Mikrobiologie sind für die Industrie von großem Interesse in der Betrachtung der gezielten Abwasserreinigung von Edelmetallen und der mikrobiologischen Brennstoffzelle in der Energieproduktion.
In der vorliegenden Arbeit werden sowohl Kompositmaterialien, wie Polymer/Bakterien - Kompositfaservliesen in Bezug auf die gezielte Bioremediation von Edelmetallen und der Stromproduktion, als auch Polymer/Metall - Kompositfaservliese für die Stromübertragung vorgestellt. Im Folgenden wird auf den Stand der Technik und die grundlegenden Methoden eingegangen. Die aufgeführten Grundlagen beinhalten die Funktionsweise der verwendeten Bakterienarten, die Herstellung der Fasern, der Partikel, der Polymer/Bakterien- und Polymer/Metall-Kompositen, als auch die Funktionsweise der Bioremediation, der mikrobiologischen Brennstoffzelle und der Funktionsweise von Elektrodenmaterialien. Nachfolgend wird das Ziel dieser Forschungsarbeit kurz erläutert. In Kapitel 2 werden die vorgestellten Publikationen detailliert zusammengefasst und nachfolgend aufgelistet.

1.1 Mikroorganismen

1.1.1 Biofilme

Biofilme sind Anhäufungen von verschiedenen Mikroorgansimen. Ein Biofilm besteht in der Regel aus 10^8 – 10^{11} Bakterien pro g Nassgewicht. [1,2] Diese Biofilme bilden sich spontan auf jeglichen Oberflächen aus. In einem Biofilm sind die Mikroorganismen durch eine sich bildende extrazelluläre Polymerschleimschicht (engl. extracellular polymeric substances EPS) von der Umgebung abgegrenzt. Polysaccharide, Lipide, Proteine und Wasser bilden diese EPS.[3,4] Die EPS hat eine schützende Wirkung auf die Mikroorganismen gegenüber äußeren Einflüssen, wie große Temperaturschwankungen, UV-Licht oder toxische Substanzen. Ein weiterer Vorteil dieser EPS ist die hohe Wasseraufnahme durch die enthaltenen neutralen Uronsäuren, wie D-Galacturon-, D-Glukuron- oder Mannuronsäure, welche Wassermoleküle binden können. Somit werden die Mikroorganismen vor Austrocknung geschützt.

Ebenfalls können Antibiotika die EPS nicht durchdringen und die Mikroorganismen in ihrer Funktion stören bzw. abtöten.

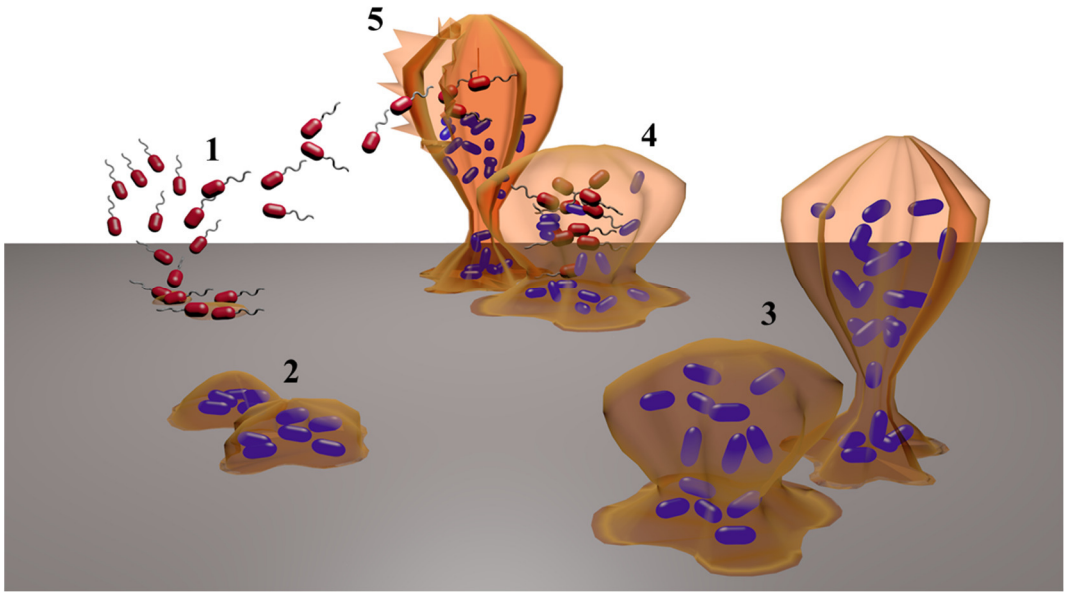

Abbildung 1.1: Schematische Darstellung der Bildung eines Biofilmes.(modifizierte Abbildung von Marius Feldmann, Makromolekulare Chemie II, Universität Bayreuth)

Die Bildung eines Biofilmes auf Oberflächen wird schematisch in Abbildung 1.1 aufgezeigt und anschließend im Detail beschrieben.[5,6]

1. Die Schwärmerzellen siedeln sich an der Oberfläche eines Materials an.
2. Anhaftung der Schwärmerzellen an der Materialoberfläche und Bildung einer EPS.
3. Bildung eines Biofilms durch das exponentielle Wachstum der Mikroorganismen durch die erhöhte Nahrungsaufnahme.
4. Neubildung der Schwärmerzellen und Freisetzung dieser aus der EPS.
5. Vermehrung der Schwärmerzellen und erneute Ansiedelung an der Oberfläche.

Biofilme sind dynamische Strukturen und folgen in der Regel diesem Kreislauf. Arbeitsteilung und Kommunikation (Quorum sensing) sind wichtig für den Erhalt eines Konsortiums durch sich schnell ändernde Umwelteinflüsse. Hochkomplexe Synthesen können somit in einem Biofilm durchgeführt werden.[7]

1.1.2 *Micrococcus luteus*

Micrococcus luteus (*M.luteus*) ist ein aerobes, gram-positives, katalase-positives Bakterium. Es gehört zur Klasse der Acetinobacter und besitzt einen hohen GC Gehalt in der DNA. *M.luteus* ist resistent gegenüber hohen Salzkonzentrationen und Wassermangel (Austrocknung).[8] Das Bakterium bildet charakteristische gelbe Kolonien und ist zwischen 0,5 und 3,5 µm groß. *M.luteus* kommt kaum als Einzelbakterium vor sondern bildet Paare bzw. Tretraden. *M.luteus* zeichnet sich durch die Aufnahme von Metallionen (Gold, Kupfer, Palladium oder Strontium) aus Abwässern aus.[9–12] Des Weiteren ist *M.luteus* bekannt dafür organische Substanzen (z. B. Naphthalin) abzubauen oder komplexe Synthesen, wie die stereospezifische Reduktion von Acetophenonen durchzuführen.[13,14]

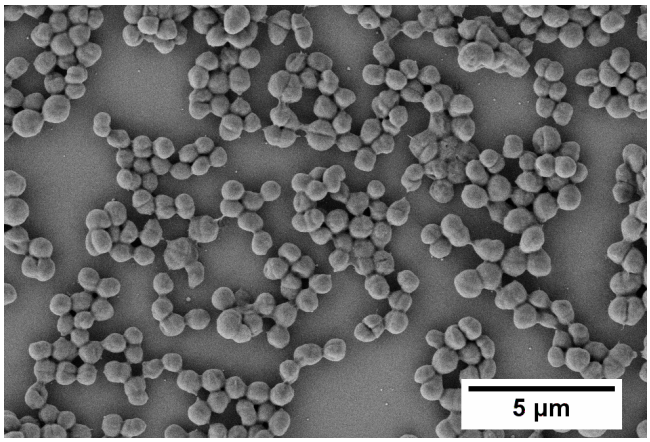

Abbildung 1.2: Elektronenmikroskopische Aufnahme der M.luteus auf einem Silizium-Wafer.

Die Reduktion von Au^{3+} zu AuNP ist durch die in der Membran enthaltenen Proteine α-Amylase und Teichuronsäure möglich. Diese sind in der Lage Au^{3+}-Ionen zu elementaren Au^0 zu reduzieren und in einem zusätzlichen Schritt AuNP zu formieren. Die aus *M.luteus* extrahierten Proteine bilden Nanopartikel in zwei verschiedenen Größen. α-Amylase bildet ungefähr 6 nm große AuNP, während durch Teichuronsäure 50 nm große AuNP entstehen.[9] Ein möglicher Mechanismus zur Bildung von AuNP durch α-Amylase wurde durch Ragnekar et al. beschrieben.[15] α-Amylase besteht unter anderem aus Cystein, welches freistehende und nicht zugängliche Thiolgruppen besitzt. Freistehende Thiolgruppen sind bekannt für ihre Affinität zu Au und sind deshalb in der Lage Au^{3+} zu Au^0 zu reduzieren (1.1).

$$2Au^{3+} + 3\,HS - R - SH \;\rightarrow\; 2Au^0 + \;6H^+ + 3\,S - R - S \qquad (1.1)$$

$$R - SH + Au^0 \rightarrow R - S - Au + \tfrac{1}{2}\ H_2 \qquad (1.2)$$

Diese hohe Affinität ermöglicht zugleich die Stabilisierung der entstehenden AuNP (1.2).

1.1.3 Shewanella oneidensis MR-1

Shewanella oneidensis MR-1 (*S.oneidensis MR-1*) ist ein gram-negatives, γ-Proteobakterium. Es ist fakultativ anaerob und bildet Stäbchen mit einer Länge von 2 – 3 µm und einem Durchmesser von 0,5 µm. Der Strang wurde in Sedimenten am New Yorks Lake von Nealson et al. 1988 isoliert. *S.oneidensis MR-1* reduziert unlösliches Mangan durch eine Elektronentransferreaktion. Wenn Eisenoxid nicht vorrätig ist, verstoffwechselt dieses Bakterium Atomabfälle wie Uran.

Der Elektronentransfer kann durch drei mögliche Annahmen beschrieben werden.

1. Cytochrome

Cytochrome wie multi Haem C-Typ Cytochrom MtrC und OmcA sind an der äußeren Zellwand translokalisiert und folgen dem TypII Proteinpfad. Diese Cytochrome sind in Kontakt mit dem Protein MtrB welches an der Oberfläche der Membran bindet. MtrC und OmcA können direkt mit der Metalloberfläche in Kontakt kommen und so die Elektronen an diese abgeben.[16]

2. Riboflavine

Elektronen müssen von der äußeren Membran der Bakterien zur Metalloberfläche abgegeben werden. Dieser Elektronentransfer kann durch Riboflavine stattfinden. Riboflavine (z. B. Vitamin B_2) bestehen aus konjugierten Doppelbindungssystemen, durch die Elektronen über kurze Strecken (50 µm) übertragen werden können.[17,18]

3. Nanodrähte

S.oneidensis MR-1 ist in der Lage elektrisch leitfähige Nanodrähte herzustellen. Diese sind direkt mit dem Bakterium verbunden. *S.oneidensis MR-1* bildet diese Nanodrähte bei einer Mangelerscheinung von Sauerstoff (O_2). Zusätzlich zu dieser Mangelerscheinung wird für die

Bildung der Nanodrähte mit einer Länge von 50 bis 150 nm, MtrC und OmcA benötigt. Der Elektronentransfer kann jedoch nur bei direktem Kontakt der Nanodrähte mit der Metalloberfläche stattfinden.[19]

1.2 Methoden zur Verarbeitung von Bakterien

1.2.1 Elektrospinnen

Elektrospinnen ist eine weit verbreitete Methode um aus Polymerlösungen[20,21] oder Polymerschmelzen[20,22–24] Mikro- und Nanofasern herzustellen. Dazu ist das Anlegen eines elektrischen Feldes erforderlich. Das Setup für das Elektrospinnen ist in der Regel folgendermaßen aufgebaut und ist in Abbildung 1.3 veranschaulicht. Eine Polymerlösung oder Polymerschmelze wird in ein Reservoir gegeben und mit einer Fördereinrichtung (Pumpe) herausbefördert. Die Kanüle und die Gegenelektrode sind über eine Spannungsquelle miteinander verbunden. Für das Elektrospinnen werden elektrische Spannungen von 200 - 2000 kV/m angelegt. An der Polymerlösung wird meist eine positive und an die Gegenelektrode eine negative Spannung angelegt. Die Gegenelektrode kann auch geerdet vorliegen.[24]

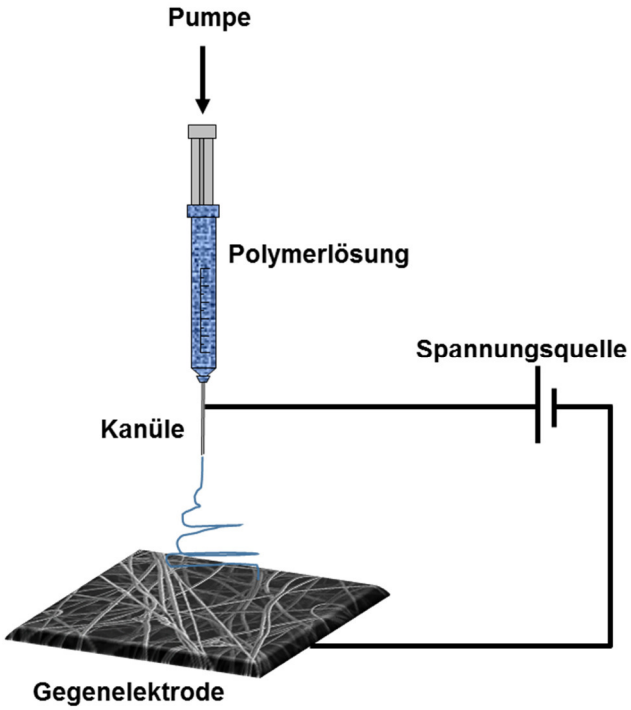

Abbildung 1.3: Schematischer Aufbau eines Setups des Elektrospinnens.

Die angelegte Spannung führt zu der Faserbildung, weshalb die Polymerlösung durch die positive Spannung an der Kanüle und der negativen Spannung an der Gegenelektrode herausgezogen wird. Die dabei entstehenden Fasern legen sich anschließend an der Gegenelektrode ab.[25,26]

Das Elektrospinnen ermöglicht die Herstellung verschiedenster Geometrien durch Variation der Prozessbedingungen. So können poröse Fasern,[27] „Janus“ Fasern,[28,29] „Perlen“ Fasern,[30] Kern-Schale Fasern,[31,32] oder Bänder[33] hergestellt werden. Ausschlaggebend für diese Geometrien oder Morphologien sind unter anderem das Molekulargewicht des Polymers, die Viskosität, die Fließgeschwindigkeit, die Oberflächenspannung, die Leitfähigkeit der Polymerlösung oder Schmelze, sowie die angelegte Spannung oder die Luftfeuchtigkeit.[34–37]

Der Nachteil eines Elektrospin-Setups mit einer Nadel sind die geringen Produktionsmengen. Hier können Polymerfasern im Bereich von 10 bis 500 mg Polymer pro Stunde hergestellt werden. Deshalb wurden Anlagen konzipiert, welche auf Basis von Scheiben oder Trommeln arbeiten, bei denen die Polymerlösung in Form eines Bad-Reservoirs vorliegt. Diese können in einem kontinuierlichen Prozess bis zu 10 g Polymer pro Stunde verarbeiten.[38–40]

Additive, wie Bakterien, Metalle oder Medikamente können durch das Elektrospinnen sehr leicht in Polymerfasern eingearbeitet werden. Diese Polymerfasern finden dann häufig ihre Anwendung in Bereichen der Industrie, wie Filtration,[41] Katalyse,[42] Medikamentenfreisetzung,[43] Wundauflagen,[44] Pflanzenschutz[45] oder Gewebezüchtung.[46] Im Folgenden wird gezielt auf die Verkapselung von Bakterien in Polymerfasern eingegangen, weil dies ein Hauptbestandteil der vorliegenden Arbeit ist. *M.luteus* und *Escherichia coli* (*E.coli)* wurden von Gensheimer et al. in PEO-Nanofasern durch das Elektrospinnen hergestellt. Diese Bakterien konnten direkt nach dem Elektrospinnen lebend nachgewiesen werden. *M.luteus* konnte im Gegensatz zu *E.coli* noch nach 250 Stunden in den Fasern nach Trockenlagerung lebend nachgewiesen werden.[47] Probiotische *Bifidobacterium animalis Bb12* wurden durch Lopez-Rubio et al. in PVA-Nanofasern immobilisiert und konnten noch nach 40 Tagen lebend nachgewiesen werden.[48] *E.coli* und *Straphylococcus albus* wurden ebenfalls in PVA-Nanofasern immobilisiert. Salalha et al. wiesen durch den Zusatz von Glycerin zu der PVA/Bakterien-Suspension eine erhöhte Zellzahl in den PVA-Nanofasern nach. Durch das Fehlen des Glycerins wurden mehrere Zellen durch den Spinnprozess oder der Trockenlagerung abgetötet.[49]

Wasserstabile Polymer/Bakterienfasern können durch Coelektrospinnen hergestellt werden. Hierbei besteht das Kernmaterial aus einem hydrophilen Polymer, in welchem die Bakterien immobilisiert sind. Das Hüllmaterial hingegen besteht aus einem hydrophoben Polymer. Klein

et al. immobilisierten *E.coli*, *Pseudomonas putida* und *Pseudomonas ADP* in PEO/PCL-Kern-Schalefasern.[50] *Corynebacterium glutamicum (C.glutamicum)* wurde von Nardi et al. in Poly(vinylfluorid-co-hexafluorpropen) (PVDF-HFP) und Polyethylenglycol (PEG) Mikroröhren verkapselt.[51] Rinderalbumin und Luciferase wurden in PVA-Nanofasern durch Zeng et al. immobilisiert und in einem weiteren Schritt mittels chemischer Gasphasenabscheidung (CVD) mit Poly(p-xylylen) (PPX) beschichtet. Diese chemische Gasphasenabscheidung wird im folgenden Kapitel beschrieben.[52]

1.2.2 Chemische Gasphasenabscheidung

Poly(p-xylylen) ist ein Polymer mit vielen chemischen und thermischen Eigenschaften für spezielle Beschichtungen.[53,54] PPX kann grundsätzlich über zwei Verfahren hergestellt werden. Erwähnenswert wäre hier die Lösungspolymerisation nach GILCH.[55] Als kontinuierlicher und industrieller Prozess wird jedoch die chemische Gasphasenabscheidung nach GORHAM verwendet.[54,56] Diese Polymerisationsart zeichnet sich durch die Vermeidung von zusätzlichen Additiven,w ie Lösungsmittel, Initiator oder Ausfällung des erhaltenen Polymers aus.
Grundsätzlich werden für die CVD folgende Bauteile benötigt. Eine Verdampfungs- bzw. Sublimationseinheit für den Präkursor [2,2]Paracyclophan, die Pyrolyseeinheit und die Abscheidungskammer. (Abbildung 1.4)

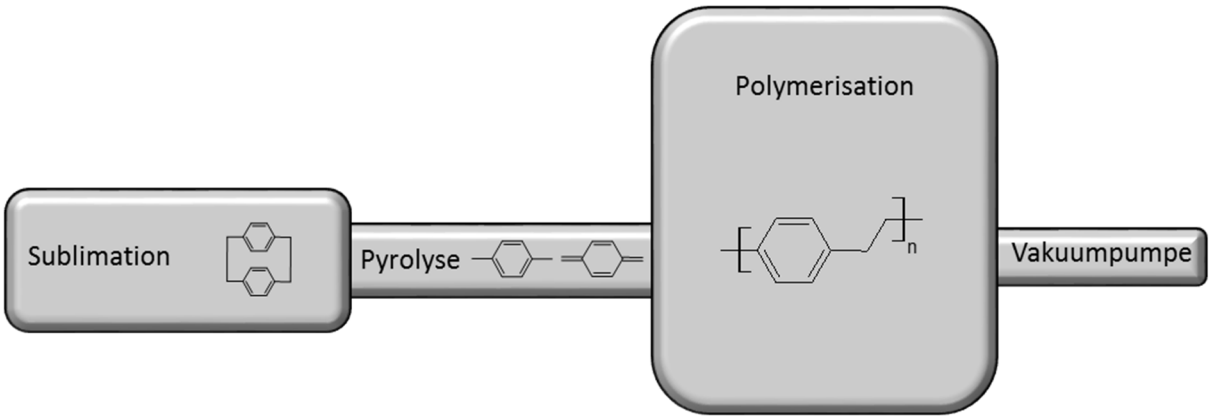

Abbildung 1.4: Darstellung des CVD Setups zur Polymerisation von PPX nach GORHAM.

Zu Beginn der Polymerisation wird der Präkursor [2,2]Paracyclophan bei ca. 150 °C im Vakuum sublimiert und in die Pyrolyseeinheit transportiert.[56–58] Hier zerfällt das [2,2]Paracyclophan bei 650 °C in zwei äquivalente p-Chinodimethan. Das reaktive p-Chinodimethan scheidet sich an der Oberfläche des Substrates ab und polymerisiert bei einer niedrigen Temperatur (T~30 °C). Es wird spekuliert, dass die Initiierung durch die Anlagerung

von p-Xylylen-Radikalen an das p-Chinodimethan erfolgt. Das Kettenwachstum wird durch die Reaktion von Makroradikalen mit p-Chinodimethan oder der Rekombination von Makroradikalen beschrieben. Das PPX wird gebildet.[53]

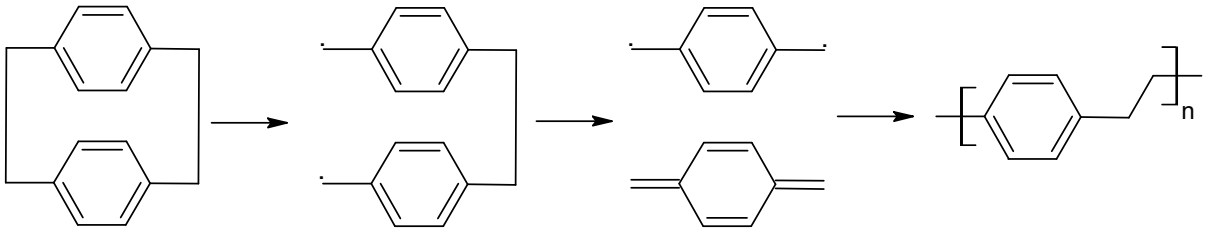

Abbildung 1.5: Schematische Darstellung der Polymerisation von PPX.

Die Schichtdicke dieses Polymers wird über die Menge an eingesetztem Präkursor gesteuert und kann bis zu wenige Nanometer betragen. Bisher wurden diese Beschichtungen an Kunststoffen, Metallen, Keramiken oder Glas durchgeführt. Diese entstehenden Beschichtungen sind hydrophob, defektfrei, transparent und beständig gegenüber UV-Strahlung und Chemikalien. [53,59,60]

1.2.3 Sprühtrocknung

Die Sprühtrocknung ist ein Verfahren, das häufig in der Lebensmittelindustrie, der Nanotechnologie und in der chemischen und pharmazeutischen Industrie eingesetzt wird.[61–66] Dieses Verfahren wird vorwiegend zur Trocknung von Lösungen, Suspensionen und Emulsionen eingesetzt.[67–69] Dabei können je nach Verwendung des Gerätes, Nano-, Mikro- oder Makropartikel hergestellt werden.[70–73] Das Sprühtrocknungsverfahren eignet sich besonders für empfindliche Substanzen, die in Lösungsmittel instabil sind. Zu nennen sind hier Medikamente, Proteine, Vitamine oder Mikroorganismen. [74–79] Die Sprühtrocknung ist jedoch nicht nur für die Trocknung von Lösungen, Suspensionen oder Emulsionen geeignet, sondern dient auch der Mikroverkapselung von diesen empfindlichen Substanzen in Polymeren. Weitere Anwendungsgebiete sind die Sprühkristallisation,[80,81] die Phasentransformation[82] oder die gezielte Agglomeration.[83,84]

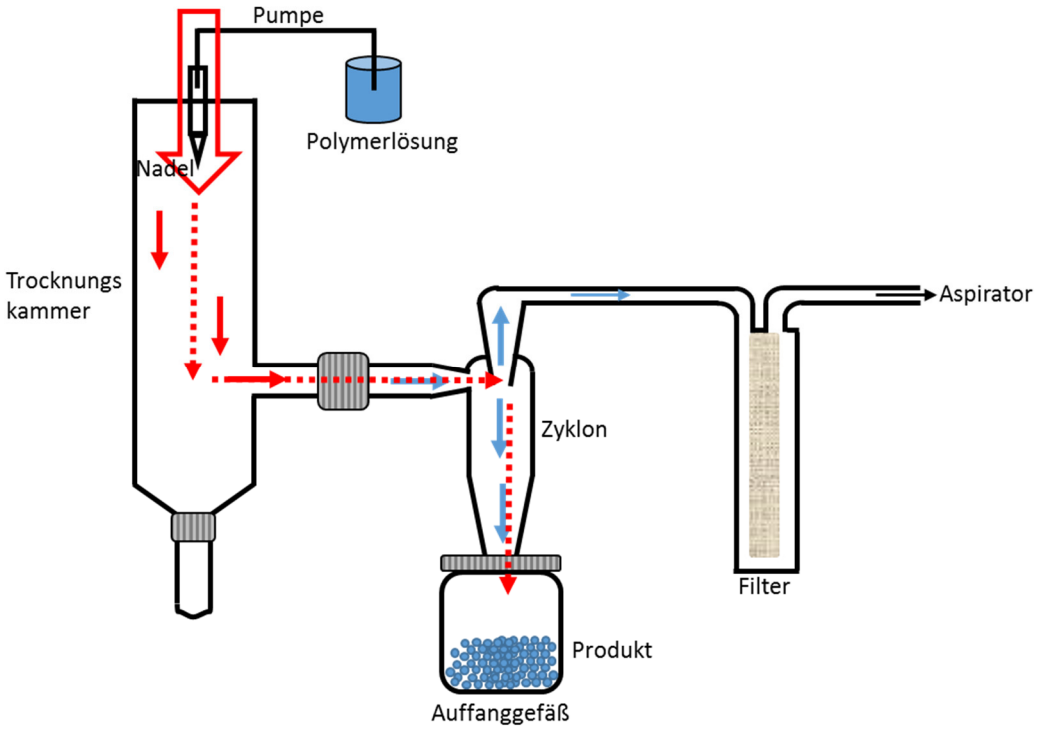

Abbildung 1.6: Schematische Darstellung des Sprühtrocknungsprozesses.

Prozess- und Lösungsparameter beeinflussen die Form und Morphologie der Partikel signifikant.[85–92] Prozessparameter sind zum Beispiel die Beförderungsgeschwindigkeit der Lösung, der Volumenstrom des Trägergases oder die Trocknungstemperatur. So entstehen poröse oder agglomerierte Partikel. Lösungsparameter wie die Konzentration, oder das eingesetzte Molekulargewicht des Polymers haben einen Einfluss auf die Größe der resultierenden Partikel. Die Sprühtrocknung besteht aus mehreren Bauteilen, die Peristaltikpumpe, Nadel, Trocknungskammer, Zyklonabscheider, Auffangbehälter, Filter und Aspirator. Der Sprühtrocknungsprozess wird in Abbildung 1.6 dargestellt und im Folgenden kurz beschrieben. Zu Beginn wird die Druckluft bzw. das Inertgas auf die erforderliche Temperatur erhitzt und anschließend mithilfe eines Aspirators durch das Sprühtrocknungssystem geführt. Die Peristaltikpumpe befördert die Polymerlösung zu der Nadel, die sich in der Trocknungskammer befindet. Es bildet sich ein Tropfen aus der Polymerlösung an der Nadel, welcher durch den heißen Luftstrom zerstäubt wird. Das Lösungsmittel der entstehenden Tröpfchen wird in der Trocknungskammer verdampft und es entstehen Partikel bzw. Kapseln. Das Partikel/Luftgemisch wird in den Zyklon geführt, wobei sich die Partikel im Auffanggefäß ablagern und das überschüssige Luft/Lösungsmittelgemisch abgeführt wird. Partikel, welche weiter im Luftstrom transportiertt wurden oder welche nicht abgelagert wurden, werden durch einen Filter gereinigt wird. Die entstehenden Kapseln dienen nun als Schutzmaterial für Mikroorganismen, Vitaminen, Proteinen, ätherischen Ölen, oder

empfindlichem Katalysatoren.[74–79] Für die Mikroverkapselung von Mikroorganismen werden hauptsächlich hydrophile Polymere, die Hydrogele bilden können, verwendet. Zu nennen sind synthetische Polymere, wie zum Beispiel PVA oder Polyacrylsäure (PAA) und natürliche Polymere wie Alginat oder Agarose. Diese Hydrogele sorgen für eine ausgeglichene Diffusion von Sauerstoff und Kohlenstoffdioxid in und aus dem Partikel sowie von Nährstoffen, Substraten und Schadstoffen. Weiter binden diese eine große Menge an Wasser, welches die Bakterien vor Austrocknung schützt. Mikroorganismen können ebenfalls durch Extrusion oder Emulsion verkapselt werden.[93–96]

1.2.4 Wet-laid Verfahren

Das Wet-laid Verfahren wird industriell angewandt um Papier bzw. Vliesstoffe herzustellen. Durch dieses Verfahren ist es einfach verschiedene Fasertypen miteinander zu kombinieren.[97] Polymerkomposite können in einer einfachen Form hergestellt werden, indem anorganische oder organische Nanostrukturen in dem Fasermedium dispergiert werden. Eine große Anforderung an die Dispersion ist die Dispergierbarkeit in wässrigem Medium.[98] Hierbei spielt die Länge und die Beschaffenheit der Fasern eine entscheidende Rolle. Lange Fasern werden einfacher dispergiert als kurze Fasern. Hydrophile Gruppen, wie Stickstoffmoleküle, oder Sauerstoffmoleküle erhöhen die Dispergierbarkeit in Wasser, da diese mit Wasser Wasserstoffbrückenbindungen eingehen können.[99] Es kommen synthetische Glas-, Polyethylen-, Polypropylen-, Polyester-, Aramid-, Carbon- oder regenerative Cellulosefasern und natürliche Flachs-, Wolle- oder Cellulosefasern zum Einsatz.[97,100–105] Die Verwendung von Polyethylen- oder Polypropylenfasern benötigen eine chemische Modifizierung, um diese in Wasser zu dispergieren. Weitere Hilfsmittel zur Dispergierbarkeit sind unter anderem Tenside, die ein hydrophobes und hydrophiles Kettenende besitzen.[106,107] Entschäumer werden eingesetzt, um die während des Prozesses entstehenden Luftblasen zu stabilisieren.[108] Die Stabilität des Faservlieses muss durch die Einführung von Hilfsmittel erfolgen. Hierbei ist die Rede von sogenannten Bindern. Typische Binder sind unter anderem Latex, schmelzbare Fasern, nicht vollständig lösliche Fasern oder wet-end Binder. [97,102,109]

Für den Wet-laid Prozess werden unter anderem Faserdispersionen, Mischer, Filtriereinheit und eine Vakuumpumpe benötigt. Der Herstellungsprozess ist in Abbildung 1.7 dargestellt. Hier werden zuerst die Faserdispersionen miteinander vermischt. Anschließend wird die Mischung in eine Filtriereinheit überführt und das wässrige Medium durch ein angelegtes Vakuum

abgesaugt. Das getrocknete Faservlies wird anschließend von dem Templat abgenommen und getrocknet. Durch ein thermisches Behandeln des Faservlieses wird die Stabilität erreicht.

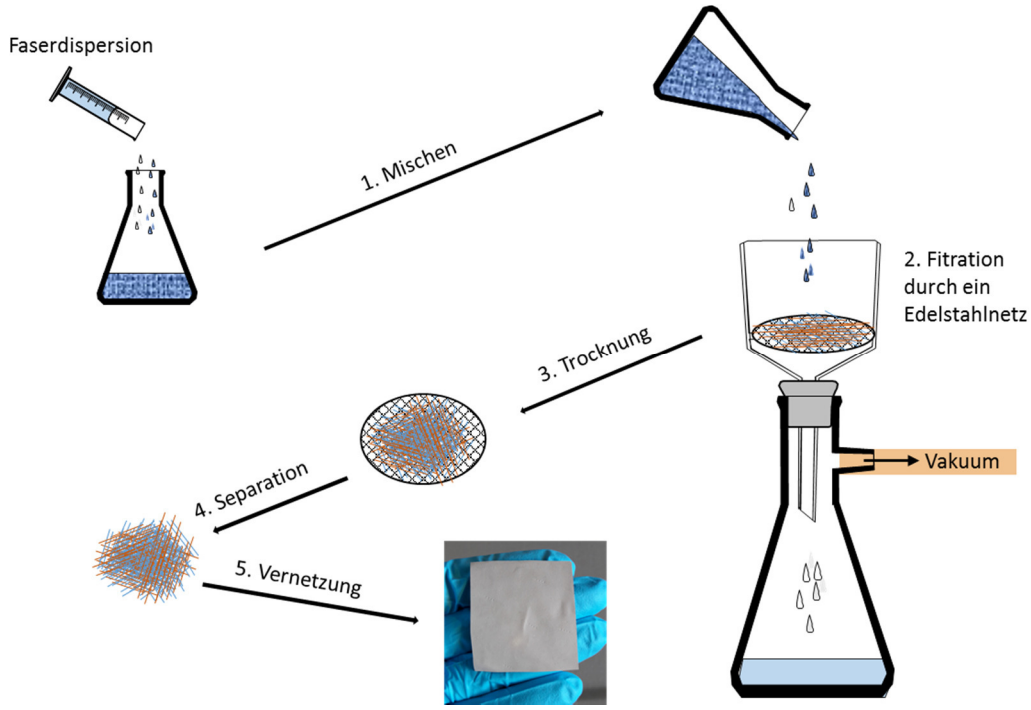

Abbildung 1.7: Schematische Darstellung des Wet-laid Verfahrens zur Herstellung von Polymervliese.Verändert aus Referenz[110], open access Journal, keine Genehmigung erforderlich.

Die Leitfähigkeit der Strukturen wird dadurch erreicht, dass durch Zugabe leitfähiger Additive (AgNW, AuNW, PdNW) Elektroden hergestellt werden können. Katalysatoren (AuNP, PdNP, PtNP) können in das Faservlies eingearbeitet werden, um Synthesen mit Hilfe eines „Teabags“ wiederholt durchzuführen.

1.3 Applikationen von verkapselten Bakterien

1.3.1 Rückgewinnung anorganischer Substanzen und deren katalytische Aktivität

Die Rückgewinnung von anorganischen Werkstoffen ist heutzutage von entscheidender Bedeutung. Industrielle Werkstoffe wie Farben, Füllstoffe oder elektronische Bauteile benötigen Metalle, die auf der Erde nur in geringen Mengen zur Verfügung stehen. Bei der Herstellung und der Entsorgung dieser Bauteile werden diese Substanzen wieder freigesetzt und sind in Abwässern oder Klärschlamm aufzufinden.[111–114] Zu diesen Substanzen gehören vor allem Edelmetalle wie Gold, Palladium und Platin.[115–118] Leitfähige Platinen der

Elektroindustrie bestehen aus Silber-, Nickel- oder Kupferverbindungen, die der Umwelt als toxische Gifte schaden.[119,120] Nukleare Elemente wie Strontium, Thorium oder Uran werden häufig in Atomkraftwerken verwendet, die anschließend aufgearbeitet werden müssen. Gängige Rückgewinnungsmethoden sind die chemische Fällung, Adsorption oder Membranprozesse.[121–126] Diese Rückgewinnung anorganischer Werkstoffe kann durch Mikroorganismen, wie Bakterien, Hefen, Pilzen, Algen oder Viren erfolgen, welche schon in der Industrie, vor allem in der Biotechnologie, erforscht und auch eingesetzt werden. Im Gegensatz zur chemischen Rückgewinnung, ist die Verwendung von Mikroorganismen eine umweltfreundliche Technologie. Dabei werden die gelösten Metallionen durch den Mikroorganismus aufgenommen (Biosorption) oder an der Oberfläche akkumuliert (Bioakkumulation). Meist werden die Metallionen zu Metallpartikeln synthetisiert. AuNP werden durch verschiedene Bakterien, *Bacillus subtilis*,[127] *E.coli*,[128] *Marinobacter Pelagius sp.*,[129] *Geobacillus sp.*[130] oder *M.luteus*.[131] Silbernanopartikel (AgNP) werden unter anderem durch *Lactobacillus sp.*,[132] *Bacillus indicus*,[133] *Enterobacter cloacae*[134] oder *Pseudonomas fluorecens*[135] biologisch synthetisiert. Weitere Nanopartikel, wie Palladium werden durch *Desulfovibrio desulfuricans*[136] oder CdS durch *Rhodobacter sphaeroides*[137] hergestellt. Bisher wurde hauptsächlich die antimikrobielle Aktivität dieser Nanopartikel untersucht. AuNP, welche durch *Hibiscus cannabinus* Stengelextrakt hergestellt wurden, zeigen eine antimikrobielle Aktivität gegenüber *Pseudomonas aeruginosa* und *Staphylococcus aureus*.[138] Annamalai et al. untersuchten die antimikrobielle Aktivität von AuNP, gegenüber *Escherichia coli*, *Pseudomonas aeruginosa* und *Klebsiella pneumonia*, die durch einen Blattextrakt von *Euphorbia hirta* synthetisiert wurden.[139] Biosynthetisierte AuNP durch *Abelmoschus esculentus* Extrakt wiesen eine antimikrobielle Aktivität gegen *Puccinia graminis trici*, *Aspergillus niger*, *Aspergillus flavus* und *Candida albicans* auf.[140] Die katalytische Aktivität, der durch Mikroorganismen hergestellten Nanopartikel, wurde bislang nur durch wenige Arbeiten nachgewiesen. Lim et al. untersuchten die Reduktion von 4-Nitrophenol zu 4-Aminophenol durch *Artemisia capillaris* Wasserextrakt hergestellte AuNP.[141] Silbernanopartikel (AgNP) synthetisiert durch *Gmelina arborea* zeigten eine katalytische Reduktion des Farbstoffes Methylenblau.[142]

Immobilisierte Mikroorganismen in Trägermaterialien haben den Vorteil gegenüber freien Mikroorganismen, dass diese mehrmals eingesetzt werden können. Weitere Vorteile sind der Schutz der Bakterien gegenüber äußeren Einflüssen, wie Temperatur, pH-Wert, UV-Strahlung, Lösungsmittel, usw. Daher wurden Mikroorganismen in hydrophilen Polymerfasern immobilisiert und mit einer hydrophoben Polymerschicht ausgestattet. Nardi et al.

immobilisierten *Corynebacterium glutamicum* (*C.glutamicum)* in PVDF-HFP-Mikroröhren und wiesen einen Phenolabbau in einem Bioreaktor nach.[51] Knierim et al. immobilisierten *M.luteus* und *Nitrobacter winogradskyi (N.winogradskyi)* in PVA-Mikrofasern und beschichteten diese mit PPX. Die Lebensfähigkeit konnte durch fluoreszenzmikroskopische Aufnahmen nachgewiesen werden. Mit diesen wasserstabilen Fasern konnten durch die Immobilisierung von *M.luteus* Au-Ionen aus einer pH 3 sauren Lösung sorbiert werden und durch eine elektronenmikroskopische Aufnahme AuNP in den Mikrofasern nachgewiesen werden. *N.winogradskyi* war in der Lage in den immobilisierten Mikrofasern Nitrit zu reduzieren.[143] Letnik et al. immobiliserten durch Coaxialelektrospinnen *Candida tropicalis* und *Saccharomyces cerevisia* in PVP-Nanofasern stabilisiert mit PVDF-HFP. Sie wiesen einen Phenolabbau und Herstellung von Ethanol aus Olivenölabwasser nach.[144] *M.luteus* wurde durch Letnik et al. in dem gleichen Fasersystem immobilisiert. Hier konnte eine Biosorption von Kupfer nachgewiesen werden.[145]

1.3.2 Mikrobielle Brennstoffzelle

Mikroorgansimen sind in der Lage elektrischen Strom herzustellen, indem sie Nährstoffe wie Acetat, Glucose, Pyruvat, Formiat usw. verstoffwechseln. Porter ist es 1911 gelungen Bakterien und Hefen für die Stromproduktion zu identifizieren.[146] Diese Bakterien waren in der Lage durch die Verwendung von Pflanzenresten Strom zu generieren. Die Stromausbeute war jedoch so gering, dass dieser Ansatz der umweltschonenden Stromproduktion kaum verfolgt wurde. 1962 gelang Yarbough und Davis die Beschreibung der Funktionsweise einer mikrobiellen Brennstoffzelle. Durch diese Beschreibung der Funktionsweise war der Grundstein für die Entwicklung neuer mikrobiellen Brennstoffzellen gelegt.
Die mikrobielle Brennstoffzelle ist ähnlich aufgebaut, wie eine handelsübliche Wasserstoff-Brennstoffzelle und besteht aus drei wesentlichen Bestandteilen. Zu nennen sind hier die biologische Zelle (Anodenseite), die chemische Zelle (Kationenseite) und die kationenselektive Membran (Abbildung 1.8).

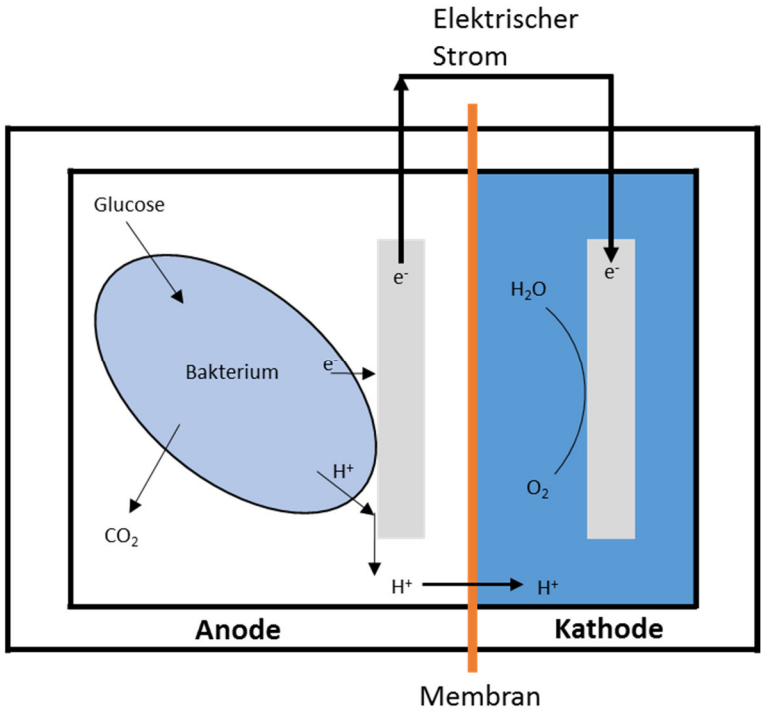

Abbildung 1.8: Schematische Darstellung einer mikrobiellen Brennstoffzelle. Verändert aus Referenz [147], mit Genehmigung..Copyright (2018) American Chemical Society.

Die biologische Zelle besteht aus einer Anode, dem entsprechenden Mikroorganismus und Substraten. Die Substrate müssen durch die Bakterien biologisch abbaubar sein. Als Substrate kommen hier nicht nur Acetat, Glucose, Ethanol, Formiat oder Pyruvat zum Einsatz,[147–151] bekannt sind ebenfalls hochkomplexe Industrieabwässer oder Abwässer aus normalen Haushalten.[152,153] Als Anode wird meist Kohlenstoff als kostengünstiges, nicht biologisch abbaubares und biokompatibles Material eingesetzt. Kohlenstoff wird hier in verschiedenen Ausführung als Anodenmaterial bereitgestellt, unter anderem als Stäbchen, Platten, Vliese, Schwämme, usw.[153–160] Jedoch ist die Leitfähigkeit, durch die Verwendung von Kohlenstoff, nachteilig gegenüber Metallen, wie Gold, Kupfer oder Silber. [161–164]

Damit eine Stromproduktion erfolgen bzw. ein messbarer Strom gemessen werden kann, muss die Anhaftung der Bakterien auf der Anodenoberfläche stattfinden bzw. eine räumliche Nähe zwischen Bakterium und Anodenoberfläche gewährleistet werden. Dies erfolgt meist durch die Ausbildung eines Biofilms an der Anodenoberfläche. Bekannte Bakterien, die einen solchen Biofilm auf Anodenoberflächen bilden, sind unter anderem Bakterienarten, wie *Geobacter*, *Escherichia*, *Ochrobactrum*, *Rhodopseudomonas* oder *Shewanella*.[165–169] Diese können ihre produzierten Elektronen direkt an die Anodenoberfläche abgeben. Redoxmediatoren sind bei den Bakterienarten *Saccharomyces* und *Pseudomonas* für den Elektronentransport zur Anodenoberfläche verantwortlich.[170,171] Bisher war nur das Aufwachsen eines Biofilmes auf

die Anodenoberfläche bekannt. Deshalb wurde in dieser Arbeit ein Anodenmaterial entwickelt, bei dem die Mikroorganismen (*S.oneidensis MR-1*) in dem Anodenmaterial immobilisiert sind.[172]

1.4 Applikationen von Wet-laid Faservliesen

1.4.1 Elektrodenmaterialien

Elektroden finden ihre Anwendung heutzutage in Bereichen der Industrie, wie den Brennstoffzellen,[173] den mikrobiellen Brennstoffzellen,[174] den Galvanischen Systemen,[175] dem Elektroschweißen,[176] dem Automobil[177] und den Glühbirnen.[178]
Elektroden bestehen heutzutage nicht nur aus Metallen[179], Salzen,[180] Kohlenstoffverbindungen[181] oder leitfähigen Polymeren,[182] sondern vielmehr aus Kompositen dieser gebräuchlichen Substanzen.[183–185] Metalle haben den Vorteil gegenüber leitfähigen Polymeren oder Salzen, dass diese die höchsten elektrischen Leitfähigkeiten von bis zu $61 \cdot 10^6$ S/m für Silber besitzen. Der Nachteil dieser Verbindungen liegt in ihrer Beschaffenheit. Metalle liegen meist in starrer Form vor und können nicht beliebig oft gefaltet, gebogen oder verdrillt werden. Weiter sind diese Materialien nicht porös und atmungsfähig. Ein weiterer Nachteil sind die hohen Kosten der Metalle für Beschaffung und Extraktion dieser aus den Natursubstanzen. Auf Basis dieser Nachteile ist es notwendig kostengünstige, flexible, biegsame, poröse und atmungsaktive Komposite, die hohe elektrische Leitfähigkeiten aufweisen, herzustellen. Als Basismaterial eignen sich Polymerfasern, die durch Elektrospinnen,[20] Wetspinning[143] oder Schmelzspinnen[24] hergestellt werden können. Die Leitfähigkeitssteigerung der Polymere kann durch die Zugabe von leitfähigen Additiven wie Silber-,[186] Kupfer-,[187] Goldnanopartikel,[188] Metallnanodrähten[189–191] oder Carbonmaterialien[192] erfolgen. Hierbei ist der Zeitpunkt der Zugabe für die resultierende Leitfähigkeit von entscheidender Bedeutung. Werden die Additive in die Verarbeitungsformulierungen gegeben, sind eine große Menge an Additiven nötig, um die elektrische Leitfähigkeit, den Perkolationspfad in der Matrix, zu erhalten. Deshalb ist es notwendig die leitfähigen Additive nachträglich auf die Oberfläche der Polymerfasern aufzubringen.[193–195]
Geeignete Verfahren zur Beschichtung der Polymerfasern sind, neben der nasschemischen und elektrochemischen Abscheidung[194,195] oder der chemischen Abscheidung in der Gasphase von Metallen auf die Polymerfasern, Eintauch- und Sprühverfahren.[193] Bei den Eintauch- und

Sprühverfahren kommen stark verdünnte Additiv-Lösungen zum Einsatz. Die Leitfähigkeitssteigerung wird durch das Wiederholen der Eintauch- oder Sprühprozesse erreicht.[193]

1.5 Ziel der Arbeit

Das Ziel der vorliegenden Arbeit war die erfolgreiche Synergie zwischen Materialwissenschaften und der Mikrobiologie. So sollten stabile Polymer/Bakterien Komposite hergestellt werden. Hierfür sollten verschiedene Systeme betrachtet werden.

Für die Herstellung von Polymer/Bakterien-Nanofasern sollte das Elektrospinnen von hydrophilen Polymeren angewandt werden. Um in Wasser stabile Fasern zu erhalten, wurden die elektrogesponnenen hydrophilen Polymerfasern mit einem hydrophoben PPX mittels CVD beschichtet. Diese Polymer/Bakterien-Nanofasern sollten dann zur Abwasserreinigung von Industrieabwässern, die Edelmetalle in gelöster Form enthielten, eingesetzt werden. Das Bakterium *M.luteus* ist in der Lage Goldionen zu Goldnanopartikeln zu synthetisieren. Deshalb ist ein wichtiger Aspekt dieser Komposite die Akkumulation von Goldionen zu Goldnanopartikeln, welche eine katalytische Aktivität besitzen. Dieses System kann nicht nur seine Anwendung in der Bioremediation von Edelmetallen und deren katalytische Aktivität finden, sondern auch in der Energieproduktion aus Abwässern dienen.

Im weiteren Verlauf werden elektronenproduzierende Bakterien, wie *S.oneidensis MR-1*, in die hydrophilen Polymer-Nanofasern mittels Elektrospinnen eingebracht und anschließend mittels CVD mit PPX zu wasserstabilen Polymerfasern verarbeitet werden. Dieser Komposit soll sein Potential als Anode für mikrobielle Brennstoffzellen unter Beweis stellen. DieVerkapselung von Mikroorganismen in Polymeren kann neben dem Elektrospinnen, auch Verfahren, wie der Dispersionsmethode und der Sprühtrocknung erfolgen.

Die Mikroverkapselung von Bakterien in Polymerpartikeln wurde in unserer Gruppe durch eine Emulsionsmethode erfolgreich durchgeführt. Die Ausbeute solcher Polymer/Bakterien-Partikel ist jedoch sehr gering, um große Mengen in einem weiteren Schritt zu verarbeiten. Deshalb sollte ein Verfahren zur Mikroverkapselung von Bakterien in Polymerpartikel für größere Mengen evaluiert werden. Hier wurde ein Sprühtrocknungsverfahren auf Basis von Polymer/Bakterienkapseln in Betracht gezogen. Dieses Verfahren umfasst die Herstellung verschiedener hydrophiler Polymerpartikel, wie PVA, Polyvinylpyrrolidon (PVP), Hydroxypropylcellulose (HPC) und Gelatine. Bakterien, wie *M.luteus* oder *E.coli*, werden in diesen Polymerpartikeln mikroverkapselt. Die Charakterisierung dieser Komposite umfasst die

Überlebensfähigkeit und die Morphologie der hergestellten Polymer/Bakterienpartikel. In einem weiteren Schritt erfolgt die Herstellung von wasserstabilen elektrogesponnene Polymerfasern, welche Polymer/Bakterienpartikel enthalten. Als hydrophobe Polymere sollen Polyvinylacetat (PVAc), Polyvinylbutyral (PVB), Polymethylmethacrylat (PMMA), Polystyrol (PS), Polyacrylnitril (PAN) und thermoplastisches Polyurethan (TPU) eingesetzt werden. Diese Komposite findet ihre Anwendung in der Bioremediation, Katalyse oder der mikrobiellen Brennstoffzelle. Hierfür werden leitfähige Komposite benötigt, die über ein Wet-laid Verfahren hergestellt werden.

Die Herstellung von Polymer/Bakterien Komposite auf Basis von elektrogesponnenen Fasern stellt für die Industrie eine große Rolle in Form einer kontinuierlichen Herstellung dar. Denn durch das Elektrospinnen ist die Industrie nicht in der Lage kontinuierlich Faservliese am Laufband herzustellen. Deshalb soll ein Verfahren angewandt werden, das die Verarbeitung von elektrogesponnenen Nanofasern im großen Stil in der Industrie erlaubt. Hierfür soll das Wet-laid Verfahren, das zur Herstellung von Papier genutzt wird, auf Basis elektrogesponnener Kurzschnittfasern entwickelt werden. Durch dieses Verfahren sollen, durch den Zusatz von Bakterien oder leitfähigen Additiven, „lebende“ oder leitfähige Komposite hergestellt werden. Leitfähige Additive und Kurzschnittfasern können einfach miteinander verarbeitet werden. Deshalb werden daraus nicht nur 2D Systeme hergestellt, sondern auch 3D Systeme. Hier soll ein System entwickelt werden, das durch Druck komprimiert werden kann. Durch die Kompression soll ein Isolator eine Leitfähigkeitssteigerung erreichen, mit der ein elektrischer Strom durch ein 3D System fließen kann. Dies soll durch die Verwendung von leitfähigen Additiven (Aspektverhältnis von 100 -500) erreicht werden.

Die möglichen Anwendungen werden in Abbildung 1.9 dargestellt. Einen Überblick über Anwendungen werden in Kapitel 2 näher erläutert.

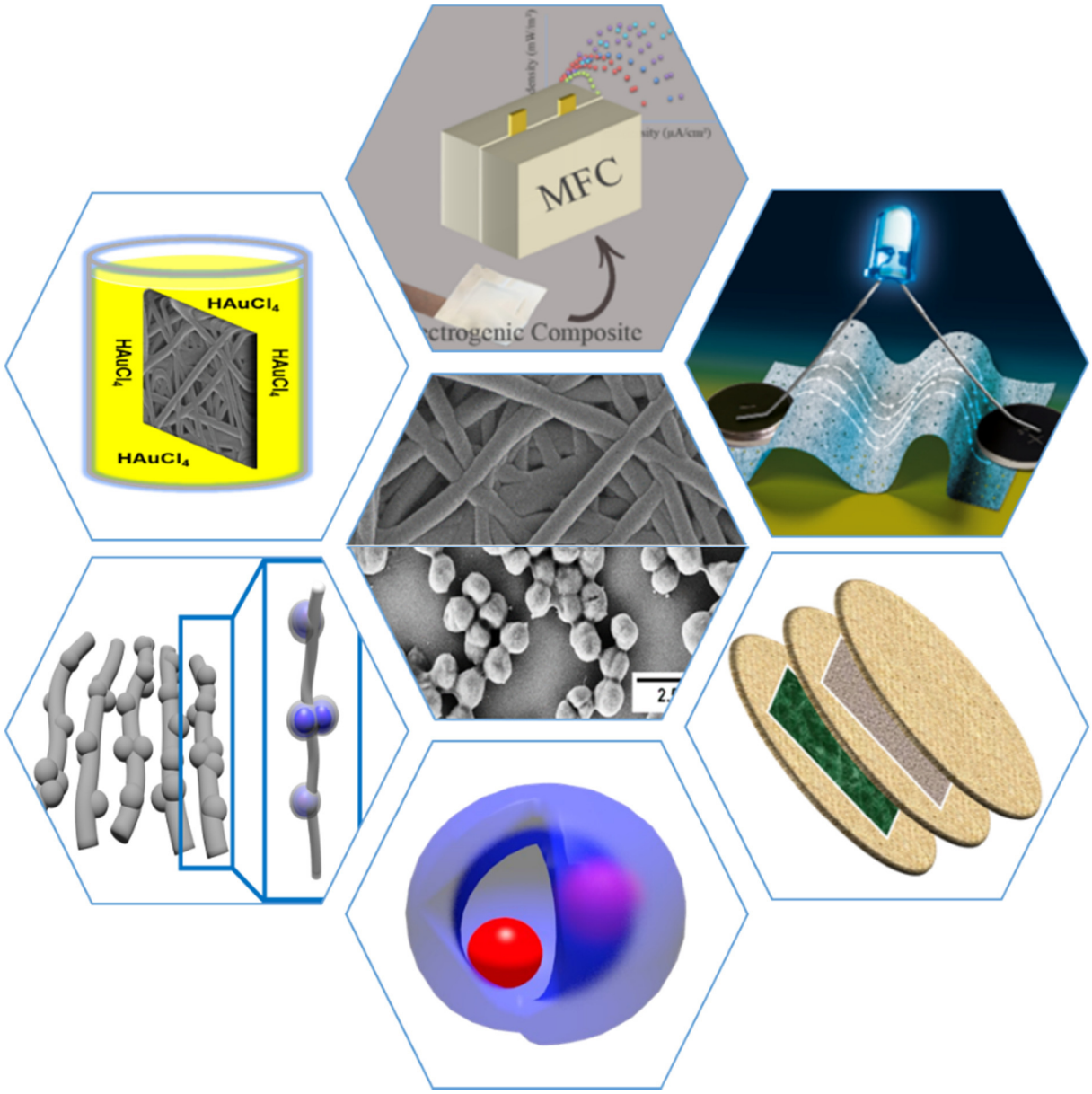

Abbildung 1.9: Darstellung der möglichen Einsatzgebiete der hergestellten funktionalen Polymer/Bakterien Komposite.

2 Überblick der Teilarbeiten

Diese Dissertation verfügt über fünf wissenschaftliche Arbeiten, die zum Teil publiziert bzw. eingereicht wurden. Die Inhalte dieser Publikationen werden in Kapitel 2.1 bis 2.5 aufgezeigt und im Detail zusammengestellt. In den Kapiteln 2.1 und 2.2 werden funktionale Bakterien in PVA/PPX-Nanofasern verarbeitet und zwei unterschiedliche Anwendungen dieser aufgezeigt. Die Anwendung in Kapitel 2.1 zeigt das Potential dieser Komposite in Bezug auf die Abwasserreinigung von Edelmetallen, die anschließend für katalytische Reaktionen verwendet werden können. In Kapitel 2.2 wird zum ersten Mal das Potential eines verkapselten Bakteriums in Bezug auf ein lebendes Polymer/Bakterium-Komposits für mikrobielle Brennstoffzellen aufgezeigt. Das Kapitel 2.3 behandelt eine Mikroverkapselungsmethode von Bakterien in Polymerkapseln im Industriemaßstab und die Weiterverarbeitung zu Polymervliesen.
Das Kapitel 2.4 und 2.5 beinhaltet die Verarbeitung von Kurzschnittfasern und leitfähigen Additiven in Bezug auf Elektrodenmaterialien. In Kapitel 2.4 werden 2D Systeme und in Kapitel 2.5 3D Systeme hergestellt und die Verwendung als Elektrodenmaterial aufgezeigt.

2.1 The preparation of bacteria based golden polymer fleece and its catalytical application

Die vorliegende Veröffentlichung beschäftigt sich mit der Verkapselung von *M.luteus* in PVA/PPX-Faservliesen für die gezielte Bioremediation von Edelmetallen (Gold) durch *M.luteus*. *M.luteus* zeigt das Potential Goldionen zu sorbieren und akkumulieren. Durch diese Biosorption und Bioakkumulation bilden sich Nanopartikel, die auf ihre katalytische Aktivität untersucht wurden (Abbildung 2.1).

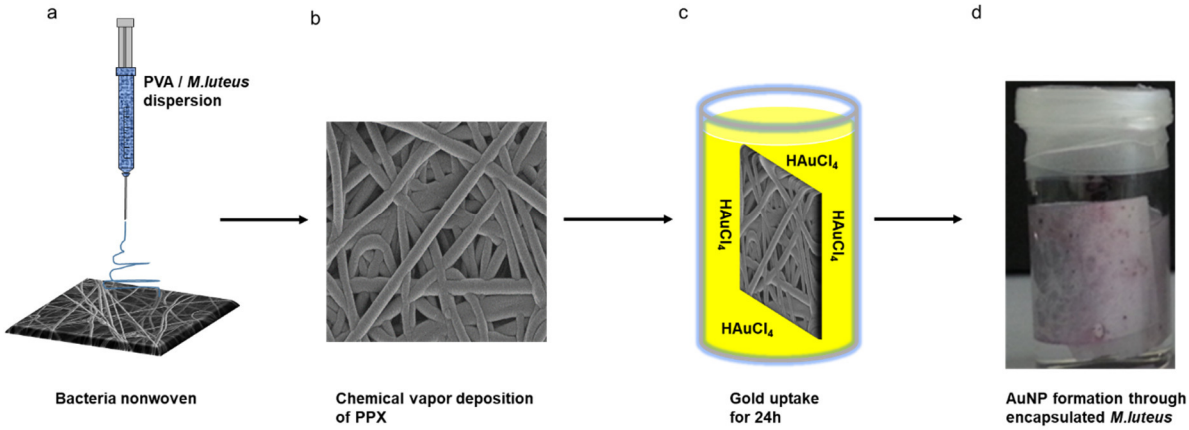

Abbildung 2.1 Schematische Vorgehensweise zur Herstellung von katalytisch aktiven Polymerfaservliesen.

Zu Beginn erfolgte die Verkapselung der *M.luteus* in PVA-Fasern durch das Elektrospinnen. Die anschließende hydrophobe Hülle wurde durch die Gasphasenabscheidung von PPX erhalten. Rasterelektronenmikroskopieaufnahmen zeigen die PVA/*M.luteus*-Fasern, wobei eine Verkapselung der *M.luteus* erreicht wurde. Die gelben Pfeile deuten auf einen hohen Gehalt an *M.luteus* hin. Der mittlere Durchmesser der PVA/*M.luteus*-Fasern beträgt 424 ± 115 nm (Abbildung 2.2a). Der mittlere Durchmesser der PVA/*M.luteus*/PPX-Fasern beträgt 1633 ± 289 nm. Die resultierende PPX-Hülle hat demnach eine Schichtdicke von ~1,2 µm (Abbildung 2.2b).

Nach diesen Prozessschritten erfolgten Überlebenstests der *M.luteus* durch Anzüchten auf einer Agarplatte nach dem Elektrospinnen und einer konfokalen Rasterfluoreszenzmikroskopie nach der Gasphasenabscheidung von PPX. Es wird deutlich, dass sowohl das Elektrospinnen, als auch die anschließende Gasphasenabscheidung keinen negativen Einfluss auf die Überlebensfähigkeit der *M.luteus* in den PVA/PPX-Faservliesen besitzt (Abbildung 2.2c,d).

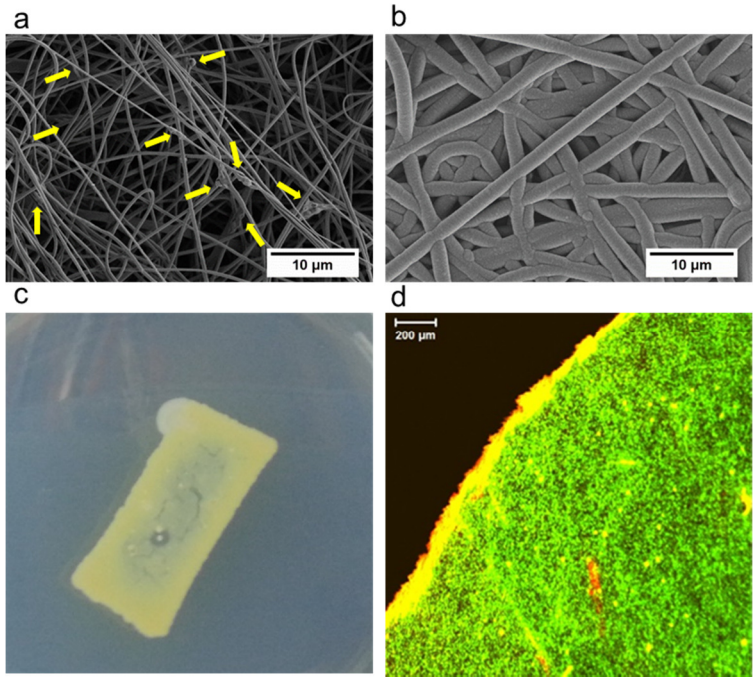

Abbildung 2.2 Charakterisierung der lebenden PVA/M.luteus/PPX-faser-vliesen. Rasterelektronen mikroskopieaufnahmen der PVA/M.luteus-Fasern (gelbe Pfeile zeigen M.luteus an) (a) und der PVA/M.luteus/PPX-Fasern (b), Überlebenstest der M.luteus nach der Elektrospinnen durch eine Agarplattentest (c) und nach der Gasphasenabscheidung von PPX durch eine Konfokale Rasterfluoreszentmikroskopie (d), rot: tote M.luteus und grün: lebende M.luteus.

Die Bioremediation von Goldionen durch die Biokomposite konnte erfolgreich durchgeführt werden. Goldionen werden durch *M.luteus* zu Goldnanopartikeln synthetisiert, welche nicht nur visuell ersichtlich wurden, da die Fasermatte eine rötliche bis violette Farbe annahm. Auch

Charakterisierungsmethoden, wie die Transmissionselektronenmikroskopie und die Rasterelektronenmikroskopie bestätigten die Bildung von Goldnanopartikel. Die Transmissionselektronenmikroskopie zeigte eine deutliche Akkumulation von Goldnanopartikeln auf der Oberfläche der *M.luteus* an. Die Rasterelektronenmikroskopie deutete durch die Verwendung eines BSE-Detektors auf metallische Nanopartikel hin, die durch die EDX-Analyse als Goldnanopartikel bestätigt werden konnten.

Die katalytische Aktivität der Goldnanopartikel wurde an einem literaturbekannten Katalysesystem, der hydrolytischen Oxidation von Dimethylphenylsilan mit Wasser, durchgeführt (Abbildung 2.3a). Hier wurde deutlich, dass die Verwendung lebender *M.luteus* in den Biokompositen zu katalytischen Goldnanopartikeln führt, während tote M.luteus keine katalytischen Goldnanopartikel herstellten. Dies ist vermutlich auf die geringe Verstoffwechselung der Goldionen und der somit gehemmten Biosynthese von Goldnanopartikeln durch die *M.luteus* zurückzuführen. Diese Erkenntnis wird in der Darstellung der hydrolytischen Oxidation von Dimethylphenylsilan deutlich, da die Katalyse nur durch die Biokomposite mit lebenden *M.luteus* einen nahezu 100%igem Umsatz aufzeigt (Abbildung 2.3b).

a

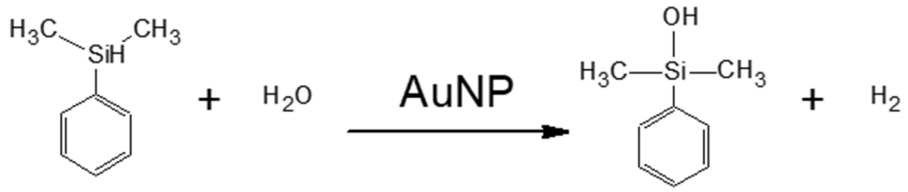

b

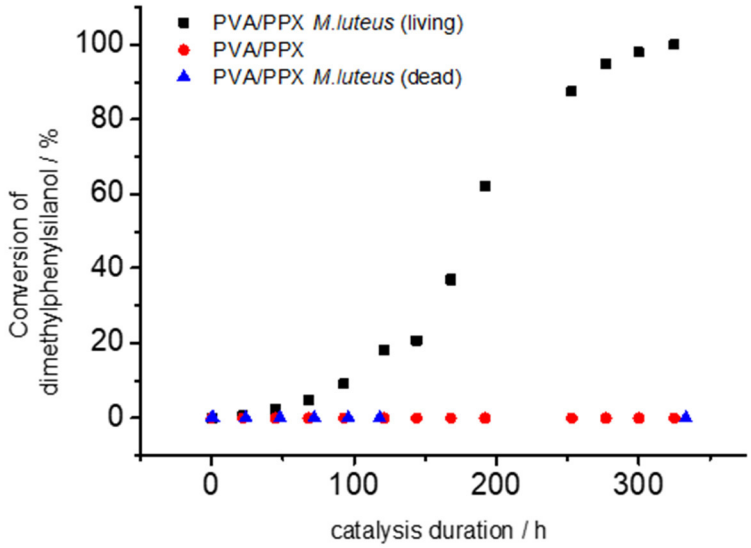

Abbildung 2.3 Schematische Darstellung der durchgeführten Katalyse von Dimethylphenylsilan mit Wasser zu Dimethylphenylsilanol durch die biosynthetisierten Goldnanopartikel (a) und Verlauf der Katalyse durch verschiedene Systeme (b); rot: PVA/PPX-Faservlies, blau: PVA/M.luteus(tot)/PPX-Faservlies und schwarz: PVA/M.luteus (lebend)/PPX-Faservlies.

2.2 Electrogenic single-species biocomposites as anodes for microbial fuel cells

Die vorliegende Veröffentlichung beschäftigt sich mit der Herstellung von Polymer-Bakterien-Vliesen, welche Anwendung als Anodenmaterial in einer mikrobiellen Brennstoffzelle finden soll. Die Herstellung erfolgt analog zu 2.1, es wurde jedoch das Bakterium *S.oneidensis MR-1* eingesetzt. Dieses Bakterium besitzt das Potential Nährstoffe zu Elektronen umzuwandeln. Der Aufbau einer mikrobiellen Brennstoffzelle wird in Abbildung 2.4 dargestellt.

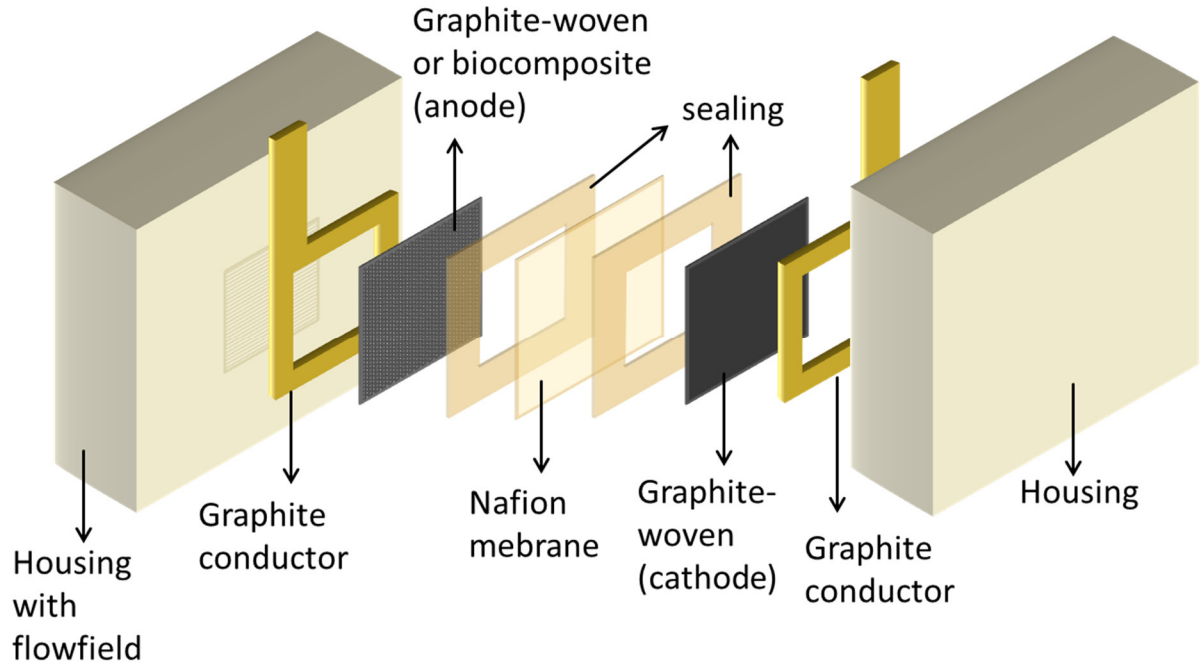

Abbildung 2.4 Schematische Darstellung einer mikrobiellen Brennstoffzelle. Verwendet aus Referenz [172], mit Genehmigung. Copyright (2018) Wiley-VCH Verlag GmbH & Co. KGaA, Weinheim.

Die Herstellung der wasserstabilen Polymer-Bakterien-Fasern wurde durch zwei Verfahren, dem Elektrospinnen und der Gasphasenabscheidung, erreicht. Die so hergestellten Biokomposite wurden durch SEM und CLSM charakterisiert. SEM-Aufnahmen zeigten PVA/*S.oneidensis MR-1*-Fasern mit einem mittleren Durchmesser von 450 ± 140 nm. Nach der Gasphasenabscheidung wurde ein mittlerer Durchmesser der Fasern von 1,7 ± 0,25 µm erhalten, was einer PPX-Schichtdicke von ~1,2 µm entspricht. Nach den Herstellungsmethoden wurde die Lebensfähigkeit der *S.oneidensis MR-1* in den wasserstabilen Polymerfasern mittels CLSM untersucht. Es wurde gezeigt, dass die *S.oneidensis MR-1* den Hestellungsprozess überleben und in diesen Polymerfasern metabolisch aktiv sind.

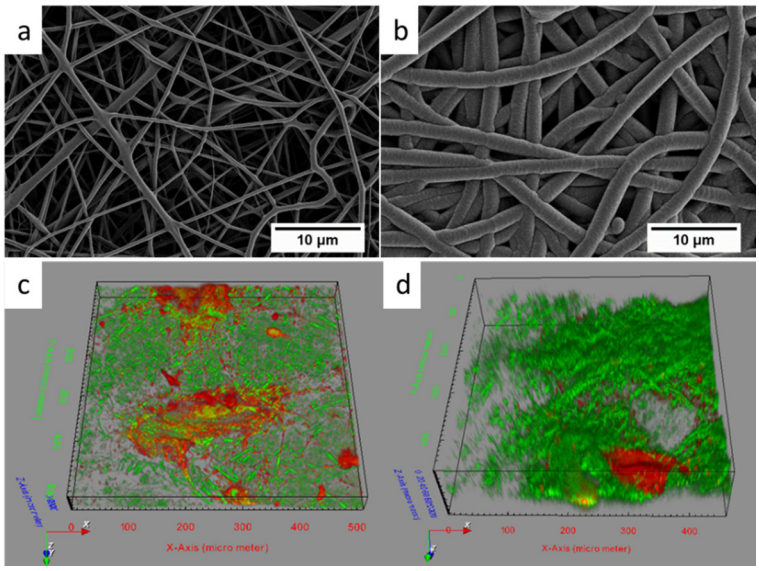

Abbildung 2.5 Charakterisierung der Biokomposite. Rasterelektronenmikroskopieaufnahme der PVA/S.oneidensis MR-1-Fasern (a) und der PVA/S.oneidensis MR-1/PPX-Fasern (b), Konfokale Rasterfluoreszenzaufnahme (CLSM) der PVA/S.oneidensis MR-1/PPX-Fasern direkt nach der Herstellung (c) und nach 7 Tagen Inkubation in Nährmedium (d), rot: tote S.oneidensis MR-1 und grün: lebende S.oneidensis MR-1.Verwendet aus Referenz[172], mit Genehmigung. Copyright (2018) Wiley-VCH Verlag GmbH & Co. KGaA, Weinheim.

Die Verwendung als Anodenmaterial in einer mikrobiellen Brennstoffzelle konnte erfolgreich gezeigt werden. Planktonische Zellen zeigten das größte Potential in einer mikrobiellen Brennstoffzelle, in dem Leistungen von 104 mW $\cdot m^{-2}$ erreicht wurden. Da hier jedoch eine *S.oneidensis MR-1*-lösung immer wieder durch die Zelle geführt wurde, ist ein Vegleich mit den anderen Materialien nur schwer durchzuführen. Ein Vergleich kann jedoch zwischen dem natürlichen Biofilm und dem Kompositmaterial erfolgen. Im Gegensatz, zu dem in der Natur vorkommenden natürlichen Biofilmen mit einer gemessenen Leistung von 30 mW $\cdot m^{-2}$, wurde eine Leistungssteigerung durch das Kompositmaterial (~65 mW$\cdot m^{-2}$) um mehr als das Doppelte gemessen. Ebenfalls ist die sterile Handhabung und die Reproduktion durch das Kompositmaterial leichter zu erhalten.

State of the bacteria	**Power density (mW m^{-2})**
control	0.04
planctonic cells	104 ± 14.1
biofilm (natural)	30
nonwoven	2.5 ± 0.5
nonwoven on copper	64.7 ± 19.4

2.3 Polymer/ Living Bacteria Capsules Spray Dried at High Temperatures

Die vorliegende Veröffentlichung beschäftigt sich mit der großtechnischen Herstellung von Polymer/Bakterien-Komposit-Kapseln und deren Weiterverarbeitung zu wasserstabilen Polymerfaservliesen. Eine von Gensheimer et al. etablierte Dispersionmethode lieferte nur eine geringe Menge von Polymer/Bakterien-Komposit-Partikeln. Die Herstellung von wasserstabilen Polymerfaservliesen erfordert große Mengen von Polymer/Bakterien-Partikeln. Deshalb wurde eine neue Methode der Partikelherstellung, das Sprühtrocknen, etabliert (Abbildung 2.6a).

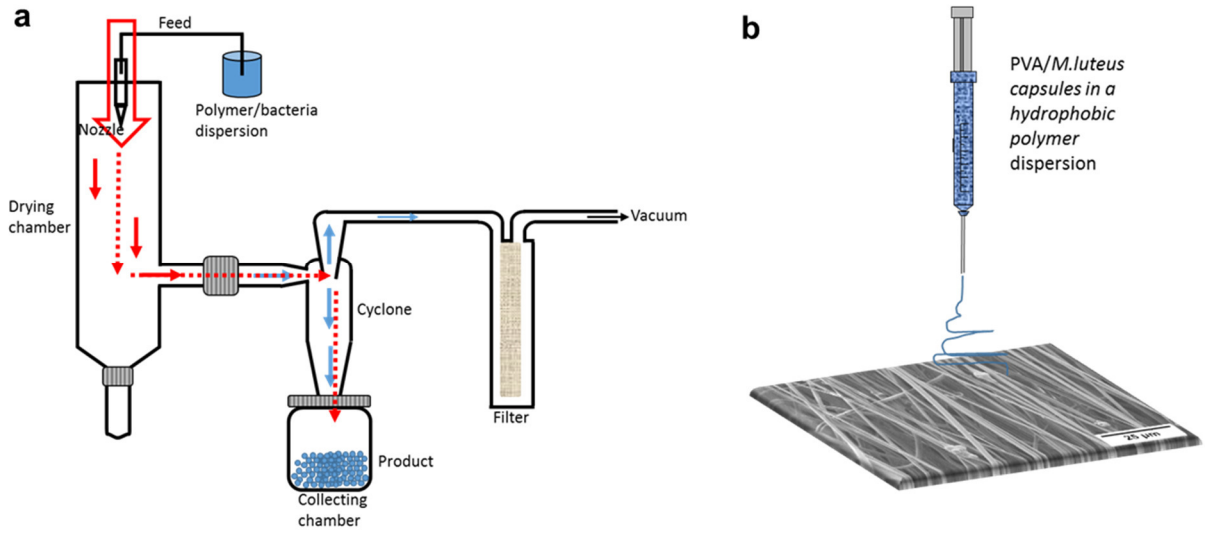

Abbildung 2.6 Schematische Darstellung der Herstellungsmethoden für die Biokomposite. Sprühtrocknung (a) und Elektrospinnen (b).

Vorversuche zeigten, dass die Temperatur einen entscheidenden Einfluss auf die Restfeuchte und somit die Agglomeration der Polymerpartikel besitzt. Temperaturen um 150 °C liefern eine Restfeuchte von 1-2% welche eine Agglomeration der Polymerpartikel zur Folge hat. Ebenfalls zeigte sich ein Einfluss des Molekulargewichts auf die Verteilung des mittleren Partikeldurchmessers. Niedrige Molekulargewichte haben einen kleineren mittleren Partikeldurchmesser, als höhere Molekulargewichte, die in größeren mittleren Partikeldurchmessern resultieren.

Bakterien, wie *M.luteus* und *E.Coli*, wurden zu Polymer/Bakterien-Komposit-Partikeln bei 150 °C verarbeitet. Hier zeigt sich, dass *M.luteus* die Prozesstemperatur von 150 °C überlebt, denn dieses Bakterium konnte erfolgreich auf Agarplatten angezüchtet werden. *E.Coli* hingegen zeigte ein anderes Verhalten, denn dieses Bakterium konnte nicht erneut auf

Agarplatten angezüchtet werden. Erst die Verringerung der Prozesstemperatur auf 120 °C hatte lebende *E.Coli* auf den Agarplatten angezeigt.

Charakterisierungsmethoden, wie TEM oder Raman-AFM-Spektroskopie zeigten eine erfolgreiche Verkapselung der Bakterien in den Polymerpartikeln an (Abbildung 2.7). Ebenfalls wird deutlich, dass diese eine Kern-Hülle-Struktur besitzen. Weiter kann durch TEM-Aufnahmen die Dicke der Polymerhülle bestimmt werden. Diese beträgt 56 ± 12 nm.

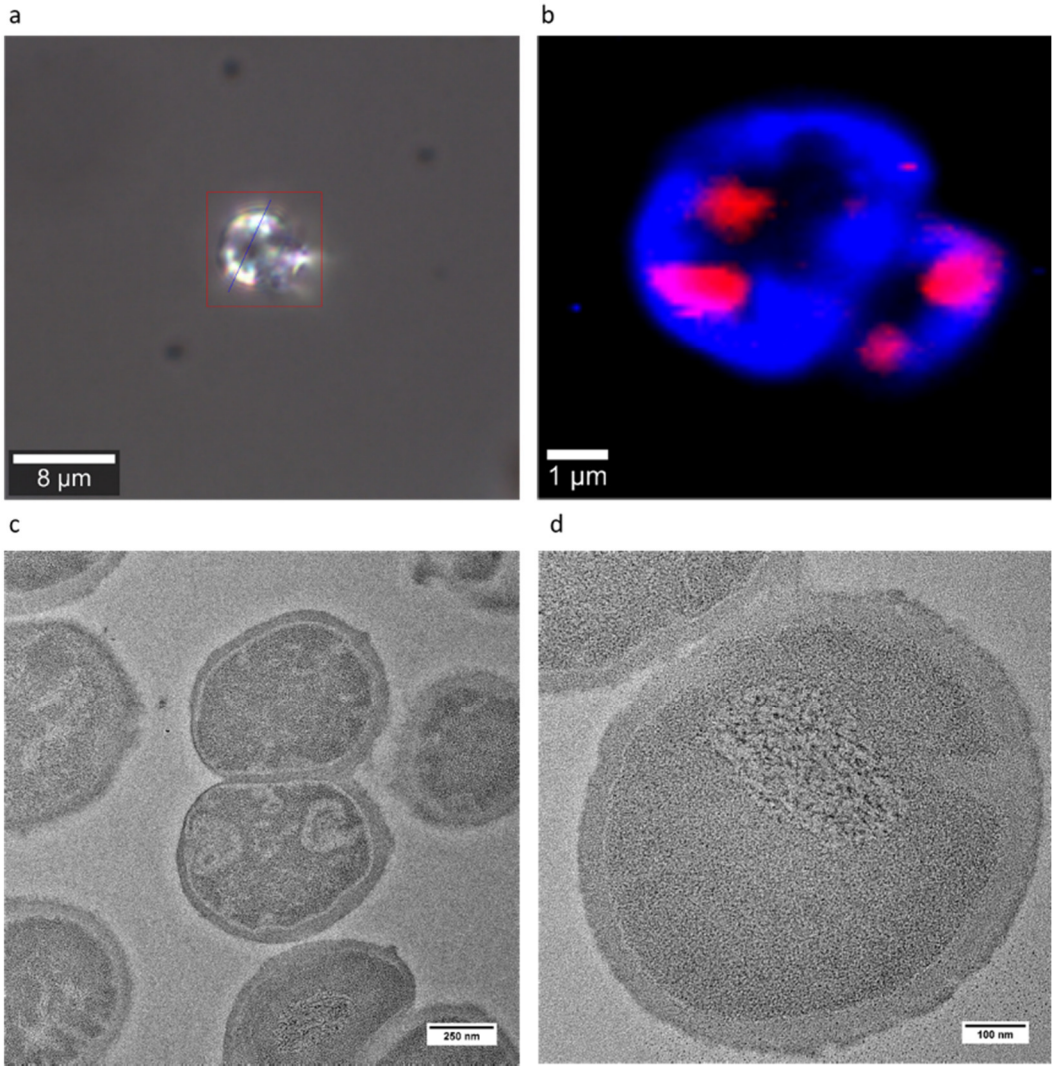

Abbildung 2.7 Charakterisierung der Polymer/Bakterien-Kapseln. Lichtmikroskopieaufnahme (a), RAMAN-Aufnahme (b), Transmissionsaufnahme geringere Auflösung (c) und höhere Auflösung (d).

Die sprühgetrockneten Polymer/Bakterien-Komposit-Kapseln konnten erfolgreich durch das Elektrospinnen zu ausgerichteten wasserstabilen Polymerfaservliesen verarbeitet werden (Abbildung 2.6b). Rasterelektronenmikroskopieaufnahmen zeigen eine Einarbeitung der Polymer/Bakterien-Komposit-Partikel in den Polymerfasern (Abbildung 2.8).

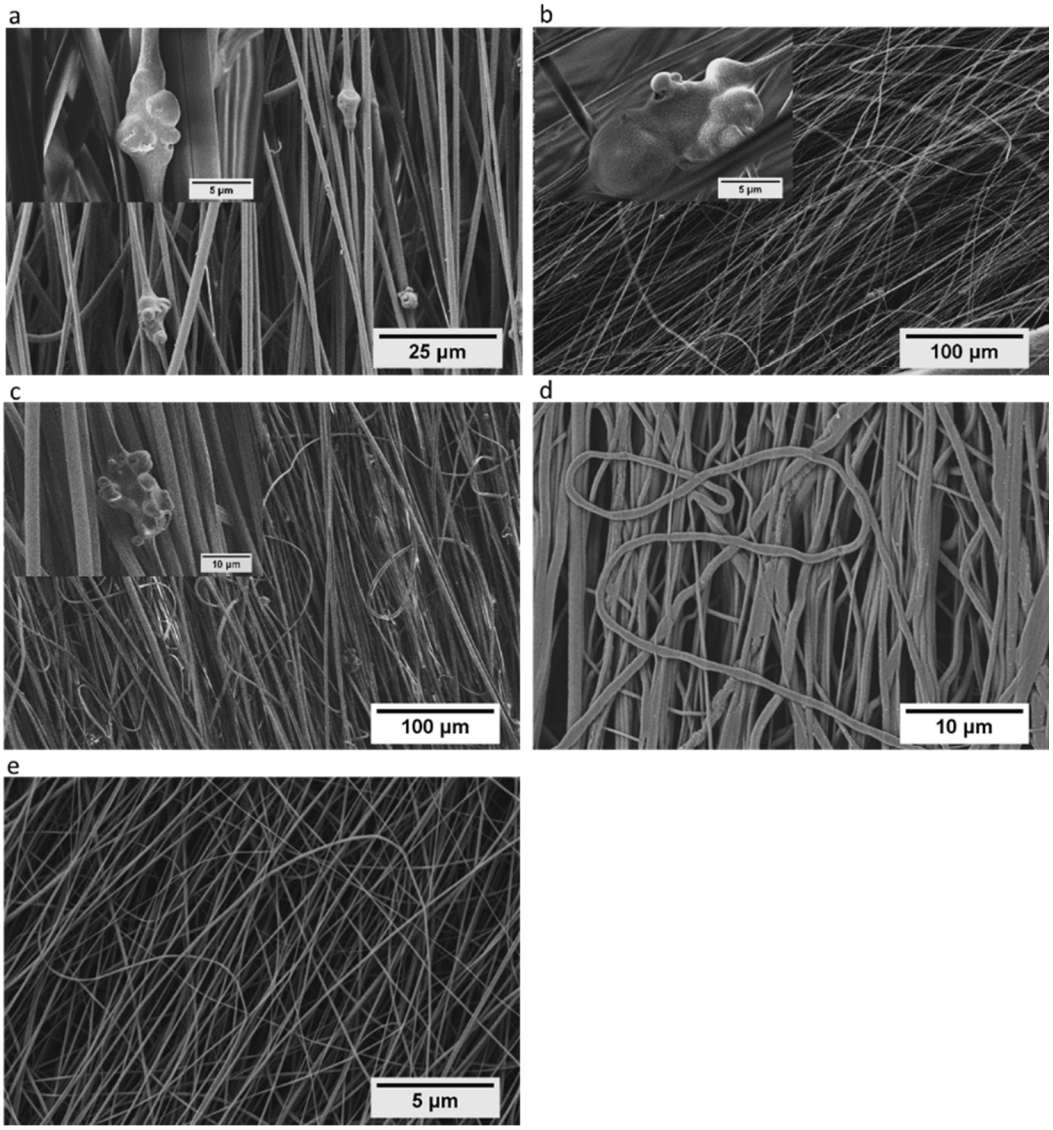

Abbildung 2.8 Rasterelektronenmikroskopieaufnahmen der ausgerichteten elektrogesponnenen Biokompositfasern. Polyacrylnitril-Fasern (a), Polymethylmethacrylat-Fasern (b), Polystyrol-Fasern (c), Thermoplastischen Polyurethan-Fasern (d) und den Polyvinylbutyral-Fasern (e).

2.4 Polymer nanofibre composite nonwovens with metal-like electrical conductivity

Die vorliegende Veröffentlichung zeigt die Herstellung von Polymerfaservliesen, welche durch die Verwendung von dispergierten Kurzschnittfasern im Industriemaßstab hergestellt werden können. Diese Herstellung bedient sich dem Wet-Laid-Verfahren, welches großtechnisch in der Papier- und Filterherstellung seine Anwendung findet.

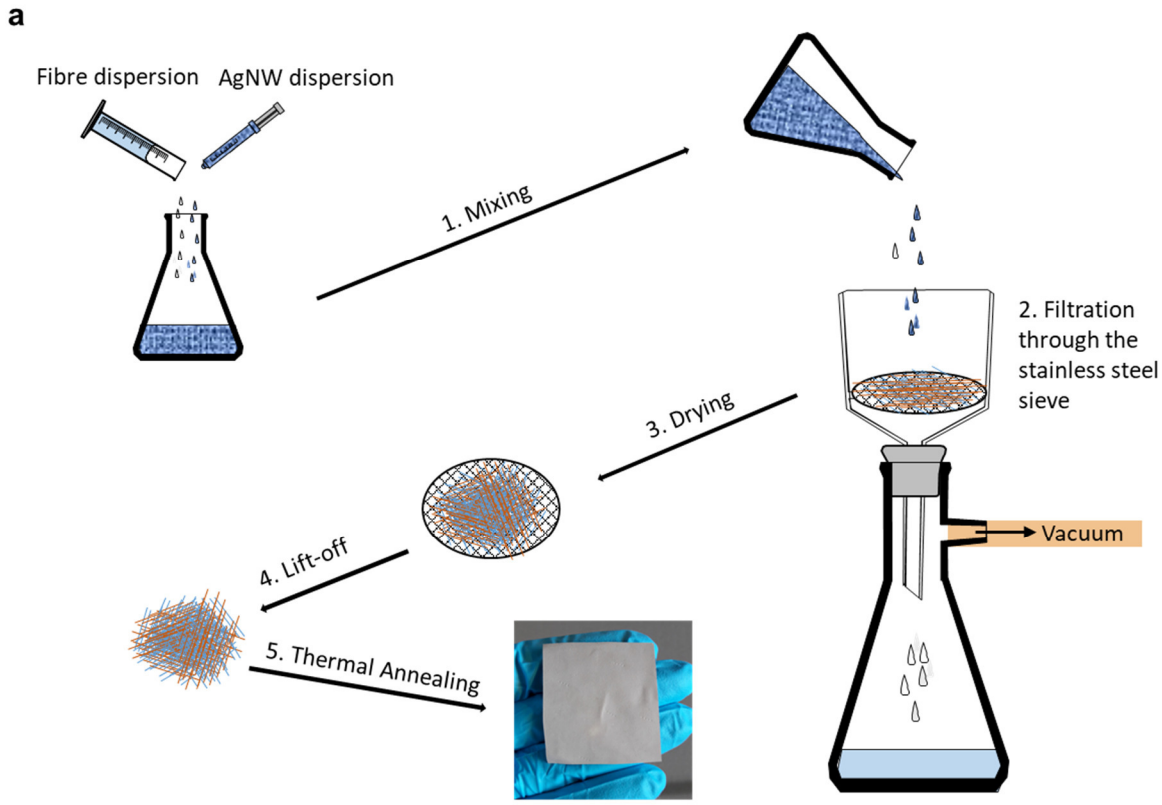

Abbildung 2.9 Schematische Darstellung der Herstellung leitfähiger Polymerfaservliesen durch das Wet-laid Verfahren.Verwendet aus Referenz[110], open access Journal, keine Genehmigung erforderlich.

Dieses Verfahren eignet sich optimal für die Herstellung von Kompositen, aufgrund der einfacheren Zugabe der Additive, wie Partikel und Fasern, welche der Faserdispersion zugemischt werden können. Hierbei is die Zumischung von leitfähigen Additiven, wie Silbernanodrähte mit einem Aspektverhältnis größer 100 möglich. Die Herstellung von leitfähigen Polymerfasern mittels klassischer Methoden, wie dem Elektrospinnen ist nicht nur durch die Dispergierbarkeit der leitfähigen Additive in der Polymerlösung beschränkt, sondern auch in der Leitfähigkeit der Polymerlösung, da eine höhere Leitfähigkeit einen negativen Einfluss auf die Faserherstellung besitzen kann.

Es wurde in der vorliegenden Veröffentlichung der Einfluss der Silbernanodrahtmenge (AgNW) auf die elektrische Leitfähigkeit des Polymerfaservlieses untersucht. Dabei wurde festgestellt, dass durch einen geringen Anteil von 0,36 vol% AgNW mit einer Länge von ~14 µm eine eindeutige Steigerung der elektrischen Leitfähigkeit erreicht wird. Hier steigt die Leitfähigkeit um sieben Zehnerpotenzen an und erreicht einen Wert von ~3000 S/m. Durch die weitere Zugabe von AgNW (~14 µm) konnte eine erneute Steigerung der elektrischen Leitfähigkeit erreicht werden. Bei einem Anteil von 1,07 vol% wurde eine elektrische Leitfähigkeit von ~ 95000 S/m erhalten (Abbildung 2.10b).

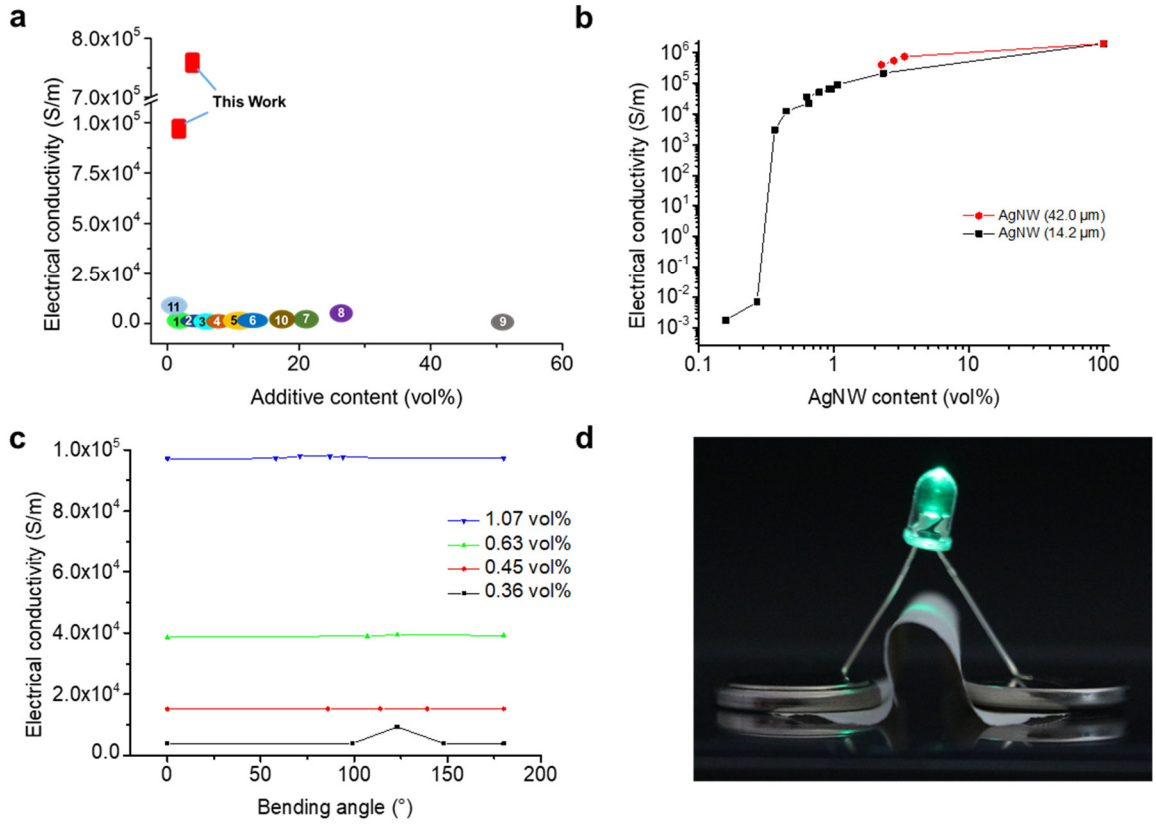

Abbildung 2.10 Vergleich der elektrischen Leitfähigkeiten unterschiedlicher Polymerfaser-Kompositen (a) 1. CNT / Polylaktat (PLA)- Fasern, 2. Ruß / PLA-Fasern, 3. Polyanilin (PANI)/ Naturkautschuk-Fasern, 4. PANI-Dodekylbenzolsulfonsäure/Co-Polyacrylnitril (PAN)-Fasern, 5. CNT/ Polyethylenterephthalat(PET)-Fasern, 6. PANI/ Bakterielle Cellulose-Fasern, 7. Poly(3,4-Ethylendioxythiophen):Polystyrolsulfonat (PEDOT:PSS/PNN)-Fasern, 8. PEDOT:PSS/ hohle Carbon-Fasern, 9. PANI/Polystyrol(PS)-Fasern, 10. MWNT/Cellulose-Fasern, 11. AgNW/Cellulose-Fasern; Elektrische Leitfähigkeiten in Abhängigkeit der AgNW-Menge (b); Elektrische Leitfähigkeit in Abhängigkeit des Beugungwinkels (c); Photoaufnahme einer LED betrieben durch 2 Batteriezellen, die durch das leitfähige Polymerfaservlies in gebogenem Zustand miteinander verbunden sind (d).Verwendet aus Referenz[110], open access Journal, keine Genehmigung erforderlich.

Die Verwendung längerer AgNW (~42 µm) ergibt eine Verdoppelung der elektrischen Leitfähigkeit im Gegensatz zu den AgNW mit einer Länge von ~14 µm bei gleichbleibenden

Anteil in dem Polymerfaservlies. Aufgrund der erhöhten Länge der AgNW werden weniger Verbindungspunkte der einzelnen Fasern benötigt, um einen effektiveren Ladungstransport im gesamten Polymervlies zu erhalten. Weiter wurde der Einfluss der Flexibilität auf die elektrische Leitfähigkeit untersucht. Es wurde keine eindeutige Beeinträchtigung der elektrischen Leitfähigkeit bei einem Beugungswinkel von 180° nachgewiesen (Abbildung 2.10c). Das Polymerfaservlies zeigt keine signifikante Verschlechterung der elektrischen Leitfähigkeit nach 10000 maliger Beugung zu einem Winkel von 180°.
Dieses Faservlies zeigt die Fähigkeit durch eine angelegte Spannung als Joule heater zu fungieren und erreicht bei einer angelegten Spannung von 1,1 Volt eine Temperatur von ~80 °C bei einem AgNW Anteil von 1,07 vol%. Dieses leitfähige Polymerfaservlies wird innerhalb von 20 Sekunden auf die jeweilige Temperatur erwärmt. Eine homogene Temperaturverteilung wird durch die homogene AgNW-Verteilung gewährleistet. Durch Ausschalten der angelegten Spannung kühlt sich das Polymerfaservlies sofort auf die Umgebungstemperatur ab.

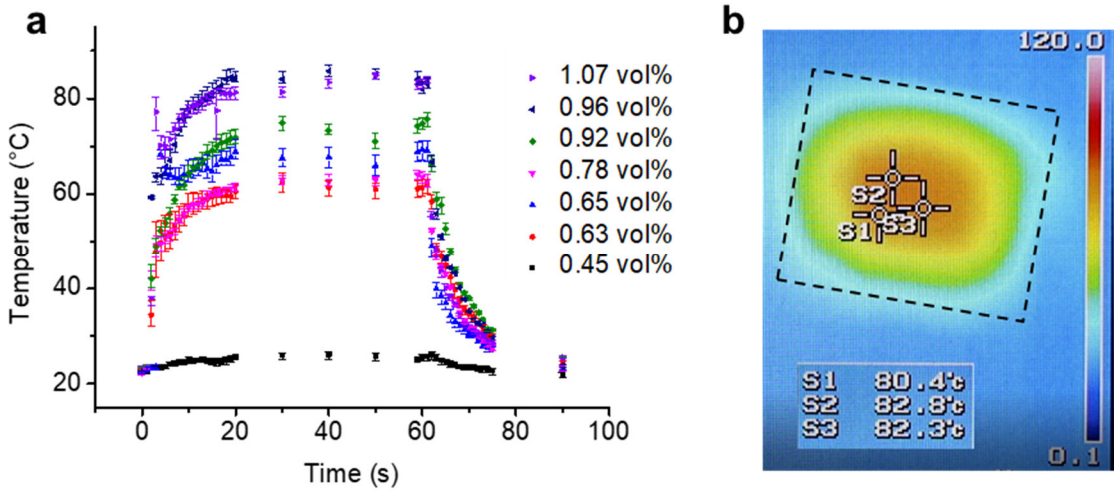

Abbildung 2.11 Joule Heizer in Abhängigkeit des AgNW-Anteils in dem Polymerfaservlies durch die angelegte Spannung von 1,1 Volt (a). IR Kameraaufnahme eines Polymerfaservlieses mit einer angelegten Spannung von 1,1 Volt (b).Verwendet aus Referenz[110], open access Journal, keine Genehmigung erforderlich.

Mögliche weitere Anwendungsgebiete können Elektrodenmaterialien für Superkondensatoren, Anodenmaterialien für mikrobielle Brennstoffzellen oder antistatische Filtermaterialien sein.

2.5 Exploration of the electrical conductivity of double-network silver nanowires/polyimide porous low-density compressible sponges

Die vorliegende Veröffentlichung beschreibt die Herstellung eines leitfähigen Kompositschwammes, bestehend aus Polyimidfasern und Silbernanodrähten, der als Joule heater in komprimierten Zustand seine Anwendung findet (Abbildung 2.12).

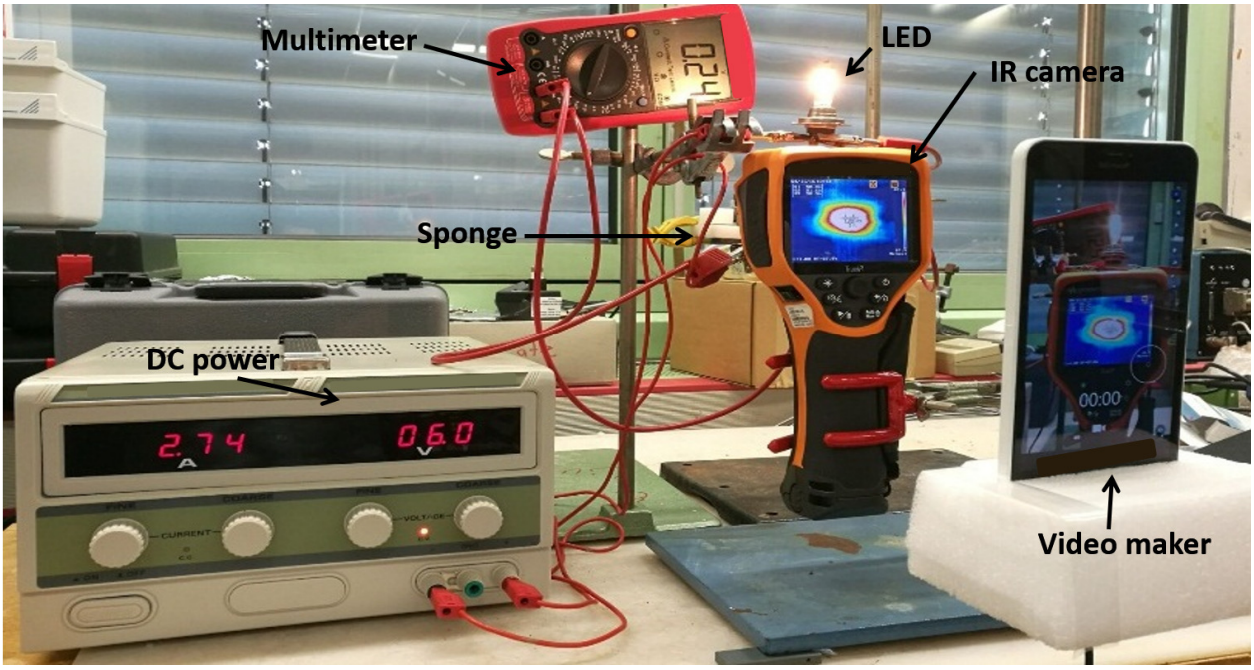

Abbildung 2.12 Setup zur Darstellung der Anwendung als Joule heater.Verwendet aus Referenz[196], mit Genehmigung. Copyright (2018) American Chemical Society.

Der Kompositschwamm wird durch Gefriertrocknen einer Dispersion aus kurzgeschnittenen Polyimidfasern und Polyamidocarbonsäurefasern, die als Binder eingesetzt werden, hergestellt. Hierbei wird die hergestellte Dispersion zuvor eingefroren und anschließend das Lösungsmittel mit Hilfe der Gefriertrocknung langsam und schonend abgeführt, so dass die strukturelle Stabilität erhalten bleibt. Anschließend wird die Polyamidocarbonsäure thermisch behandelt, wodurch diese in dem 3D-Netzwerk schmilzt und so die Polyimidfasern miteinander verklebt. Dieser kompressionsstabile Schwamm wird mit Polyethylenimin benetzt und in eine Silbernanodraht-Dispersion getaucht. Polyethylenimin, das an der Oberfläche der Polyimidfasern anhaftet, dient als Stabilisator der Silbernanodrähte, die nun ein Perkolationsnetzwerk ausbilden können. Im Ausgangszustand wird keine Leitfähigkeit

erhalten, während durch die Kompression eine eindeutige Leitfähigkeitssteigerung erhalten wird (Abbildung 2.13).

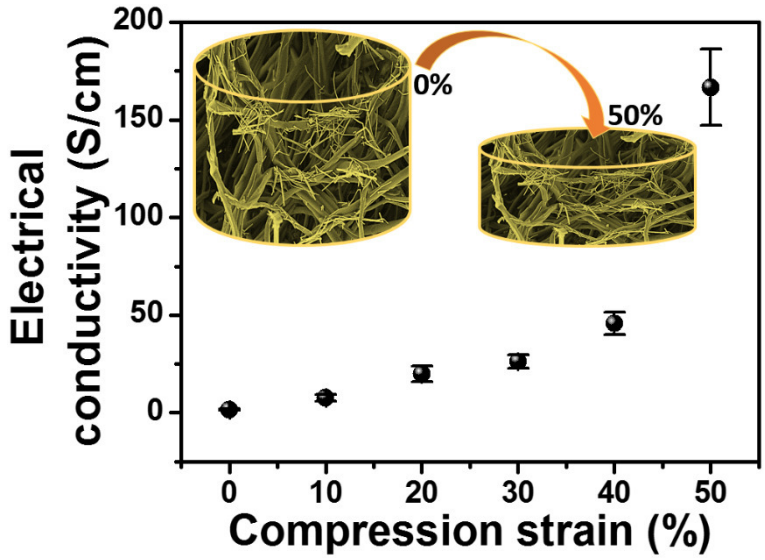

Abbildung 2.13 Elektrische Leitfähigkeit des PI/AgNW Schwammes in Abhängigkeit der Kompression.Verwendet aus Referenz[196], mit Genehmigung. Copyright (2018) American Chemical Society.

Dieser Schwamm fungiert als Elektrodenmaterial in einem Joule heater. Dabei wird eine elektrische Spannung an das Material angelegt und die Temperaturerhöhung mit Hilfe einer IR-Kamera bestimmt. Hier zeigt sich eine homogene Temperaturverteilung in dem PI/AgNW Schwamm, beim Anlegen eines elektrischen Stromes von 3,05 A (Abbildung 2.14).

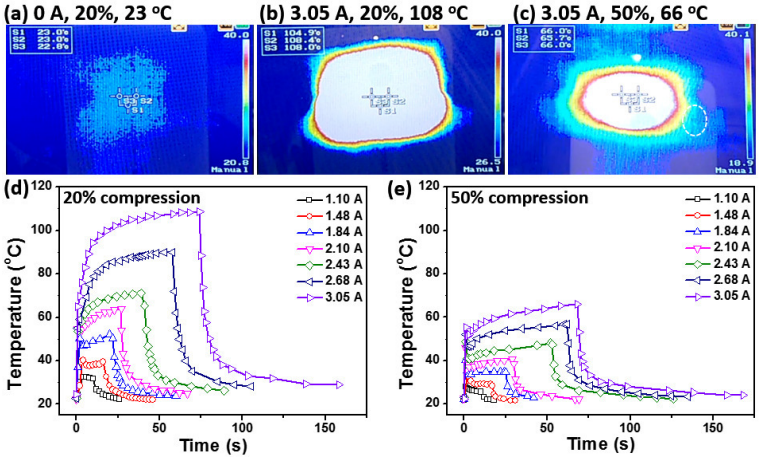

Abbildung 2.14 IR-Kamera Aufnahmen des PI/AgNW Schwammes in Abhängigkeit der Kompression und der angelegten Spannung. (a-c). Joule heating des PI/AgNW Schwammes bei unterschiedlicher Kompression d) 20% und e) 50%.Verwendet aus Referenz[196], mit Genehmigung. Copyright (2018) American Chemical Society.

2.6 Individuelle Beiträge zu den Publikationen

Nachfolgend werden die individuellen Beiträge der Autoren und Co-Autoren für die einzelnen Veröffentlichungen detailliert beschrieben.

The preparation of bacteria based golden polymer fleece and its catalytical application

Zur Einreichung
Von Steffen Reich, Andreas Greiner.

Das Konzept der vorliegenden Veröffentlichung wurde von Herrn Prof. Andreas Greiner und mir erarbeitet. Die Herstellung der Biokompositvliese, die Bioremediation von Gold und die anschließende Katalyse wurden von mir durchgeführt. Unter anderem werden dafür Mikroorganismen verwendet, die von mir kultiviert und nach der Verarbeitung auf ihre Überlebensfähigkeit getestet wurden. SEM-Messungen der Biokompositvliese wurden von mir durchgeführt. Weiter wurde die Katalyse mittels GC-MS von mir verfolgt. ICP-OES wurden durch Dr. Gunter Ilgen durchgeführt. SEM/BSE-Messungen wurden von Matthias Burgard und SEM/EDX-Messungen von Martina Heider bereitgestellt. Das Manuskript wurde von mir und unterstützt durch Prof. Andreas Greiner angefertigt.

Electrogenic single-species biocomposites as anodes for microbial fuel cells

Publiziert in *Macromolecular Bioscience* **2017**, 17, 1600442
Von Patrick Kaiser, Steffen Reich, Daniel Leykam, Monika Willert-Porada, Andreas Greiner, Ruth Freitag

Das Konzept dieser Veröffentlichung wurde von Herrn Prof. Andreas Greiner zusammen mit Frau Prof. Ruth Freitag erarbeitet und mit mir und Patrick Kaiser vervollständigt. Die Bereitstellung der Biokompositvliese erfolgte von mir. Die SEM-Messungen wurden von mir durchgeführt. Der entsprechende Abschnitt der Veröffentlichung wurde von mir verfasst. Die Kultivierung der Mikroorganismen erfolgte durch Patrick Kaiser. Patrick Kaiser führte die weiteren Charakterisierungen in Bezug auf Überlebensfähigkeit der Biokomposite und den Einsatz in der mikrobiellen Brennstoffzelle durch. Die Veröffentlichung wurde von Patrick

Kaiser und Prof. Ruth Freitag verfasst und durch Daniel Leykam, Monika Willert-Porada, Prof. Andreas Greiner und mir korrigiert.

Polymer/ Living Bacteria Capsules Spray Dried at High Temperatures

Zur Einreichung
Von Steffen Reich, Patrick Kaiser, Holger Schmalz, Daniel Rhinow, Ruth Freitag, Andreas Greiner.

Das Konzept dieser Veröffentlichung wurde von Prof. Andreas Greiner zusammen mit Prof. Ruth Freitag erarbeitet und von Patrick Kaiser und mir vervollständigt. Die Herstellung der Biokompositkapseln und die Weiterverarbeitung zu Biokompositfaservliesen wurden von mir durchgeführt. Die Charakterisierung in Bezug auf SEM, TGA, Kultivierung und Überlebensfähigkeit der *M.luteus* wurde von mir bereitgestellt. Die Kultivierung und Überlebensfähigkeit der *E.coli* erfolgte durch Patrick Kaiser. Raman-AFM-Messungen der Polymerkapseln erfolgten durch Holger Schmalz. TEM-Messungen wurden von Daniel Rhinow durchgeführt. Die vorliegende Veröffentlichung wurde von mir und unterstützt durch Prof. Andreas Greiner verfasst und von Patrick Kaiser, Holger Schmalz, Daniel Rhinow und Prof. Ruth Freitag korrigiert.

Polymer nanofibre composite nonwovens with metal-like electrical conductivity

Publiziert in *npj Flexible Electronics*, **2018**, 2, 1417
Von Steffen Reich, Matthias Burgard, Markus Langner, Shaohua Jiang, Xueqin Wang, Seema Agarwal, Bin Ding, Jianyong Yu, Andreas Greiner.

Das Konzept dieser Arbeit wurde von Prof. Andreas Greiner zusammen mit mir und Markus Langner erarbeitet. Die Herstellung und Charakterisierung der Silberdrähte, die Herstellung und Charakterisierung der Polymerfasern durch Elektrospinnen, sowie die Herstellung und Charakterisierung der Kurzschnittfaserdispersion erfolgte durch mich. Weiter wurde die Herstellung der Kompositvliese und Charakterisierungen von mir durchgeführt. Markus Langner war an der Herstellung der Fasern und Faserdispersionen maßgeblich beteiligt. Matthias Burgard führte SEM/BSE-Messungen und Zug-Dehnungs-Messungen durch. Shaohua Jiang synthetisierte einen zweiten Batch an Silbernanodrähten. Xueqin Wang führte die Messung der Biegesteifigkeit durch. Diese Veröffentlichung wurde von mir und unterstützt

durch Prof. Andreas Greiner verfasst und von Matthias Burgard, Markus Langner, Shaohua Jiang, Xueqin Wang, Seema Agarwal, Bin Ding und Jianyong Yu korrigiert.

Exploration of the electrical conductivity of double network silver nanowires - polyimide porous low density compressible sponges

Publiziert in *ACS Applied Materials & Interfaces*, **2017**, 9(39), 34286-34293.
Shaohua Jiang, Steffen Reich, Bianca Uch, Pin Hu, Seema Agarwal, Andreas Greiner

Das Konzept dieser Veröffentlichung wurde von Herrn Prof. Greiner zusammen mit mir erarbeitet und von Shaohua Jiang, Bianca Uch und Pin Hu vervollständigt. Shaohua Jiang finalisierte das Projekt, führte Charakterisierungen, wie SEM/EDX, Kompressionstests, Wärmeleitfähigkeit und Joule heating Experimente durch. Die Silbernanodrähte wurden von mir synthetisiert und in das Projekt eingeführt. Unter meiner Leitung stellte Bianca Uch die Silbernanodrähte, die Kompositschwämme her und charakterisierte diese durch TEM, SEM und elektrischer Leitfähigkeit. Pin Hu reproduzierte die Kompositschwämme. Die vorliegende Veröffentlichung wurde von Shaohua Jiang unterstützt durch Prof. Andreas Greiner verfasst und von Prof. Seema Agarwal und mir korrigiert.

3 Literatur

1. Balzer, M., Witt, N., Flemming, H.-C. & Wingender, J. Faecal indicator bacteria in river biofilms. *Water science and technology : a journal of the International Association on Water Pollution Research* **61,** 1105–1111 (2010).
2. Morgan-Sagastume, F., Larsen, P., Nielsen, J. L. & Nielsen, P. H. Characterization of the loosely attached fraction of activated sludge bacteria. *Water research* **42,** 843–854 (2008).
3. Vert, M. *et al.* Terminology for biorelated polymers and applications (IUPAC Recommendations 2012). *Pure and Applied Chemistry* **84,** 1410 (2012).
4. Flemming, H.-C. & Wingender, J. The biofilm matrix. *Nature reviews. Microbiology* **8,** 623–633 (2010).
5. O'Toole, G., Kaplan, H. B. & Kolter, R. Biofilm formation as microbial development. *Annual review of microbiology* **54,** 49–79 (2000).
6. Satpathy, S., Sen, S. K., Pattanaik, S. & Raut, S. Review on bacterial biofilm. An universal cause of contamination. *Biocatalysis and Agricultural Biotechnology* **7,** 56–66 (2016).
7. Gross, R., Lang, K., Bühler, K. & Schmid, A. Characterization of a biofilm membrane reactor and its prospects for fine chemical synthesis. *Biotechnology and bioengineering* **105,** 705–717 (2010).
8. Zheng, C., Qu, B., Wang, J., Zhou, J. & Lu, H. Isolation and characterization of a novel nitrobenzene-degrading bacterium with high salinity tolerance: Micrococcus luteus. *Journal of Hazardous Materials* **165,** 1152–1158 (2009).
9. Arunkumar, P., Thanalakshmi, M., Kumar, P. & Premkumar, K. Micrococcus luteus mediated dual mode synthesis of gold nanoparticles: involvement of extracellular α-amylase and cell wall teichuronic acid. *Colloids and surfaces. B, Biointerfaces* **103,** 517–522 (2013).
10. Puyen, Z. M. *et al.* Biosorption of lead and copper by heavy-metal tolerant Micrococcus luteus DE2008. *Bioresource technology* **126,** 233–237 (2012).
11. Deplanche, K. *et al.* Catalytic activity of biomass-supported Pd nanoparticles. Influence of the biological component in catalytic efficacy and potential application in 'green' synthesis of fine chemicals and pharmaceuticals. *Applied Catalysis B: Environmental* **147,** 651–665 (2014).
12. Faison, B. D., Cancel, C. A., Lewis, S. N. & Adler, H. I. Binding of Dissolved Strontium by Micrococcus luteus. *Applied and environmental microbiology* **56,** 3649–3656 (1990).

13. Zhuang, W.-Q., Tay, J.-H., Maszenan, A. M., Krumholz, L. R. & Tay, S.-L. Importance of Gram-positive naphthalene-degrading bacteria in oil-contaminated tropical marine sediments. *Letters in Applied Microbiology* **36,** 251–257 (2003).

14. Yamazaki, Y., Maruyama, A., Hosono, K., Higashihara, T. & Kobayashi, H. Asymmetric Reduction of Synthetic Ketones by Marine Microorganisms. *Zeitschrift für Naturforschung,* 451–456 (1993).

15. Rangnekar, A. *et al.* Retention of enzymatic activity of alpha-amylase in the reductive synthesis of gold nanoparticles. *Langmuir : the ACS journal of surfaces and colloids* **23,** 5700–5706 (2007).

16. Fredrickson, J. K. *et al.* Towards environmental systems biology of Shewanella. *Nature reviews. Microbiology* **6,** 592–603 (2008).

17. Lies, D. P. *et al.* Shewanella oneidensis MR-1 uses overlapping pathways for iron reduction at a distance and by direct contact under conditions relevant for Biofilms. *Applied and environmental microbiology* **71,** 4414–4426 (2005).

18. Marsili, E. *et al.* Shewanella secretes flavins that mediate extracellular electron transfer. *Proceedings of the National Academy of Sciences of the United States of America* **105,** 3968–3973 (2008).

19. Gorby, Y. A. *et al.* Electrically conductive bacterial nanowires produced by Shewanella oneidensis strain MR-1 and other microorganisms. *Proceedings of the National Academy of Sciences of the United States of America* **103,** 11358–11363 (2006).

20. Greiner, A. & Wendorff, J. H. Electrospinning: a fascinating method for the preparation of ultrathin fibers. *Angewandte Chemie (International ed. in English)* **46,** 5670–5703 (2007).

21. Peng, M. *et al.* Nanoporous structured submicrometer carbon fibers prepared via solution electrospinning of polymer blends. *Langmuir : the ACS journal of surfaces and colloids* **22,** 9368–9374 (2006).

22. Lyons, J., Li, C. & Ko, F. Melt-electrospinning part I. Processing parameters and geometric properties. *Polymer* **45,** 7597–7603 (2004).

23. Zhou, H., Green, T. B. & Joo, Y. L. The thermal effects on electrospinning of polylactic acid melts. *Polymer* **47,** 7497–7505 (2006).

24. Brown, T. D., Dalton, P. D. & Hutmacher, D. W. Melt electrospinning today. An opportune time for an emerging polymer process. *Progress in Polymer Science* **56,** 116–166 (2016).

25. Reneker, D. H. & Yarin, A. L. Electrospinning jets and polymer nanofibers. *Polymer* **49,** 2387–2425 (2008).

26. Reneker, D. H., Yarin, A. L., Fong, H. & Koombhongse, S. Bending instability of electrically charged liquid jets of polymer solutions in electrospinning. *Journal of Applied Physics* **87,** 4531–4547 (2000).

27. Huang, Z.-M., Zhang, Y.-Z., Kotaki, M. & Ramakrishna, S. A review on polymer nanofibers by electrospinning and their applications in nanocomposites. *Composites Science and Technology* **63,** 2223–2253 (2003).

28. Chen, G. *et al.* Structure-tunable Janus fibers fabricated using spinnerets with varying port angles. *Chemical communications (Cambridge, England)* **51,** 4623–4626 (2015).

29. Srivastava, Y., Marquez, M. & Thorsen, T. Microfluidic electrospinning of biphasic nanofibers with Janus morphology. *Biomicrofluidics* **3,** 12801 (2009).

30. Lim, J.-M., Moon, J. H., Yi, G.-R., Heo, C.-J. & Yang, S.-M. Fabrication of one-dimensional colloidal assemblies from electrospun nanofibers. *Langmuir : the ACS journal of surfaces and colloids* **22,** 3445–3449 (2006).

31. Bazilevsky, A. V., Yarin, A. L. & Megaridis, C. M. Co-electrospinning of core-shell fibers using a single-nozzle technique. *Langmuir : the ACS journal of surfaces and colloids* **23,** 2311–2314 (2007).

32. Li, D. & Xia, Y. Direct Fabrication of Composite and Ceramic Hollow Nanofibers by Electrospinning. *Nano Lett.* **4,** 933–938 (2004).

33. Koombhongse, S., Liu, W. & Reneker, D. H. Flat polymer ribbons and other shapes by electrospinning. *J. Polym. Sci. B Polym. Phys.* **39,** 2598–2606 (2001).

34. Koski, A., Yim, K. & Shivkumar, S. Effect of molecular weight on fibrous PVA produced by electrospinning. *Materials Letters* **58,** 493–497 (2004).

35. Casper, C. L., Stephens, J. S., Tassi, N. G., Chase, D. B. & Rabolt, J. F. Controlling Surface Morphology of Electrospun Polystyrene Fibers. Effect of Humidity and Molecular Weight in the Electrospinning Process. *Macromolecules* **37,** 573–578 (2004).

36. Deitzel, J., Kleinmeyer, J., Harris, D. & Beck Tan, N. The effect of processing variables on the morphology of electrospun nanofibers and textiles. *Polymer* **42,** 261–272 (2001).

37. Kirecci, A., Özkoç, Ü. & İçoğlu, H. İ. Determination of optimal production parameters for polyacrylonitrile nanofibers. *J. Appl. Polym. Sci.* **53,** n/a-n/a (2011).

38. Niu, H., Lin, T. & Wang, X. Needleless electrospinning. I. A comparison of cylinder and disk nozzles. *J. Appl. Polym. Sci.* **114,** 3524–3530 (2009).

39. Yarin, A. L. & Zussman, E. Upward needleless electrospinning of multiple nanofibers. *Polymer* **45,** 2977–2980 (2004).

40. Nazir, A. *et al.* Using the Taguchi method to investigate the effect of different parameters on mean diameter and variation in PA-6 nanofibres produced by needleless electrospinning. *RSC Adv.* **5,** 76892–76897 (2015).

41. Park, H.-S. & Park, Y. O. Filtration properties of electrospun ultrafine fiber webs. *Korean J. Chem. Eng.* **22,** 165–172 (2005).

42. Fang, X. *et al.* Facile immobilization of gold nanoparticles into electrospun polyethyleneimine/polyvinyl alcohol nanofibers for catalytic applications. *J. Mater. Chem.* **21,** 4493 (2011).

43. Lu, Y. *et al.* Coaxial electrospun fibers: applications in drug delivery and tissue engineering. *Wiley interdisciplinary reviews. Nanomedicine and nanobiotechnology* **8,** 654–677 (2016).

44. Zahedi, P., Rezaeian, I., Ranaei-Siadat, S.-O., Jafari, S.-H. & Supaphol, P. A review on wound dressings with an emphasis on electrospun nanofibrous polymeric bandages. *Polym. Adv. Technol.* **35,** n/a-n/a (2009).

45. Buchholz, V. *et al.* Protection of Vine Plants against Esca Disease by Breathable Electrospun Antifungal Nonwovens. *Macromolecular bioscience* **16,** 1391–1397 (2016).

46. Sill, T. J. & Recum, H. A. von. Electrospinning: applications in drug delivery and tissue engineering. *Biomaterials* **29,** 1989–2006 (2008).

47. Gensheimer, M. *et al.* Novel Biohybrid Materials by Electrospinning. Nanofibers of Poly(ethylene oxide) and Living Bacteria. *Adv. Mater.* **19,** 2480–2482 (2007).

48. López-Rubio, A., Sanchez, E., Sanz, Y. & Lagaron, J. M. Encapsulation of living bifidobacteria in ultrathin PVOH electrospun fibers. *Biomacromolecules* **10,** 2823–2829 (2009).

49. Salalha, W., Kuhn, J., Dror, Y. & Zussman, E. Encapsulation of bacteria and viruses in electrospun nanofibres. *Nanotechnology* **17,** 4675–4681 (2006).

50. Klein, S. *et al.* Encapsulation of bacterial cells in electrospun microtubes. *Biomacromolecules* **10,** 1751–1756 (2009).

51. Nardi, A., Avrahami, R., Zussman, E., Rokem, J. S. & Greenblatt, C. L. Phenol Biodegradation by *Corynebacterium glutamicum*; Encapsulated in Electrospun Fibers. *JEP* **03,** 164–168 (2012).

52. Zeng, J. *et al.* Poly(vinyl alcohol) nanofibers by electrospinning as a protein delivery system and the retardation of enzyme release by additional polymer coatings. *Biomacromolecules* **6,** 1484–1488 (2005).

53. Greiner, A., Mang, S., Schäfer, O. & Simon, P. Poly(p-xylylene)s: Synthesis, polymer analogous reactions, and perspectives on structure-property relationships. *Acta Polym.* **48,** 1–15 (1997).

54. Simon, P., Mang, S., Hasenhindl, A., Gronski, W. & Greiner, A. Poly(p -xylylene) and Its Derivatives by Chemical Vapor Deposition. Synthesis, Mechanism, and Structure. *Macromolecules* **31,** 8775–8780 (1998).

55. Gilch, H. G. & Wheelwright, W. L. Polymerization of α-halogenated p-xylenes with base. *J. Polym. Sci. A-1 Polym. Chem.* **4,** 1337–1349 (1966).

56. Gorham, W. F. A New, General Synthetic Method for the Preparation of Linear Poly-p-xylylenes. *J. Polym. Sci. A-1 Polym. Chem.* **4,** 3027–3039 (1966).

57. Roth, W. R. *et al.* Zur Rekombinationsenthalpie von Radikalen — Thermochemie der Ringöffnung von Cyclophanen. *Liebigs Ann.* **1996,** 2141–2154 (1996).

58. Smalara, K., Giełdoń, A., Bobrowski, M., Rybicki, J. & Czaplewski, C. Theoretical study of polymerization mechanism of p-xylylene based polymers. *The journal of physical chemistry. A* **114,** 4296–4303 (2010).

59. Hanefeld, P., Sittner, F., Ensinger, W. & Greiner, A. Investigation of the ion permeability of poly(p-xylylene) films. *e-Polymers* **6** (2006).

60. Tung, N. T., Yu, Y. J., Kim, K., Joo, S.-H. & Jin, J.-I. Synthesis of Poly(p-xylylene) from α,α'-Bis(alkoxy or aryloxy)-p-xylenes by Chemical Vapor Deposition Polymerization. *Bulletin of the Korean Chemical Society* **25,** 31–32 (2004).

61. Fuchs, M. *et al.* Encapsulation of oil in powder using spray drying and fluidised bed agglomeration. *Journal of Food Engineering* **75,** 27–35 (2006).

62. Ahn, J.-H. *et al.* Optimization of microencapsulation of seed oil by response surface methodology. *Food Chemistry* **107,** 98–105 (2008).

63. Bae, E. K. & Lee, S. J. Microencapsulation of avocado oil by spray drying using whey protein and maltodextrin. *Journal of microencapsulation* **25,** 549–560 (2008).

64. Partanen, R. *et al.* Effect of relative humidity on oxidation of flaxseed oil in spray dried whey protein emulsions. *Journal of agricultural and food chemistry* **56,** 5717–5722 (2008).

65. Quinlan, E. *et al.* Controlled release of vascular endothelial growth factor from spray-dried alginate microparticles in collagen-hydroxyapatite scaffolds for promoting vascularization and bone repair. *Journal of tissue engineering and regenerative medicine* **11,** 1097–1109 (2017).

66. Gholampour, N. *et al.* Simultaneous creation of metal nanoparticles in metal organic frameworks via spray drying technique. *Chemical Engineering Journal* **322,** 702–709 (2017).

67. Gómez-Gaete, C., Fattal, E., Silva, L., Besnard, M. & Tsapis, N. Dexamethasone acetate encapsulation into Trojan particles. *Journal of controlled release : official journal of the Controlled Release Society* **128,** 41–49 (2008).

68. Grenha, A., Seijo, B. & Remuñán-López, C. Microencapsulated chitosan nanoparticles for lung protein delivery. *European journal of pharmaceutical sciences : official journal of the European Federation for Pharmaceutical Sciences* **25,** 427–437 (2005).

69. Jafari, S. M., Assadpoor, E., Bhandari, B. & He, Y. Nano-particle encapsulation of fish oil by spray drying. *Food Research International* **41,** 172–183 (2008).

70. Huang, S. *et al.* Spray drying of probiotics and other food-grade bacteria. A review. *Trends in Food Science & Technology* **63,** 1–17 (2017).

71. Iskandar, F. *et al.* Enhanced Photocatalytic Performance of Brookite TiO2 Macroporous Particles Prepared by Spray Drying with Colloidal Templating. *Adv. Mater.* **19,** 1408–1412 (2007).

72. Li, X., Anton, N., Arpagaus, C., Belleteix, F. & Vandamme, T. F. Nanoparticles by spray drying using innovative new technology: the Büchi nano spray dryer B-90. *Journal of controlled release : official journal of the Controlled Release Society* **147,** 304–310 (2010).

73. Motskin, M. *et al.* Hydroxyapatite nano and microparticles: correlation of particle properties with cytotoxicity and biostability. *Biomaterials* **30,** 3307–3317 (2009).

74. Silva, N. K. *et al.* Influence of shell material on vitamin C content, total phenolic compounds, sorption isotherms and particle size of spray-dried camu-camu juice. *Fruits* **68,** 175–183 (2013).

75. Silva, J., Carvalho, A. S., Teixeira, P. & Gibbs, P. A. Bacteriocin production by spray-dried lactic acid bacteria. *Lett Appl Microbiol* **34,** 77–81 (2002).

76. Paudel, A., Worku, Z. A., Meeus, J., Guns, S. & van den Mooter, G. Manufacturing of solid dispersions of poorly water soluble drugs by spray drying: formulation and process considerations. *International journal of pharmaceutics* **453,** 253–284 (2013).

77. Maa, Y., Nguyen, P., Sweeney, T., Shire, S. J. & Hsu, C. C. Protein Inhalation Powders: Spray Drying vs Spray Freeze Drying. *Pharmaceutical Research* **16,** 249–254 (1999).

78. Teixeira, P., Castro, H. & Kirby, R. Spray drying as a method for preparing concentrated cultures of Lactobacillus bulgaricus. *Journal of Applied Bacteriology* **78,** 456–462 (1995).

79. Gardiner, G. E. *et al.* Comparative Survival Rates of Human-Derived Probiotic Lactobacillus paracasei and L. salivarius Strains during Heat Treatment and Spray Drying. *Applied and environmental microbiology* **66,** 2605–2612 (2000).

80. Costantino, H. R. *et al.* Effect of mannitol crystallization on the stability and aerosol performance of a spray-dried pharmaceutical protein, recombinant humanized anti-IgE monoclonal antibody. *Journal of pharmaceutical sciences* **87,** 1406–1411 (1998).

81. Yu, L. & Ng, K. Glycine crystallization during spray drying: the pH effect on salt and polymorphic forms. *Journal of pharmaceutical sciences* **91,** 2367–2375 (2002).

82. Roos, Y. & Karel, M. Phase transitions of mixtures of amorphous polysaccharides and sugars. *Biotechnol. Prog.* **7,** 49–53 (1991).

83. Francia, V., Martín, L., Bayly, A. E. & Simmons, M. J. Agglomeration during spray drying: Airborne clusters or breakage at the walls? *Chemical Engineering Science* **162,** 284–299 (2017).

84. Chever, S. *et al.* Agglomeration during spray drying. Physical and rehydration properties of whole milk/sugar mixture powders. *LWT - Food Science and Technology* **83,** 33–41 (2017).

85. BROADHEAD, J., ROUAN, S. K. E., HAU, I. & RHODES, C. T. The Effect of Process and Formulation Variables on the Properties of Spray-dried β-Galactosidase. *Journal of Pharmacy and Pharmacology* **46,** 458–467 (1994).

86. Ståhl, K., Claesson, M., Lilliehorn, P., Lindén, H. & Bäckström, K. The effect of process variables on the degradation and physical properties of spray dried insulin intended for inhalation. *International journal of pharmaceutics* **233,** 227–237 (2002).

87. Corrigan, D. O., Corrigan, O. I. & Healy, A. M. Predicting the physical state of spray dried composites: salbutamol sulphate/lactose and salbutamol sulphate/polyethylene glycol co-spray dried systems. *International journal of pharmaceutics* **273,** 171–182 (2004).

88. Corrigan, D. O., Corrigan, O. I. & Healy, A. M. Physicochemical and in vitro deposition properties of salbutamol sulphate/ipratropium bromide and salbutamol sulphate/excipient spray dried mixtures for use in dry powder inhalers. *International journal of pharmaceutics* **322,** 22–30 (2006).

89. Mosén, K. *et al.* Particle Formation and Capture During Spray Drying of Inhalable Particles. *Pharmaceutical Development and Technology* **9,** 409–417 (2004).

90. Lindeløv, J. S. & Wahlberg, M. Spray drying for processing of nanomaterials. *J. Phys.: Conf. Ser.* **170,** 12027 (2009).

91. Elversson, J. & Millqvist-Fureby, A. Particle size and density in spray drying-effects of carbohydrate properties. *Journal of pharmaceutical sciences* **94,** 2049–2060 (2005).

92. Elversson, J., Millqvist-Fureby, A., Alderborn, G. & Elofsson, U. Droplet and particle size relationship and shell thickness of inhalable lactose particles during spray drying. *Journal of pharmaceutical sciences* **92,** 900–910 (2003).

93. Green, K. D., Gill, I. S., Khan, J. A. & Vulfson, E. N. Microencapsulation of yeast cells and their use as a biocatalyst in organic solvents. *Biotechnol. Bioeng.* **49,** 535–543 (1996).

94. Graff, S., Hussain, S., Chaumeil, J.-C. & Charrueau, C. Increased intestinal delivery of viable Saccharomyces boulardii by encapsulation in microspheres. *Pharmaceutical Research* **25,** 1290–1296 (2008).

95. Sheu, T. Y., Marshall, R. T. & Heymann, H. Improving survival of culture bacteria in frozen desserts by microentrapment. *Journal of dairy science* **76,** 1902–1907 (1993).

96. Lee, K. Y. & Heo, T. R. Survival of Bifidobacterium longum immobilized in calcium alginate beads in simulated gastric juices and bile salt solution. *Applied and environmental microbiology* **66,** 869–873 (2000).

97. Hubbe, M. A. & Koukoulas, A. A. Wet-Laid Nonwovens Manufacture – Chemical Approaches Using Synthetic and Cellulosic Fibers. *BioResources* **11** (2016).

98. Safavi, A., Fathi, S., Babaei, M. R., Mansoori, Z. & Latifi, M. Experimental and numerical analysis of fiber characteristics effects on fiber dispersion for wet-laid nonwoven. *Fibers Polym* **10,** 231–236 (2009).

99. Rebouillat, S., Letellier, B. & Steffenino, B. Wettability of single fibres – beyond the contact angle approach. *International Journal of Adhesion and Adhesives* **19,** 303–314 (1999).

100. Sun, K. C. *et al.* Highly efficient and durable dye-sensitized solar cells based on a wet-laid PET membrane electrolyte. *J. Mater. Chem. A* **4,** 458–465 (2016).

101. Zhang, B. *et al.* Wet-Laid Formation and Strength Enhancement of Alkaline Battery Separators Using Polypropylene Fibers and Polyethylene/Polypropylene Bicomponent Fibers as Raw Materials. *Ind. Eng. Chem. Res.* **56,** 7739–7746 (2017).

102. Fages, E., Gironés, S., Sánchez-Nacher, L., García-Sanoguera, D. & Balart, R. Use of wet-laid techniques to form flax-polypropylene nonwovens as base substrates for eco-friendly composites by using hot-press molding. *Polym Compos* **33,** 253–261 (2012).

103. Martin, N., Davies, P. & Baley, C. Evaluation of the potential of three non-woven flax fiber reinforcements. Spunlaced, needlepunched and paper process mats. *Industrial Crops and Products* **83,** 194–205 (2016).

104. Li, C.-D., Chen, Z.-F. & Saeed, M.-U. Characterization of hybrid glass wool suspensions and optimization of microstructure and tensile strength of the associated wet-laid mats by various blendings and numbers of beating revolutions. *Mater Struct* **49,** 1861–1869 (2016).

105. Lee, J. *et al.* Ultrahigh electromagnetic interference shielding performance of lightweight, flexible, and highly conductive copper-clad carbon fiber nonwoven fabrics. *J. Mater. Chem. C* **5,** 7853–7861 (2017).

106. Cai, B., Zheng, Q.-K., Li, R.-X. & Wu, D.-C. Adsorption mechanism of surfactants on nonwoven fabrics. *J. Appl. Polym. Sci.* **89,** 3210–3215 (2003).

107. Prosser, A. J. & Franses, E. I. Adsorption and surface tension of ionic surfactants at the air–water interface. Review and evaluation of equilibrium models. *Colloids and Surfaces A: Physicochemical and Engineering Aspects* **178,** 1–40 (2001).

108. Karakashev, S. I. & Grozdanova, M. V. Foams and antifoams. *Advances in colloid and interface science* **176-177,** 1–17 (2012).

109. Fages, E. *et al.* The use of wet-laid techniques to obtain flax nonwovens with different thermoplastic binding fibers for technical insulation applications. *Textile Research Journal* **83,** 426–437 (2012).

110. Reich, S. *et al.* Polymer nanofibre composite nonwovens with metal-like electrical conductivity. *npj Flex Electron* **2,** 1417 (2018).

111. Cornwall, W. Sewage sludge could contain millions of dollars worth of gold. *Science* (2015).

112. Dobson, R. S. & Burgess, J. E. Biological treatment of precious metal refinery wastewater. A review. *Minerals Engineering* **20,** 519–532 (2007).

113. Umeda, H. *et al.* Recovery and Concentration of Precious Metals from Strong Acidic Wastewater. *Mater. Trans.* **52,** 1462–1470 (2011).

114. Carey, J. B. Inner Workings: Finding precious metals in unlikely places. *Proceedings of the National Academy of Sciences of the United States of America* **112,** 8803–8804 (2015).

115. Han, Y.-L. *et al.* Recovery of gold from industrial wastewater by extracellular proteins obtained from a thermophilic bacterium Tepidimonas fonticaldi AT-A2. *Bioresource technology* **239,** 160–170 (2017).

116. Kakoi, T., Horinouchi, N., Goto, M. & Nakashio, F. Recovery of Palladium from an Industrial Wastewater Using Liquid Surfactant Membranes. *Separation Science and Technology* **31,** 381–399 (1996).

117. Ju, X. *et al.* Effective and selective recovery of gold and palladium ions from metal wastewater using a sulfothermophilic red alga, Galdieria sulphuraria. *Bioresource technology* **211,** 759–764 (2016).

118. Won, S. W., Mao, J., Kwak, I.-S., Sathishkumar, M. & Yun, Y.-S. Platinum recovery from ICP wastewater by a combined method of biosorption and incineration. *Bioresource technology* **101,** 1135–1140 (2010).

119. Cui, J. & Forssberg, E. Mechanical recycling of waste electric and electronic equipment. A review. *Journal of Hazardous Materials* **99,** 243–263 (2003).

120. Wong, M. H. *et al.* Export of toxic chemicals - a review of the case of uncontrolled electronic-waste recycling. *Environmental pollution (Barking, Essex : 1987)* **149,** 131–140 (2007).

121. Ku, Y. & Jung, I. L. Photocatalytic reduction of Cr(VI) in aqueous solutions by UV irradiation with the presence of titanium dioxide. *Water research* **35,** 135–142 (2001).

122. Huisman, J. L., Schouten, G. & Schultz, C. Biologically produced sulphide for purification of process streams, effluent treatment and recovery of metals in the metal and mining industry. *Hydrometallurgy* **83,** 106–113 (2006).

123. Kang, K. C., Kim, S. S., Choi, J. W. & Kwon, S. H. Sorption of Cu2+ and Cd2+ onto acid- and base-pretreated granular activated carbon and activated carbon fiber samples. *Journal of Industrial and Engineering Chemistry* **14,** 131–135 (2008).

124. Iijima, S. Helical microtubules of graphitic carbon. *Nature* **354,** 56–58 (1991).

125. Landaburu-Aguirre, J., García, V., Pongrácz, E. & Keiski, R. L. The removal of zinc from synthetic wastewaters by micellar-enhanced ultrafiltration. Statistical design of experiments. *Desalination* **240,** 262–269 (2009).

126. Figoli, A. *et al.* Influence of operating parameters on the arsenic removal by nanofiltration. *Water research* **44,** 97–104 (2010).

127. Beveridge, T. J. & Murray, R. G. Sites of metal deposition in the cell wall of Bacillus subtilis. *Journal of bacteriology* **141,** 876–887 (1980).

128. Srivastava, S. K., Yamada, R., Ogino, C. & Kondo, A. Biogenic synthesis and characterization of gold nanoparticles by Escherichia coli K12 and its heterogeneous catalysis in degradation of 4-nitrophenol. *Nanoscale research letters* **8,** 70 (2013).

129. Sharma, N. *et al.* Exploitation of marine bacteria for production of gold nanoparticles. *Microbial cell factories* **11,** 86 (2012).

130. Correa-Llantén, D. N., Muñoz-Ibacache, S. A., Castro, M. E., Muñoz, P. A. & Blamey, J. M. Gold nanoparticles synthesized by Geobacillus sp. strain ID17 a thermophilic bacterium isolated from Deception Island, Antarctica. *Microbial cell factories* **12,** 75 (2013).

131. Arunkumar, P., Thanalakshmi, M., Kumar, P. & Premkumar, K. Micrococcus luteus mediated dual mode synthesis of gold nanoparticles: involvement of extracellular α-amylase and cell wall teichuronic acid. *Colloids and surfaces. B, Biointerfaces* **103,** 517–522 (2013).

132. Fu, X., Wang, Y., Wu, N., Gui, L. & Tang, Y. Shape-Selective Preparation and Properties of Oxalate-Stabilized Pt Colloid. *Langmuir* **18,** 4619–4624 (2002).

133. Shivaji, S., Madhu, S. & Singh, S. Extracellular synthesis of antibacterial silver nanoparticles using psychrophilic bacteria. *Process Biochemistry* **46,** 1800–1807 (2011).

134. Shahverdi, A. R., Minaeian, S., Shahverdi, H. R., Jamalifar, H. & Nohi, A.-A. Rapid synthesis of silver nanoparticles using culture supernatants of Enterobacteria. A novel biological approach. *Process Biochemistry* **42,** 919–923 (2007).

135. Silambarasan, S. & Abraham, J. Biosynthesis of silver nanoparticles. *African Journal of Biotechnology* **12,** 3088–3098 (2013).

136. Yong, P., Rowson, N. A., Farr, J. P. G., Harris, I. R. & Macaskie, L. E. Bioreduction and biocrystallization of palladium by Desulfovibrio desulfuricans NCIMB 8307. *Biotechnology and bioengineering* **80,** 369–379 (2002).

137. Bai, H., Zhang, Z., Guo, Y. & Jia, W. Biological Synthesis of Size-Controlled Cadmium Sulfide Nanoparticles Using Immobilized Rhodobacter sphaeroides. *Nanoscale research letters* **4,** 717–723 (2009).

138. Bindhu, M. R., Vijaya Rekha, P., Umamaheswari, T. & Umadevi, M. Antibacterial activities of Hibiscus cannabinus stem-assisted silver and gold nanoparticles. *Materials Letters* **131,** 194–197 (2014).

139. Annamalai, A., Christina, V. L. P., Sudha, D., Kalpana, M. & Lakshmi, P. T. V. Green synthesis, characterization and antimicrobial activity of Au NPs using Euphorbia hirta L. leaf extract. *Colloids and surfaces. B, Biointerfaces* **108,** 60–65 (2013).

140. Jayaseelan, C., Ramkumar, R., Rahuman, A. A. & Perumal, P. Green synthesis of gold nanoparticles using seed aqueous extract of Abelmoschus esculentus and its antifungal activity. *Industrial Crops and Products* **45,** 423–429 (2013).

141. Lim, S. H., Ahn, E.-Y. & Park, Y. Green Synthesis and Catalytic Activity of Gold Nanoparticles Synthesized by Artemisia capillaris Water Extract. *Nanoscale research letters* **11,** 474 (2016).

142. Saha, J., Begum, A., Mukherjee, A. & Kumar, S. A novel green synthesis of silver nanoparticles and their catalytic action in reduction of Methylene Blue dye. *Sustainable Environment Research* **27,** 245–250 (2017).

143. Knierim, C. *et al.* Living Composites of Bacteria and Polymers as Biomimetic Films for Metal Sequestration and Bioremediation. *Macromolecular bioscience* **15,** 1052–1059 (2015).

144. Letnik, I. *et al.* Living Composites of Electrospun Yeast Cells for Bioremediation and Ethanol Production. *Biomacromolecules* **16,** 3322–3328 (2015).

145. Letnik, I. *et al.* Biosorption of copper from aqueous environments by Micrococcus luteus in cell suspension and when encapsulated. *International Biodeterioration & Biodegradation* **116,** 64–72 (2017).

146. Potter, M. C. Electrical Effects Accompanying the Decomposition of Organic Compounds. *Proceedings of the Royal Society B: Biological Sciences* **84,** 260–276 (1911).

147. Logan, B. E. *et al.* Microbial fuel cells: methodology and technology. *Environmental science & technology* **40,** 5181–5192 (2006).

148. Cheng, S., Liu, H. & Logan, B. E. Increased Power Generation in a Continuous Flow MFC with Advective Flow through the Porous Anode and Reduced Electrode Spacing. *Environ. Sci. Technol.* **40,** 2426–2432 (2006).

149. Heilmann, J. & Logan, B. E. Production of electricity from proteins using a microbial fuel cell. *Water environment research : a research publication of the Water Environment Federation* **78,** 531–537 (2006).

150. Liu, H., Grot, S. & Logan, B. E. Electrochemically Assisted Microbial Production of Hydrogen from Acetate. *Environ. Sci. Technol.* **39,** 4317–4320 (2005).

151. Logan, B. E., Murano, C., Scott, K., Gray, N. D. & Head, I. M. Electricity generation from cysteine in a microbial fuel cell. *Water research* **39,** 942–952 (2005).

152. Oh, S. E. & Logan, B. E. Hydrogen and electricity production from a food processing wastewater using fermentation and microbial fuel cell technologies. *Water research* **39,** 4673–4682 (2005).

153. Liu, H., Ramnarayanan, R. & Logan, B. E. Production of Electricity during Wastewater Treatment Using a Single Chamber Microbial Fuel Cell. *Environ. Sci. Technol.* **38,** 2281–2285 (2004).

154. Logan, B., Cheng, S., Watson, V. & Estadt, G. Graphite Fiber Brush Anodes for Increased Power Production in Air-Cathode Microbial Fuel Cells. *Environ. Sci. Technol.* **41,** 3341–3346 (2007).

155. Chen, S. *et al.* Electrospun and solution blown three-dimensional carbon fiber nonwovens for application as electrodes in microbial fuel cells. *Energy Environ. Sci.* **4,** 1417 (2011).

156. Guerrini, E., Grattieri, M., Trasatti, S. P., Bestetti, M. & Cristiani, P. Performance explorations of single chamber microbial fuel cells by using various microelectrodes applied to biocathodes. *International Journal of Hydrogen Energy* **39,** 21837–21846 (2014).

157. Santoro, C. *et al.* Current generation in membraneless single chamber microbial fuel cells (MFCs) treating urine. *Journal of Power Sources* **238,** 190–196 (2013).

158. Santoro, C. *et al.* The effects of carbon electrode surface properties on bacteria attachment and start up time of microbial fuel cells. *Carbon* **67,** 128–139 (2014).

159. Ieropoulos, I., Greenman, J. & Melhuish, C. Microbial fuel cells based on carbon veil electrodes. Stack configuration and scalability. *Int. J. Energy Res.* **32,** 1228–1240 (2008).

160. Cheng, S. & Logan, B. E. Ammonia treatment of carbon cloth anodes to enhance power generation of microbial fuel cells. *Electrochemistry Communications* **9,** 492–496 (2007).

161. Zhou, X. *et al.* Surface oxygen-rich titanium as anode for high performance microbial fuel cell. *Electrochimica Acta* **209,** 582–590 (2016).

162. Wang, H. *et al.* High power density microbial fuel cell with flexible 3D graphene-nickel foam as anode. *Nanoscale* **5,** 10283–10290 (2013).

163. Ketep, S. F., Bergel, A., Calmet, A. & Erable, B. Stainless steel foam increases the current produced by microbial bioanodes in bioelectrochemical systems. *Energy Environ. Sci.* **7,** 1633–1637 (2014).

164. Baudler, A., Schmidt, I., Langner, M., Greiner, A. & Schröder, U. Does it have to be carbon? Metal anodes in microbial fuel cells and related bioelectrochemical systems. *Energy Environ. Sci.* **8,** 2048–2055 (2015).

165. Richter, H. *et al.* Electricity generation by Geobacter sulfurreducens attached to gold electrodes. *Langmuir : the ACS journal of surfaces and colloids* **24,** 4376–4379 (2008).

166. Wang, Y. *et al.* Polyaniline/mesoporous tungsten trioxide composite as anode electrocatalyst for high-performance microbial fuel cells. *Biosensors & bioelectronics* **41,** 582–588 (2013).

167. Xing, D., Zuo, Y., Cheng, S., Regan, J. M. & Logan, B. E. Electricity generation by Rhodopseudomonas palustris DX-1. *Environmental science & technology* **42,** 4146–4151 (2008).

168. Yong, Y.-C., Dong, X.-C., Chan-Park, M. B., Song, H. & Chen, P. Macroporous and monolithic anode based on polyaniline hybridized three-dimensional graphene for high-performance microbial fuel cells. *ACS nano* **6,** 2394–2400 (2012).

169. Zuo, Y., Xing, D., Regan, J. M. & Logan, B. E. Isolation of the exoelectrogenic bacterium Ochrobactrum anthropi YZ-1 by using a U-tube microbial fuel cell. *Applied and environmental microbiology* **74,** 3130–3137 (2008).

170. Lovley, D. R., Coates, J. D., Blunt-Harris, E. L., Phillips, E. J. P. & Woodward, J. C. Humic substances as electron acceptors for microbial respiration. *Nature* **382,** 445–448 (1996).

171. Pham, T. H. *et al.* Metabolites produced by Pseudomonas sp. enable a Gram-positive bacterium to achieve extracellular electron transfer. *Applied microbiology and biotechnology* **77,** 1119–1129 (2008).

172. Kaiser, P. *et al.* Electrogenic Single-Species Biocomposites as Anodes for Microbial Fuel Cells. *Macromolecular bioscience* **17** (2017).

173. Haile, S. M. Materials for fuel cells. *Materials Today* **6,** 24–29 (2003).

174. Zhou, M., Chi, M., Luo, J., He, H. & Jin, T. An overview of electrode materials in microbial fuel cells. *Journal of Power Sources* **196,** 4427–4435 (2011).

175. Beck, F., Junge, H. & Krohn, H. Graphite intercalation compounds as positive electrodes in galvanic cells. *Electrochimica Acta* **26,** 799–809 (1981).

176. Kim, C. Micropatterning of Organic Electronic Devices by Cold-Welding. *Science* **288,** 831–833 (2000).

177. Walter, M., Eilebrecht, B., Wartzek, T. & Leonhardt, S. The smart car seat. Personalized monitoring of vital signs in automotive applications. *Pers Ubiquit Comput* **15,** 707–715 (2011).

178. Gather, M. C., Köhnen, A. & Meerholz, K. White organic light-emitting diodes. *Advanced materials (Deerfield Beach, Fla.)* **23,** 233–248 (2011).

179. Yang, W., Yang, S., Sun, W., Sun, G. & Xin, Q. Nanostructured palladium-silver coated nickel foam cathode for magnesium–hydrogen peroxide fuel cells. *Electrochimica Acta* **52,** 9–14 (2006).

180. Posada-Quintero, H. F. *et al.* Dry carbon/salt adhesive electrodes for recording electrodermal activity. *Sensors and Actuators A: Physical* **257,** 84–91 (2017).

181. Suzuki, K., Yamaguchi, M., Kumagai, M. & Yanagida, S. Application of Carbon Nanotubes to Counter Electrodes of Dye-sensitized Solar Cells. *Chem. Lett.* **32,** 28–29 (2003).

182. Balint, R., Cassidy, N. J. & Cartmell, S. H. Conductive polymers: towards a smart biomaterial for tissue engineering. *Acta biomaterialia* **10,** 2341–2353 (2014).

183. Yan, J. *et al.* Preparation of graphene nanosheet/carbon nanotube/polyaniline composite as electrode material for supercapacitors. *Journal of Power Sources* **195,** 3041–3045 (2010).

184. Gelves, G. A., Lin, B., Sundararaj, U. & Haber, J. A. Low Electrical Percolation Threshold of Silver and Copper Nanowires in Polystyrene Composites. *Adv. Funct. Mater.* **16,** 2423–2430 (2006).

185. Gong, T. *et al.* Low percolation threshold and balanced electrical and mechanical performances in polypropylene/carbon black composites with a continuous segregated structure. *Composites Part B: Engineering* **99,** 348–357 (2016).

186. Jiang, H., Moon, K.-s., Li, Y. & Wong, C. P. Surface Functionalized Silver Nanoparticles for Ultrahigh Conductive Polymer Composites. *Chem. Mater.* **18,** 2969–2973 (2006).

187. Chan, K. L., Mariatti, M., Lockman, Z. & Sim, L. C. Effects of the size and filler loading on the properties of copper- and silver-nanoparticle-filled epoxy composites. *J. Appl. Polym. Sci.* **121,** 3145–3152 (2011).

188. Janovák, L. & Dékány, I. Optical properties and electric conductivity of gold nanoparticle-containing, hydrogel-based thin layer composite films obtained by photopolymerization. *Applied Surface Science* **256,** 2809–2817 (2010).

189. Bergin, S. M. *et al.* The effect of nanowire length and diameter on the properties of transparent, conducting nanowire films. *Nanoscale* **4,** 1996–2004 (2012).

190. Guo, H. *et al.* Copper nanowires as fully transparent conductive electrodes. *Scientific reports* **3,** 2323 (2013).

191. He, Y., Chen, Y., Xu, Q., Xu, J. & Weng, J. Assembly of Ultrathin Gold Nanowires into Honeycomb Macroporous Pattern Films with High Transparency and Conductivity. *ACS applied materials & interfaces* **9,** 7826–7833 (2017).

192. Stankovich, S. *et al.* Graphene-based composite materials. *Nature* **442,** 282–286 (2006).

193. Lee, T.-W., Lee, S.-E. & Jeong, Y. G. Highly Effective Electromagnetic Interference Shielding Materials based on Silver Nanowire/Cellulose Papers. *ACS applied materials & interfaces* **8,** 13123–13132 (2016).

194. Langner, M., Agarwal, S., Baudler, A., Schröder, U. & Greiner, A. Large Multipurpose Exceptionally Conductive Polymer Sponges Obtained by Efficient Wet-Chemical Metallization. *Adv. Funct. Mater.* **25,** 6182–6188 (2015).

195. An, S. *et al.* Self-Junctioned Copper Nanofiber Transparent Flexible Conducting Film via Electrospinning and Electroplating. *Advanced materials (Deerfield Beach, Fla.)* **28,** 7149–7154 (2016).

196. Jiang, S. *et al.* Exploration of the Electrical Conductivity of Double-Network Silver Nanowires/Polyimide Porous Low-Density Compressible Sponges. *ACS applied materials & interfaces* **9,** 34286–34293 (2017).

4. The preparation of bacteria based golden polymer fleece and its catalytic application

To be submitted (non final version)

Steffen Reich[1], Andreas Greiner[1]

[1]Macromolecular Chemistry II and Bayreuth Center for Colloid and Interface Science, University of Bayreuth, D-95440 Bayreuth, Germany

4.1 Abstract *Polymer composite fleeces with living bacteria were prepared by electrospinning followed by coating via chemical vapor deposition (CVD) of poly(p-xylylene) (PPX). These fleeces converted gold ions to gold nanoparticles (AuNP) which could be used for catalytic reactions. Interesting the catalytic reaction was only possible when the bacteria in the fleece were alive. In contrast, fleeces with dead bacteria did not show any significant catalytic activity.*

4.2 Introduction

Gold nanoparticles range in the size between 1-100 nm. Generally gold nanoparticles find their applications in catalysis, biosensors, food industry, drug delivery, cancer therapy, anti-microbiology, cyto-genetoxicity. Typical methods for the production of nanoparticles are chemical and electrochemical reduction,[1] co-reduction of metal ions,[2] photochemical and sonochemical irradiation,[3] impregnation,[4] deposition- and co-precipitation,[5] vapor deposition or liquid preparation.[6] AuNP are of interest for catalysis, for example for the oxidation of benzylalcohol to benzaldehyde,[7] the conversion of cyclohexane to adipic acid,[8] and the hydrolysis of dimethylphenylsilane to dimethylphenylsilanol or the alcoholysis to butoxydimethylphenylsilane in PPX microtubes.[9] AuNP were used in the confinement of

microbes for the antimicrobial effect against other harmful microbes or in catalysis. The implementation of AuNP in microbes could be achieved by bioremediation.[10,11] Bioremediation is also known for other noble metals like silver and palladium by *Lactobacillus sp.*,[12] *Bacillus indicus*,[13] *Enterobacter cloacae*,[14] *Pseudonomas fluorecens*[15] or *Desulfovibrio desulfuricans*.[16]

AuNP prepared by *Hibiscus cannabinus* stem extract showed antimicrobial activity against *Pseudomonas aeruginosa* and *Staphylococcus aureus*,[17] leaf extract of *Euphorbia hirta* against *Escherichia coli*, *Pseudomonas aeruginosa* and *Klebsiella pneumonia*[18] or synthesized AuNP through *Abelmoschus esculentus* extract showed antifungal activity against *Puccinia graminis trici*, *Aspergillus niger*, *Aspergillus flavus* and *Candida albicans*.[19] The catalytic activity of biosynthesized nanoparticles didn't get that attention like the antimicrobial studies. The potential of the catalytic activity is still under observation. Biosynthesized AuNP are used for the reduction of 4-nitrophenol to 4-aminophenol.[20] Silver nanoparticles (AgNP) synthesized through *Gmelina arborea* showed the catalytic reduction of methylene blue dye.[21] The challenge for the wide use of microbes in harmful environments, for example during catalytic reactions in organic solvents is the preservation of the functional state of the microbes, which carry the active catalytic sites. The protection of microbes could be achieved for example by encapsulation in electrospun water soluble poly(ethylene oxide) (PEO) fibers,[22] by electrospinning of microencapsulated bacteria[23] or by encapsulation of bacteria in poly(methyl methacrylate) PMMA coated hydrogel microparticles.[24] *M.luteus* in PPX wet-spun poly(vinylalcohol) PVA microfibers could be used for gold sequestration from aqueous Au(III) solutions.[25] The formation of AuNP in the shell of the bacteria were observed. From the biological point of view, we wanted to explore how *M.luteus* synthesized AuNP in PVA/PPX nanofibers which has not been reviewed to the best of our knowledge in catalysis. In fact, we discovered the formation of AuNP inside the polymer fleece. Surprisingly the catalytic

performance was found using living *M.luteus* while no catalytic performance was received by dead *M.luteus*.

Herein we report the preparation of a biohybrid polymer fleece composite as a tool for the production of gold nanoparticles and its catalytic performance in a polymer fleece. We examined in detail the preparation of biohybrid polymer fibers, their encapsulation of *M.luteus* in PVA nanofibers, the hydrophobic stabilization with PPX through CVD, and the biosynthesis of AuNP inside the core-shell fibers. The survival of the *M.luteus* during the preparation steps were studied as well as the catalytic activity of the biosynthesized AuNPs.

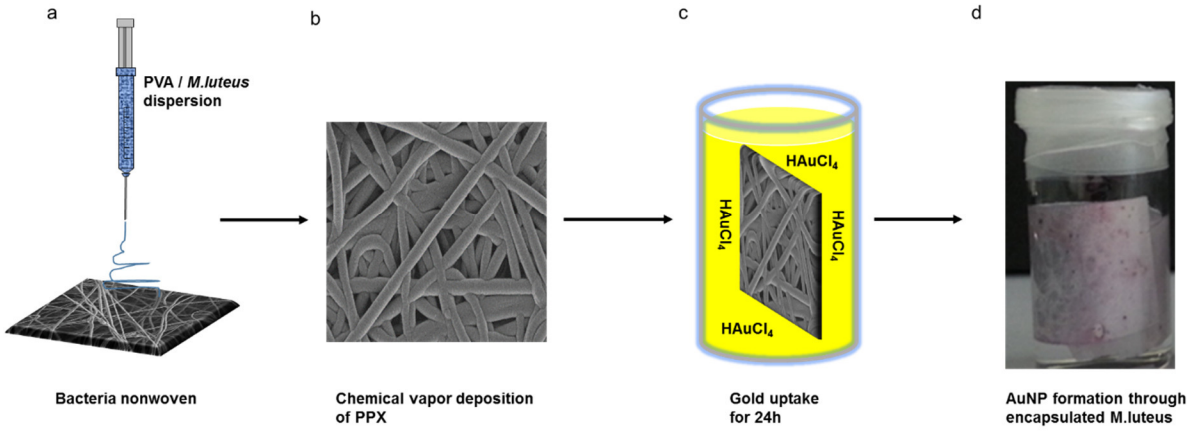

Sheme 4.1. Shematic preparation of biosynthesis of gold nanoparticles. a) Electrospinning of biohybrid PVA nanofibers, b) hydrophobic PPX coating by chemical vapor deposition (CVD), c) gold biosorption by M.luteus and d) gold nanoparticle biosynthesis by *M.luteus*.

Sheme 4.1 presents the approach for the preparation of biohybrid polymer fiber fleece composites. First a dispersion of *M.luteus* and sterile PVA were electrospun to a stainless steel mesh using high applied voltage. Several biohybrid polymer systems are known to be used for waste water treatment where microorganism show the performance of detoxifying waste water. After the hydrophobic coating with PPX by CVD the resulted biohybrid polymer fiber fleece

composite is a versatile tool for the removal of precious metal ions and the biosynthesis of nanoparticles.

Biohybrid nanofibers were electrospun from a dispersion of 10 wt% PVA and *M.luteus* in water (Sheme 4.1a). The 10 wt% PVA water solution was previously sterilized to overcome contaminations through other microorganism. Scanning electron microsopy (SEM) of biohybrid PVA nanofibers illustrates average diameters of 424 ± 115 nm (Figure 4.1a). According to the SEM images *M.luteus* were encapsulated in the PVA nanofibers (arrows Figure 4.1a). Survival tests were performed directly after electrospinning were the biohybrid nanofibers were dissolved on an agar plate containing nutrients. The growth of the *M.luteus* can be observed after 3 days (Figure 4.1b). After the hydrophobic coating with PPX of the biohybrid nanofibers the fiber diameter increased to an average dimeter of 1633 ± 289 nm (Sheme 4.1b, Figure 4.1c) resulting in a hydrophobic PPX thickness of approximately 1.2 µm. Confocal laser scanning microcopy was investigated to proof the survival of the *M.luteus* after PPX caoting. Living (green) and dead (red) *M.luteus* indicated that most of the *M.luteus* survived this stabilization process (Figure 4.1d). Just a few red dots (dead *M.luteus*) can be observed.

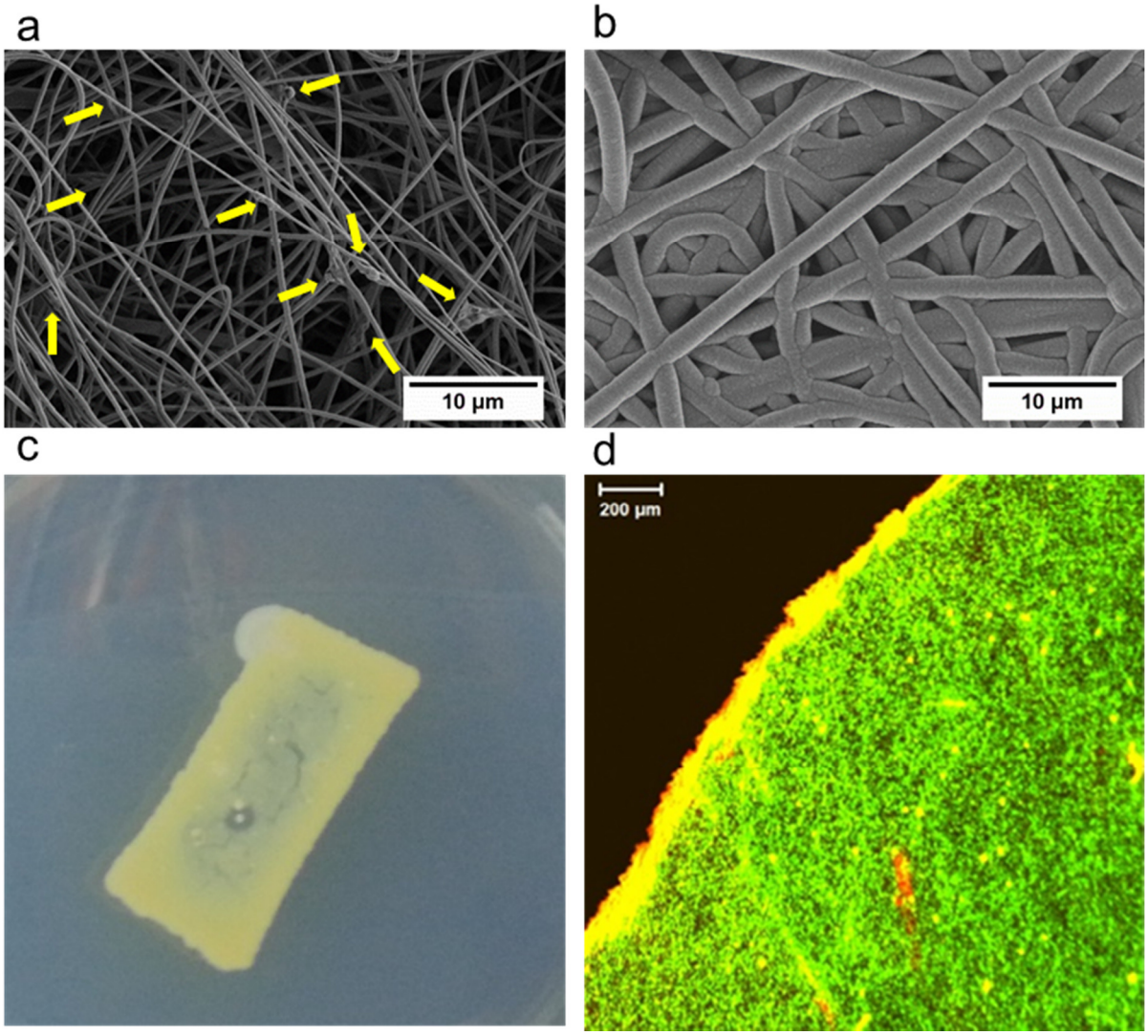

Figure 4.1. Characterization of the biohybrid nanofibers. a) SEM image of the PVA/*M.luteus* nanofibers arrows indicates the *M.luteus*, b) SEM image of the PVA/*M.luteus*/PPX nanofibers, c) Agarplate with living *M.luteus* after electrospinning in PVA and d) CLSM image of living (green) and dead (red) *M.luteus* after PPX coating.

Next the biohybrid polymer composite fleece was dipped in a chloroauric acid solution of pH 3 for 24 hours (Sheme 4.1c). We assume that the gold ions in the solution penetrates through the PPX layer were *M.luteus* can biosorp and/or bioaccumulate the gold ions to produce gold nanoparticles according to Arunkumar et al.[11] Free *M.luteus* show the formation of gold nanoparticles on its surface which are well dispersed, as manifested by TEM measurements

(Figure 4.2a). The AuNPs encapsulated in the biohybrid polymer composite fleece are separated and are located near the *M.luteus* as characterized by SEM using a backscattered electron detector (BSE) (Figure 4.2b). The AuNPs don't seem bright as they are encapsulated in a layer of 1.2 µm. The elemental composition of the produced AuNPs were studied by SEM using an energy dispersive X-ray detector (Figure 4.2e). The signal at 2.2 keV is characteristic for the element gold. In contrast non biohybrid polymer composite fleece seem to reduce gold ions as well, as shown by SEM/BSE image (Figure 4.2c). The gold uptake was determined by inductively coupled plasma optical emission spectroscopy (ICP-OES). Nevertheless the gold uptake through biohybrid polymer composite fleece was three times higher than in case of the non biohybrid polymer composite fleece (Figure 4.2d) using high starting concentration of 100 and 1000 µmol · L^{-1}, as shown in Table 4.1. Low concentration of chloroauric acid solution (1 µmol · L^{-1}) lead to the same gold uptake by non and biohybrid polymer composite fleece.

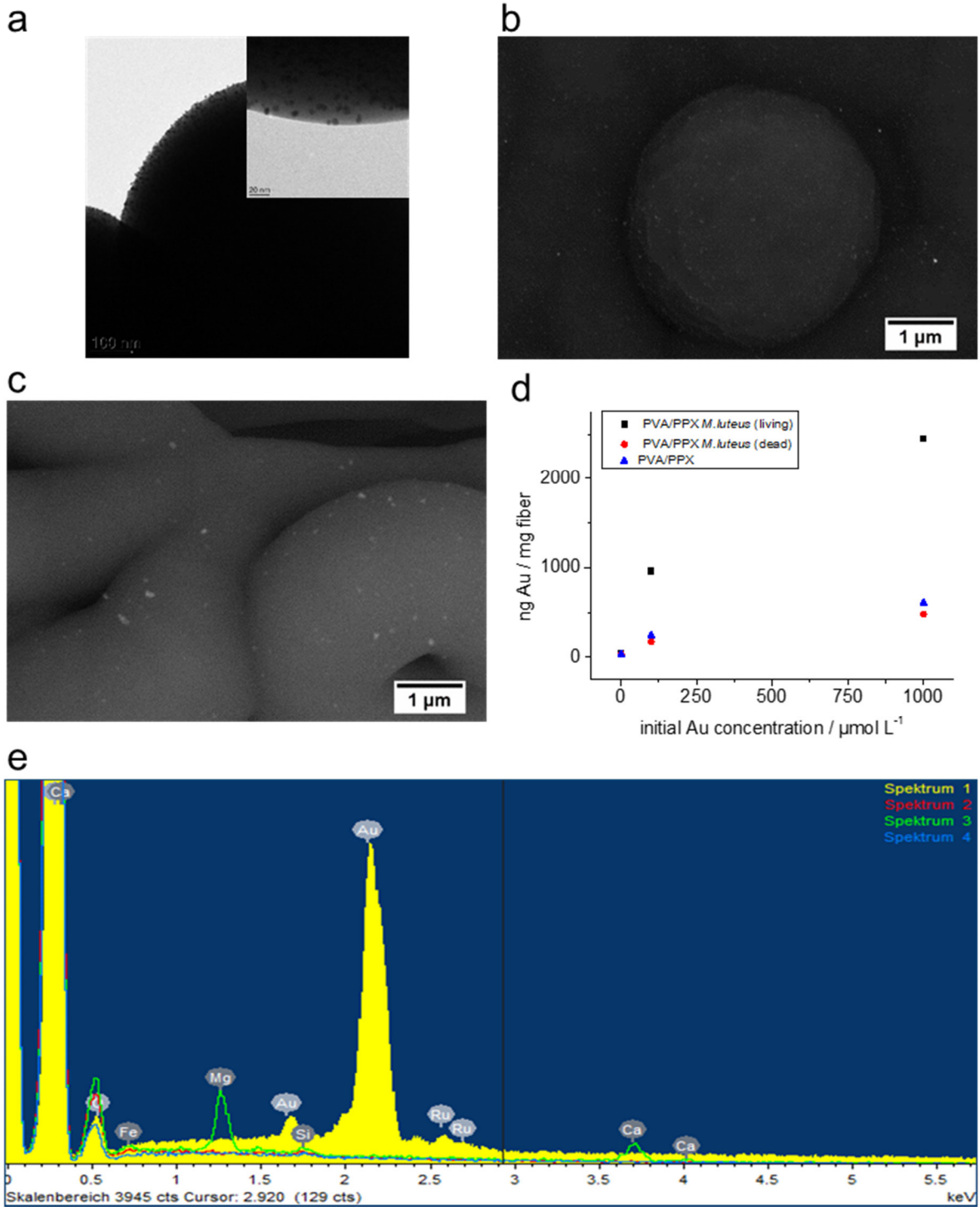

Figure 4.2. Characterization of the biohybrid polymer composite nonwoven after gold uptake. a) TEM image of *M.luteus*, b) SEM/BSE image of PVA/*M.luteus*/PPX nonwoven, c) SEM/BSE image of PVA/PPX nonwoven, d) comparison of the gold uptake through different systems out

of increasing chloroauric acid concentrations and e) SEM/EDX spectra of the PVA/M.luteus/PPX nonwoven.

Table 4.1. Comparison of the gold uptake through the systems determined via ICP-OES.

Chloroauric acid solution µmol/L	PVA/*M.luteus* (living)/PPX µg Au	PVA/*M.luteus* (dead)/PPX µg Au	PVA/PPX µg Au
1000	180.81 (2.2 %)	17.36 (0.2 %)	36.54 µg (0.5 %)
100	67.60 (8.6 %)	6.16 (0.8 %)	14.55 (1.8 %)
1	2.23 (28.3 %)	0.72 (9.1 %)	1.87 (23.7 %)

The behavior in gold uptake through dead *M.luteus* was studied as well as they have proteins on its surface which are present in the bioreduction of gold ions. According to the ICP-OES studies *M.luteus* is much more effective in AuNP production when it is used in the living state. We studied the catalytic activity of the biosynthesized AuNP in the hydrolysis of dimethylphenylsilane with water as a model reaction (Figure 4.3a). Particulated gold is a common used catalyst for the hydrolysis of dimethylphenylsilane. Table 4.2 summarizes the used gold supported catalysts. Various literature known systems where AuNPs are supported on substrates showed hydrolytic oxidations of dimethylphenylsilane between 1 and 60 minutes using 0.04 to 1 mol% gold with respect to dimethylphenylsilane.[26–29] Our system where AuNP were biosynthesized through encapsulated *M.luteus* showed quantitative conversion after 21000 minutes at room temperature using 0.001 mol% AuNP with respect to dimethylphenylsilane. This amount of AuNP was 870 times lower than a comparable system where AuNP were located in PPX-tubes and hydrolytic oxidation yielded in over 99% after 210 minutes.[9]

Following the catalytic oxidation of dimethylphenylsilane through biosynthesized AuNP (low starting concentration (1 µmol · L^{-1} chloroauric acid solution)) no product was formed by the use of dead *M.luteus* in the biohybrid polymer composite fleece and the non biohybrid polymer composite fleece, where the amount of gold is approximately the same (Table 4.1). This can be an explanation that *M.luteus* is much more effective in AuNP biosynthesis when *M.luteus* is alive and encapsulated.

The hydrolytic conversion of dimethylphenylsilane to dimethylphenylsilanol follows a reaction pseudo first order because water was added in a big excess. The reaction rate can be calculated as follows and determines to k = 7.307 10-6 l/mol s.

$$-\frac{d[silane]}{dt} = k\,[silane]\,[H_2O] \quad (1)$$

$$-\frac{d\,[silane]}{dt} = k_{app}\,[silane] \quad (2)$$

$$\ln\frac{[A]_0}{[A]_t} = k\,t \quad (3)$$

In all cases neither disiloxanes nor side products can be found (Figure S4.1). Catalytic hydrolysis was done for blank samples as well where no conversion can be found by the use of PVA/PPX fleeces, PVA/*M.luteus* (living)/PPX fleeces and the pure catalytic solution without gold nanoparticles (Figure S4.2).

a

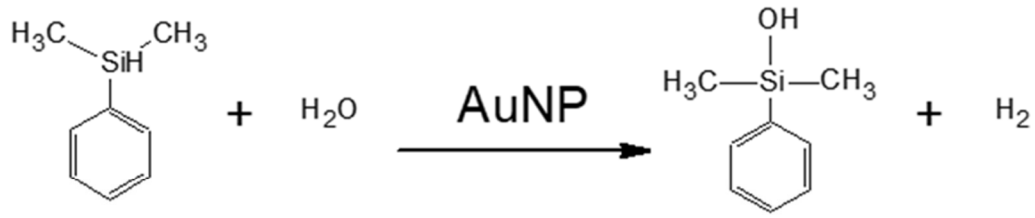

b

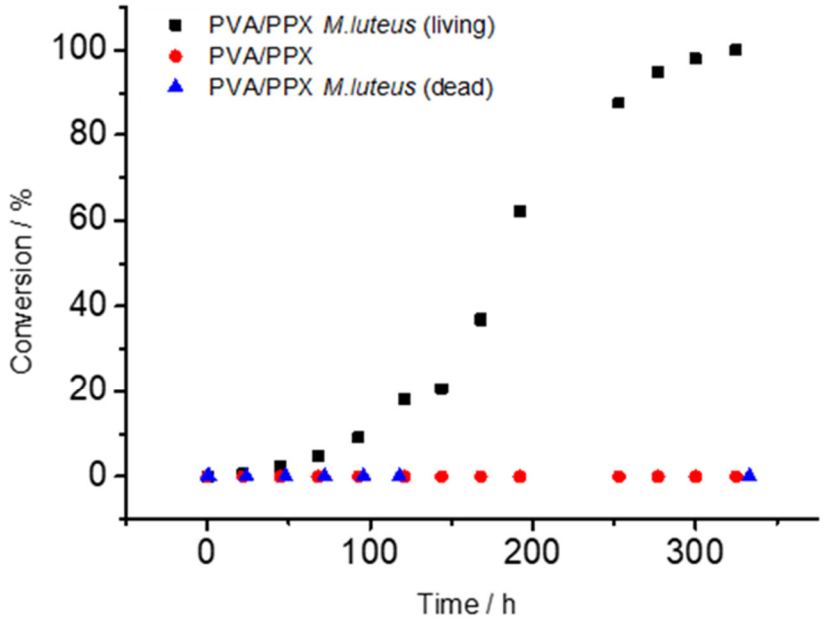

Figure 4.3. Schematic catalytic conversion of dimethylphenylsilane to dimethylphenylsilanol through AuNP (a) and catalytic conversion through biosynthesized AuNP (b).

Table 4.2. Hydrolytic oxidation of dimethylphenylsilane via gold supported catalysts.

Catalyst	Time (min)	Conversion (%)	Reference
Au/HAP (0.04 mol%)	5	>99	[28]
Au/SiO_2 (0.4 mol%)	1	>99	[29]
AuCNT (0.1 mol%)	45	98	[26]
AuNPore (1 mol%)	60	100	[27]
AuNP/PPX-tubes (0.87 mol%)	210	>99	[9]
bioAuNP (0.001 mol%)	21000	100	This work

In conclusion living *M.luteus* were encapsulated in PVA nanofibers by the electrospinning process and further stabilized with hydrophobic PPX using a CVD device to create a versatile approach for waste water treatment and catalytically active fleece. Confocal laser scanning microscopy revealed the survival of *M.luteus* in the biohybrid polymer composite fleece after processing. This biohybrid polymer composite fleece was successfully used for the removal of gold ions and in addition the production of AuNP through encapsulated *M.luteus*. These biosynthesized AuNP show catalytic performance in the hydrolytic oxidaion of dimethylphenylsilane. This tea bag like system show the use in a step by step application like waste water treatment for removal of pollutants such as metals and in a following step in catalysis. Furthermore other kind of microorganism or biofilms can be used in this system to be much more effective in waste water treatment or catalysis, which will be focus of this research.

4.3 Acknowledgements

This work was funded by the German Research Foundation (DFG) in the GIP-project. The authors thank Dr. Rakesh Kumar of the SCS for the DIMER-N, Tobias Moss for thickness measurements of the coatings, Dr. Jürgen Ilgen for ICP-OES measurements, Martina Heider

for SEM-EDX measurements, Matthias Burgard for SEM-BSE measurements, Judith Schöbel and Marina Krekhova for TEM maesurements.

4.4 Conflict of interest

The authors declare no conflict of interes.

4.5 References

[1] a) J. Turkevich, G. Kim, *Science (New York, N.Y.)* **1970**, 169, 873; b) M. S. Chen, D. W. Goodman, *Science (New York, N.Y.)* **2004**, 306, 252.

[2] a) L. Prati, A. Villa, *Catalysts* **2012**, 2, 24; b) S. Nishimura, A. Takagaki, K. Ebitani, *Green Chem.* **2013**, 15, 2026.

[3] a) M. Ahmed, R. Narain, *Langmuir : the ACS journal of surfaces and colloids* **2010**, 26, 18392; b) A. Akhavan, H. R. Kalhor, M. Z. Kassaee, N. Sheikh, M. Hassanlou, *Chemical Engineering Journal* **2010**, 159, 230; c) Y.-C. Cheng, C.-C. Yu, T.-Y. Lo, Y.-C. Liu, *Materials Research Bulletin* **2012**, 47, 1107; d) F. Kim, J. H. Song, P. Yang, *J. Am. Chem. Soc.* **2002**, 124, 14316.

[4] D. P. Debecker, P. H. Mutin, *Chemical Society reviews* **2012**, 41, 3624.

[5] a) M. Haruta, M. Daté, *Applied Catalysis A: General* **2001**, 222, 427; b) X. Fu, Y. Wang, N. Wu, L. Gui, Y. Tang, *Langmuir* **2002**, 18, 4619; c) N. Toshima, M. Kuriyama, Y. Yamada, H. Hirai, *Chem. Lett.* **1981**, 10, 793.

[6] a) S. U. Son, Y. Jang, J. Park, H. B. Na, H. M. Park, H. J. Yun, J. Lee, T. Hyeon, *Journal of the American Chemical Society* **2004**, 126, 5026; b) S. Alayoglu, A. U. Nilekar, M. Mavrikakis, B. Eichhorn, *Nature materials* **2008**, 7, 333.

[7] A. Abad, P. Concepción, A. Corma, H. García, *Angewandte Chemie (International ed. in English)* **2005**, 44, 4066.

[8] A. Alshammari, A. Koeckritz, V. N. Kalevaru, A. Bagabas, A. Martin, *ChemCatChem* **2012**, 4, 1330.

[9] F. Mitschang, H. Schmalz, S. Agarwal, A. Greiner, *Angewandte Chemie (International ed. in English)* **2014**, 53, 4972.

[10] a) T. J. Beveridge, R. G. Murray, *Journal of bacteriology* **1980**, 141, 876; b) S. K. Srivastava, R. Yamada, C. Ogino, A. Kondo, *Nanoscale research letters* **2013**, 8, 70; c) N. Sharma, A. K. Pinnaka, M. Raje, A. Fnu, M. S. Bhattacharyya, A. R. Choudhury, *Microbial cell factories* **2012**, 11, 86; d) D. N. Correa-Llantén, S. A. Muñoz-Ibacache, M. E. Castro, P. A. Muñoz, J. M. Blamey, *Microbial cell factories* **2013**, 12, 75.

[11] P. Arunkumar, M. Thanalakshmi, P. Kumar, K. Premkumar, *Colloids and surfaces. B, Biointerfaces* **2013**, 103, 517.

[12] F. Jinkun, L. Yueying, G. Pingying, T. Dingliang, L. Zhongyu, Y. Bingxin, W. Shengzhou, *Acta Physico-Chimica Sinica* **2000**, 16, 779.

[13] S. Shivaji, S. Madhu, S. Singh, *Process Biochemistry* **2011**, 46, 1800.

[14] A. R. Shahverdi, S. Minaeian, H. R. Shahverdi, H. Jamalifar, A.-A. Nohi, *Process Biochemistry* **2007**, 42, 919.

[15] S. Silambarasan, J. Abraham, *African Journal of Biotechnology* **2013**, 12, 3088.

[16] P. Yong, N. A. Rowson, J. P. G. Farr, I. R. Harris, L. E. Macaskie, *Biotechnology and bioengineering* **2002**, 80, 369.

[17] M. R. Bindhu, P. Vijaya Rekha, T. Umamaheswari, M. Umadevi, *Materials Letters* **2014**, 131, 194.

[18] A. Annamalai, V. L. P. Christina, D. Sudha, M. Kalpana, P. T. V. Lakshmi, *Colloids and surfaces. B, Biointerfaces* **2013**, 108, 60.

[19] C. Jayaseelan, R. Ramkumar, A. A. Rahuman, P. Perumal, *Industrial Crops and Products* **2013**, 45, 423.

[20] S. H. Lim, E.-Y. Ahn, Y. Park, *Nanoscale research letters* **2016**, 11, 474.

[21] J. Saha, A. Begum, A. Mukherjee, S. Kumar, *Sustainable Environment Research* **2017**, 27, 245.

[22] M. Gensheimer, M. Becker, A. Brandis-Heep, J. H. Wendorff, R. K. Thauer, A. Greiner, *Adv. Mater.* **2007**, 19, 2480.

[23] M. Gensheimer, A. Brandis-Heep, S. Agarwal, R. K. Thauer, A. Greiner, *Macromolecular bioscience* **2011**, 11, 333.

[24] C. Knierim, C. L. Greenblatt, S. Agarwal, A. Greiner, *Macromolecular bioscience* **2014**, 14, 537.

[25] C. Knierim, M. Enzeroth, P. Kaiser, C. Dams, D. Nette, A. Seubert, A. Klingl, C. L. Greenblatt, V. Jérôme, S. Agarwal et al., *Macromolecular bioscience* **2015**, 15, 1052.

[26] J. John, E. Gravel, A. Hagège, H. Li, T. Gacoin, E. Doris, *Angewandte Chemie (International ed. in English)* **2011**, 50, 7533.

[27] N. Asao, Y. Ishikawa, N. Hatakeyama, Menggenbateer, Y. Yamamoto, M. Chen, W. Zhang, A. Inoue, *Angewandte Chemie (International ed. in English)* **2010**, 49, 10093.

[28] T. Urayama, T. Mitsudome, Z. Maeno, T. Mizugaki, K. Jitsukawa, K. Kaneda, *Chem. Lett.* **2015**, 44, 1062.

[29] W. Li, A. Wang, X. Yang, Y. Huang, T. Zhang, *Chemical communications (Cambridge, England)* **2012**, 48, 9183.

4.6 Supporting Information

Experimental Section

Materials

PVA (Sigma Aldrich, 124'000- 186'000 g/mol, 87-89mol% hydrolysis), $HAuCl_4 \cdot 3H_2O$ (Acros Organics), LIVE/DEAD BacLight Bacterial Viability Kit (life technologies, USA), and standard chemicals were from established suppliers and used as received. Unless otherwise indicated, plastic materials, supplements and culture devices for experiments involving microorganisms were from established suppliers and used as received. High quality water was prepared by a Millipore unit. Dimethylphenylsilane (Sigma Aldrich, 98%), Acetone (Acros Organics); [2.2]paracyclophane (Specialty Coating System; Indianapolis, US)

Micrococcus luteus (M.luteus) DSM-No. 20300 (DSMZ Braunschweig), LB medium was prepared by dissolving 32 g LB-powder (Carl Roth) in 1 L of Millipore-water, Phosphate buffered saline (PBS) was prepared in house as follows: 8.0 g NaCl, 0.2 g KCl, 1.42 g Na2HPO4 and 0.24 g KH2PO4 per liter of Millipore-water, pH adjusted to 7.3 with 2 M NaOH, sterilized by autoclaving (121 °C, 20 min).

Analytical Methods

A fluorescence microscope (DMRX) from Leica (Wetzlar, Germany) were used for the optical characterizations of bacteria and composites as indicated below. For optical microscopy of culture supernatants, a phase contrast microscope Olympus BX51 equipped with 600x oil immersion objective UPlanFI, Olympus and camera CC-12 from Olympus Soft Imaging Systems (Tokio, Japan) was used. Software analysis package 3.2 (Build 883) from Olympus Soft Imaging Systems was used for illustrating and storing the pictures. For staining of *M.luteus*

with baclight Bacterial Viability-kit from lifetechnologies, nonwovens were treated as indicated in the instructions.For scanning electron microscopy (SEM) a Zeiss LEO 1530 with a Schottky-field-emission cathode was employed for characterization of the silver nanowires and the resulting nonwovens. The samples were stuck on a sample holder with a double sided adhesive tape and coated subsequently with 2.0 nm of platinum by a high resolution sputter coater 208 HR from Cressington. A SE2 detector was used for SE2 images at an acceleration voltage of 2 kV and a working distance of ca. 4.5 mm. BSE measurements were performed with a Robinson detector and an acceleration voltage of 10 kV and a working distance of 10 mm. The samples were processed with aluminium strips previously. EDX- measurements were performed with a Zeiss Ultra Plus with a Schottky-field-emission cathode with an acceleration voltage of 10 kV. The samples were vapor coated with carbon with a Balzer Union MED 010 prior measurements. Gas Chromatography Coupled with Mass-Spectrometry (GC-MS). For GC-MS, a GC 7890 B with a 30 m capillary column (Agilent HP-5ms; 30 m x 0.25 mm x 0.25 µm) and a mass spectrometer 5977 A from Agilent Technologies were used. The heating profile was set as following: the starting temperature of 50 °C was kept for 2 min; subsequently, the temperature of the oven was raised to 150 °C applying a heating rate of 10 K min 1, followed by heating to 300 °C at 35 K min 1. The applied carrier gas was helium (5.6; purified with a Agilent CP17973 gas clean filter). For calculation, the ratio of integrals of dimethylphenylsilane (R_t = 6.43 min, m z 1 = 136 [M], 121 [M-(CH3)]+, 105 [C6H5Si]+) and dimethylphenylsilanol (R_t = 9.20 min, m z 1 = 152 [M], 137 [C6H5Si(CH3) (OH)]+, 119 [C6H5SiCH3]+).Inductively Coupled Plasma-Optical Emission Spectrometry (ICP-OES). ICP-OES was measured on a VARIAN Vista-Pro (40 MHz, Argon Plasma) equipped with an ASX-510 autosampler, an Echelle polychromator and an Argon humidifier. Before measurement, 0.3 g of the samples were dried at 60 °C. The residue was dissolved in 0.5 mL aqua regia and diluted with 9.5 mL of ultrapure water. A CCD semiconductor detector was used for the detection. Dynamic light scattering (DLS). The DLS measurements were performed on an ALV system equipped with an ALV-SP

125 compact goniometer, an ALV 5000/E cross correlator, and a He-Ne Laser (λ = 632.8 nm). UV-Vis Spectroscopy. Reflection spectra were recorded with a Cary 5000 (2.23) from Agilent Technologies equipped with a universal measurement accessory (UMA) unit. Spectra were recorded in the wavelength range of 200 to 800 nm. The spectra were background corrected. The gold containing *M.luteus* were characterized with an elastic bright-field transmission electron microscope (TEM, Zeiss 922 Omega EFTEM) at a voltage of 200 kV.

Cultivation of M.luteus

M.luteus were cultivated with LB medium in a shaking flask (200 mL, 37 °C, 100 rpm) for 72 hours. The *M.luteus* were harvested by centrifugation (4000 rpm, 4 °C, 10 min). The *M.luteus* pellet was washed with PBS three times.

Preparation of PVA/PPX core-shell nonwovens

A solution of 10 wt% poly(vinyl alcohol) in PBS was produced and sterilized. The solution was mixed with *M.luteus* to a concentration of $2x10^9$ CFU / mL polymer solution and stirred for 1 hour to obtain a homogenous solution. The polymer *M.luteus* solution was filled in 2 mL syringes stocked with a cannula (hole diameter 0.9 mm). The collector electrode (rotary plate) was covered with a stainless steel mesh (6 x 2 cm) in a distance of 15 cm. Both the collector electrode and the cannula were connected to a power supply a voltage of – 5 kV and +23 kV was applied. Electrospun PVA/*M.luteus* nonwovens were stored over night at 4°C and were coated with PPX at the next day.

PPX-coating of the PVA/*M.luteus*-composites by chemical vapor deposition (CVD) employing [2.2]paracyclophane as a precursor was done using a labcoter from SCS (Indianapolis, IN, USA). PPX was deposited onto the samples at 20 °C at a pressure of 40-50 mbar. Evaporation

of the precursor took place at 150 °C, pyrolysis at 650 °C. Coating took approximately 6 h. Fibers without *M.luteus* were prepared as negative controls.

Gold uptake by PVA/M.luteus/PPX- and PVA/PPX-nonwoven

The PVA/*M.luteus*/PPX- and PVA/PPX-nonwovens were immersed in different concentrations (1, 100 and 1000 $\mu mol \cdot L^{-1}$) of chloroauric acid solutions for 24 hours. The solution was shaked with a velocity of 200 rpm at 25 °C. The nonwovens were washed three times with Millipore®-water and three times with acetone (pure).

Catalytic reaction of the biosynthesized gold nanoparticles

Catalytic reactions take place in a glass vial. Therefore a mixture was prepared consisting of dimethylphenylsilane (~ 110 mg; 0.81 mmol), water (~ 100 mg; 0.18 mmol) and acetone (~ 5000 mg; 86.09 mmol) (pure). The gold containing nonwovens (~ 40 mg; (~ 2 µg Au; $1.02 \cdot 10^{-5}$ mmol) were put into the solutions and in time distances of 24 hours samples were measured via GC-MS to determine the hydrolytic oxidation of dimethylphenylsilane to dimethylphenylsilanol.

Synthesis of the citrate stabilized gold nanoparticles

In a typical experiment 90 mL of Millipore water was heated to 100 °C. Afterwards 10 mg chloroauric acid trihydrate was immersed in the boiling water. Afterwards 50 mg of trisodiumcitrate dehydrate dissolved in 5 mL of Millipore water was added to the solution. After 10 minutes the color changed from yellow to wine red. The reaction was stirred for 1 hour at 100 °C. The gold nanoparticles solution was cooled to room temperature as was filled in a Shott flask and was stored at 4 °C under dark conditions. The gold nanoparticles were characterized with TEM, DLS, UV/Vis-spectroscopy to obtain the diameter of 14.5 to 14.6 nm. The concentration amounted to ~34 $\mu g \cdot mL^{-1}$ determined via ICP-MS.

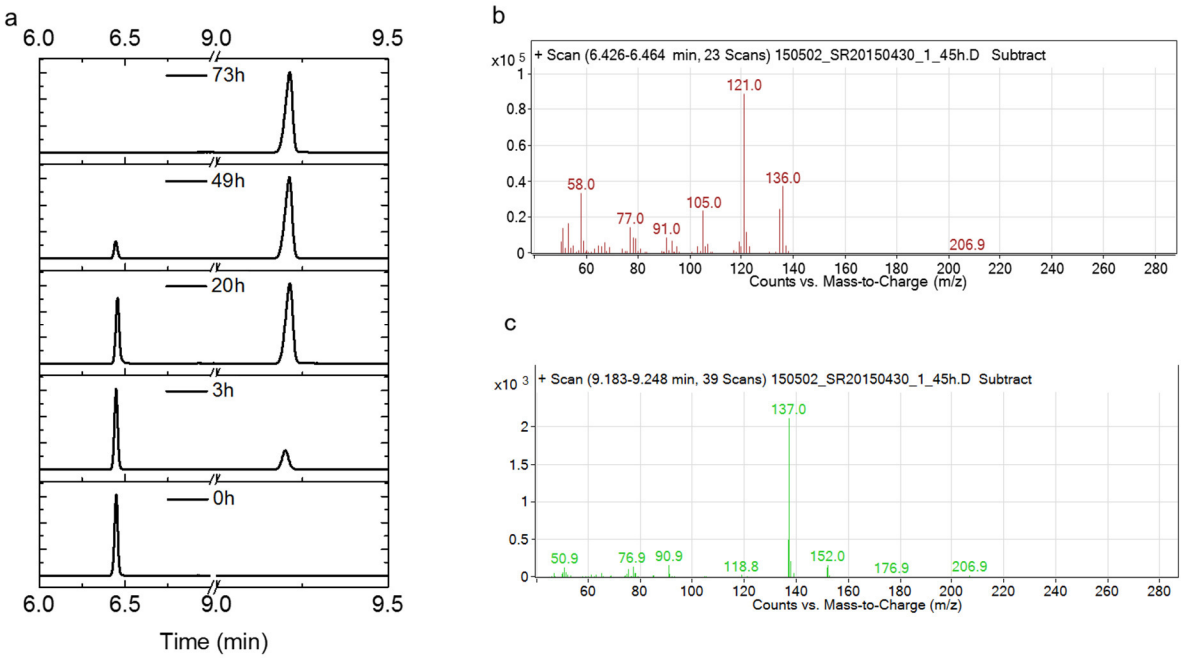

Figure S4.1. GC/MS chromatogram of the hydrolytic oxidation of dimethylphenylsilane to dimethylphenylsilanol (a), Mass-to-charge chromatogram of dimethylphenylsilane (b) and dimethylphenylsilanol (c).

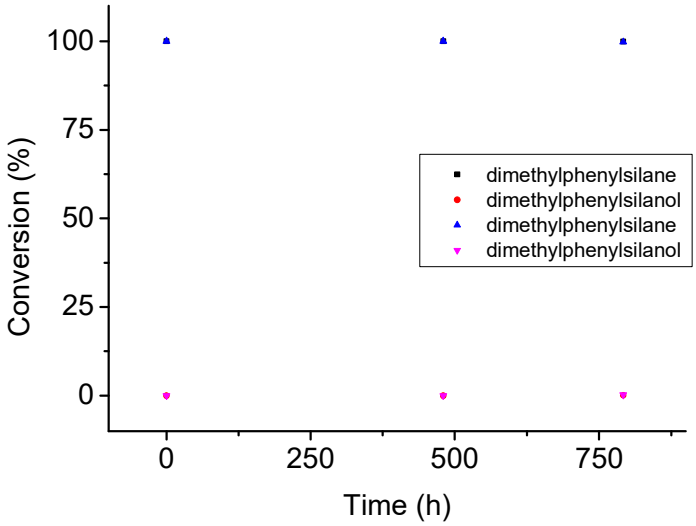

Figure S4.2. Hydrolytic oxidation of dimethylphenylsilane through PVA/PPX nonwovens.

5. Electrogenic single-species biocomposites as anodes for microbial fuel cells

Published in *Macromolecular Bioscience* ***2017****, 17, 1600442*

Patrick Kaiser[1*], *Steffen Reich*[2*], *Daniel Leykam*[3], *Monika Willert-Porada*[3], *Seema Agarwal*[2], *Andreas Greiner*[2], *Ruth Freitag*[1,§]

[*]Both authors contributed equally in this work

[1] Process Biotechnology, University of Bayreuth, D-95447 Bayreuth, Germany

[2] Macromolecular Chemistry II and Bayreuth Center for Colloid and Interface Science, University of Bayreuth, D-95447 Bayreuth, Germany

[3] Chair of Materials Processing, University of Bayreuth, D-95447 Bayreuth, Germany

§ Corresponding author: Process Biotechnology, University of Bayreuth, 95440 Bayreuth, Germany, phone: +49 921 557371, e-mail: ruth.freitag@uni-bayreuth.de

5.1 Abstract

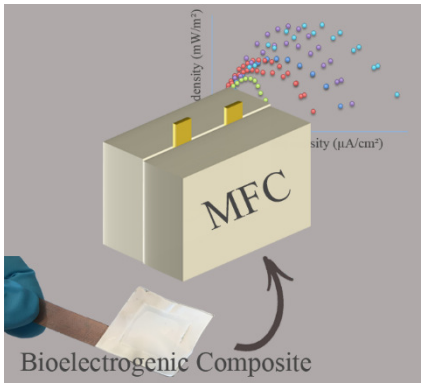

Integration of electrogenic microorganisms remains a challenge in biofuel cell technology. Here, synthetic biocomposites (‘artificial biofilms’) are proposed. Bacteria (*S. oneidensis*) are embedded in a hydrogel matrix (poly(vinyl alcohol)) *via* wet- and electro-spinning, creating fibers and non-woven gauzes. The bacteria remain viable and metabolically active. The

performance is compared to *S. oneidensis* suspension cultures and 'natural' biofilms. While lower than with the suspension cultures, the power output from the fuel cells with the artificial biofilms is higher than with the natural one. Handling, reproducibility, and stability are also better. Artificial biofilms could therefore contribute to resolving fundamental issues of design, scale up, and monosepsis in biofuel cell technology.

5.2 Introduction

Fuel cells continuously convert chemical into electrical energy. For this purpose an oxidation reaction at the anode is coupled to a reduction reaction at the cathode. The electrons released by the oxidation travel to the cathode via an external circuit and thereby become available for electrical work. The circuit is completed by the movement of charged molecules, often H^+, through an ion-selective barrier from the anode to the cathode space. A common set-up is the polymer electrolyte membrane fuel cell (PEM-FC), which burns hydrogen and oxygen and hence does not produce any hazardous waste[1]. Among the drawbacks of these systems are the need for comparatively high operating temperatures as well as the difficulties in providing and storing the hydrogen.[2,3] Since the 1990ies it has been recognized that the range of fuel cell technology can be considerably broadened, both in terms of chemical energy sources and operating conditions, when biological oxidation processes are exploited. Subsequently, both enzymatic and microbial fuel cells (MFCs) were described.[3-5]

The integration of the biological and the electrochemical processes is currently the major challenge in developing efficient biofuel cells. For continuous operation the biological component should be retained within the system. Enzymes can directly be immobilized onto the electrodes, but lack in stability. Microorganisms have the potential to regenerate themselves and may spontaneously attach to surfaces to form a so-called 'biofilm'. However, microorganisms typically do not leak catabolic electrons into their aqueous environment.

Instead chemical mediators are used and the first microbial fuel cells 'solved' the problem of electron transfer by supplying such mediators. However, most of the proposed mediators are costly and many are also toxic. Mass transfer limitations and overpotentials restrict the efficiency of the fuel cell, if too many electron transfer reactions are coupled. In consequence, the current densities provided by the first generation MFCs were in the low μA m^{-2} range.[3]

Research in MFC technology was boosted when starting in the early 2000s exoelectrogenic bacteria, such as *Shewanella* and *Geobacter spp.* were described, which were capable of transferring electrons to the electrodes without the need for any added mediator.[6-12] The mechanism, through which the electron transfer is achieved, is still under debate. The respiratory chain enzymes of some metal-reducing bacteria span the outer membrane and directly transfer electrons to external acceptors such as Fe (III) or Mn (IV) ions.[13] To such bacteria the anode of an MFC could presumably act as direct electron acceptor in the absence of oxygen (anaerobic conditions). However, the production of indigenous mediators has also been proposed [14]. Regardless of the actual mechanism of electron transfer, it is preferable that the electrogenic bacteria should grow directly on the anode. This will retain them in the system for continuous use, while electron transfer limitations are minimized. Bacteria that easily form biofilms are therefore attractive for MFC applications.[15] In 2003 the group of Bond and Lovley reported current densities of up to 65 mA m^{-2} in case of an MFC using *Geobacter sulfurreducens* attached to the electrode.[16]

Biofilms are ubiquitous in nature and form on any kind of surface. They are composed of microorganisms embedded in a hydrogel matrix formed by various extracellular polymeric substances (EPS) produced by the organisms themselves.[17] Natural biofilms tend to contain microbial communities rather than single species' and all natural biofilms require significant time to establish and mature.[18] Spontaneously formed, multi-species biofilms are the norm in bioelectricity generation from wastewater, due to their excellent long-term stability and robustness.[19] However, these are large-scale, low efficiency applications, characterized by

maximum power densities well below 20 mW m^{-2}. [20] Higher power densities and/or smaller units presumably could benefit from the use of selected highly active exoelectrogenic bacteria. Unfortunately, single-species biofilms are much less common in nature and significantly less stable than multi-species ones. Biofilms of *Shewanella oneidensis* MR-1 have been described to detach, whenever the oxygen content of the environment becomes low, i.e. precisely under conditions suitable for electricity production in the fuel cell.[21] Moreover, unless sterility of the system is strictly maintained, other organisms will sooner or later contaminate the single-species biofilm.

Over the last few years, some chemical immobilization strategies have been proposed as alternatives to natural biofilm formation in MFCs. The group of Luckarift fixed *S. oneidensis* MR-1 physisorbed on a graphite felt electrode *via* vapor deposition of tetramethylorthosilicate (TMOS) followed by sol-gel formation of a silica matrix.[15] With a similar aim, the group of Chen coated a biofilm pre-formed on the anode of the MFC with poly(vinyl alcohol).[22] Afterwards, the biofilm was shown to protect the bacteria against harsh environmental conditions such as pH values above 11 or ultrasonic vibrations. Analogous approaches involving other types of coatings can be imagined. However, all of these entail the initial deposition of the bacteria as such and often require the formation of a full natural biofilm as initial step.

We have recently proposed the concept of the 'artificial biofilm', i.e. biocomposites where the desired microorganisms are embedded into a synthetic hydrogel matrix of adjustable properties, originally for environmental applications.[23] Herein we propose that this concept can also be used to produce defined and highly reproducible biocomposites as anodes for MFCs, thereby overcoming current fundamental challenges in the integration of biological components into biofuel cells.

5.3. Experimental Section

5.3.1 Materials

Standard chemicals, culture media components, supplements, plastic materials, and culture flasks were from established suppliers and used as received. High quality water was prepared by a Millipore unit. Poly(vinyl alcohol), PVA, were *Clariant Mowiol 28-99* (M_w 145'000 g mol^{-1}, 99.4 ± 0.4 mol% hydrolysis) and PVA (M_w 128'000 to 186'000 g mol^{-1}, 87-89 mol% hydrolysis) both from Sigma Aldrich. Phosphate buffered saline (PBS) was prepared in house as follows: 8.0 g NaCl, 0.2 g KCl, 1.42 g Na_2HPO_4 and 0.24 g KH_2PO_4 per liter of Millipore-water, pH adjusted to 7.3 with 2 M NaOH, sterilized by autoclaving (121°C, 20 min). LB medium was prepared by weighting 25 g of LB-Powder (Carl Roth, Karlsruhe, Germany) in 1 L of Millipore-water, pH adjusted to 7.0, if necessary, and also sterilized by autoclaving. *Shewanella* basal medium (SB medium) was prepared in house as follows: 0.225 g K_2HPO_4, 0.225 g KH_2PO_4, 0.46 g NaCl, 0.225 g $(NH_4)_2SO_4$, 0.117 g $MgSO_4$ x 7 H_2O, 23.83 g HEPES and 1.802 g L-lactic acid per liter of Millipore-water, pH adjusted to 7.2 with 2 M NaOH and sterilized by autoclaving. Afterwards the medium was supplemented with 5 mL of a mineral mix (1.5 g nitrilotriaceticacid, 3 g $MgSO_4$ x 7 H_2O, 0.5 g $MnSO_4$ x 2 H_2O, 1 g NaCl, 0.1 g $FeSO_4$ x 7 H_2O, 0.183 g $CoCl_2$ x 6 H_2O, 0.1 g $CaCL_2$ x 2 H_2O, 0.13 g $ZnCl_2$, 0.01 g $CuSO_4$, 0.01 g $AlK(SO_4)_2$, 0.01 g H_3BO_3, 0.025 g Na_2MoO_4 x 2 H_2O, 0.027 g $NiCl_2$ x H_2O, and 0.025 g Na_2WO_4 x 2 H_2O per liter of Millipore-water) as well as with 1 mL of a vitamin mix (0.1 g biotin, 0.5 g pyridoxine HCl, 0.25 g thiamine HCl, 0.25 g riboflavin, 0.25 g nicotinic acid, 0.25 g pantothenic acid, 0.005 g cobalamin, 0.25 g 4-aminobenzoic acid, and 0.25 g thioctic acid, per liter of Millipore-water) and 10 mL of a folic acid stock solution (0.01 g L^{-1}). The mineral mix, vitamin mix and the folic acid stock solution were sterilized by sterile filtration (cellulose acetate syringe filter, 0.2 µm, VWR Collection, Radnor, PA).

5.3.2 Analytical Methods

For light microscopy a phase contrast microscope Olympus BX51 equipped with a 600x oil immersion objective UPlanFI, Olympus and camera CC-12, all from Olympus Soft Imaging Systems (Tokyo, Japan) was used. Software analysis package 3.2 (Build 883) from Olympus Soft Imaging Systems was used for treating and storing the pictures. The concentration of L-lactic acid was determined by the enzymatic L-lactic acid test-kit from r-biopharm, Darmstadt, Germany following the supplier's instructions. For viability testing, biocomposites were stained ('Life/Dead' stain) with the BacLight Bacterial Viability Kit from life technologies (Eugene, OR) according to the manufacturer's instructions using Syto9 (green, living bacteria) and propidium iodide (red, dead bacteria) as dyes. Stained biocomposites were subsequently analyzed by confocal microscopy (LSM510, Zeiss, Oberkochen, Germany). Biocomposites were in addition characterized by scanning electron microscopy (LEO 1530, also Zeiss). For this purpose, samples were attached to the holder with water-based conductive carbon glue and sputter coated with Pt (coat thickness: 1.3 nm, sputter coater: 208 HR from Cressington, Watford, England).

5.3.3 Microbiology

For initial built up of bacterial mass, 30 mL of LB medium were inoculated with *S. oneidensis* strain MR-1 (ATCC) from kryo stock and cultivated overnight in shake flasks at 30°C and 150 rpm in a Forma Orbital shaker (Thermo Fisher Scientific, Marietta, OH). The OD_{600} of the culture was determined photometrical (Biophotometer, Eppendorf, Hamburg, Germany), with an OD_{600} of 1 equaling 8.5×10^8 bacteria mL^{-1}. Bacteria from a volume corresponding to 4×10^{10} bacteria were harvested by centrifugation (10 min, 1200 *g*), followed by two washes with PBS. Afterwards, the bacteria were either integrated into biocomposites, see below, or cultured in planktonic form (starting OD_{600}: 0.1, i.e. 8.5×10^7 bacteria mL^{-1}) in shake flasks (30 mL SB medium) under aerobic or anaerobic conditions as indicated. To establish anaerobic conditions,

the medium was sparged with nitrogen for 20 minutes prior to inoculation and the culture flask sealed with a turnover flange stopper. To obtain a natural biofilm of *S. oneidensis*, a 2 x 2 cm piece of the MFC electrode material (graphite-woven ELAT 1400, ElectroChem, Woburn, MA) was suspended in a planktonic shake flask culture of *S. oneidensis* for 120 h. Afterwards the graphite-woven with the established biofilm was directly inserted into the MFC.

5.3.4 Biocomposite preparation

For biocomposite preparation the necessary amount of bacteria was recovered by centrifugation from an exponentially growing culture and resuspended at a final concentration of 2 x 10^9 bacteria mL^{-1} in the indicated 10 wt% PVA-solution in sterile PBS. The mixture was stirred with a magnetic stirrer (RH basic, IKA, Staufen, Germany) at 150 rpm for 1 hour to obtain a homogenous suspension. For wet-spinning *Clariant Mowiol 28-99* PVA (M_w 145'000 g mol^{-1}, 99.4 % hydrolysis) was used. 2 mL of the suspension were filled into a 5 mL syringe (0.8 x 120 mm cannula) connected by an adapter to a compressed air hose. Biocomposite fibers were produced by steadily pressing (0.5 bar) the suspension through the cannula into an acetone bath for hardening. The resulting PVA/bacterial composite fibers were collected on 6 x 2 cm metal frames and stored over-night at 4 °C. PPX coating, see below, was done the next day. For the preparation of the non-woven biocomposites a PVA (10 wt% solution in sterile PBS) with a lower degree of hydrolysis was used (M_w: 128,000 – 186,000 g mol^{-1}, 87 – 89 % hydrolysis). Four syringes (0.9 x 40 mm cannula), each filled with 2 mL of suspension, were integrated into a homemade electro-spinning apparatus. The collector electrode (rotary plate) of the apparatus was covered with a 4 x 4 cm stainless steel mesh (325 mesh size, material 1.4432 V4A / 316L, Zivipf, Treuchtlingen, Germany) and placed at a distance of 15 cm from the syringes. The collector electrode and the syringe cannula were connected to the power supply and voltages of – 5 kV and +23 kV were applied causing the deposition of hydrogel nanofibers onto the steel mesh. The preparation of a nonwoven biocomposite gauze required 3 to 4 h. In addition,

PVA/bacteria-nonwovens were also prepared on a copper mesh (99% purity, 100 mesh size, AlfaAesar, Karlsruhe, Germany) instead of the steel mesh using otherwise identical conditions. Nonwovens were stored over night at 4°C, prior to PPX coating, see below, the next day. PPX-coating of the biocomposites (fibers, nonwovens) was by chemical vapor deposition (Labcoater®1 Parylene Deposition Unit Model PDS 2010, SCS, Indianapolis, IN) using [2.2]paracyclophane as a precursor. PPX was deposited at 20 °C and 40-50 mbar, the evaporation of the precursor took place at 150 °C and the following pyrolysis at 650 °C. Unless indicated otherwise, the coating time was 6 h and resulted in a coating thickness of approximately 600 nm. In case of the biocomposites prepared on the copper mesh, the coating thickness was approximately 350 to 400 nm. Biocomposites without bacteria (fibers, nonwovens) were prepared as negative controls under otherwise identical conditions.

5.3.5 Cultivation of biocomposites

For cultivation, nonwovens (2 x 2 cm pieces, cut under sterile conditions from the 4 x 4 cm gauzes) were peeled from the steel mesh support and suspended in 30 mL of medium in shake flasks, similar to the planktonic cultures (see above). Fibers were cultivated on the metal frames using 150 mL of medium and otherwise identical conditions. Plates for agar plate cultures were prepared according to standard laboratory protocols with 15 g L^{-1} agar-agar and SB medium. 2 x 1.5 cm cut outs from the nonwovens were put on the agar plate. The plates were incubated for 72 h at 30°C in a standard incubator (BD240, Binder, Tuttlingen, Germany).

5.3.6 Microbial fuel cell (MFC)

The set-up of the two chamber MFC is shown in Figure **5.1**. A 2 x 2 cm graphite-woven (ELAT 1400, ElectroChem, Woburn, MA) in contact with a graphite conductor was used as cathode. In the experiments involving planktonic cultures and natural biofilms of *S. oneidensis* the anode was also a 2 x 2 cm graphite-woven in contact with a graphite conductor. In case of the artificial

biofilms, the PPX-coated biocomposites (2 x 2 cm) were peeled off the steel mesh and inserted to replace the graphite-woven into the MFC (in direct contact with the graphite conductor).

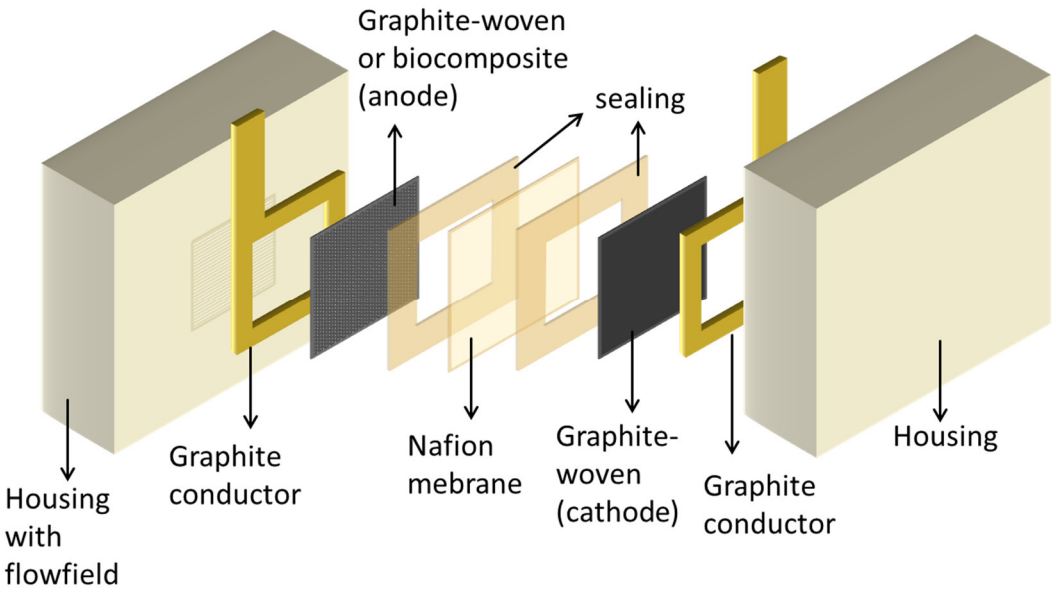

Figure 5.1. Set-Up of the microbial fuel cell.

Alternatively, the nonwoven biocomposites prepared on the copper mesh were used as a whole; in this case replacing both the graphite-woven *and* the graphite conductor of the standard MFC set up. A proton-selective Nafion membrane (117, Dupont, Wilmington, DE) was placed between anode and cathode. On the cathode side oxygen was supplied as final electron accepter *via* an air stream (3 NL min^{-1}). During operation, 300 mL of SB medium (or bacteria suspension) were recirculated by peristaltic pump (25 mL h^{-1}) through the anode chamber. To assure anaerobic conditions, the medium in was continuously sparged with nitrogen. Potentials were maintained using either the one-channel potentiostat IM6e from Zahner (Kronach, Germany) or the multi-channel potentiostat VMP3 from BioLogic Science Instruments (Claix, France) as indicated. The Software Thales 4.0 (Zahner) was used to control the Zahner potentiostat, the potentiostat from BioLogic was controlled by the Ec-lab software also from BioLogic. Power outputs of the MFC were taken at 24 hours intervals. Each measurement was

repeated 3 times for reproducibility. Power (P) was calculated by P = U x I and normalized by the anode area.

5.4 Results and Discussion

5.4.1 Preparation of the biocomposites

Biocomposite fibers of *S. oneidensis* MR-1 embedded in PVA (2 x 10^9 cells mL^{-1}) were prepared by wet-spinning. The fibers had an average diameter of 100 µm (± 25 µm), as determined by electron microscopy, and a length of approximately 2.5 m. As part of the wet-spinning protocol, the fibers were passed through an acetone bath for hardening (contact time 3 to 5 s). Afterwards the fibers were first stored over night at 4°C and then coated with PPX (coating thickness 0.5 to 1 µm) to stabilize them in aqueous solution, where PVA would otherwise dissolve. Coating takes up to 6 hours, during which the fibers are dry and no nutrients are supplied to the organisms.

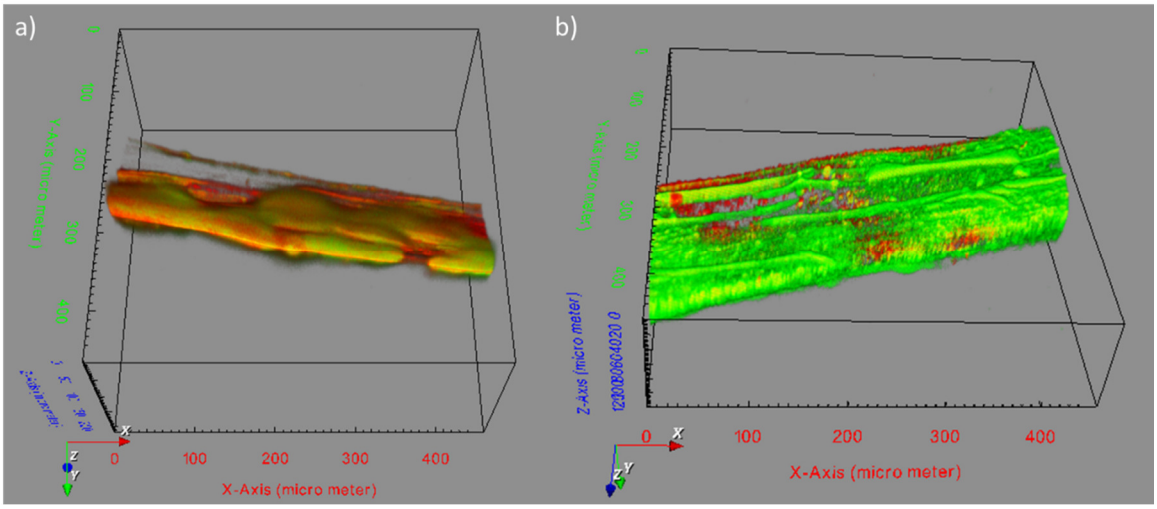

Figure 5.2. Life Dead stain of biocomposite fibers a) directly after spinning / coating, b) after 7 d in culture (shake flask, 150 mL LB medium, aerobic conditions).

Neither the contact with the toxic acetone nor the long coating procedure caused significant damage to the embedded bacteria. To demonstrate this, fibers were stained with the Life Dead stain. Directly after spinning / coating a thin layer of dead bacteria was found close to the surface (red color, indicating dead cells), the majority of the cells was alive (areas stained in green), Figure 5.2a. When the fibers were reexamined after several days in culture (shake flasks, 150 ml LB medium, aerobic conditions), the regions close to the fiber surface had been re-settled by life bacteria, Figure 5.2b. At this point, red areas indicative of dead bacteria were seen mainly at points where fibers crossed or were in direct contact with the holder. It cannot be excluded that bacteria in these spots were less well supplied with nutrients and/or oxygen. If this were the case, it may have consequences for the preparation of woven tissues from the biocomposite fibers.

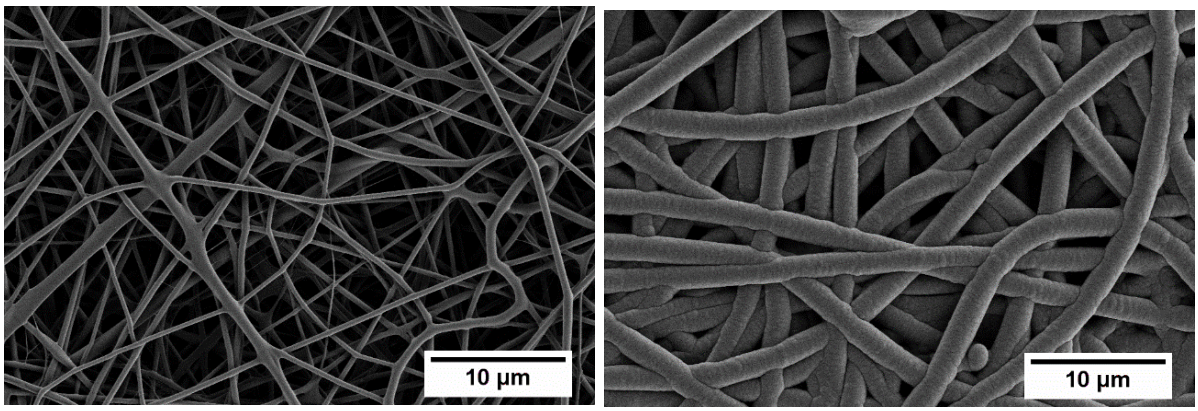

Figure 5.3. SEM images of biocomposite nonwovens, left: before and right: after PPX coating. Thickness distributions discussed in the text were determined with the software ImageJ from the SEM data.

While the fibers would still require weaving to produce a two-dimensional tissue, the electro-spinning process directly produces a two-dimensional material (nonwoven gauze). Such materials are characterized by high surface areas and little resistance to liquid transfer, while electro-spinning can easily be scaled up to the multi m^2 scale as previously shown.[24] This

would inter alia resolve the issue of electrode scale up in MFC technology. Average fiber diameters in the electro-spun material produced in this study were 450 nm (± 140 nm), a value that increased to approximately 1.7 µm (± 0.25 µm) after PPX coating, Figure 5.3. A different PVA, namely one with a lower degree of hydrolysis, had to be used in the electro-spinning procedure, since the PVA with a > 99% degree of hydrolysis used for wet-spinning did not result in the formation of depositable microfibers. In our opinion this is due to an increase in viscosity, possibly caused by physical interactions (cross-linkage) between the hydroxyl-groups of the PVA and ions from the buffer-system. In the Life Dead stain, areas of dead cells were observed close to the surface of the gauzes directly after electro-spinning / coating, whereas after 7 days in culture (30 mL SB medium, aerobic conditions) all electro-spun biocomposites showed a strong green color indicative of a high density of living bacteria in spite of the pronounced degree of fiber crossing, Figure 5.4.

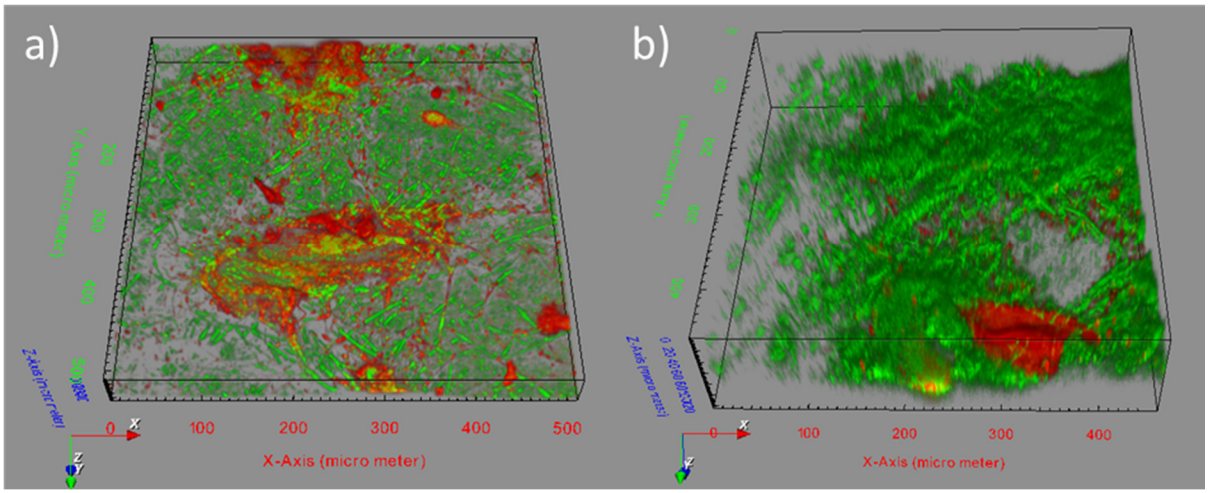

Figure 5.4. Live Dead stain of a biocomposite nonwoven a) directly after spinning / coating, b) after 7 days in culture (shake flask, 30 mL SB medium, aerobic conditions)

This rises questions of how well the bacteria are supported in the biocomposites and of the main mass transfer limitations. The PPX coating is of similar thickness in both types of biocomposite. We know from previous work that with increasing thickness the PPX-coating represents a more and more important barrier to diffusional mass transfer, e.g. of nutrients and metabolites.[23] The thickness of the coating can be adjusted *via* the duration of the coating procedure and a coating thickness of less than 1 µm, as adjusted here, typically does not present a significant resistance. The diameter of the hydrogel core in the electro-spun nanofibers was more than a 100-fold smaller than in the wet-spun fibers. This should improve the nutrient supply of the embedded cells in particular those close to the center and may explain the better vitality of the bacteria at the points of fiber crossing in the electro-spun material.

As a final demonstration of bacterial fitness, 2 x 1.5 cm cuttings were prepared under sterile conditions from standard 2 x 2 cm nonwovens and placed on a solid SB medium agar plate. Bacteria were found to grow out from the gauze, thus demonstrating viability (organisms identified as *S. oneidensis* by microscopic observation). However, outgrowth was observed only from the edges, where the gauze had been cut, i.e. where the PPX shell had been damaged. No such outgrowth was observed from areas with intact PPX coating. By inference, it can be assumed that an intact PPX shell would in a similar manner also prevent ingrowth of contaminating bacteria into the synthetic biofilm, thereby facilitating the operation of a single species MFC under non-sterile conditions.

5.4.2 Metabolic activity of the biocomposites

S. oneidensis spp. are able to use L-lactate as carbon source,[25] and lactate consumption has been proposed as means to quantify their metabolic activity.[26] After transformation into pyruvate, the further processing follows standard metabolic pathways (citric acid cycle, oxidative phosphorylation) using oxygen as final electron acceptor. Alternatively, in the near absence of oxygen, metal ions may apparently also function as electron acceptors. [27] In

addition, a linkage to the C1 metabolism has been proposed by the group of Luo, which has mainly electrogenic purposes.[25]

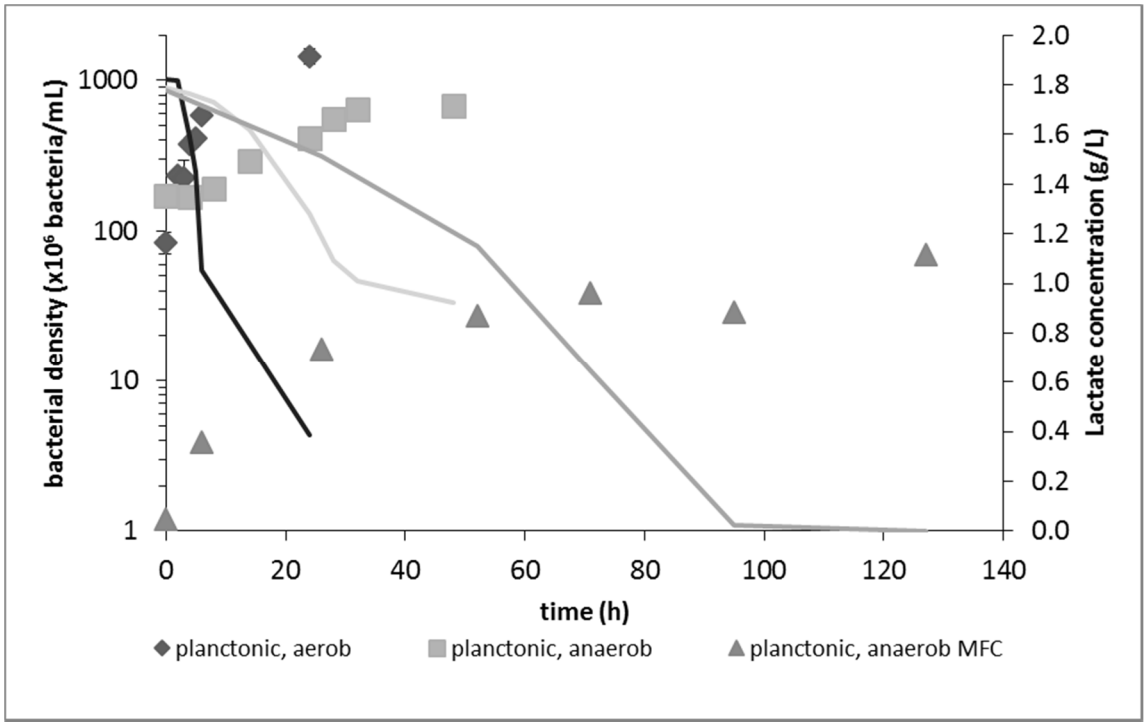

Figure 5.5. Bacterial densities and lactate concentrations in shake flask and MFC cultures of planktonic *S. oneidensis*. Symbols correspond to bacterial densities, lines serve a guide to the eye and connect lactate concentrations.

Figure 5.5 summarizes bacterial densities and lactate concentrations in shake flask cultures (SB medium, initial lactate concentration 1.8 g L^{-1}) of planktonic *S. oneidensis* MR-1 under aerobic and anaerobic conditions. Bacterial densities and lactate concentrations determined in an MFC operated under standard conditions with planktonic cultures of *S. oneidensis* MR-1 are also included in that figure. Under standard conditions MFCs are operated *an*aerobically to enforce the bacteria to use the anode as metabolic sink for the electrons. Lactate consumption data were in addition determined for both types of biocomposite (fibers: 2.65 m x 100 µm, gauzes: 2 x 2 cm) cultivated under aerobic conditions in the shake flask. A determination of the bacterial density within a given biocomposite is at present not possible. Exclusively for the biocomposite

gauzes, lactate consumption data were established for *an*aerobic shake flask cultures and under standard operating conditions in the MFC. Biocomposite fibers can at present not be integrated into the MFC. 'Empty' biocomposites containing no bacteria served as negative controls. Total lactate consumption rates (mg h^{-1}) calculated for the investigated cultures are given in Table 5.1.

Table 5.1. Lactate consumption in the different cultures

		State of the bacteria	Lactate consumption (mg h^{-1})
shake flasks	aerobic	planktonic	6.45 ± 1.95
		fiber	0.12 ± 0,04
		nonwoven	0.19 ± 0.03
		control (fibers, gauzes)	b.d.l.
	anaerobic	planktonic	0.88 ± 0.19
		nonwoven	0.22 ± 0.01
		control (gauzes)	b.d.l.
MFC	anaerobic	planktonic	5.83 ± 0.39
		biofilm (natural)*	6.17
		nonwoven	2.00 ± 0.22
		nonwoven on copper	4.79 ± 0.59
		control (gauzes)	b.d.l.

b.d.l.: below the detection limit, *best value given

Under aerobic conditions in the shake flask, planktonic cultures of S. *oneidensis MR-1* (μ_{max}: 0.325 h^{-1}) showed a total lactate consumption rate of 6.45 ± 1.95 mg h^{-1}. This compares

well with values determined by others, e.g. the 2.6 mM h^{-1} reported by the group of Tang[28] and corresponds to a specific maximum lactate consumption rate of 2.85 mg h^{-1} 10^{-8} cells. If one assumes a similar or a slightly reduced specific lactate consumption rate for the embedded bacteria in the biocomposites, the 0.12 ± 0.04 mg h^{-1} and 0.19 ± 0.03 mg h^{-1} lactate consumption measured in the aerobic shake flask cultures of the biocomposites, correspond to an activity of 5 x 10^6 bacteria in case of the fibers and of roughly 6 x 10^6 cells for the gauze. A wet-spun fiber with a length of 265 cm and a diameter of 0.01 cm has a volume of 21 µL. In view of the 2 x 10^9 bacteria per mL adjusted during spinning and the observed overall lactate consumption, this would mean that only 12 % of the bacteria in the fiber are metabolically active. A determination of the volume of the gauze is at present not possible. However, based on the volume processed during spinning, the volumes of the biocomposites prepared by wet- and electro-spinning should be similar. Using similar reasoning, the observed metabolic activity of the gauzes can be correlated to a vitality of 15 %. This is low, both in view of biocomposites prepared in the past[23] and in particular since the Life Death stain had not given any indication of massive cellular death during biocomposite preparation.

When planktonic *S. oneidensis* were subsequently cultured under *an*aerobic conditions in the shake flask, both the maximum specific lactate consumption rate (0.35 mg h^{-1} 10^{-8} cells) and the maximum specific growth rate (μ_{max}: 0.05 h^{-1}) declined by an order of magnitude. This is not surprising, since under *an*aerobic conditions in the shake flask, the bacteria have no suitable acceptor for their metabolic electrons. The metal ion concentration in the SB medium is not high enough for this purpose. The nonwoven biocomposite, on the other hand, showed no corresponding reduction in lactate consumption under anaerobic compared to aerobic culture conditions, Table 5.1. If anything a slightly higher total lactate consumption rate is observed in the *an*aerobic shake flask cultivations. Moreover, if biocomposite vitalities are calculated for *an*aerobic conditions based on the specific lactate consumption rates of the corresponding planktonic *Shewanella* cultures, values close to 100 % are found. We therefore hypothesize that

the low, but similar lactate consumption rates found in case of the biocomposites under aerobic and anaerobic conditions can be explained by the assumption that even in the formally aerobic cultures the bacteria in the synthetic biofilm were already operating under oxygen limitation. In consequence, the low biological activity of the biocomposites found above under aerobic conditions is not due to low vitality, but rather to the lack of a suitable electron acceptor.

This hypothesis was corroborated when lactate consumption was quantified in the MFC under operating conditions. The results are also listed in Table 5.1. In this set of experiments, the performance of the planktonic *Shewanella* culture was also compared to that of a natural *Shewanella* biofilm, pre-grown under aerobic conditions on the graphite anode by incubating pieces of the corresponding graphite woven in *Shewanella* shake flask cultures. No natural biofilms could be produced in strictly *an*aerobic shake flask cultures. In the MFC the performance of the planktonic culture and the natural biofilm were similar. In fact, conditions in both experiments approached each other with time, as the planktonic culture produced a biofilm similar to the pre-grown one, while the OD_{600} in the recirculating medium of the MFC containing the pre-grown biofilm increased. For both cultures, total lactate consumption rates were in the same range as in aerobic planktonic shake flask cultivations, the same was the case for the maximum specific growth rate (μ_{max}: 0.575 h^{-1}) in the planktonic MFC culture. The anode in the fuel cell thus showed a similar electron acceptor quality as molecular oxygen. In these experiments 300 mL of suspension were continuously pumped through the MFC. This creates two different environments, anaerobic conditions without an electron acceptor in > 99% of the culture volume and the possibility to transfer electrons to the anode within the MFC (volume of the flow field < 1 mL). In addition a biofilm was forming on the anode. We therefore refrained from calculating specific lactate consumption rates for these experiments.

In case of the biocomposites the lactate consumption measured in the MFC experiments, was at least an order of magnitude higher than in any of the shake flask experiments and for the first time approached that of the planktonic cultures. This supports our hypothesis that the

comparatively low metabolic activity of the biocomposites in the aerobic shake flask cultures was due to limited access to oxygen as final electron acceptor. Moreover, when the MFC anode (graphite woven plus graphite conductor) was completely replaced by a biocomposite electro-spun on a copper mesh as conductor, the lactate consumption was yet two and a half fold higher than in the experiments were a simple biocomposite replaced just the graphite woven. In fact, lactate consumption in the MFC operated with a biocomposite-on-copper anode was fully comparable to that of an MFC operated with a planktonic *S. oneidensis* culture. Presumably both the better electron acceptor quality of the copper conductor and the slightly reduced thickness of the PPX coating contributed to this result.

Finally, it should be noted that no lactate consumption whatsoever was observed for any of the controls containing no bacteria. This indicates that the embedded bacteria in the 'artificial biofilms' are indeed biologically active and responsible for the observed conversions.

5.4.3 Performance of the bioelectrogenic composites as anodes in the MFC

The experimental set up to evaluate the electrical performance of the various *Shewanella* cultures in the MFC was identical to the one used in the MFC / lactate consumption experiments. In particular, the performance of the biocomposites (standard nonwoven and copper supported nonwoven) was compared to that of planktonic cultures of *S. oneidensis MR-1*, but also to that of naturally grown S. *oneidensis MR-1* biofilms. Nonwovens without bacteria served again as negative controls. All experiments were performed under anaerobic conditions in SB medium. Figure 5.6 shows the polarization curves as well as the power density curves recorded for the artificial biofilm (standard nonwoven) as function of the operating time.

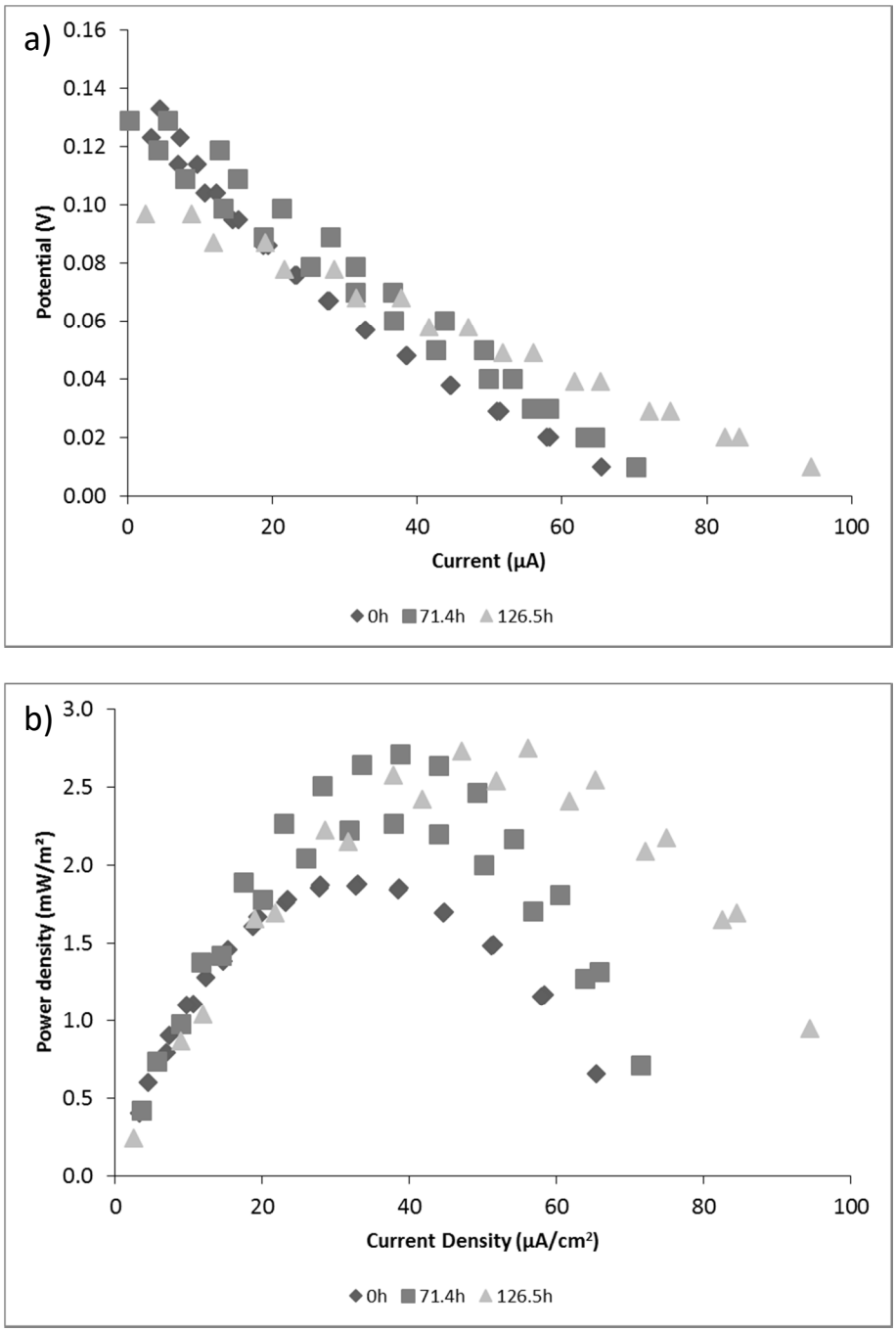

Figure 5.6. a) polarization curves and b) power densities recorded by the Zahner potentiostat for the MFC operated with an artificial biofilm (standard nonwoven)

Table 5.2. Comparison of the power densities measured for MFCs using the indicated means to integrate *S. oneidensis MR-1*.

State of the bacteria	Power density (mW m^{-2})
control	0.04
planctonic cells	104 ± 14.1
biofilm (natural)	30
nonwoven	2.5 ± 0.5
nonwoven on copper	64.7 ± 19.4

With cultivation time the current increased and reached a maximum value of 37.8 µA, corresponding to a current density of 94.4 mA m^{-2} after 126 hours. The control ('empty' gauze) reached a maximum value of only 1.9 mA m^{-2}. The measured current density can therefore be ascribed to the metabolic activity of the bacteria. During operation / cultivation, a maximum power density of 2.5 ± 0.5 mW m^{-2} was reached in the MFC operated with the standard biocomposite, Table 5.2. By comparison, the maximum power density of the MFC continuously operated with a planktonic *S. oneidensis* culture was 104 ± 14.1 mW m^{-2}, Table 5.2. The maximum power density was reached after 52 hours in this case and did not increase any further throughout the remainder of the cultivation (130 h). The same was true for the bacterial density, which also stabilized after roughly 50 h of cultivation, Figure 5-5. Interestingly, power in the range of 110 mW m^{-2} was still provided by the MFC, when lactate had already been completely consumed after 96 h, Figure 5.5. No explanation can at present be given. However, since bacterial densities were in steady state at that time, consumption of dead bacteria may have taken place.

With ca. 104 ± 14.1 mW m^{-2} the power output for the planktonic culture is in the same order of magnitude as values obtained, e.g., by the group of Wu, who reported 73.9 mW m^{-2} for an MFC operated with planktonic *S. oneidensis* in the absence of any mediators.[29] However, while

operating the MFC with a planktonic culture is straightforward in case of a closed loop, using a similar approach, e.g., for continuous processing of wastewater would be impossible, since this would mean to continuously add the bacteria to the MFC, while preventing other microorganisms from entering.

Attempts to operate the MFC with a natural *Shewanella* biofilm were not met with success in our case. When the anodes with the biofilms pre-formed under aerobic conditions were integrated into the MFC, some bioelectrogenic activity could be seen, albeit at a lower level than with the planktonic cultures. The obtainable maximum power density increased during the first 50 h, reaching values of up to 30 mW m^{-2} after 48 h in the best cases. Reproducibility was an issue in case of the natural biofilms, where in about 50 % of the experiments no electrogenic material was obtained. In general operating the MFC with a preformed biofilm was difficult and stable performance was seen in less than 30% of the experiments. Moreover, while performance stabilized close to the maximum value for the reminder of the experiment in case of the planktonic culture, this was not the case for the natural biofilm, where the power density decreased rapidly to only 0.17 mW m^{-2} after 120 h, when the experiment was terminated.

With approximately 2.5 ± 0.5 mW m^{-2}, the maximum output from the MFC operated with a standard artificial biofilm was yet below that of the natural biofilm. However, the performance was stable and reproducibly obtained. We did not observe significant outgrowth of *S. oneidensis* bacteria from the biocomposite into the circulating culture medium throughout the experiment (OD_{600} < 0.01) and more importantly, the MFC could be operated under non-sterile conditions without significant overgrowth of the *S. oneidensis* population in the system by contaminating bacteria.

When the MFC was operated with an artificial biofilm directly prepared on the copper conductor, the maximum power density increased to 64.7 ± 19.4 mW m^{-2}, Table 5.2, which is twice as high as for the best natural biofilms. Moreover, compared to the natural biofilm, the maximum power density was reached after 24 h instead of 50 h and was stable thereafter. The

difference in performance between the standard and the copper based artificial biofilm is even more pronounced in regard to current / power density than in regard to the lactate consumption experiments discussed above. Again the better electron acceptor quality of the copper conductor, but also the slightly reduced thickness of the PPX shell may contribute to this phenomenon.

5.5 Conclusions

Single-species biocomposite anodes with defined chemical and biological properties constitute a major advantage for the design of robust MFCs. Here such biocomposites were produced with *S. oneidensis*, but the approach could be extended to other bioelectrogenic species. The biocomposite anodes were produced as electro-spun nonwovens. The bacteria inside the artificial biofilm were alive and metabolic active both in terms of lactate degradation and production of electricity in the MFC. Artificial biofilms can be produced on demand and, if necessary, at large scale, since electro-spinning can easily be scaled to the multi m^2-range. Contamination of the biocomposite by other microorganisms is unlikely under operating conditions, thereby removing the need for sterile operation in case of single-species MFCs.

5.6 Appendix/Nomenclature/Abbreviations

Acknowledgements: The bacteria strain *S. oneidensis MR-1* was kindly made available to us by Dirk Holtmann from the DECHEMA Forschungsinstitut, Frankfurt, Germany. PK, SR, AG, and RF thank the Bavarian State Ministry of the Environment and Consumer Protection for financial funding of this work within the BayBiotech program.

Received: Month XX, XXXX; Revised: Month XX, XXXX; Published online

Conflict of interest statement: The authors declare no conflict of interest.

Keywords: biological application of polymers, electro-spinning, fibers, hydrogels, Shewanella oneidensis

5.7 References

[1] V. Mehta, J.S. Cooper, *Journal of Power Sources*, 2003, 114(1), 32-53

[2] J. Larminie, A. Dicks: Fuel cell systems explained, Wiley VCH, Weinheim **2000**

[3] R.A. Bullen, T.C. Arnot, J.B. Lakeman, F.C. Walsh, *Biosensors and Bioelectronics* **2006**, 21, 2015–2045

[4] F. Davis, S.P.J. Higson, *Biosensors and Bioelectronics* **2007**, 22, 1224-1235

[5] A. Ramanavicius, A. Kausaite, A. Tamanaviciene, *Biosensors and Bioelectronics* **2008**, 24, 761-766

[6] H. Liu, S. Grot, B.E. Logan, *Environ. Sci. Technol*. **2004**, 38, 2281-2285

[7] G.C. Gil, I.S. Chang, B.H. Kim, M. Kim, J.K. Jang, H.S. Park, H.J. Kim, *Biosensors and Bioelectronics* **2003**,18(4), 327-334

[8] J.H. Kim, M.S. Hyun, I.S. Chang, B.H. Kim, *J Microbiol Biotechnol* **1999**, 9, 365-367

[9] C.A. Pham, S.J. Jung, N.T. Phung, J. Lee, I.S. Chang, B.H. Kim, H. Yi, J. Chun, *FEMS Microbiol Lett.* 2003, 223(1), 129-34

[10] B.E. Logan, J.M. Regan, *Trends Microbiol* **2006**, 14, 512-518

[11] Y.A. Gorby, S. Yanina, J.S. Malean, *PNAS* **2006**, 103, 11358-11363

[12] G.J. Newton, S. Mori, R. Nakamura, K. Hashimoto, K. Watanabe, *Appl Environ Microbiol*. **2009**, 75 (24), 7674–7681,

[13] A. Kouzuma, T. Kasai, A. Hirose, K. *Front. Microbiol*. **2015,** 6, 609

[14] B.E. Logan, *Nature Reviews Microbiology*, **2009**, 7, 375-381

[15] H.R. Luckarift, S.R. Sizemore, J. Roy, C. Lau, G. Gupta, P. Atanassov, G.R. Johnson, *Chem. Commun.* **2010**, **46**, 6048-6050

[16] D.R. Bond, D.R. Lovley, *Appl Environ Microbiol* **2003**, 69(3), 1548-1555

[17] G. O´Toole, H.B. Kaplan, K. Roberto, *Annu. Rev. Microbiol.* **2000**, 54, 49-79

[18] J.R. Kim, B. Min, B.E. Logan, *Appl. Microbiol. Biotechnol*. **2005**, 68, 23–30

[19] B. Zhang, H. Zhao, S. Zhou, C. Shi, C. Wang, J. Ni, *Bioresource Technol*. **2009**, 100(23), 5687-5693

[20] W.W. Li., H.Q. Yu and Z. He, *Energy Environ. Sci*., **2014**, 7, 911-924

[21] K.M. Thormann, R.M. Saville, S. Shukla and A.M. Spormann, *J. Bacteriol.* **2005**, 187(3), 1014-1021

[22] S. Chen, F. Yang, C. Li, S. Zheng, H. Zhang, M. Li, H. Yao, F. Zhao, H. Hou, *J. Mater. Chem. B*, **2015**, 3, 4641-4646

[23] C. Knierim, M. Enzeroth, P. Kaiser, C. Dams, D. Nette, A. Seubert, A. Klingl, C.L. Greenblatt, V. Jérôme, S. Agarwal, R. Freitag, A. Greiner, *Macromol. Biosci.* **2015**, 15(8), 1052-1059

[24] A. Greiner, J.H. Wendorff, *Angew. Chem. Int*. **2007**, 46, 5670–5703

[25] S. Luo, W. Guo, K.H. Nealson, X. Feng, Z. He, *Sci Rep* **2016**, 6, 20941

[26] B.R. Ringeisen, E. Henderson, P.K. Wu, J. Pietron, R. Ray, B. Little, J.C. Biffinger, J.M. Jones-Meehan, *Environ.Sci.Technol*. **2006**, 40(8), 2629-2634

[27] H.J. Kim, H.S. Park, M.S. Hyun, I.S. Chang, M. Kim, B. H. Kim, *Enzyme and Microbial Technology* **2002**, 30, 145–152

[28] Y.J. Tang, A.L. Meadows, J.D. Keasling, *Biotechnol. Bioeng*. **2007**, 96, 125–133

[29] D. Wu, D. Xing, L. Lu, M. Wie, B. Liu, N. Ren, *Bioresource Technology* **2013**, 135, 630-634

6. Polymer/Living Bacteria Capsules Spray Dried at High Temperatures

To be submitted (non final version)

Steffen Reich[1], Patrick Kaiser[2], Holger Schmalz[1], Daniel Rhinow[3], Ruth Freitag[2] and Andreas Greiner[1]

[1]Chair of Macromolecular Chemistry II and Bavarian Polymer Institute, University of Bayreuth, D-95440 Bayreuth, Germany

[2]Chair for process biotechnology, University of Bayreuth, D-95447 Bayreuth, Germany

[3]Department of Structural Biology, Max Planck Institute of Biophysics, D-60438 Frankfurt am Main, Germany

6.1 Abstract

Living *Micrococcus luteus* (*M.luteus*) and *Escherichia coli* (*E.coli*) were encapsulated in poly(vinyl alcohol) (PVA), poly(vinyl pyrrolidone) (PVP), hydroxypropyl cellulose (HPC) and gelatin by high temperature spray drying. The bacteria survived the spray drying process at temperatures of 150 °C (*M.luteus*) and 120 °C (*E.coli*), while short contact times were adjusted. Raman-AFM-spectroscopy and transmission electron microscopy (TEM) measurements indicates encapsulated bacteria in hollow polymer capsules. The polymer bacteria capsules were successfully used in standard polymer solution processing techniques such as electrospinning to aligned water-insoluble polyacrylonitrile (PAN), thermoplastic polyurethane (TPU), polystyrene (PS), poly(methyl methacrylate) (PMMA) and poly(vinyl butyrate) (PVB) nanofiber nonwovens.

6.2 Introduction

Encapsulation of living bacteria in polymer systems such as particles,[1,2] microfibers,[3] and nanofibers[4–6] is important for the exploitation of their functions. Encapsulation techniques have their major reason in protection of sensitive additives of the surrounding environment such as temperature, moisture, solvents, interaction with other materials and UV irradiation or the controlled release of the core material.[7] The challenge for the preparation of water-insoluble polymer nanofibers containing bacteria, is the use of hostile solvents in the fiber production which destroy the bacteria. Therefore, the encapsulation of bacteria is inevitable. Methods, such as emulsion, dispersion, spray drying and electrospinning setups are known for the encapsulation of bacteria. Inconveniently, emulsion or dispersion techniques require high amounts of processing solutions and lots of purification steps.[1,8] Fortunately, spray drying is a well-known method for the production of high amount of polymer capsules containing additives which are sensitive, fluid or alive.[2,7,9] These water soluble polymer capsules have to be processed to water-insoluble polymer composites to find multifarious applications in bioremediation, in microbial fuel cells, in synthesis of fine chemicals or in catalysis.

Previously, we reported on the encapsulation of living *M.luteus*, *E.coli* and *S.oneidensis MR-1* in hydrophilic polymer (e.g. poly(ethylene oxide) (PEO), PVA) nanofibers,[4,6] wet fibers[3] and particles.[1] These structures were coated with hydrophobic polymers[1,3,4,8] (e.g. PMMA, poly(p-xylylene) (PPX)) shell to prevent the release of the bacteria to the environment and protect the bacteria against pH, temperature or toxic chemicals and find their application in bioremediation and in microbial fuel cells. Due to these results, the development of novel biohybrid polymer nonwovens is of interest where interaction of different bacteria are required.[10] The combination of different species of microorganism in water-insoluble polymer fiber nonwoven will be processed easily, when bacteria capsules can be stored for a long time and including one species of microorganism. Herein, we demonstrate the encapsulation of living *M.luteus* and *E.coli* in PVA, PVP, HPC and gelatin capsules. Raman spectroscopy and

TEM images indicate the hollow polymer capsule structure and the location of the bacteria inside these polymer capsules. The viability of *M.luteus* and *E.coli* in the polymer capsules was verified with an agarplate test where living bacteria were determined. The polymer/bacteria capsules were electrospun to water-insoluble poly(vinyl acetate) (PVAc), PVB, PAN, PS and PMMA nanofibers by electrospinning.

As schematically shown in **Sheme 6.1**, bacteria were first encapsulated in polymer microcapsules (PVA, PVP, HPC and gelatin). After spray drying, dry and hollow polymer capsules containing bacteria were ready for standard processing methods such as electrospinning. Hydrophobic polymer nonwovens were reached by electrospinning. Here a dispersion of polymer capsules including bacteria, hydrophobic polymer and toxic solvents were processed to water-insoluble polymer nanofibers.

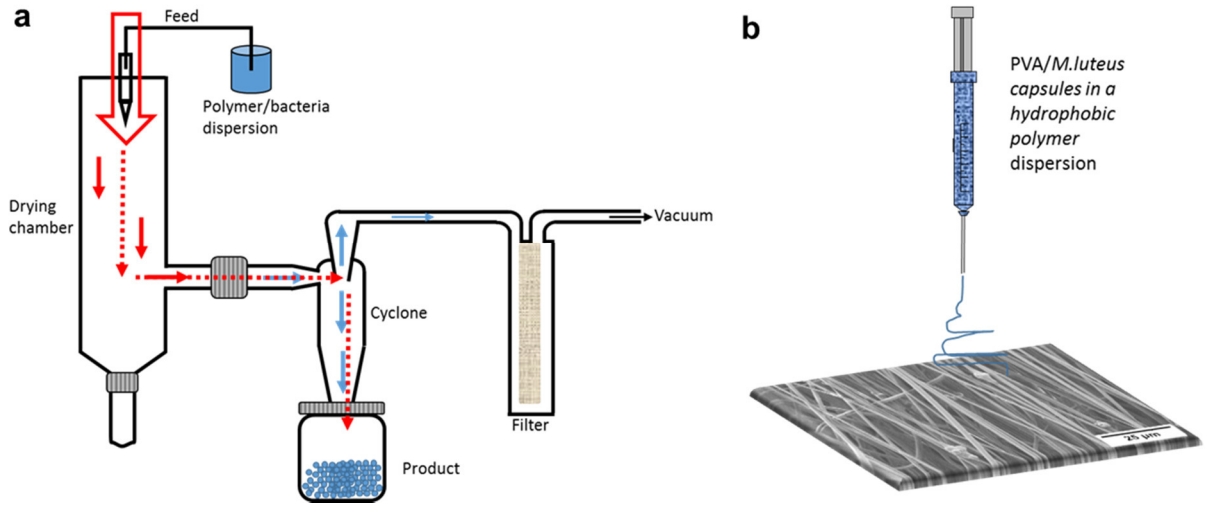

Sheme 6.1. Sheme for the preparation of the spray dried polymer bacteria capsules in aligned electrospun nanofibers. a) Spray drying procedure and b) Electrospinning

6.2 Results and Discussion

Micrococcus luteus (M.luteus) is a well-known aerobic, gram-positive and catalase-positive bacteria. It is a member of the *Acetinobacteria* and shows a high GC-concentration in its DNA. The *M.luteus* is relatively resistant against high salt concentration and low water contents (dryness). The bacteria forms characteristic yellow colonies and has a size of 0.5 to 3.5 µm. *Escherichia coli (E.coli)* is a gram-negative bacteria has a size of 1.1 to 6.0 µm and is much more sensitive instead of *M.luteus*. Both types of bacteria were selected for the encapsulation in microcapsules and the processing to aligned electrospun fibers. First the bacteria were encapsulated in bacteria friendly polymer microcapsules (e. g. PVA, PVP, HPC and gelatin) as schematically shown in Sheme 1.

The Zytotox assay with Resazurin is a common assay to determine the viability of bacteria and cells.[11] This test is used to determine the toxicity of the polymers towards the bacteria (**Table 6.1**). The vitalities of the bacteria, which were in contact with the polymer, are as high as bacteria, which had no contact to the polymers. Therefore the polymers have no toxic influence towards the bacteria. The vitality was, in some cases like *M.luteus* with PVA (13-23 kDa) and PVP or *E.coli* with PVP, higher than the negative control. The polymer solutions with 10 wt% are highly viscous and difficult to pipette an exact volume into the wells of the 96-well-plate. Thus, the concentration of the bacteria could be raised up, resulting to a better transformation of Resazurin to Resorufin, which is determined by the plate reader. Resazurin salt can also be transferred to Resorufin salt by a pH shift below pH 3.8. To avoid such a pH shift, the solution was buffered with PBS.

Table 6.1. Relative vitalities of bacteria in contact with polymers compared to bacteria without contact to polymers, n = 5

	M.luteus	***E.coli***
PVA (13-23 kDa)	*119.6 ± 5.2 %*	*90.5 ± 6.4 %*
PVP	*126.3 ± 9.5 %*	*123.9 ± 5.2 %*
HPC	*109.6 ± 2.7 %*	*94.3 ± 1.2 %*

Polymer capsules were prepared by spray drying of an aqueous solution consisting of 2.5 wt% polymer at 150 °C. Dry PVA microcapsules with a mean diameter of 2.6 ± 1.0 µm were reached without additionally purification steps (**Figure 6.1**a). Dryness was determined to 1-2 wt% water content due to thermogravimetric analysis (Supplementary Figure S6.1). The associated diameters of the PVP, HPC and gelatin capsules weren't determined due to deflated and collapsed microspheres as shown in Figure 6.1 b-d. Raman spectroscopy analysis showed hollow microspheres of the PVA microcapsules (Supplementary Figure S6.2). The PVA microcapsules were re-dispersed in an organic solvent (dimethylformamide (DMF) used in electrospinning of hydrophobic polymers. Hydrophobic PVAc and PVB nanofibers containing polymer capsules were successfully electrospun (Supplementary Figure S6.3).

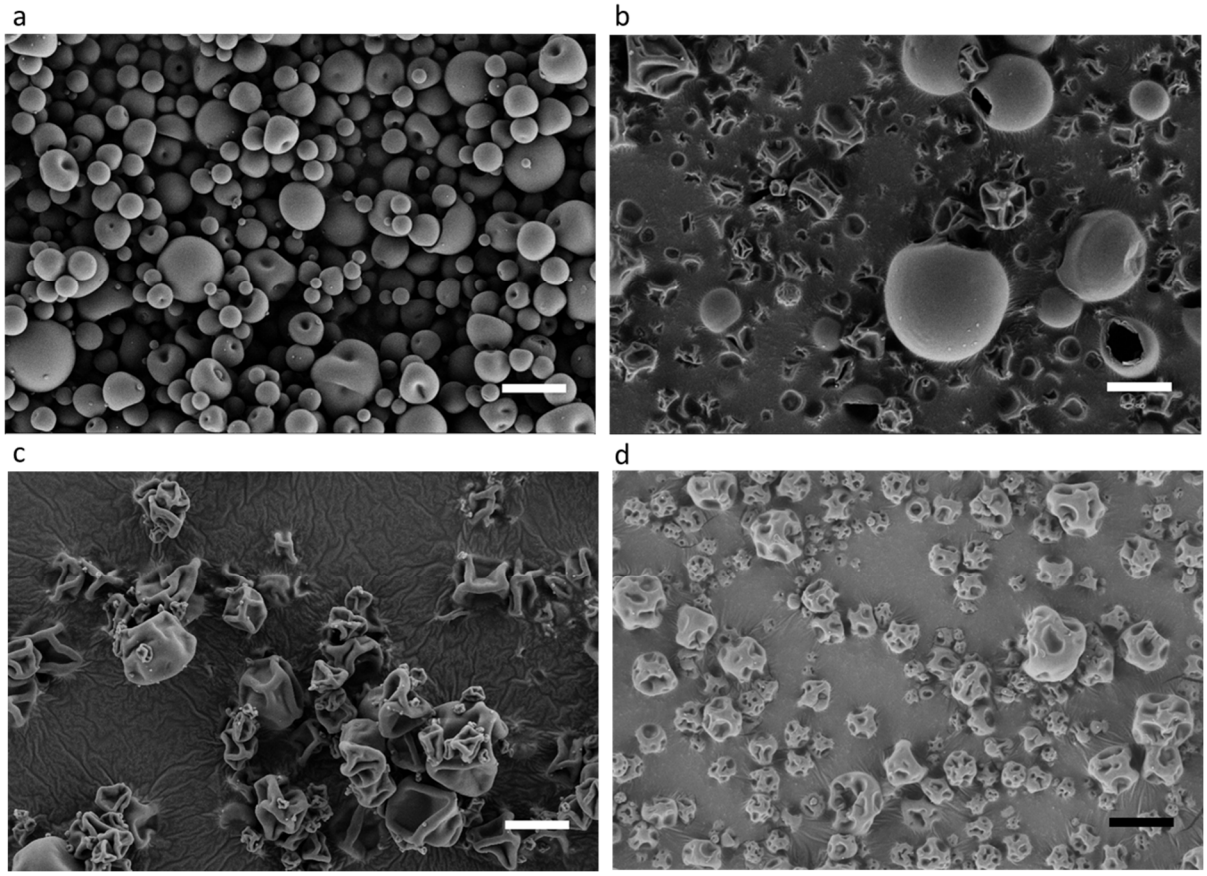

Figure 6.1. SEM images of different polymer microcapsules, a) PVA capsules, b) gelatin capsules, c) HPC capsules and d) PVP capsules. Scale bar: 5µm.

Bacteria-containing capsules were produced the same way by adding bacteria pellets to the polymer solution. Raman spectroscopy localized the bacteria inside the PVA microcapsule (**Figure 6.2**a,b) and are confirmed by transmission electron microscopy (Figure 6.2c,d). Detailed investigation of the localization of the bacteria and the morphology of the spray dried polymer/bacteria composites the PVA/*M.luteus* capsule was measured by Raman-AFM-Spectroscopy. First *M.luteus* was characterized with the Raman-AFM-spectroscopy to determine the Raman Shift signals of the *M.luteus*. In observation of the PVA and *M.luteus* spectra there is a big difference in the Raman Shift of 1500 – 1750 cm^{-1} (Supplementary Figure S6.4). After measuring the PVA/*M.luteus* beads via Raman-AFM-spectroscopy the PVA/*M.luteus* composites were examined as hollow PVA/*M.luteus* capsules. The prepared Raman image show blue, red and black regions. The blue colour indicates PVA, red *M.luteus*

and black empty regions. We conclude that the PVA capsules are hollow and the *M.luteus* are located inside the PVA capsules. Acquired from thin sections, TEM microscopy confirm this observation (Figure 6.2c,d). The thickness of the shell is determined to 56 ± 12 nm. The spray dried bacteria containing capsules were stored at 4°C and it is found to be alive up to 12 months. The viability of the bacteria were accomplished by incubating the capsules on lyogeny broth media for *M.luteus* and *E.coli*, respectively (Figure 6.2e,f). Spray dried capsules included living *M.luteus* when spray dried at 150 °C and contained living *E.coli* in case of 120 °C (**Table 6.2**).

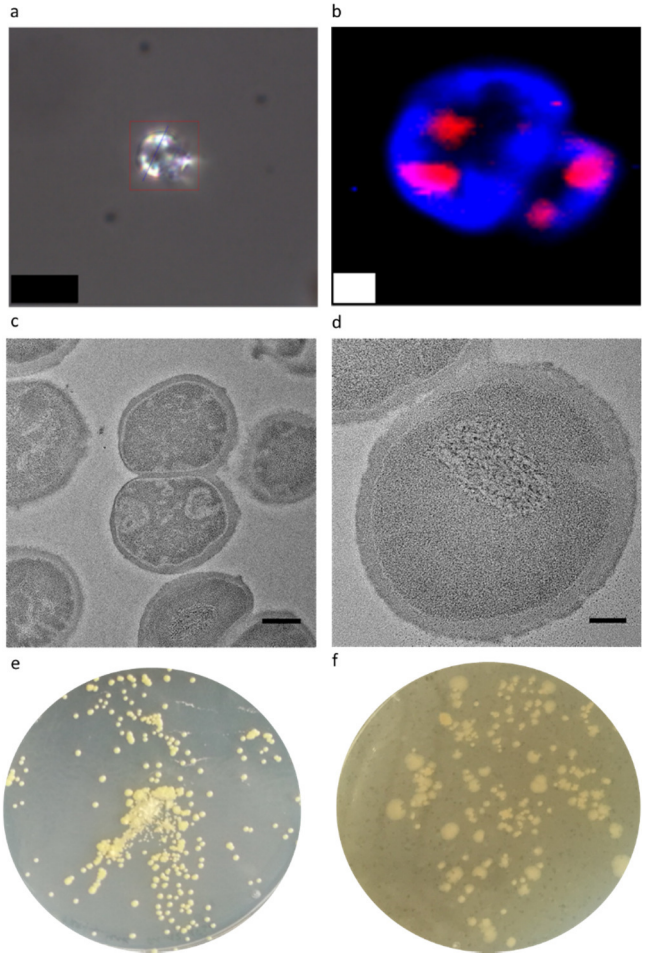

Figure 6.2. Characterization of the spray dried polymer bacteria capsules. a) light microscopy image of PVA/*M.luteus* capsules, scale bar: 8 µm, b) Raman image of PVA(blue)/*M.luteus*(red) capsules, scale bar: 1 µm. TEM images of thin sections obtained from PVA/*M.luteus* capsules. c) Cross-sectional view of PVA/*M.luteus* capsules, scale bar: 250 nm. d) Magnified view, scale bar: 100 nm. Viability tests of encapsulated living bacteria capsules, e) *M.luteus* and f) *E.coli*.

Table 6.2. Summary of the viability of the bacteria after spray drying.

	M.luteus (150°C)	***E.coli (120°C)***
PVA	*Living*	*Living*
PVP	*Living*	*Living*
HPC	*Living*	*Living*
Gelatin	*Living*	*Living*

In order to verify the production of water-insoluble composites, the bacteria containing polymer capsules were incorporated in aligned polymer fibers. Consequently, capsules including *M.luteus* were re-dispersed in polymer solutions used for electrospinning. The polymer solutions contained PAN, PMMA, PS, TPU and PVB in DMF. Polymer fibers were reached in all cases by electrospinning containing capsules (**Figure 6.3**). Aligned fibers were prepared using a fast rotating collector. One or more capsules were observed in the polymer fibers due to non-perfect distribution of the polymer capsules in the electrospinning solution (Figure 6.3a-c).

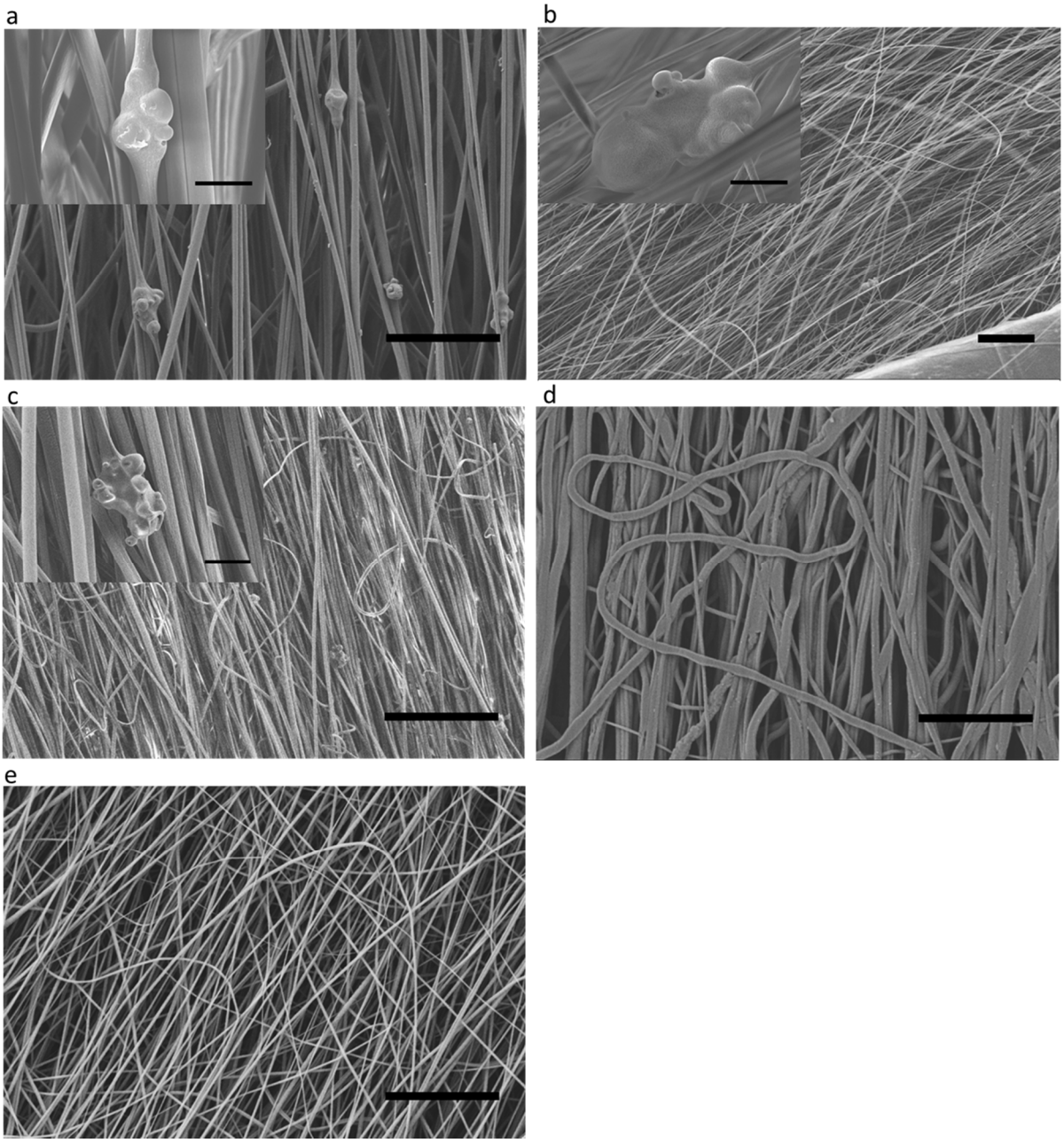

Figure 6.3. SEM images of PVA/*M.luteus* capsules in electrospun aligned polymer nanofibers. a) PAN nanofibers, scale bars: 25 µm, 5 µm (inner image); b) PMMA nanofibers, scale bars: 250 µm, 5 µm (inner image); c) PS nanofibers, scale bars: 100 µm, 5 µm (inner image); d) TPU nanofibers, scale bar: 10 µm and e) PVB nanofibers, scale bar: 100 µm.

6.3 Conclusion

M.luteus and *E.coli* were successfully encapsulated in different polymer microspheres by spray drying technique. *M.luteus* can be processed at high temperatures of 150 °C while *E.coli* at 120 °C. The survival of the bacteria were verified with an agarplate test. Location of the bacteria and the morphology of the polymer capsules were successfully performed with Raman-AFM-Spectroscopy and TEM measurements. Obviously, the survival of bacteria even at high temperature is plausible by the short contact time in spray drying which opens many new perspectives for the encapsulation of functional bacteria. The encapsulation of functional bacteria is extremely useful for further processing of bacteria in harmful solvent, for example by electrospinning for the preparation of nonwovens.

6.4 Experimental Section

Materials: Poly(vinyl alcohol) (PVA) (Sigma Aldrich 13,000 – 23,000 g/mol, 99 % hydrolysis; 31,000-50,000 g/mol, 98-99% hydrolysis; 145,000 g/mol, 99% hydrolysis), poly(vinyl alcohol) (Kuraray Mowiol 3-96 (16,000 g/mol, 96 % hydrolysis), Mowiol 6-98 (47,000 g/mol, 96 % hydrolysis), Mowiol 10-98 (61,000 g/mol, 96 % hydrolysis)), hydroxypropyl cellulose (HPC) (Sigma Aldrich 80,000 g/mol), poly(vinyl pyrollidone) (PVP, Kollidon 17 PF (7,000 - 11,000 g/mol), polyacrylonitrile (PAN, 120,000 g/mol), thermoplastic polyurethane (TPU, Desmopan 2590A, 88,000 g/mol), poly(vinyl acetate) (PVAc), poly(vinyl butyral) (PVB, Mowital B60T,), polystyrene (PS, 94,000 g/mol), poly(methyl methacrylate) (PMMA, 120,000 g/mol) and gelatin were used as received. *Micrococcus luteus (M.luteus)* (DSMZ Braunschweig; DSM-No. 20030), LB media (Roth), *Escherichia Coli (E.coli)(*NEB® 5-alpha, #C2987, New England Biolabs Inc) and Resazurin (Sigma-Aldrich) were used as received. Lyogeny browth (LB) medium was prepared by weighting 25 g of LB-Powder (Roth) in 1 L of Millipore-water, pH adjusted to 7.0, if necessary, and also sterilized by autoclaving.

Analytical Methods: Scanning electron microscope (SEM) from LEO 1530 was employed for characterization of the polymer and the polymer bacteria capsules. The samples were stuck on a holder with water-based conductive carbon glue and coated with 2.0 nm of platinum by a sputter coater 208 HR from Cressington. Polymer bacteria capsules were fixed with 2.5 % glutaraldehyde, 1 % OsO_4, and 1 % uranyl acetate. Subsequently samples were dehydrated and embedded in Agar low viscosity resin. Thin sections were prepared with a diamond knife and transferred to 100 mesh Cu TEM grids. Samples were analyzed in a FEI Tecnai Spirit transmission electron microscope at an acceleration voltage of 120 kV. Images were recorded with a Gatan 4k * 4k CCD camera. Thermogravimetric analysis (TGA) were done on a TGA Libra F1 (Netzsch) with corundum crucibles. The heating rate was set to 10 K/min and the samples were analyzed under nitrogen from 25 °C to 800 °C. A confocal WITec alpha 300 RA+ imaging system equipment with a UHTS 300 spectrometer and a back-illuminated Andor Newton 970 EMCCD camera was used for co-local Raman/AFM measurements. Raman spectra were acquired using an excitation wavelength of $\lambda = 532$ nm, a step size of 10 pixels/µm and integration times of 0.1 - 0.5 s/pixel (100x objective, NA = 0.9, software WITec Control FOUR 4.1). All spectra were subjected to a cosmic ray removal routine and baseline correction. The spatial distribution of *M.luteus* and PVA in the PVA/*M.luteus* capsules was determined by basis analysis, using the Raman spectra of the neat components (Figure S6.3) as reference (software WITec Project FOUR 4.1). Zytotox Assay: Bacteria, which were in the exponential growth phase were seeded in wells of a 96-well plate with bacteria concentrations of 100 x 10^6 bacteria/mL. The bacteria were zentrifuged (1800 *g*, 10 min) and the supernatant removed. The bacteria were washed twice with DPBS (8.0 g NaCl, 0.2 g KCl, 1.78 g Na_2HPO_4 x 2 H_2O and 0,27 g KH_2PO_4). The bacteria were resuspend with a mastermix containing LB-Medium, Resazurin (0,625 mg/L) and the polymer solution (10 wt% in DPBS). PVA (13-23 kDA and 146-186 kDa, Sigma Aldrich), HPC and PVP were used as polymers. Mastermix without the polymer solution was used for negative control. After resuspension, the bacteria were incubated

by 30 °C (*M.luteus*) and 37 °C (*E.coli*) respectively. The fluorescence (Excitation: 535 nm, Emission: 590 nm, 10 flashes) was determined with a plate reader (Genius Pro, Tecan). The Emission rates were correlated to the Emission from the negative control.

Cultivation and Preparation of M.luteus and E.coli: A mixture of 1.6 g LB media and 160 mL Millipore® water was used for the nutrient media. All materials which will be in contact with the bacteria were sterilized at 121 °C for 20 minutes with an autoclave. *M.luteus* (*E.coli*) was grown in liquid media for 72 hours (18 hours) at 37 °C and shaking at 150 rpm. The cells were harvested with a centrifuge at 4000 rpm for 10 minutes. The pellet was washed three times with phosphate buffer saline (PBS).

Preparation of polymer/bacteria capsules: PVA/ bacteria capsules were prepared using a spray drying device (mini spray dryer b290 advanced from Büchi (Suisse)). The bacteria were immersed in 2.5 wt% PVA in phosphate buffer saline. Spray drying was done with a mini spray dryer b290 advanced from the company Büchi (Suisse). Therefore the pump was adjusted to 10 % which is a feed of 2.5 mL/min. The aspirator was 100 % with a gas of 600 L/h, Inlet temperature was set to 150 °C and the outlet temperature was 90 °C. The dry polymer bacteria capsules were measured by thermogravimetric analysis (TGA) to determine the water content of the capsules. Meanwhile the viability of the *M.luteus* and *E.coli* in the polymer capsules were verified with an agarplate test. Other polymer capsules such as PVP, HPC and gelatin were prepared the same way as previous mentioned.

Electrospinning of PVA/M.luteus capsules in hydrophobic polymer nanofibers: The PVA/*M.luteus* capsules were electrospun in hydrophobic polymer nanofibers. For each experiment approximately 20 mg PVA/*M.luteus* capsules were immersed in 3 mL polymer solution. The polymer solution consist of 15 % in DMF/acetone (v,v; 86/14%), 5 % PVAc in DMF, 20 % TPU in DMF, 25 % PMMA in DMF, 25 % PS in DMF and 13 % PVB in DMF. The electrospun fibers were collected on a rotating wheel with a velocity of 700 rpm in a distance of 10 cm.

6.4 Supporting Information

Supporting Information is available from the Wiley Online Library or from the author.

6.5 Acknowledgment

We thank the Bavarian State Ministry of the Environment and Consumer Protection for financial funding of this work within the BayBiotech program.

We thank Mark Linder (MPI of Biophysics) for assistance with the preparation of thin sections.

6.6 Conflict of Interest

The authors declare no conflict of interest.

6.7 Keywords

Spray drying, microorganism, encapsulation, electrospinning, RAMAN-imaging.

6.8 References

[1] C. Knierim, C. L. Greenblatt, S. Agarwal, A. Greiner, *Macromolecular bioscience* **2014**, 14, 537.

[2] P. E. Johnson, P. Muttil, D. MacKenzie, E. C. Carnes, J. Pelowitz, N. A. Mara, W. M. Mook, S. D. Jett, D. R. Dunphy, G. S. Timmins et al., *ACS nano* **2015**, 9, 6961.

[3] C. Knierim, M. Enzeroth, P. Kaiser, C. Dams, D. Nette, A. Seubert, A. Klingl, C. L. Greenblatt, V. Jérôme, S. Agarwal et al., *Macromolecular bioscience* **2015**, 15, 1052.

[4] P. Kaiser, S. Reich, D. Leykam, M. Willert-Porada, A. Greiner, R. Freitag, *Macromolecular bioscience* **2017**.

[5] I. Letnik, R. Avrahami, J. S. Rokem, A. Greiner, E. Zussman, C. Greenblatt, *Biomacromolecules* **2015**, 16, 3322.

[6] M. Gensheimer, M. Becker, A. Brandis-Heep, J. Wendorff, R. Thauer, A. Greiner, *Adv. Mater.* **2007**, 19, 2480.

[7] M. I Ré, *Drying Technology* **1998**, 16, 1195.

[8] M. Gensheimer, A. Brandis-Heep, S. Agarwal, R. K. Thauer, A. Greiner, *Macromolecular bioscience* **2011**, 11, 333.

[9] P. Schuck, A. Dolivet, S. Méjean, C. Hervé, R. Jeantet, *International Dairy Journal* **2013**, 31, 12.

[10] R. M. Stubbendieck, C. Vargas-Bautista, P. D. Straight, *Frontiers in microbiology* **2016**, 7, 1234.

[11] a) J.-C. Palomino, A. Martin, M. Camacho, H. Guerra, J. Swings, F. Portaels, *Antimicrobial Agents and Chemotherapy* **2002**, 46, 2720; b) D. A. Hudman, N. J. Sargentini, *SpringerPlus* **2013**, 2, 55.

6.9 Supplementary Information

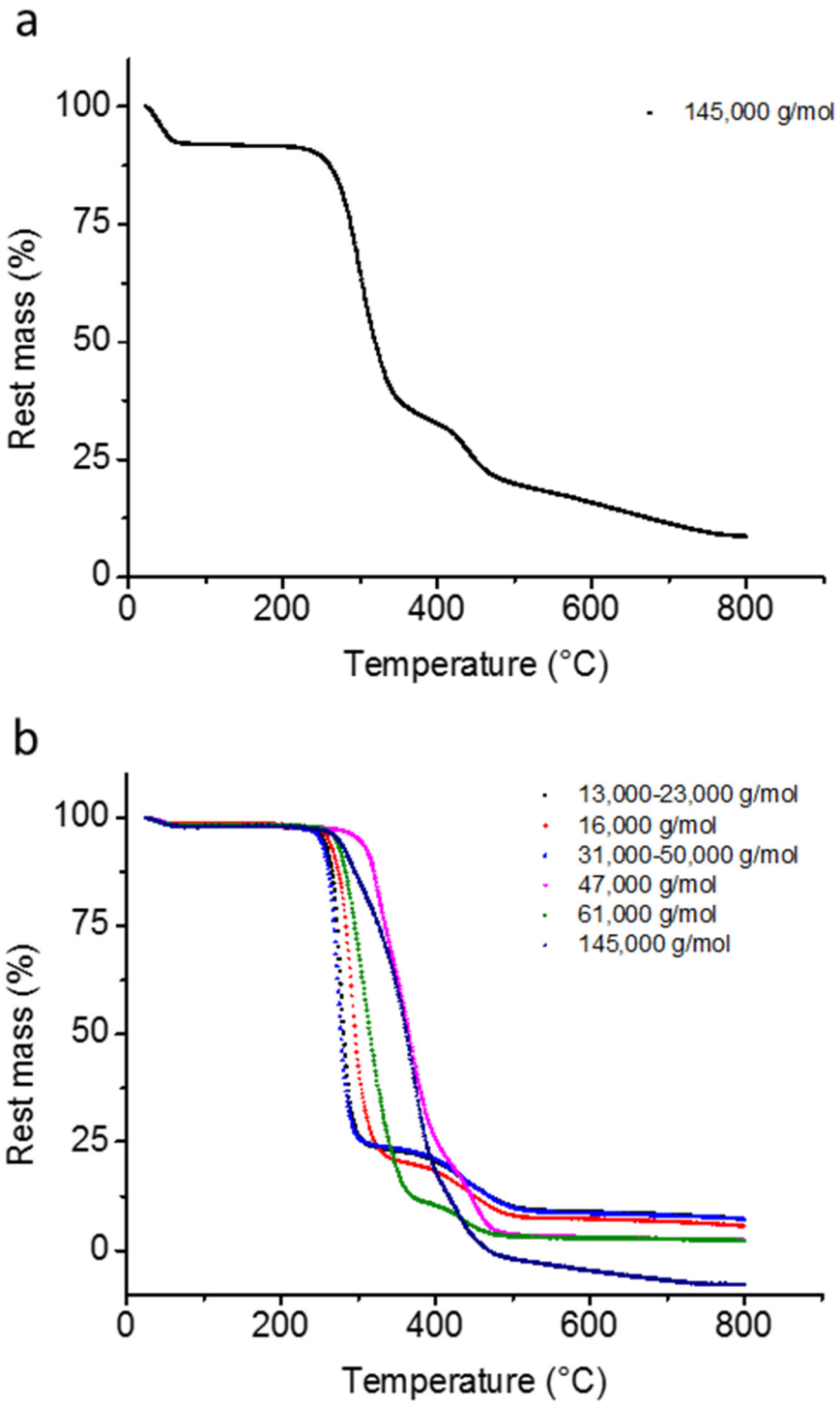

Figure S6.1. (a) Thermogravimetric analysis (TGA) of PVA particles prepared via dispersion method. (b) TGA of different PVA capsules prepared via spray drying.

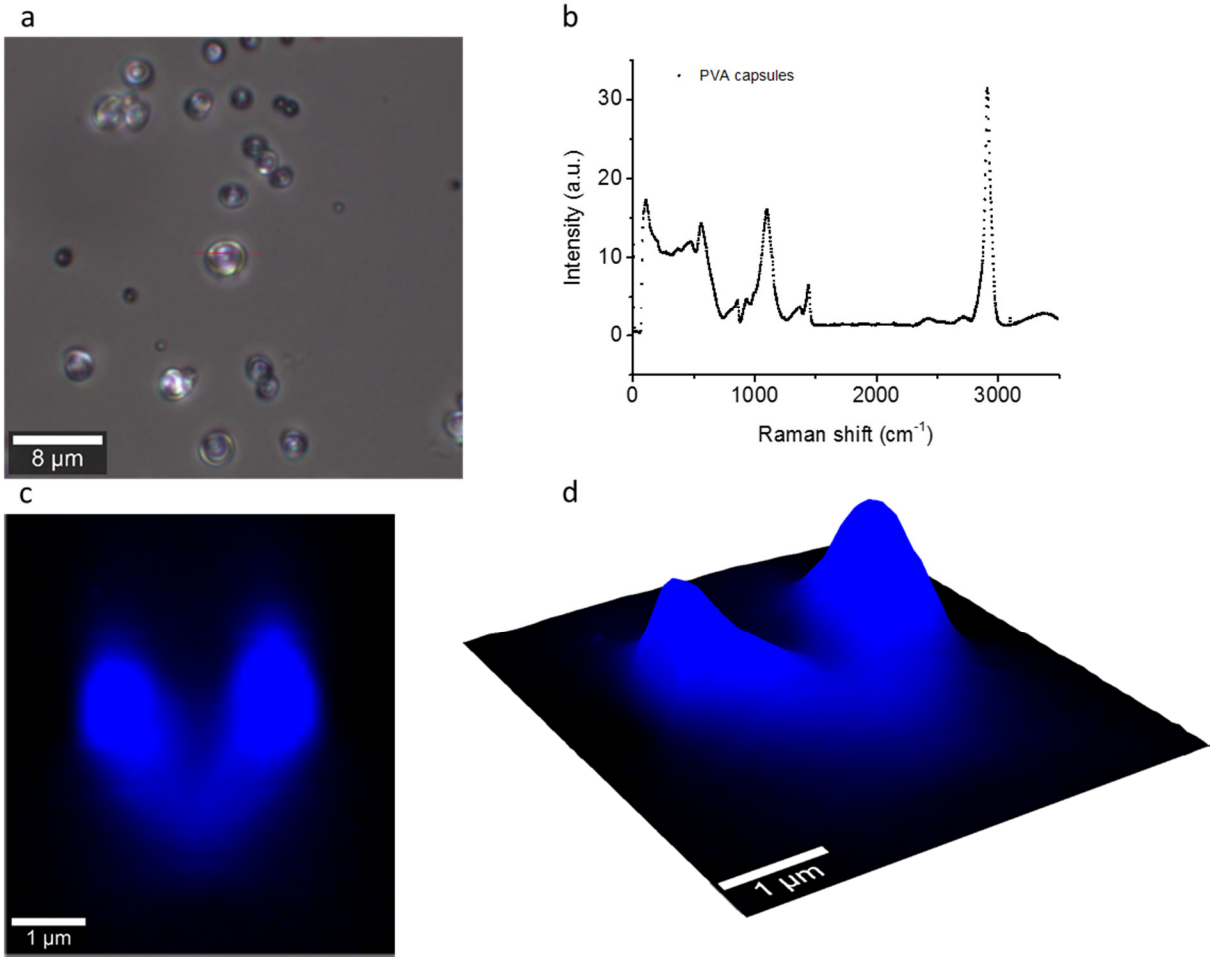

Figure S6.2. Raman-AFM-Spectroscopy on spray dried PVA capsules, a, light microscopy image of PVA capsules; b, Raman spectrum of the spray dried PVA capsules, c, 2D image of the PVA capsules (blue), d, 3D image of the PVA capsules (blue).

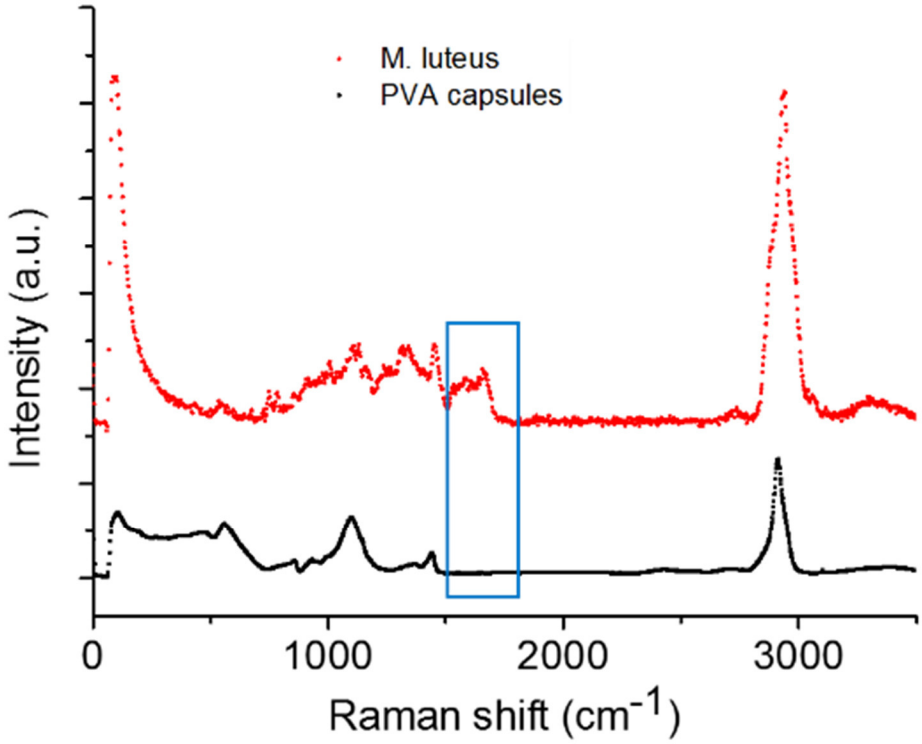

Figure S6.3. Raman spectrum of the spray dried PVA capsules (blue) and the M.luteus (red).

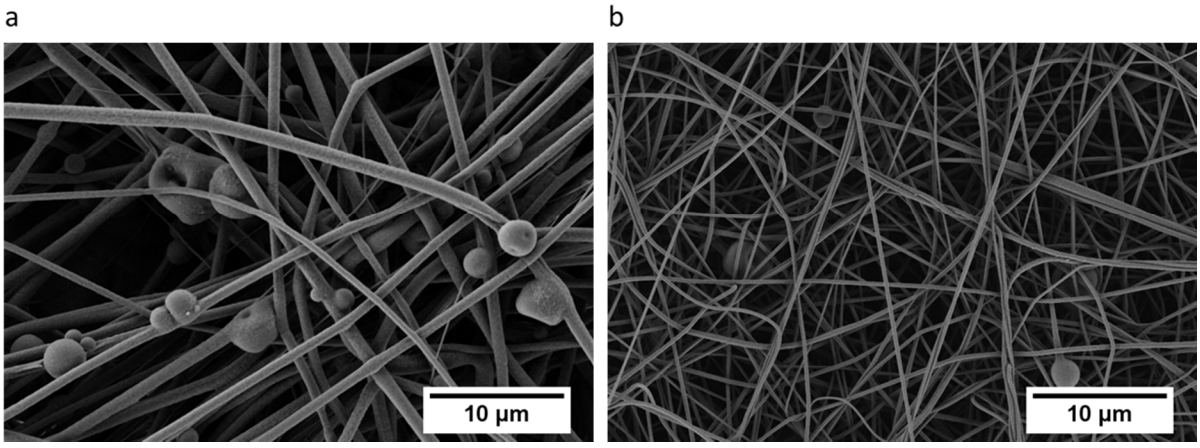

Figure S6.4. SEM images of PVA/bacteria capsules in electrospun polymer nanofibers. a) PVAc nanofibers and b) PVB nanofibers.

7. Polymer nanofibre composite nonwovens with metal-like electrical conductivity

Published in *npj Flexible Electronics, **2017,** in press*

Steffen Reich[1], Matthias Burgard[1], Markus Langner[1], Shaohua Jiang[2], Xueqin Wang[3], Seema Agarwal[1], Bin Ding[3,4], Jianyong Yu[3,4], Andreas Greiner[1]

[1]Macromolecular Chemistry, Bavarian Polymer Institute, University of Bayreuth, 95440 Bayreuth, Germany

[2]College of Materials Science and Engineering, Nanjing Forestry University, 210037 Nanjing, China

[3]Key Laboratory of Textile Science & Technology, Ministry of Education, College of Textile, Donghua University, 201620 Shanghai, China

[4]Innovation Center for Textile Science and Technology, Donghua University, 20051 Shanghai, China

7.1 Abstract

Bendable and breathable polymer nanofibre nonwovens with metal-like electrical conductivity are required for lightweight electrodes and electric shielding design with applications in batteries, functional textiles, sensors, cars, aerospace, constructions, mobile phones, and medical devices. Metal-like conductivity in polymer nonwovens has not been achieved till now due to the limitation of the existing processing techniques. We show here, the metal-like electrical conductivity of 750,000 S/m in polyacrylonitrile (PAN), poly(ε-caprolactone) (PCL) nonwoven using very low content of silver nanowires (AgNW; 3.35 vol%). The key to the high conductivity was the homogenous distribution of AgNW in nonwoven made by wet-laid process using short electrospun fibre and AgNW

dispersion. Above a threshold of 0.36 vol% AgNW, the conductivity of the nonwoven increased by 7 orders of magnitude which we attribute to the onset of percolation of the AgNW. Our nonwoven-AgNW composites show fast heating and cooling within a few seconds at a voltage of 1.1 V which is in the range of portable devices. These composites are also breathable and bendable. The electrical conductivity was independent of the bending angle of the composite which is important for applications mentioned above and would help other scientists to design new conductive materials in the future.

Electrically conductive sponges, nonwovens, films, and fibres are of major importance for energy production[1], energy storage[2], sensors[3], and actuators[4]. Polymers often form an integral part of nanostructured materials, as they are mechanically flexible, easily processable, have low thermal conductivity, chemical stability, high strength to weight ratio, and are lightweight. However, most polymers are also electrically insulating, which limits their applications in electrodes.

Besides, metal coating (aluminium, copper, silver)[5,6], two primary strategies are used to produce polymer-based materials capable of conducting electricity: the use of conductive polymers (such as polyaniline (PANI), polypyrrole (PPy) polythiophene, and polyfluorene)[7], or the use of polymer composites with silver, copper or gold nanoparticles[6,8], metal nanowires[9-11] or carbon materials as conductive additives[12-15]. The inherent conductivity, and the amount and shape of the additive are important parameters for the conductivity of the composite. Lower amount of additives with elongated shape in a composite is required for high conductivity as compared to spherical additives.[16] Lower amount of additive could be favourable for reduced specific weight and mechanical or optical properties. For example, polymer composites with spherical metal particles and carbon black feature decent conductivities at volume fractions of over 5 vol%[17] and 20 vol%[18], respectively. In contrast, wire shaped additives, such as conductive metallic or carbon nanowires, with high aspect ratios from 100–500, show in films

high conductivities even with volume fractions ≤1 vol%[19]. Over the past decade, the use of conductive silver nanowires (AgNW) has been investigated for several applications[20] including organic light-emitting diodes (OLED)[13,21], solar cells[22], touch panels[23], wearable electronics[24], strain sensors[25], piezoelectric energy harvester[26], and paper-based electronics[27], because of the conductivity and transparency of polymer composite films. Nevertheless, the electrical conductivity of AgNW polymer composite films could not reach metal-like conductivity due to the inherent insulation of AgNW by the polymer matrix. Like in polymer films metal-like conductivity was also not achieved in polymer nonwovens. Reason for this is the limited processability of micro- and nanofibre together with AgNW or similar conductive additives. The state-of-the-art method for the preparation of micro- and nanofibre nonwovens is electrospinning[28]. In electrospinning a materials jet is formed from a droplet of a viscous polymer solution by the action of a strong electrical field. This material jet is pulled continuously towards the counter electrode and deposits as a nanofibre nonwoven. Electrospinning of polymer solutions with suspended conductive additives such as AgNW has been reported but resulted in encapsulation of the AgNW in the nanofibres of the nonwovens[29]. Consequently, the conductivity of the resulting nonwovens is relatively low and does not exceed 0.2 S/m[30].

In the present work, we present a straightforward methodology for the preparation of polymer composite nanofibre nonwovens with metal-like electrical conductivity of up to 750,000 S/m at very low content of AgNW (< 3.4 vol%) as conductive additive. These composites are also breathable, bendable, and mechanically stable. Key to the metal-like conductivity was the homogenous distribution of long AgNW in the nonwoven and the percolation of the AgNW electrical contacts. The homogenous distribution of AgNW in the nonwoven was achieved by the so-called wet-laid method[31], which is the formation of a nonwoven by filtration of a fibre suspension in a solvent. Obstacles in the processing of high aspect ratio AgNW with homogenous distribution can be overcome by the utilization of the wet-laid process. Besides

homogenous distribution of high aspect ratio AgNW, other advantages of the wet-laid process are that composite nonwovens could be fabricated by a roll-to-roll process and many other additives could be added for multifunctionality. For the formation of our composite nonwovens we have used in the suspensions for the wet-laid process AgNW in combination with short electrospun PAN and PCL fibres. The electrospun fibres had to be shortened since with as-electrospun fibres no homogenous suspension could be achieved. After moderate annealing of the composite which was required for the bonding of the composite nonwoven by melting of the PCL fibres, we obtained the nonwovens with metal-like conductivity. We discuss in detail the impact of the amount of AgNW on the electrical conductivity and provide a qualitative as well as quantitative explanation based on the percolation theory. We answer the question why a low amount of conductive additive, here AgNW, is sufficient for the achievement of metal-like electrical conductivity. We are convinced that our concept will have a broad impact on application in battery electrodes, supercapacitors, functional textiles, sensors, medical implants and as conductive construction parts in cars, aeronautics, and mobile phone. Our concept of making metal-like electrically conductive porous nonwovens by wet-laid process in combination with high aspect ratio metal nanowires is highly versatile and could be applied to numerous other materials as well.

7.2 Results and Discussion

Nonwovens composed of short electrospun PAN nanofibres and PCL microfibres were prepared with different amounts of AgNW (PAN/PCL/AgNW nonwovens) by the recently established wet-laid process[31] as illustrated schematically in Fig. 7.1a and parameters as given in Tab. S7.1. The wet-laid process is ideal for the preparation of composite nonwovens as fibre dispersions are used, which has been exploited here for the mixture of electrospun fibres with AgNW. Firstly, dispersions of short electrospun PAN and PCL were prepared by mechanical cutting of the as-electrospun fibres in a solvent mixture of 2-propanol and water (7:3 by volume)

followed by the addition of AgNW. PCL served here as glue for the stabilization of the nonwovens while the AgNW served as conductive additive. Secondly, the composite nonwovens of PAN and PCL fibres and AgNW were wet-laid by filtration of the dispersion on stainless steel sieve. After drying, the nonwovens were stabilized by gentle pressing between 2 glass plates at 75 °C.

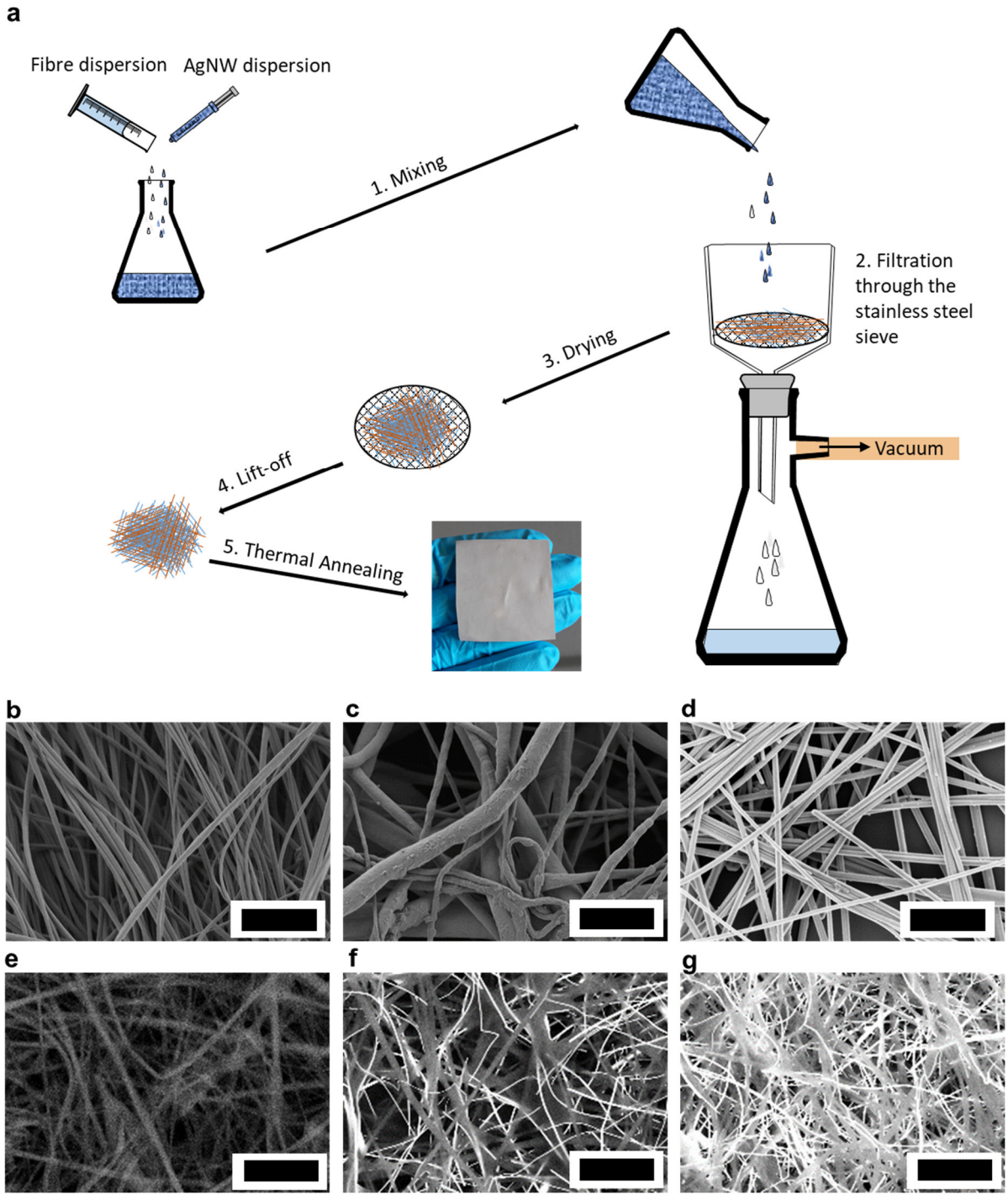

Figure 7.1 | Preparation and morphology of PAN/PCL/AgNW nonwovens prepared by the wet-laid process. a, Schematic of the procedure for the preparation of the PAN/PCL/AgNW nonwovens. (1-5) 1**,** Mixing of PAN nanofibres, PCL nanofibres and AgNW. 2, Filtration of the PAN/PCL/AgNW dispersion through the stainless steel sieve. 3, Drying of the PAN/PCL/AgNW nonwoven. 4, Lift-off of the PAN/PCL/AgNW nonwoven from the stainless steel sieve. 5, Thermal annealing of the PAN/PCL/AgNW nonwoven. SEM images of the polymeric and metallic fibres: **b**, as-electrospun PAN fibres, **c**, as-electrospun PCL fibres, **d**, AgNW; SEM/BSE images of the composite nonwovens with increasing AgNW content: **e,** 0.00 vol%, **f,** 0.36 vol% and **g,** 1.07 vol%. scale bar 5 μm (**d** 1 μm).

In general, fibrous nonwovens are characterized by the diameter of the fibres, the porosity, and the pore size. The diameter of the electrospun PAN and PCL fibres, respectively ranged from 307 ± 82 nm and 714 ± 593 nm according to SEM images (Fig. 7.1b, c). The porosity (78%) and the pore size (1.3 μm) of the wet-laid PAN/PCL nonwovens without AgNW compare well to the porosity (87%) and pore size (3.9 μm) of the electrospun PAN nonwovens. The length of the AgNW ranged from 5 – 34 μm and their diameter from 25 – 150 nm for batch A (Fig. 7.1d, Supplementary Fig. S7.1a-d) and from length of 10 – 95 μm and a diameter from 27 – 143 nm for batch B (Fig. S7.1e). The scanning electron microscopy with backscattered electron detector (SEM/BSE) and energy-dispersive X-ray analysis (EDX) displayed homogeneous distribution of the PAN fibres and AgNW in the composite nonwovens obtained by the wet-laid process (Fig. 7.1f, 7.1g and Figs. S7.2-S7.5). The PCL fibres are no more visible as they were molten during the stabilization step at 75 °C. The porosity of composite nonwovens PAN/PCL/AgNW increased up to 93% with increasing amount of AgNW (Tab. S7.1). A detailed discussion of the nonwoven morphology for all compositions is given in the supplementary information. The inherent porosity of the composite nonwovens provide gas flow through the system and thereby breathability. In a qualitative experiment to confirm

breathability, the PAN/PCL/AgNW nonwoven is fixed to one end of a rubber tube. Carbon dioxide gas generated from solid carbon dioxide at room temperature passed through the nonwoven tied at the end of the tube and bubbled through a phenolphthalein/limewater solution and discoloured it (Video S7.1). The non-porous polyethylene film was used as a negative blank (Video S7.2). The breathability is controlled by the mean pore size, which was nearly independent of the AgNW content (Fig. S7.6). AgNW showed a weight loss of about 3 wt% in thermogravimetric analysis (Fig. S7.7), which we attribute to the presence of poly(vinyl pyrrolidone) (PVP). PVP was used in the synthesis of AgNW. The content of AgNW in the nonwoven, given as the volume percentage (vol%), ranged from 0.16 to 3.35 vol%. The content of AgNW was calculated using Equations S7.1 and S7.2 (see supplementary information) based on the weight percent (wt%) of AgNW obtained by thermogravimetric analysis (Fig. S7-8; ranged from 1.8 to 77.15 wt%). The mechanical properties of the composite nonwovens were in the typical range for electrospun nonwoven (Fig. S7.9). They showed a slight increase in Young's modulus up to about 140 MPa with increasing AgNW content, which was three-fold higher compared to the pure wet-laid PAN/PCL composite nonwoven. The elongation at break decreased slightly with increasing amount of AgNW content. The bending stiffness of the composite nonwovens was low and varied insignificantly between 28 – 90 mN (Tab. S7.2), which is in the typical range of soft electrospun nonwovens[32].

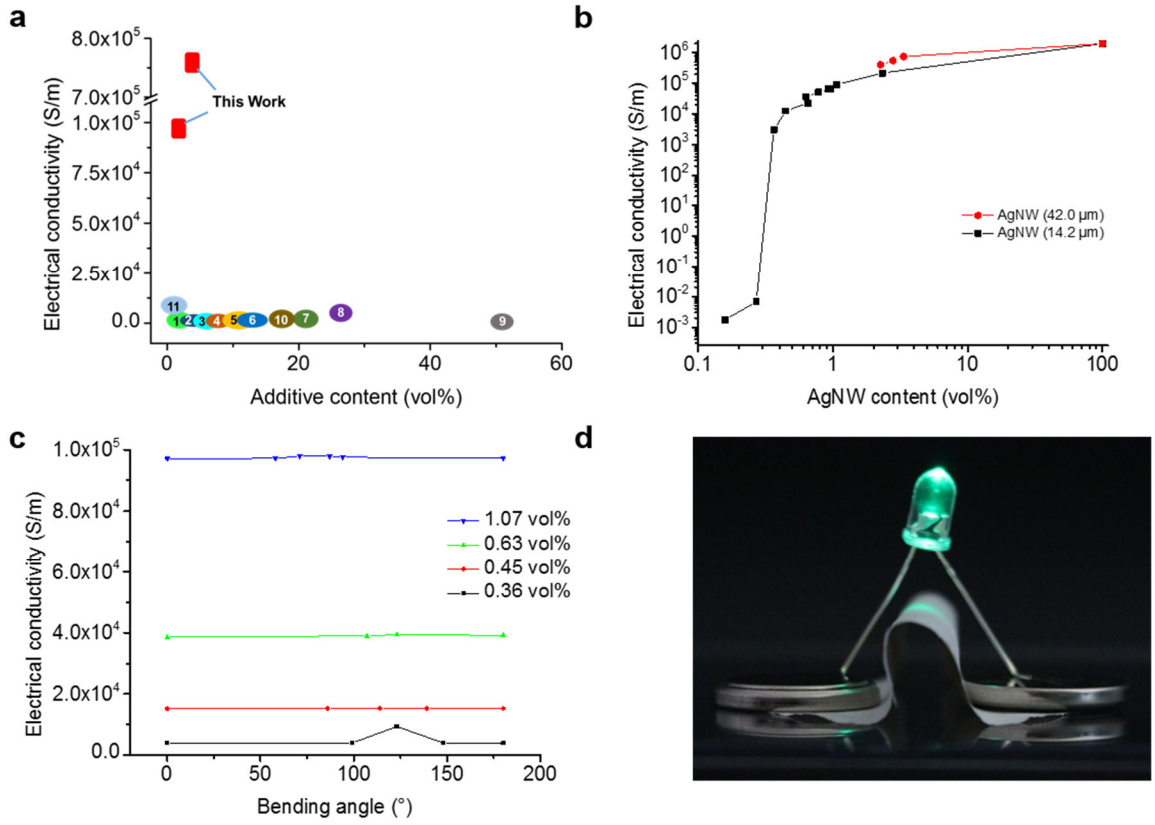

Figure 7.2 | Electrical properties of conductive nonwovens. a, Ashby plot showing the electrical conductivity of different conductive composite nonwovens against their conductive additive content: 1, carbon nanotube/polylactide(PLA) fibres[39]; 2, carbon black/PLA fibres[39]; 3, PANI/natural rubber fibres[40]; 4, PANI-dodecylbenzene sulfonic acid/Co-PAN fibres[41]; 5, carbon nanotube/PET fibres[42]; 6, PANI/bacterial cellulose fibres[43]; 7, poly(3,4-ethylenedioxythiophene):polystyrene sulfonate (PEDOT:PSS/PNN) fibres[44]; 8, PEDOT:PSS/hollow carbon fibres[45]; 9, PANI/polystyrene fibres[46]; 10, MWNT/cellulose fibres[47]; 11, AgNW/cellulose fibres[48]. b, Electrical conductivity with respect to the AgNW content. c, Electrical conductivity dependence on bending angle. d, Photograph of an LED operated by two coin batteries connected by a flexible conductive PAN/PCL nonwoven with 1.07 vol% AgNW.

The electrical conductivity of the composite nonwovens was calculated according to equations S7.3-S7.5 in the supplementary information based on the resistance of the nonwovens (Tab.

S7.1). Composite nonwoven with the highest electrical conductivity of 750,000 S/m was achieved with a AgNW (batch B) content of 3.35 vol%. This conductivity was 5 orders of magnitude higher compared to conductive composite nonwovens with an additive content < 10 vol% (Fig. 7.2a). The AgNW with diameter ca. 25 nm and length up to 5 and 10 µm showed percolation threshold in the range of 0.50-0.75 vol% for polystyrene composite films.[10] The electrical conductivity of our composite nonwovens increased with increasing AgNW content with a discontinuous jump between 0.27 – 0.36 vol% AgNW in the composite nonwoven (Fig. 2b). Above 0.36 vol% the electrical conductivity could be extrapolated as a function of the AgNW content by volume to the electrical conductivity of the pure AgNW (1,970,000 S/m, batch A). The conductivity of the composite nonwoven with 0.27 vol% AgNW was 0.1 S/m, whereas the composite nonwoven 0.36 vol% AgNW showed a conductivity of 3050 S/m. This jump in conductivity by a small increase in AgNW content could be rationalized as the percolation threshold of AgNW throughout the whole sample, as supported by SEM analysis (Fig. 7.1f, 7.1g and Figs. S7.2, S7.3). Qualitative inspection of the SEM images of the nonwovens with 0.36 vol% or more AgNW clearly shows overlapping of the nanowires (Fig. 7.1f, 7.1g), which is the prerequisite of the percolation for the conductivity. The increase in the conductivity at very low volume content of AgNW in the composite nonwoven can be rationalized by the percolation theory which predicts that with rod-like additives significantly less amount additive is required as compared to spherical particles in order to achieve property (for example conductivity) percolation in a composite. This prediction has been fully exploited in the concept of our conductive composite nonwovens with AgNW as conductive additive. The number of AgNW in a defined volume can be calculated using Equation (7.1):

$$Number\ of\ nanowires = \frac{4CV}{D_{Ag}\pi d^2 L} \qquad (7.1)$$

where C is the concentration of the AgNW dispersion (183 mg/mL), V is the volume of the AgNW dispersion, D_{Ag} is the density of Ag (10.5 g/cm^3), d is the diameter (76 ± 28 nm) and L

is the length of the AgNW (14.24 ± 6.27 µm). The number of AgNWis given N = 0.8476 V/µm^3 for the given volume of the AgNW dispersion. In order to describe the correlation of the conductivity quantitatively by the density of the AgNW in our composite nonwovens the value for the critical exponent in Equation (7.2) for the dimensionality (α) should be 1.33 (for two dimensional (2D) system) or 1.9 (for three dimensional (3D) system).[33]

$$\sigma \sim (N - N_c)^{\alpha} \tag{7.2}$$

σ is the conductivity in 3D and N_c is the critical nanowire density for the onset of percolation. N_c is obtained by plotting of the sheet resistance versus the volume of the nanowire dispersion (Fig. S10). The relationship between σ and the sheet resistance, R_{sh}, is $\sigma = 1/R_{sh}$, and the relationship between the volume V of the AgNW dispersion and R_{sh} is given by Equation (7.3). From this calculation the critical exponent α can be derived (inset of Fig. S7.10).

$$R_{sh} \sim (V - V_c)^{-\alpha} \tag{7.3}$$

According to these calculations based on the percolation theory the value for α for our composite nonwovens with AgNW is 1.60 ± 0.07, which is centred between 1.33 for 2D systems and 1.9 for 3D systems. The results obtained for the value α match the morphology of the composite nonwovens, which are neither flat films nor real 3D object but voluminous (porosity up to 93%).

The level of conductivity could be almost doubled by use of longer AgNW with an average length of 42.0 µm (AgNW batch B, Fig. S7.1e) as compared to shorter AgNW with average length of 14.2 µm (AgNW batch A, Fig. S7.1d). The electrical conductivity of the composite nonwoven made with shorter AgNW (2.30 vol %) was about 220,000 S/m. In contrast, the electrical conductivity was almost doubled to about 407,000 S/m with longer AgNW (batch B) at similar content (2.25 vol%). The length of the AgNWs plays very important role to achieve superior electrical conductivity. The longer AgNW provide an effective and longer percolation network thereby better conductivity as shown in other literatures.[34,35]

The percolation of the AgNW is obviously not affected by the bending of the composite nonwovens as the conductivity is nearly independent of the bending angle (Fig. 7.2c). Consequently, the operation of a commercial light-emitting diode by a bended nonwoven with coin batteries was possible (Fig. 7.2d). The durability of the nonwovens can be demonstrated by bending the nonwoven 10,000 times without changing the electrical conductivity. For example, PAN/PCL/AgNW nonwoven with 0.90 vol% AgNW (batch A) after bending for 10,000 times (Video S7.3) show the electrical conductivity of 10,6625 ± 8,347 S/m which is comparable to the electrical conductivity of 10,0185 ± 9,927 S/m before bending. There are several reports about conductive and stretchable conductors[20] in which conductive metal nanowires are typically deposited on top of substrates, such as poly (ethylene terephthalate) (PET), polydimethylsiloxane (PDMS) and polyacrylates.[34,36] In such systems, nanowires exist as a network layer on a flexible substrate or embedded in polymer film where just one network layer of the AgNW creates the electrical conductive pathways. The conductivity is decreased after a limited tensile / compressive strain due to the weakening and detachment of the NW contacts.

Moreover, delamination under repeated mechanical loading could also occur.[37,38] In our system lot of AgNW layers are over and under each other in the whole bulk of the material and they are not embedded in the polymer. So if the membrane is bended there will be other connections (percolation network) between the silver nanowires created causing almost no change in conductivity.

A very interesting feature of the electrically conductive composite nonwovens is their ability to act as Joule heaters at a constant voltage of 1.1 V which is in the range of portable devices. The maximum temperature increased at constant voltage of 1.1 V with the content of AgNW (Fig. 7.3a). Within 20 seconds the composite nonwoven with 1.07 vol% AgNW heats up to about 80 °C and cools down immediately when the voltage is off. The polymer-AgNW Joule heaters are

known in the literature[49] and fast heating and cooling of our PAN/PCL/AgNW nonwoven compares well with the fastest heating and cooling rates of other AgNW based films[50]. The IR camera image of the heated sample showed homogenous distribution of temperature with gradual cooling towards the edges of the sample (Fig. 7.3b). This Joule heating and cooling can be performed for a sample with 0.90 vol% AgNW (batch A) in the bended or unbended state while the temperature for unbended reached 67 °C and bended reached 61 °C.

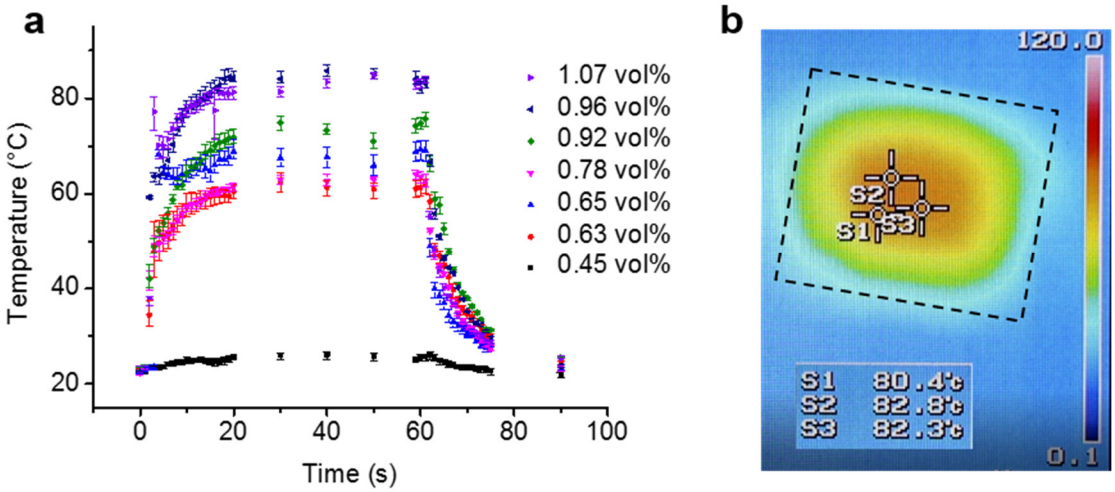

Figure 7.3 | Heating at constant voltage with increasing AgNW content. a, Joule heating at 1.1 V for nonwovens with different AgNW contents. b, IR camera image with an applied voltage of 1.1 V and 1.07 vol% AgNW nonwoven material (dotted lines). Scale unit: °C.

The joule heating is shown to affect the deformation of the low glass transition temperature (*T*g) polymers, such as polyethylene terephthalate (PET) substrate (*T*g ~75 °C) in literature.[51] In our case, there was no burning or distortion of sample observed even after 3 cycles of heating and cooling. This might be due to the fact that the maximum temperature did not exceed the *T*g of PAN, the matrix polymer.

7.3 Conclusion

Novel polymer nanofibre composite nonwovens with metal-like electrical conductivity were achieved by exploitation of the versatility of the wet-laid process. This process enabled the homogenous distribution of AgNW in the polymer nanofibre composites with percolation of the electric contacts between the AgNW. As a result the composites show metal-like conductivities at extremely low volume content of the AgNW, which is plausible by the rod-like shape of AgNW and its low percolation threshold. The increase in length of the AgNW increases the electrical conductivity of the composite very significantly. The design of AgNW will provide more opportunities for further increase of the conductivity of the nonwovens. The concept of conductive composite nonwoven preparation should be widely applicable to other nonwovens based on short micro- and nanofibres prepared by the wet-laid process. Consequently, future work will focus on the implementation of other shape-anisotropic conductive additives in wet-laid micro- and nanofibre nonwovens, the translation of the process to 3D shaped objects, and its application as electrodes in textiles, capacitors, batteries, functional textile, and as basis for sensor devices.

7.4 Methods

Methods, including statements of data availability and any associated accession codes and references, are available in the online version of the paper.

7.5 Data Availability Statement

The authors declare that the data supporting the findings of this study are available within the article (and its Supplementary Information files)

7.6 Acknowledgements

We thank the DFG (Deutsche Forschungsgemeinschaft) for financial support. The authors would also like to thank Franka Gruschwitz for help fabricating the membranes and performing the material characterisation, Martina Heider of BIMF for supporting the SEM/EDX measurements and Judith Schöbel for the TEM measurements.

7.7 Author contributions

S.R. carried out the synthesis and characterisation of the AgNW; the electrospinning, prepared and characterized the nonwovens and wrote the manuscript. M.B. carried out the tensile tests and SEM/BSE measurements. M.L. carried out the electrospinning, cutting of the fibres and the preparation of the fibre dispersions. S.J. provided a second batch of AgNW and revised the manuscript. S.A. discussed the project and revised the manuscript. H.W. and B.D. performed the bending stiffness analysis. A.G. directed the project and wrote the manuscript.

7.8 Additional information

Supplementary and chemical compound information are available in the online version of the paper. Reprints and permissions information is available at www.nature.com/reprints. Correspondence and requests for materials should be addressed to A.G.

7.9 Competing financial interests

The authors declare no competing financial interests.

7.10 References

1. Chen, S. *et al.* Electrospun and solution blown three-dimensional carbon fibre nonwovens for application as electrodes in microbial fuel cells. *Energy Environ. Sci.* **4**, 1417–1421 (2011).

2. Arico, A. S., Bruce, P., Scrosati, B., Tarascon, J. M. & van Schalkwijk, W. Nanostructured materials for advanced energy conversion and storage devices. *Nat. Mater.* **4**, 366–377 (2005).

3. Tee, B. C.-K., Wang, C., Allen, R. & Bao, Z. An electrically and mechanically self-healing composite with pressure- and flexion-sensitive properties for electronic skin applications. *Nat. Nanotech.* **7**, 825–832 (2012).

4. Lu, W., Smela, E., Adams, P., Zuccarello, G. & Mattes, B. R. Development of solid-in-hollow electrochemical linear actuators using highly conductive polyaniline. *Chem. Mater.* **16**, 1615–1621 (2004).

5. Lee, H. M. *et al.* Long-term sustainable aluminium precursor solution for highly conductive thin films on rigid and flexible substrates. *ACS Appl. Mater. Interfaces* **6**, 15480–15487 (2014).

6. Langner, M., Agarwal, S., Baudler, A., Schröder, U. & Greiner, A. Large multipurpose exceptionally conductive polymer sponges obtained by efficient wet-chemical metallization. *Adv. Funct. Mater.* **25**, 6182–6188 (2015).

7. Balint, R., Cassidy, N. J. & Cartmell, S. H. Conductive polymers: towards a smart biomaterial for tissue engineering. *Acta Biomater.* **10**, 2341–2353 (2014).

8. Janovák, L. & Dékány, I. Optical properties and electric conductivity of gold nanoparticle-containing, hydrogel-based thin layer composite films obtained by photopolymerization. *Appl. Surf. Sci.* **256**, 2809–2817 (2010).

9. Bergin, S. M. *et al.* The effect of nanowire length and diameter on the properties of transparent, conducting nanowire films. *Nanoscale* **4**, 1996–2004 (2012).

10. Gelves, G. A., Lin, B., Sundararaj, U. & Haber, J. A. Low electrical percolation threshold of silver and copper nanowires in polystyrene composites. *Adv. Funct. Mater.* **16**, 2423–2430 (2006).

11. Gong, S. *et al*. A wearable and highly sensitive pressure sensor with ultrathin gold nanowires. *Nat. Commun.* ***5***, 3132 (2014).

12. Gong, T. *et al*. Low percolation threshold and balanced electrical and mechanical performances in polypropylene/carbon black composites with a continuous segregated structure. *Composites, Part B* **99**, 348–357 (2016).

13. Zhang, D. *et al.* Transparent, conductive, and flexible carbon nanotube films and their application in organic light-emitting diodes. *Nano Lett.* **6**, 1880–1886 (2006).

14. Sengupta, R., Bhattacharya, M., Bandyopadhyay, S. & Bhowmick, A. K. A review on the mechanical and electrical properties of graphite and modified graphite reinforced polymer composites. *Prog. Polym. Sci.* **36**, 638–670 (2011).

15. Stankovich, S. *et al.* Graphene-based composite materials. *Nature* **442**, 282–286 (2006).

16. Jason, N. N., Ho, M. D. & Cheng, W. Resistive electronic skin. *J. Mater. Chem. C* **5**, 5845-5866 (2017).

17. Chan, K. L., Mariatti, M., Lockman, Z. & Sim, L. C. Effects of the size and filler loading on the properties of copper- and silver-nanoparticle-filled epoxy composites. *J. Appl. Polym. Sci.* **121**, 3145–3152 (2011).

18. Saleem, A., Frormann, L. & Iqbal, A. Mechanical, thermal and electrical resistivity properties of thermoplastic composites filled with carbon fibres and carbon particles. *J. Polym. Res.* **14**, 121–127 (2007).

19. Gelves, G. A., Al-Saleh, M. H. & Sundararaj, U. Highly electrically conductive and high performance EMI shielding nanowire/polymer nanocomposites by miscible mixing and precipitation. *J. Mater. Chem*. **21**, 829–836 (2011).

20. Gong, S. & Cheng, W. One-dimensional nanomaterials for soft electronics. *Adv. Electron. Mater.* **3**, 1600314 (2017).

21. Zeng, X.-Y., Zhang, Q.-K., Yu, R.-M. & Lu, C.-Z. A new transparent conductor: silver nanowire film buried at the surface of a transparent polymer. *Adv. Mater.* **22**, 4484–4488 (2010).

22. Hu, L. *et al.* Scalable coating and properties of transparent, flexible, silver nanowire electrodes. *ACS Nano* **4**, 2955–2963 (2010).

23. Lee, J. *et al.* Very long Ag nanowire synthesis and its application in a highly transparent, conductive and flexible metal electrode touch panel. *Nanoscale* **4**, 6408–6414 (2012).

24. Lee, P. *et al*. Highly stretchable or transparent conductor fabrication by a hierarchical multiscale hybrid nanocomposite. *Adv. Funct. Mater.* **24**, 5671–5678 (2014).

25. Kim, K. K. *et al.* Highly sensitive and stretchable multidimensional strain sensor with prestrained anisotropic metal nanowire percolation metworks. *ACS Nano* **15**, 5240–5247 (2015).

26. Jeong, C. K. *et al*. A hyper-stretchable elastic-composite energy harvester. *Adv. Mater.* **27**, 2866–2875 (2015).

27. Santhiago, M., Bettini, J., Araujo, S. R., & Bufon, C. C. B. Three-dimensional organic conductive networks embedded in paper for flexible and foldable devices. *ACS Appl. Mater. Interfaces* **8**, 10661–10664 (2016).

28. Greiner, A. & Wendorff, J. H. Electrospinning: a fascinating method for the preparation of ultrathin fibres. *Angew. Chem. Int. Ed.* **46**, 5670–5703 (2007).

29. Song, J. *et al.* Direct electrospinning of Ag/polyvinylpyrrolidone nanocables. *Nanoscale* **3**, 4966–4971 (2011).

30. Satoungar, M. T., Fattahi, S., Azizi, H., & Mehrizi, M. K. Electrospinning of polylactic acid/silver nanowire biocomposites: antibacterial and electrical resistivity studies. *Polym. Compos.* http://onlinelibrary.wiley.com/doi/10.1002/pc.24241/full (2017).

31. Langner, M. & Greiner, A. Wet-laid meets electrospinning: nonwovens for filtration applications from short electrospun polymer nanofibre dispersions. *Macromol. Rapid Commun.* **37,** 351–355 (2016).

32. Si, Y., Mao, X., Zheng, H., Yu, J. & Ding, B. Silica nanofibrous membranes with ultra-softness and enhanced tensile strength for thermal insulation. *RSC Adv.* **5**, 6027–6032 (2015).

33. Madaria, A. R., Kumar, A., Ishikawa, F. N. & Zhou, C. Uniform, highly conductive, and patterned transparent films of a percolating silver nanowire network on rigid and flexible substrates using a dry transfer technique. *Nano Res.* **3**, 564–573 (2010).

34. Lee, P. *et al.* Highly stretchable and highly conductive metal electrode by very long metal nanowire percolation network. *Adv. Mater.* **24**, 3326–3332 (2012).

35. Lee, J. H., Lee, P., Lee, D., Lee, S. S. & Ko, S. H. Large-scale synthesis and characterization of very long silver nanowires via successive multistep growth. *Cryst. Growth Des*. **12**, 5598–5605 (2012)

36. Xu, F. & Zhu, Y. Highly conductive and stretchable silver nanowire conductors. *Adv. Mater.* **24**, 5117–5122 (2012).

37. Yu, Z. *et al.* Highly flexible silver nanowire electrodes for shape-memory polymer light-emitting diodes. *Adv. Mater.* **23**, 664–668 (2011).

38. Yun, S. *et al*. Compliant silver nanowire-polymer composite electrodes for bistable large strain actuation. *Adv. Mater.* **24**, 1321–1327 (2012).

39. Li, Y. *et al.* Tuning of vapor sensing behaviors of eco-friendly conductive polymer composites utilizing ramie fibre. *Sens. Actuators, B* **221**, 1279–1289 (2015).

40. Sukitpaneenit, P., Thanpitcha, T., Sirivat, A., Weder, C. & Rujiravanit, R. Electrical conductivity and mechanical properties of polyaniline/natural rubber composite fibres. *J. Appl. Polym. Sci*. **106**, 4038–4046 (2007).

41. Jianming, J., Wei, P., Shenglin, Y. & Guang, L. Electrically conductive PANI-DBSA/Co-PAN composite fibres prepared by wet spinning. *Synth. Met.* **149**, 181–186 (2005).

42. Li, Z., Luo, G., Wei, F. & Huang, Y. Microstructure of carbon nanotubes/PET conductive composites fibres and their properties. *Compos. Sci. Technol.* **66**, 1022–1029 (2006).

43. Hu, W., Chen, S., Yang, Z., Liu, L. & Wang, H. Flexible electrically conductive nanocomposite membrane based on bacterial cellulose and polyaniline. *J. Phys. Chem. B* **115**, 8453–8457 (2011).

44. Huang, S.-R. *et al.* Thermoresponsive conductive polymer composite thin film and fibre mat: Crosslinked PEDOT:PSS and P(NIPAAm-*co*-NMA) composite. *J. Polym. Sci. Part A: Polym. Chem.* **54**, 1078–1087 (2016).

45. Qu, G. *et al*. A Fibre supercapacitor with high energy density based on hollow graphene/conducting polymer fibre electrode. *Adv. Mater.* **28**, 3646–3652 (2016).

46. Yin, X. H. *et al.* Percolation conduction in polymer composites containing polypyrrole coated insulating polymer fibre and conducting polymer. *Synth. Met.* **96**, 367–368 (1995).

47. Imai, M., Akiyama, K., Tanaka, T. & Sano, E. Highly strong and conductive carbon nanotube/cellulose composite paper. *Compos. Sci. Technol.* **70**, 1564–1570 (2010).

48. Lee, T.-W., Lee, S.-E. & Jeong, Y. G. Highly effective electromagnetic interference shielding materials based on silver nanowire/cellulose papers. *ACS Appl. Mater. Interfaces* **8**, 13123–13132 (2016).

49. Suh, Y. D. et al. Nanowire reinforced nanoparticle nanocomposite for highly flexible transparent electrodes: borrowing ideas from macrocomposites in steel-wire reinforced concrete. *J. Mater. Chem. C* **5**, 791–798 (2017).

50. Lan, W. *et al.* Ultraflexible transparent film heater made of Ag nanowire/PVA composite for rapid-response thermotherapy pads. *ACS Appl. Mater. Interfaces* **9**, 6644–6651 (2017).

51. Jang, D.-W., Lee, J.-H., Kim, A., Lee, S.-B. & Hong, S.-G. Self-heating-induced deterioration of electromechanical performance in polymer-supported metal films for flexible electronics. *Sci. Rep.* **7**, 12506 (2017).

7.11 Supplementary Information

Supplementary Methods

Materials

In this study we used PAN (M_w 150,000 g/mol, Polysciences, Inc., Warrington, PA, United States), PCL (Capa 6800, M_w 120,000 g/mol, Perstorp UK Ltd. Cheshire, United Kingdom), dimethylformamide (DMF, p.a. 99.8%, WR International GmbH, Darmstadt, Germany), silver nitrate ($AgNO_3$, p.a. 99.9999%, Sigma-Aldrich Chemie GmbH, Taufkirchen, Germany), polyvinylpyrrolidone (PVP K30, M_w 40,000 g/mol, Sigma-Aldrich Chemie GmbH, Taufkirchen, Germany), ethylene glycol (p.a. ≥99.5%, Fluka), iron chloride ($FeCl_3$, p.a. 98.0%, Sigma-Aldrich Chemie GmbH, Taufkirchen, Germany) and sodium chloride (NaCl, p.a. 99.0% VWR International GmbH, Darmstadt, Germany). 2-propanol and technical-grade acetone were distilled prior to use.

Analytical Methods

For scanning electron microscopy (SEM) analysis, a Zeiss LEO 1530 (Jena, Germany) with a Schottky field-emission cathode was employed for characterisation of the silver nanowires (AgNW) and the resulting nanowire-polymer nonwovens. The samples were stuck onto a sample holder with double-sided adhesive tape and subsequently coated with 2.0 nm of platinum by a high-resolution sputter coater (208 HR, Cressington). A secondary electron (SE2) detector was used for SE2 images at an acceleration voltage of 2 kV and a working distance of ca. 4.5 mm. Backscattered electron (BSE) measurements were performed with a Robinson detector at an acceleration voltage of 10 kV and a working distance of 10 mm. The samples for the BSE measurements were previously conducted with alumina strips.

EDX measurements were performed with a Zeiss Ultra Plus (Jena, Germany) with a Schottky field-emission cathode with an acceleration voltage of 10 kV. The samples were vapour coated with carbon using a Balzer Union MED 010 prior to measurement.

The AgNW were characterized with an elastic bright-field transmission electron microscope (TEM, Zeiss 922 Omega EFTEM, Jena, Germany) at a voltage of 200 kV. The original AgNW dispersion was dropped on a carbon-coated copper grid on filter paper. After drying in air, TEM characterisation was performed. To determine the AgNW diameter, 100 AgNW were measured using the ImageJ software.

Thermogravimetric analysis (TGA Libra F1, Netzsch, Selb, Germany) was performed with corundum crucibles to determine the content of AgNW in composite nonwoven. The heating rate was set to 20 K/min, and the samples were analysed under synthetic air atmosphere from 25 °C to 650 °C.

Pore size measurements were performed with a PSM 165/H (pore size metre, Dresden, Germany) from Topas with Topor as the test liquid (surface tension of 16.0 mN/m). An adapter with an inner diameter of 11 mm was used as the sample holder, and a flow rate of up to 70 L/min was applied. The presented values are averages of at least three measurements.

Resistivity measurements (Four point measurements) were performed using a Keithley 2420 High-Current Source Meter coupled with a Signatone SYS-301. The resistivity was measured ten times for each sample. The durability of the conductive nonwoven was shown by making same measurements after bending for 10000 times.

Voltage source heating was performed with a DF-3010 lab power source with fixed voltages of 1.1 V. The heating and cooling time was set to 60 s. The temperature was recorded at three sites with a Keysight U5856A IR camera. This was done in bended and unbended state.

For the tensile tests, specimens with a length of 3 cm and a width of 1 cm were cut from each nonwoven sample. The specimen was mounted on the tensile tester (zwickiLine Z0.5; BT1-FR0.5TN.D14; Zwick/Roell, Germany), with a clamping length of 2 cm, a crosshead speed of

2 mm/min at 20 °C and a pre-tension of 0.05 N/mm. The load cell was a Zwick/Roell KAF TC with a nominal load of 200 N. The thickness of the samples was measured with a screw micrometer.

The bending stiffness of the resultant nonwovens was tested using a softness analyser (RRY-1000, Hangzhou Qingtong & Boke Automation Technology Co., Ltd., China) following ASTM standard D 2923-01. The pressed depth of the indenter path was 8 mm with a slit width of 5 mm, and the pressure exerted on the nonwovens was recorded by a pressure sensor as the bending stiffness (sample parameters: area of 10 cm × 10 cm and thickness of 50 ± 5 μm).

Breathing test was performed with a self-made assembly. The conductive nonwoven was fixed at one end of a rubber tube which was fixed (air-tight) to a flask containing solid carbon dioxide. The other end of the rubber tube was immersed in phenolphthalein/limewater mixture. The carbon dioxide gas generated at room temperature from solid carbon dioxide permeated through the nonwoven and could be seen bubbling in the lime water solution. Moreover, the carbon dioxide neutralised the limewater solution and therefore the color of the phenolphthalein containing solution changed from pink to colorless (Video S7.1). A dense polyethylene (PE) film was used as a negative blank (Video S7.2).

Experimental Procedures

Synthesis of AgNW batch A

The AgNW were synthesized using the polyol process by Bergin *et al.*[1] First, 160 mL of ethylene glycol (EG) was added to a 500 mL Schlenk flask, stirred at 500 rpm and preheated in an oil bath at 130 °C for 1 hour. Next, 0.2 mL of NaCl (0.1985 g in 10 mL EG), 0.1 mL of $FeCl_3$ (0.054 g in 10 mL EG), 20.76 mL of PVP K30 (1.05 g in 25 mL EG) and 20.76 mL of $AgNO_3$ (1.05 g in 25 mL EG) were added to the nitrogen-purged flask. The reaction was carried out at 130 °C for 6 h. The reaction solution was cooled to room temperature, and acetone was added until the AgNW flocculated. This purification process with acetone was repeated three

times. During the last purification process, the AgNW were centrifuged at 1000 rpm for 10 min. The obtained AgNW were dispersed in water to give an AgNW dispersion with a concentration of 183 mg/mL.

The AgNW were hydrophilic due to the application of a PVP coating on their surface and consequently could be dispersed in water (Supplementary Fig. S7.1). The AgNW had diameters in the range of 30 to 280 nm (average diameter: 76 nm). The length of the AgNW was in the range of 5 to 35 µm (average length: 14 µm), resulting in an aspect ratio of approximately 190. The silver content in the AgNW was 97%, according to TGA (Supplementary Fig. S7.6).

The AgNW of batch B were prepared according to the same protocol but the solution was not stirred.

Preparation of PAN nanofibres and PCL nanofibres

PAN nanofibre nonwovens were obtained by electrospinning of 10 wt% PAN in DMF solution. The PAN fibres were collected on aluminium foil at a distance of 15 cm. The electrospinning process involved a KD Scientific syringe pump with a 20 mL syringe and a 0.9-mm-diameter needle at a positive voltage of 20 kV at 25 °C and a relative humidity of 35%.

PCL fibres were electrospun from 15 wt% PCL in a mixture of THF/DMF (70/30 wt%). The PCL fibres were collected on aluminium foil at a distance of 15 cm under the same conditions as used in the PAN fibre preparation, except for a positive voltage of 14 kV.

The SEM images of the PAN or PCL nonwovens are shown in Figs. 1b, 1c. PAN nanofibres were obtained with an average diameter of 307 ± 82 nm, and the PCL fibres had an average diameter of 714 ± 593 nm.

Preparation of short PAN nanofibre and PCL nanofibre dispersions

Dispersions of short PAN or PCL nanofibres were obtained by cutting 1.00 g of the electrospun PAN or PCL nanofibre mat and blending it in a mixture of 700 mL of 2-propanol and 300 mL

of demineralized water at -18 °C (Robot Coupe Blixer 4, Rudolf Lange GmbH & Co. KG) for 2 min at 3500 rpm.

Preparation of conductive PAN/PCL/AgNW short fibre nonwoven

The preparation of the PAN/PCL/AgNW nonwovens was accomplished as shown schematically in Fig. 7.1a. A 2:1 ratio of PAN/PCL suited well for the desired application. First, 20 mL of the PAN nanofibre dispersion containing 1.00 g/L PAN nanofibres and 10 mL of the PCL nanofibre dispersion containing 1.00 g/L PCL nanofibres were mixed. Then, the AgNW (183 mg/mL AgNW dispersion in water) were immersed in this dispersion. The non-conductive nonwovens were prepared without AgNW as earlier mentioned (Fig. 7.1e). The mixture was shaken and passed through a round 325-mesh stainless-steel sieve with a diameter of 60 mm. The sieve was pressed to a glass frit to achieve a homogeneous flow through the stainless-steel sieve. The short PAN and PCL fibers and the AgNW formed the nonwoven on top of the stainless steel sieve. During this process, some AgNW passed through the stainless-steel sieve. The achieved fibre mat was dried under vacuum for 10 min at a pressure of 0.1 mbar. To induce thermal annealing, the nonwovens were pressed between two glass plates and heated at a temperature of 75 °C for 15 s to melt the PCL fibres and fabricate high mechanical stable composite nonwovens.

Supplementary Table 7.1 | Preparation and properties of composite nonwovens.

Experiment No.	PAN dispersion[1] (mL)	PCL dispersion[2] (mL)	AgNW dispersion[3] (µL)	Fraction of AgNW in nonwoven[4] (vol%)	Density (g/cm^3)	Porosity (%)	Resistance (Ω m)	Electrical conductivity (S/m)
1	20	10	0	0.00	0.245	79.5	333 ± 143	0.003 ± 0.004
2	20	10	32	0.16	0.248	86.4	566 ± 532	0.002 ± 0.002
3	20	10	64	0.27	0.253	88.7	148 ± 110	0.007 ± 0.009
4	20	10	96	0.36	0.258	90.0	$3.28 \times 10^{-4} \pm 1.18 \times 10^{-3}$	3047 ± 845
5	20	10	128	0.45	0.259	91.0	$7.96 \times 10^{-5} \pm 2.40 \times 10^{-4}$	12570 ± 4170
6	20	10	160	0.65	0.295	91.1	$4.42 \times 10^{-5} \pm 2.62 \times 10^{-4}$	22640 ± 3010
7	20	10	192	0.63	0.263	92.6	$2.73 \times 10^{-5} \pm 3.32 \times 10^{-4}$	36670 ± 3810
8	20	10	224	0.78	0.297	92.1	$1.97 \times 10^{-5} \pm 2.02 \times 10^{-4}$	50720 ± 4950
9	20	10	256	0.96	0.284	93.0	$1.52 \times 10^{-5} \pm 9.71 \times 10^{-5}$	66000 ± 7200
10	20	10	288	0.92	0.302	93.5	$1.46 \times 10^{-5} \pm 1.39 \times 10^{-5}$	68530 ± 10300
11	20	10	320	1.07	0.307	93.3	$1.07 \times 10^{-5} \pm 6.94 \times 10^{-5}$	93610 ± 14400

12	**20**	**10**	**690**	**2.30**	**0.487**	**91.6**	**$4.56 \times 10^{-6} \pm 4.18 \times 10^{-6}$**	**219519 ± 19729**
13	**20**	**10**	**690**	**2.25**	**0.414**	**93.6**	**$2.46 \times 10^{-6} \pm 2.33 \times 10^{-6}$**	**406811 ± 23167**
14	**20**	**10**	**835**	**2.79**	**0.441**	**94.0**	**$1.79 \times 10^{-6} \pm 1.67 \times 10^{-6}$**	**557929 ± 41027**
15	**20**	**10**	**1003**	**3.35**	**0.467**	**94.1**	**$1.32 \times 10^{-6} \pm 9.37 \times 10^{-7}$**	**756375 ± 310993**

[1]Concentration of PAN dispersion = 1.00 g/L

[2]Concentration of PCL dispersion = 1.00 g/L

[3]Concentration of AgNW dispersion = 183 g/L

[4]Determined gravimetrically by TGA

Supplementary Table 7.2 | The electrical conductivity and bending stiffness of composite nonwovens.

PAN nanofibre dispersion volume[1] (mL)	PCL nanofibre dispersion volume[2] (mL)	Amount of AgNW in nonwoven[3] (vol%)	Electrical conductivity (S/m)	Bending stiffness (mN)
250	125	0	0	99 ± 4
180	90	0.21	2	28 ± 3
180	90	0.33	1218	57 ± 3
180	90	0.75	44634	80 ± 4

[1]Concentration of PAN dispersion = 1.00 g/L

[2]Concentration of PCL dispersion = 1.00 g/L

[3]Determined gravimetrically by TGA

Supplementary Table 7.3 | Electrical conductivity of the composite nonwovens in dependence of the bending angle.

AgNW content (vol%)	Beding angle (°)	Electrical conductivity (S/m)
0.36	0	3932
	99	3942
	123	9347
	148	3949
	180	3949
0.45	0	15214
	86	15237
	114	15293
	139	15292
	180	15274
0.63	0	38554
	107	38993
	123	39372
	180	39145
1.07	0	97064
	58	97179
	71	97901
	87	97877
	94	97543
	180	97259

Supplementary Table 7.4 | Summary of the electrical conductivity of composite nonwovens with different additives.

Point	Material	Additive content (vol%)	Elctrical conductivity (S/m)	Reference
1	CNT/PLA fibres	1.3	0.1	2
2	Carbon black/PLA fibres	5	0.1	2
3	PANI/natural rubber fibres	5	1	3
4	PANI-dodecylbenzene sulfonic acid/Co-PAN fibres	10	0.1	4
5	CNT/PET fibres	10	5	5
6	PANI/bacterial cellulose fibres	10.7	0.5	6
7	PEDOT:PSS/PNN fibres	19,9	1120	7
8	PEDOT:PSS/hollow carbon fibres	25	4700	8
9	PANI/PS fibres	50	0.1	9
10	MWCNT/cellulose fibres	16.5	671	10
11	AgNW/cellulose fibres	0.53	6751	11
This work	PAN/PCL/AgNW(A) nonwoven	1.07	95000	
This work	PAN/PCL/AgNW(B) nonwoven	3.35	756000	

Supplementary Table 7.5 | Summary of the mechanical properties of the PAN/PCL/AgNW nonwovens with different AgNW contents.

AgNW content (vol%)	Young's modulus (MPa)	Elongation at break (%)	Tensile strength (MPa)
0.00	50.04 ± 10.13	17.55 ± 1.28	2.95 ± 0.55
0.16	89.35 ± 7.01	19.42 ± 0.89	4.95 ± 0.29
0.27	93.37 ± 15.99	15.97 ± 2.60	4.61 ± 0.52
0.36	75.61 ± 3.30	19.43 ± 1.46	4.09 ± 0.26
0.45	92.05 ± 16.73	18.08 ± 1.41	4.59 ± 0.60
0.63	114.07 ± 3.99	19.51 ± 2.55	5.62 ± 0.20
0.65	108.13 ± 5.44	16.76 ± 1.17	4.99 ± 0.08
0.78	102.41 ± 8.51	14.90 ± 1.59	3.45 ± 0.28
0.92	89.82 ± 13.63	14.20 ± 2.01	3.66 ± 0.28
0.96	130.98 ±9.55	14.08 ± 0.58	4.93 ± 0.35
1.07	141.83 ± 56.46	11.72 ± 2.93	3.40 ± 1.02

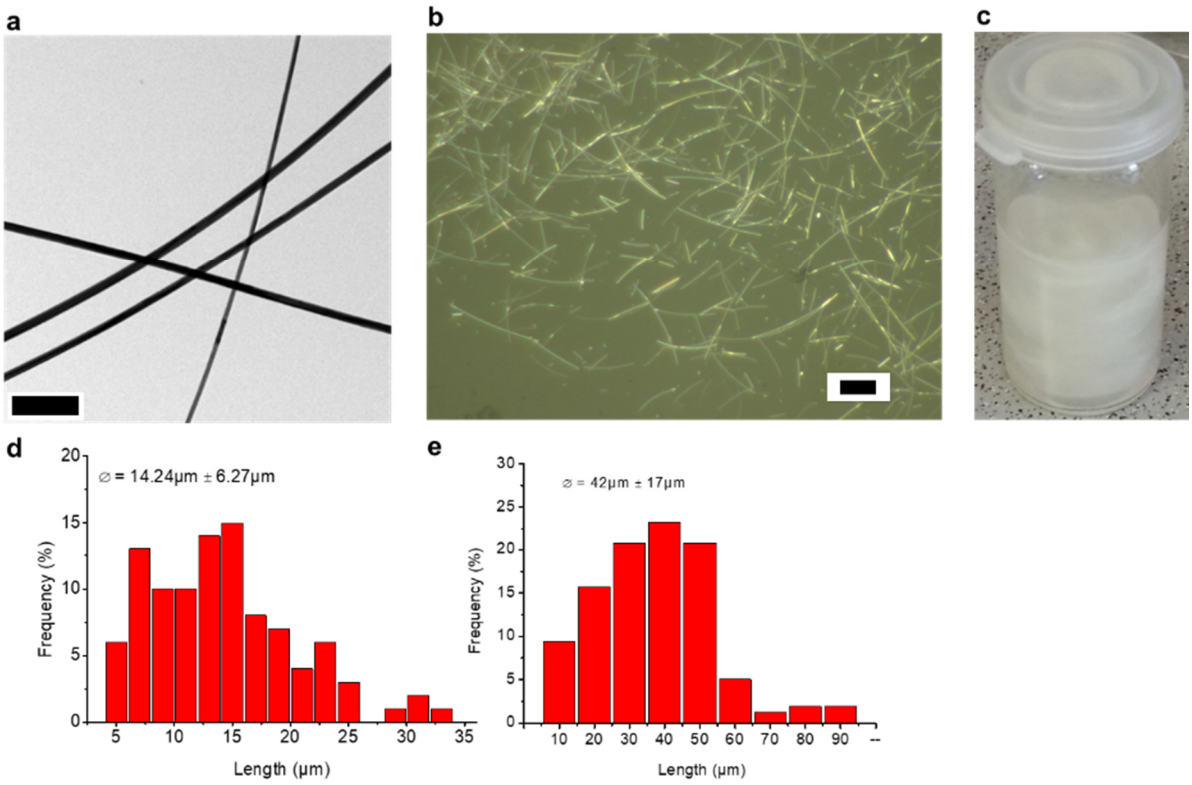

Supplementary Figure 7.1 | Characterisation of AgNW. a, TEM image of the AgNW. Scale bar 500 nm, b, Optical microscopy image of the AgNW. Scale bar 10 µm, c, Dispersion of the AgNW in water. d, Frequency distribution of the AgNW length of AgNW batch A as determined using ImageJ software. e, Frequency distribution of the length of AgNW batch B as determined using ImageJ software. Ø is used as a symbol for the mean value.

Discussion of the morphology of the nonwovens

The AgNW could not be detected with a normal SE detector (Supplementary Fig. S2). The BSE detector showed the material contrast between the polymer fibres and the AgNW. The polymer fibres appear dull, while the AgNW appear bright. The SEM/BSE images show the increasing content of AgNW with the addition of the AgNW dispersion (Supplementary Fig. S3).

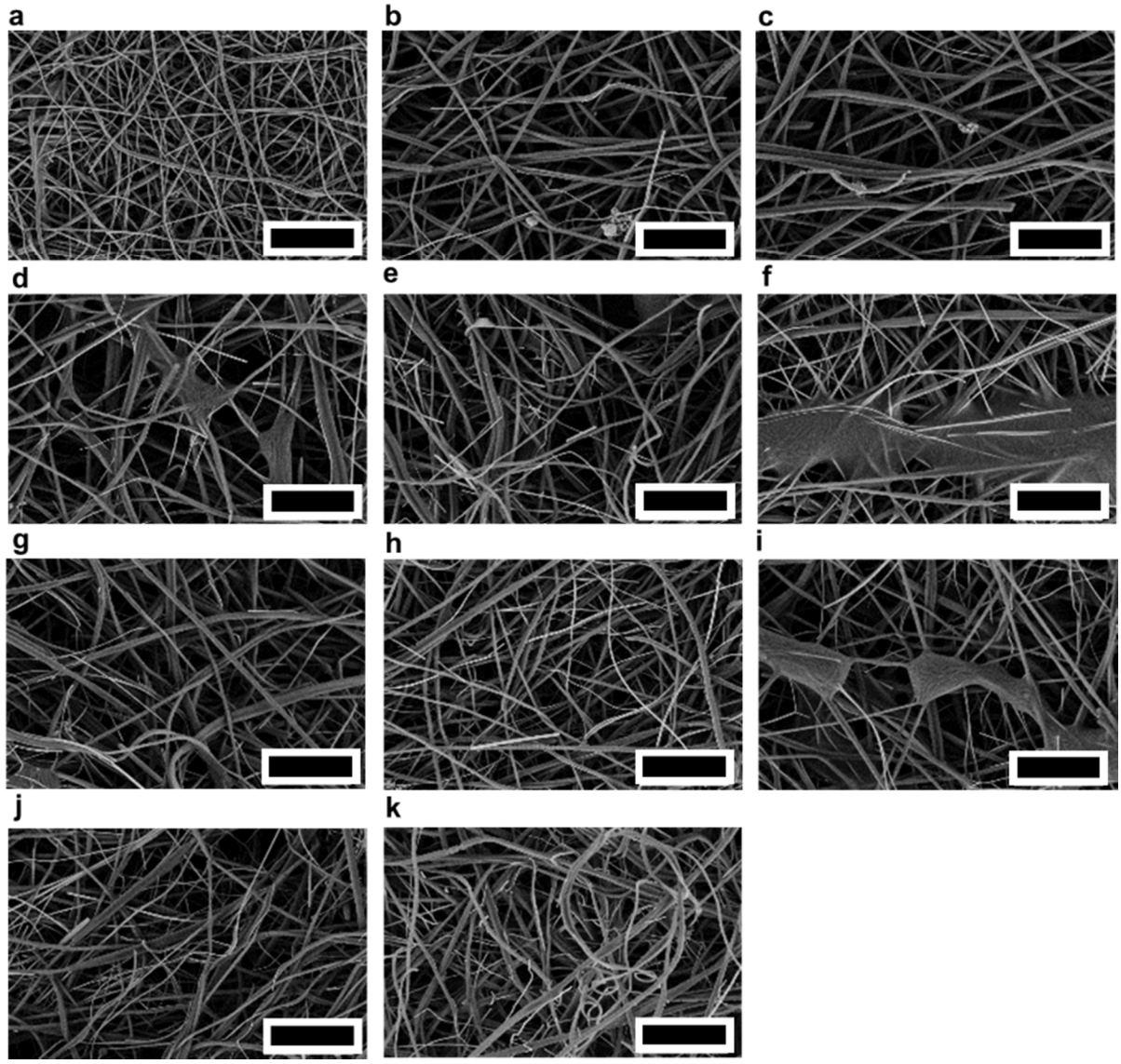

Supplementary Figure 7.2 | SEM images of the conductive PAN/PCL/AgNW nonwovens with increasing AgNW content. a, 0.00 vol% AgNW. b, 0.16 vol% AgNW. c, 0.27 vol% AgNW. d, 0.36 vol% AgNW. e, 0.45 vol% AgNW. f, 0.63 vol% AgNW. g, 0.65 vol% AgNW. h, 0.78 vol% AgNW. i, 0.92 vol% AgNW. j, 0.96 vol% AgNW. k, 1.07 vol% AgNW. Scale bar 5 µm.

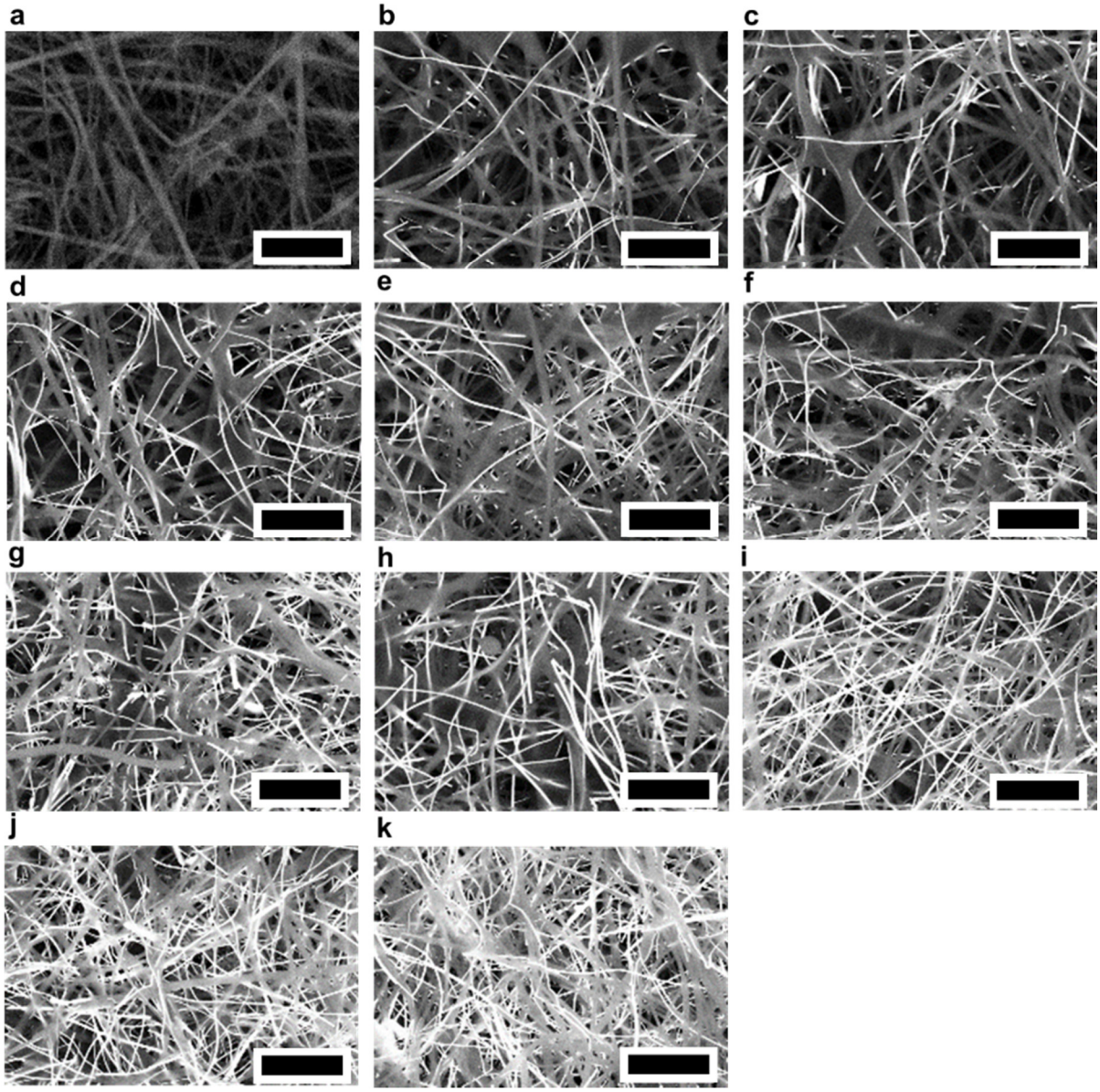

Supplementary Figure 7.3 | SEM images with the BSE detector of the conductive PAN/PCL/AgNW nonwovens with increasing AgNW content. a, 0.00 vol% AgNW. b, 0.16 vol% AgNW. c, 0.27 vol% AgNW. d, 0.36 vol% AgNW. e, 0.45 vol% AgNW. f, 0.63 vol% AgNW. g, 0.65 vol% AgNW. h, 0.78 vol% AgNW. i, 0.92 vol% AgNW. j, 0.96 vol% AgNW. k, 1.07 vol% AgNW. Scale bar 5 µm.

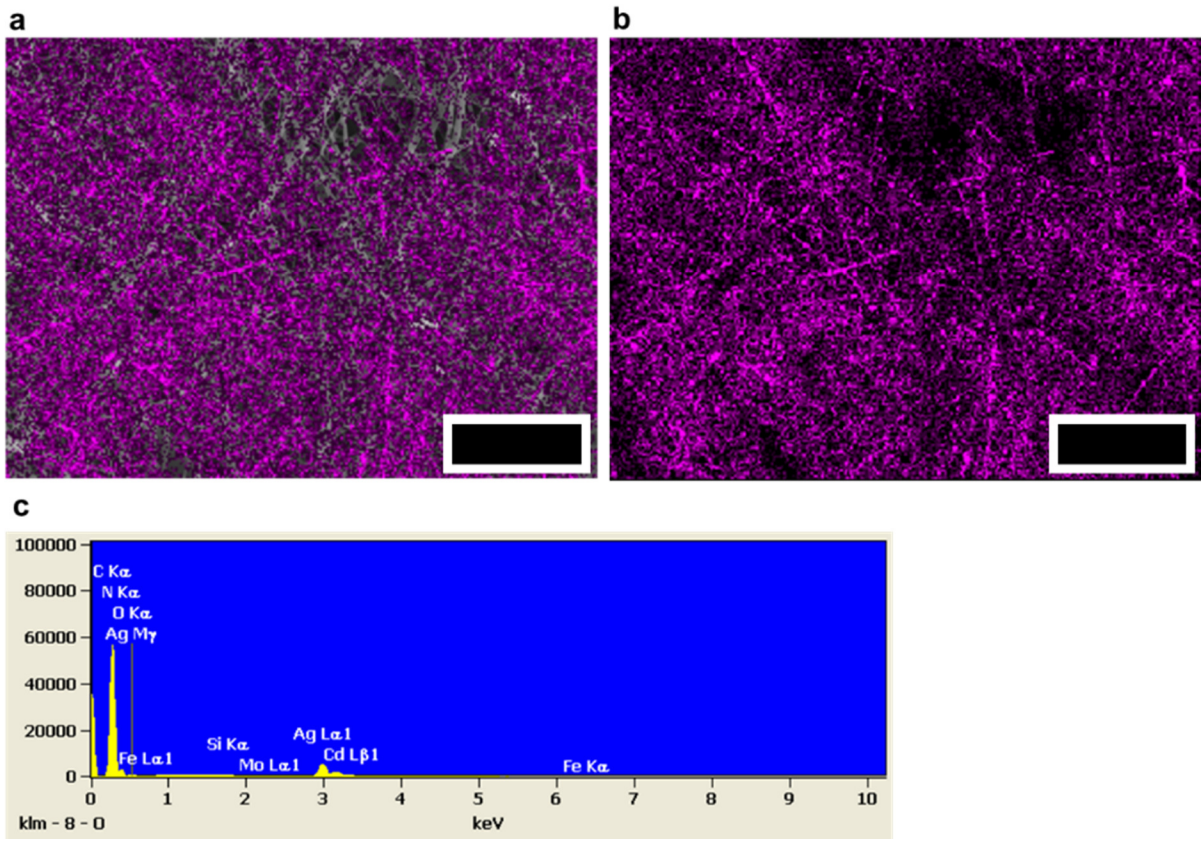

Supplementary Figure 7.4 | SEM/EDX images of the conductive nonwoven with 0.36 vol% AgNW (a–c). a, Overlapped EDX mapping of the conductive nonwoven. b, Single EDX mapping of the conductive nonwoven. c, Corresponding EDX spectra of the EDX mapping of the conductive nonwoven. Scale bar 10 µm.

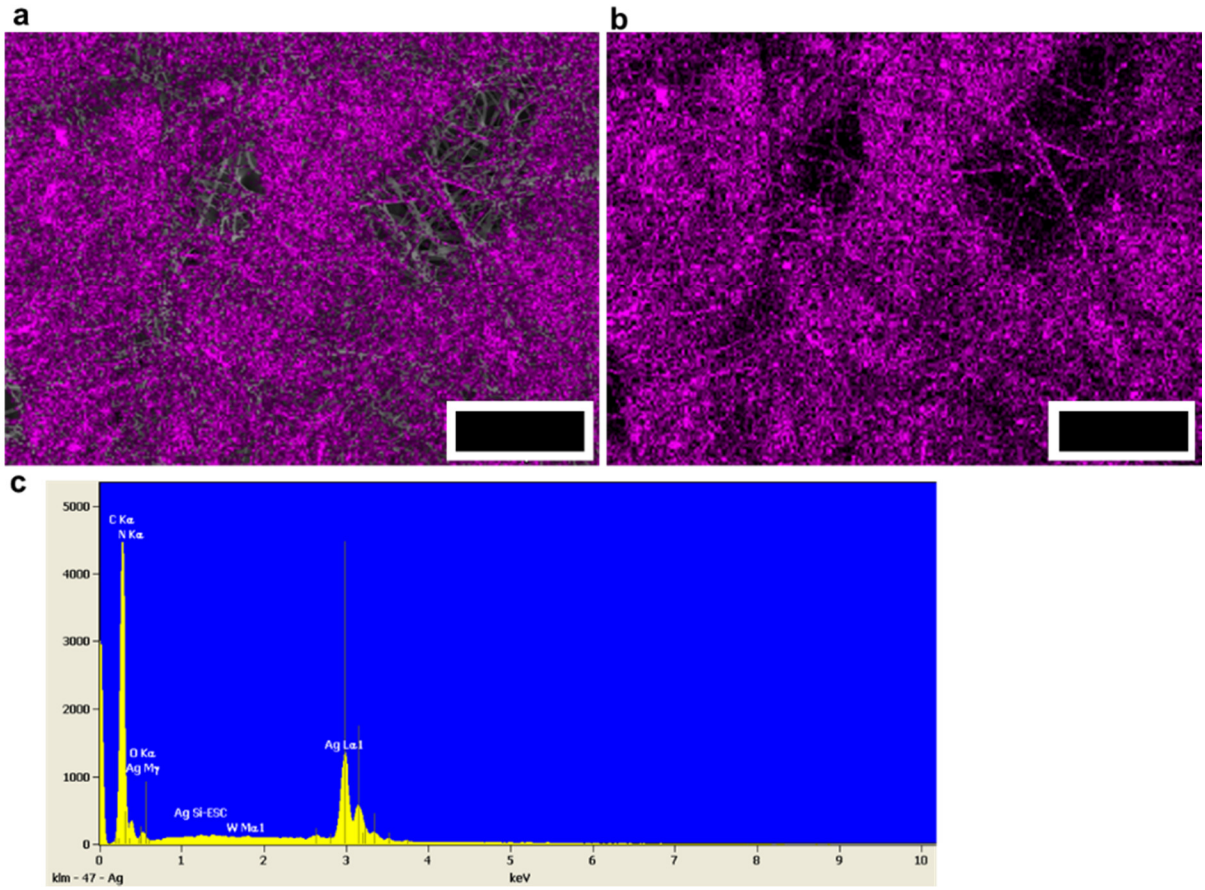

Supplementary Figure 7.5 | SEM/EDX images of the conductive nonwoven with 1.07 vol% AgNW (a–c). a, Overlapped EDX mapping of the conductive nonwoven. b, Single EDX mapping of the conductive nonwoven. c, Corresponding EDX spectra of the EDX mapping of the conductive nonwoven. Scale bar 10 µm

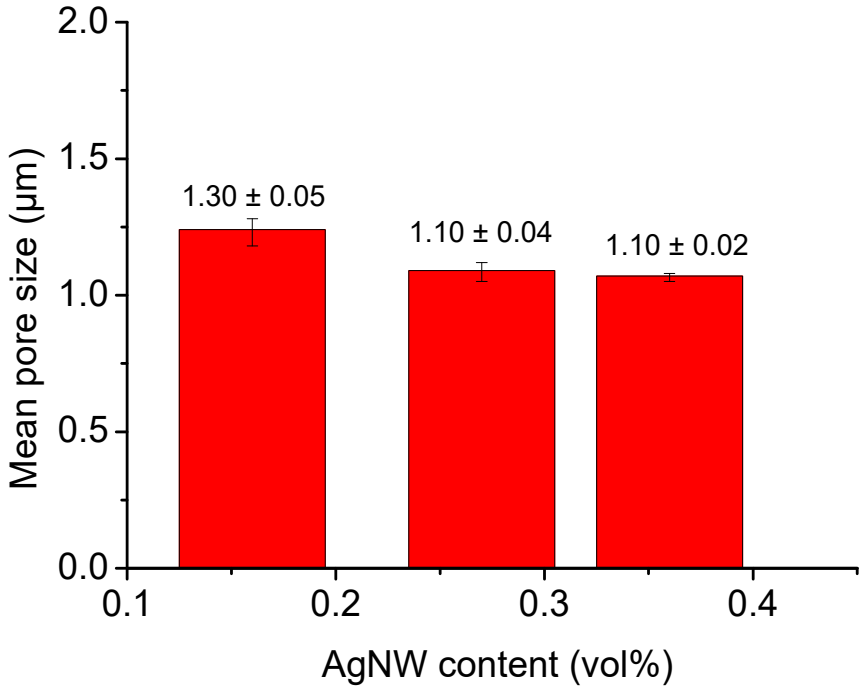

Supplementary Figure 7.6 | Pore size measurements with respect to AgNW content.

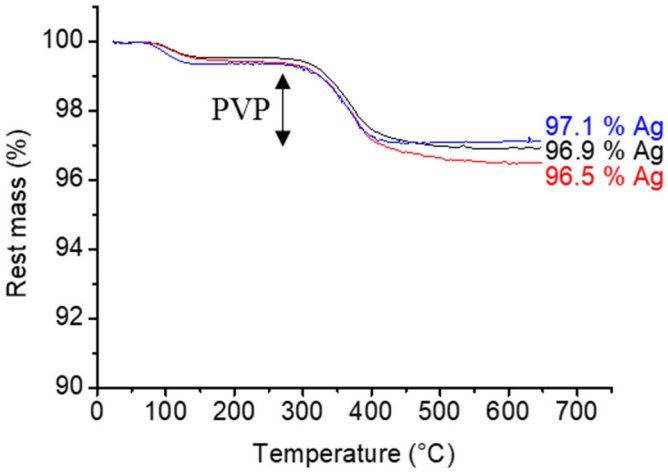

Supplementary Figure 7.7 | Thermogravimetric analysis of the AgNW.

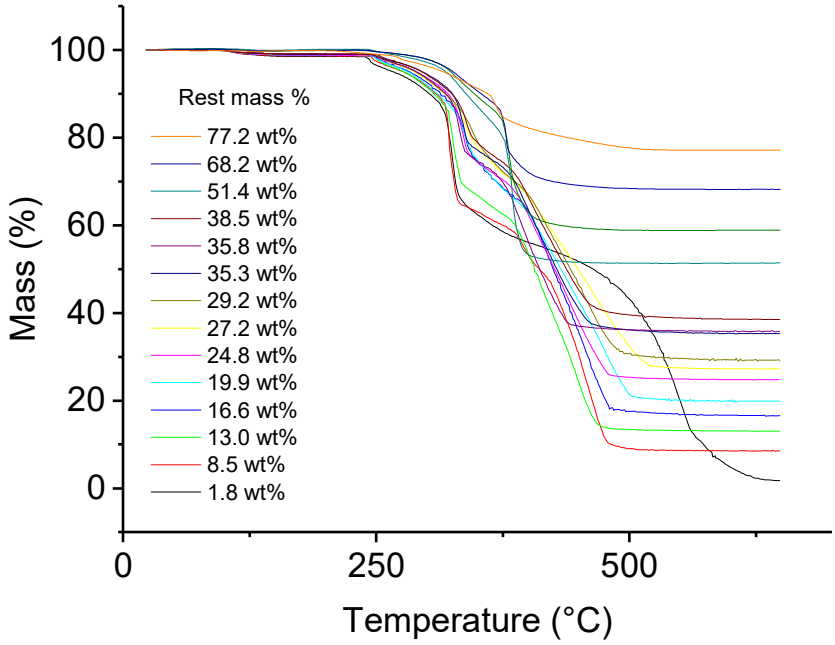

Supplementary Figure 7.8 | Thermogravimetric analysis of the conductive nonwovens with different amounts of AgNW. The black curve represents the non conductive nonwoven.

The volume percentage of AgNW in the nonwovens was calculated using Equations (S1) and (S2) as follows:

$$vol\%(Ag) = \frac{V_{Ag}}{V_{membrane}} = \frac{\frac{m_{Ag}}{\rho_{Ag}}}{\pi r^2 h} \quad \text{(S1)}$$

$$m_{Ag} = (wt\%_{sample} - 1.8\ wt\%) \times m_{membrane} \quad \text{(S2)}$$

where ρ_{Ag} is the density of silver (10.5 g/cm^3), r is the radius of the nonwoven (2.75 cm) (a circular sample was used) and h is the thickness of the nonwoven (approximately 53 µm). $wt\%_{sample}$ is the amount of AgNW in the sample. It is the mass of the sample left after heating to 650ºC as determined from thermogravimetric analysis (refer figure S8). 1.8 $wt\%$ is the amount of sample left after heating for non-conductive nonwoven till 650ºC.

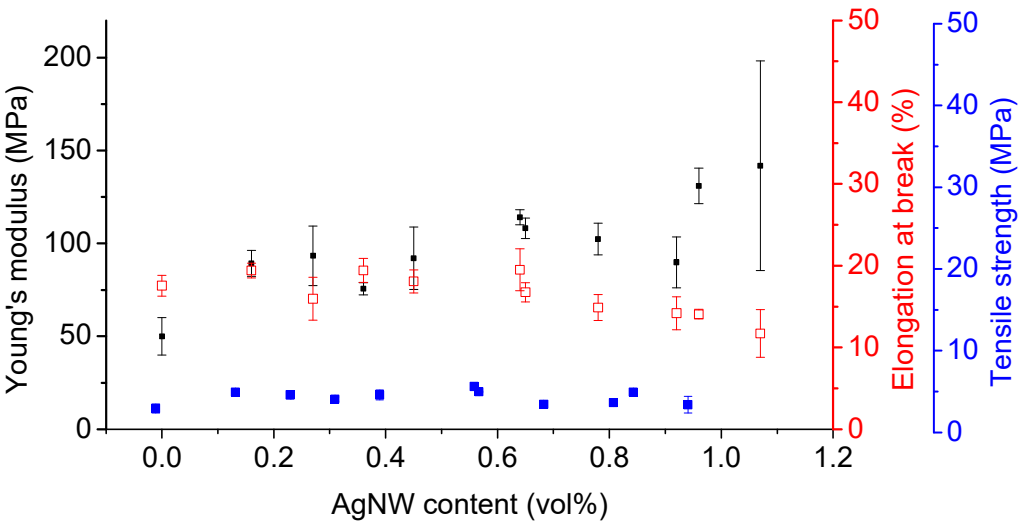

Supplementary Figure 7.9 | Values for tensile tests with increasing AgNW content. By increasing the additive content, the membrane modulus increased, and the elongation at break and the tensile strength had the same value.

Electrical conductivity of the nanofibre composite nonwovens

Electrical conductivities of the PAN/PCL/AgNW nonwovens were calculated according to Equations (S7.3)–(S7.5).

$$R_{sh} = 0.1526 \times 10^{0} \frac{\Omega}{sqr} = 0.1526 \times 10^{0} \frac{\Omega\,\mathrm{m}}{m} \quad \text{(S7.3)}$$

$$\rho = R_{sh} \times l \quad \text{(S7.4)}$$

$$\rho = 0.1526 \times 10^{0} \frac{\Omega \times 1000\,\mathrm{mm}}{m} \times 0.056\,mm = 8.55 \frac{\Omega\,\mathrm{mm}^2}{m}$$

where ρ is the resistivity, R_{sh} is the sheet resistance, l is the thickness of the nonwoven, where σ is the electrical conductivity.

$$\sigma = \frac{1}{\rho} = \frac{1}{8.55 \frac{\Omega\,\mathrm{mm}^2}{m}} = 0.116959 \frac{m}{\Omega\,\mathrm{mm}^2} = 116959 \frac{S}{m} \quad \text{(S7.5)}$$

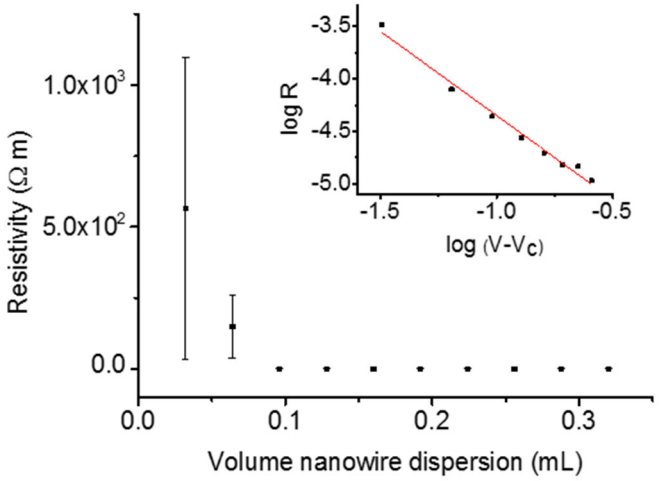

Supplementary Figure 7.10 | Correlation of the resistance with the volume of the nanowire dispersion and the calculation of the critical exponent α (inset figure).

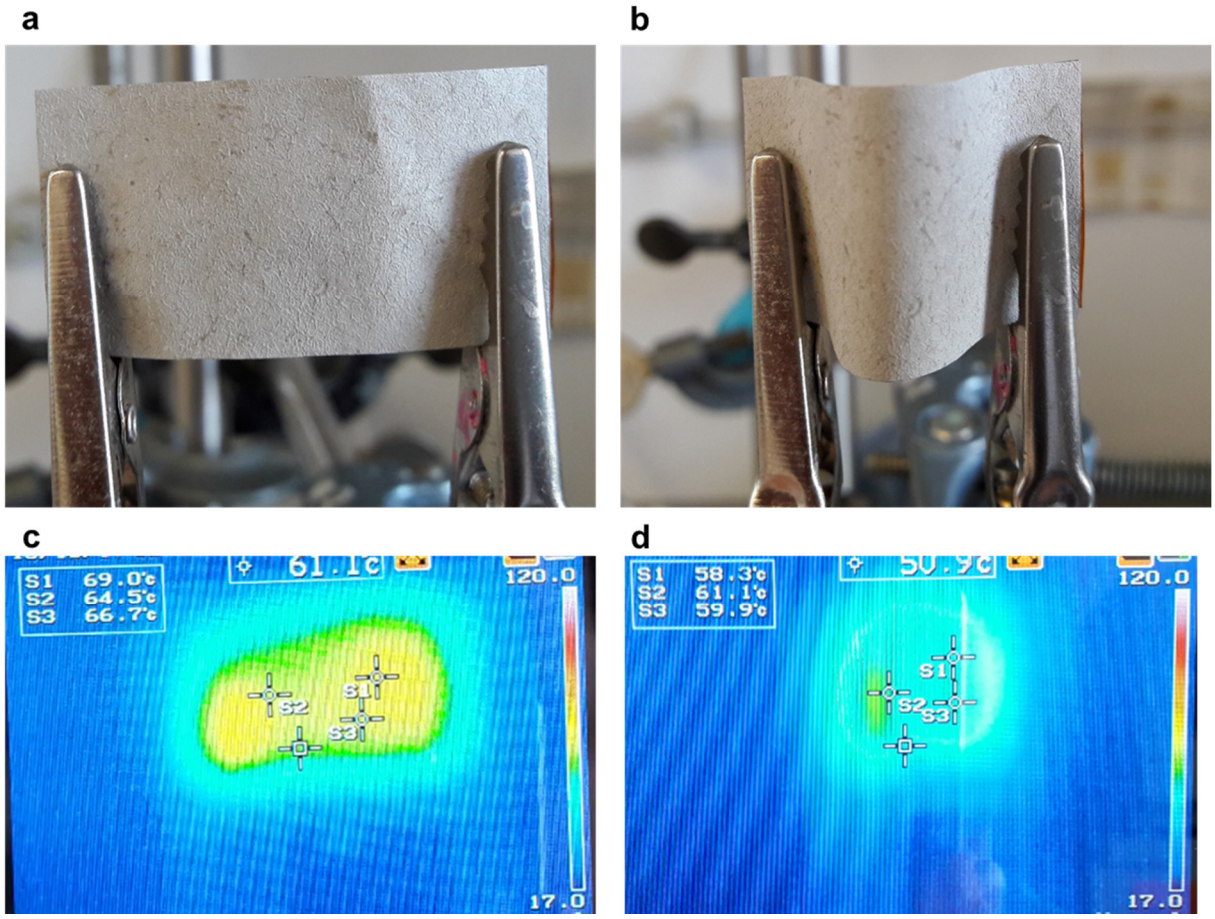

Supplementary Figure 7.11 | Electrical current heating for a sample with 0.90 vol% AgNW. Image of the conductive nonwoven in a, unbended and b, bended state. IR camera image with an applied voltage of 1.1 V in c, unbended and d, bended state. Scale unit: °C

Supplementary References

1. Bergin, S. M. *et al.* The effect of nanowire length and diameter on the properties of transparent, conducting nanowire films. *Nanoscale* **4**, 1996–2004 (2012).

2. Li, Y. *et al.* Tuning of vapor sensing behaviors of eco-friendly conductive polymer composites utilizing ramie fibre. *Sens. Actuators, B* **221**, 1279–1289 (2015).

3. Sukitpaneenit, P., Thanpitcha, T., Sirivat, A., Weder, C. & Rujiravanit, R. Electrical conductivity and mechanical properties of polyaniline/natural rubber composite fibres. *J. Appl. Polym. Sci*. **106**, 4038–4046 (2007).

4. Jianming, J., Wei, P., Shenglin, Y. & Guang, L. Electrically conductive PANI-DBSA/Co-PAN composite fibres prepared by wet spinning. *Synth. Met.* **149**, 181–186 (2005).

5. Li, Z., Luo, G., Wei, F. & Huang, Y. Microstructure of carbon nanotubes/PET conductive composites fibres and their properties. *Compos. Sci. Technol.* **66**, 1022–1029 (2006).

6. Hu, W., Chen, S., Yang, Z., Liu, L. & Wang, H. Flexible electrically conductive nanocomposite membrane based on bacterial cellulose and polyaniline. *J. Phys. Chem. B* **115**, 8453–8457 (2011).

7. Huang, S.-R. *et al.* Thermoresponsive conductive polymer composite thin film and fibre mat: Crosslinked PEDOT:PSS and P(NIPAAm-*co*-NMA) composite. *J. Polym. Sci. Part A: Polym. Chem.* **54**, 1078–1087 (2016).

8. Qu, G. *et al*. A Fibre supercapacitor with high energy density based on hollow graphene/conducting polymer fibre electrode. *Adv. Mater.* **28**, 3646–3652 (2016).

9. Yin, X. H. *et al.* Percolation conduction in polymer composites containing polypyrrole coated insulating polymer fibre and conducting polymer. *Synth. Met.* **96**, 367–368 (1995).

10. Imai, M., Akiyama, K., Tanaka, T. & Sano, E. Highly strong and conductive carbon nanotube/cellulose composite paper. *Compos. Sci. Technol.* **70**, 1564–1570 (2010).

11. Lee, T.-W., Lee, S.-E. & Jeong, Y. G. Highly effective electromagnetic interference shielding materials based on silver nanowire/cellulose papers. *ACS Appl. Mater. Interfaces* **8**, 13123–13132 (2016).

8. Exploration of the electrical conductivity of double network silver nanowires - polyimide porous low density compressible sponges

Published in *ACS Applied Materials & Interfaces* ***2017****, 9(39), 34286-34293.*

*Shaohua Jiang, Steffen Reich, Bianca Uch, Pin Hu, Seema Agarwal, Andreas Greiner**

Macromolecular Chemistry, Bavarian Polymer Institute, University of Bayreuth, Universitätsstraße 30, 95440 Bayreuth, Germany

* E-mail: greiner@uni-bayreuth.de *

8.1 KEYWORDS

Responsivity; conductivity; sponge; electrospinning; compression; electric heating.

8.2 ABSTRACT

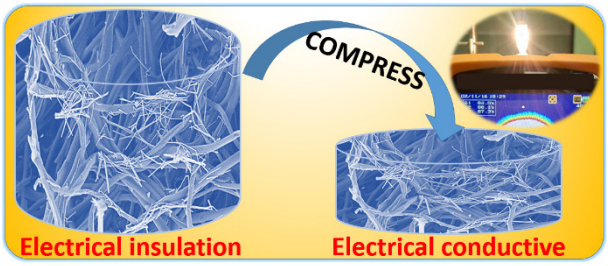

Stress-responsive, highly flexible, and breathable nanocomposite sponges show electric conductivity from 170 –16660 S/m depending on the applied stress. Key for the responsive electric conductivity of the sponges is the change of percolation of the silver nanowires. These sponges made of short electrospun fibers and silver nanowires could be applied without any amplifier for the operation of automobile bulbs and as an efficient Joule heater. The times required for electric heating (current on) and cooling are very short. Interestingly, the maximum

temperature reached by electric heating depend on the compression status. The higher the compression status the lower is the maximum temperature which is in accordance with the understanding for Joule heaters. It is noteworthy that these sponges are thermally, chemically, and mechanically very stable. These conductive sponges will open a new area for novel conductive devices with relevance for real-world applications.

8.3 INTRODUCTION

Three dimensional (3D) polymer sponges with interconnected networks have promising features, such as low density, high porosity, gas permeability, and mechanical stability.[1] Sponges with this set of properties could find applications for electrodes, filtration, oil/water separation, solvent absorption, catalysts, tissue engineering and pressure sensors.[2-8] Most of the reported studies on conductive sponges are focused on the carbonaceous materials made from carbon nanotubes (CNTs), carbon nanofibers (CNFs), and graphenes.[4, 9-20] The conductive materials are self-assembled in the form of 3D networks. For example, the graphene ultralight 3D network (graphene foam) show an electrical conductivity of 7 ~ 10 S/cm.[17] The electrical conductivity of carbon nanotubes network is in general < 10 S/cm. The conductivity of carbon nanofiber aerogel of density ~ 6 mg/cm^3 was 0.21 S/cm.[10] For making conductive polymer composites, the polymer is penetrated into the conductive networks. The PDMS-carbon nanotube aerogels and PDMS-graphite show a conductivity of 1.08 S/cm and 2 S/cm, respectively.[18-19] 3D interconnected graphene networks made by a self-assembly process of graphene oxide and polymer particles at 4.8 vol% graphene shows a high electrical conductivity of 10.8 S/cm.[20] In further efforts to enhance conductivity, the silver nanowires (AgNWs)/graphene/polymer sponge composites were made. They show electrical conductivity of ~10 S/cm for ~18 mg/cm^3, which corresponds to a porosity of ~ 99.7 vol%.[21] Infiltration of

silver nanowires in commercially available PU sponges are also tried and showed conductivity < 20 S/cm.[22] Metallization of 3D polymer sponges by a very thin coating of metals or other conductive materials is another method for making insulating polymer sponges conductive.[23-24] The polymer sponges used for conductivity modifications, in general are mostly commercially available polyurethane, polydimethylsiloxane (PDMS) and melamine-formaldehyde sponges with macropores and high density.

Recently, a new concept has been applied for the preparation of polymeric ultralight open-cell sponges based on the self-assembly of short electrospun fibers during freeze-drying.[6-7, 25-28] The sponges have bimodal pore size distribution with big pores (~ 100 μm) and the small pores < 10 μm in diameter and density as low as 4 ~ 5 mg/cm^3 possible. Several different types of polymer sponges can be made using this method. It would be interesting to study high temperature stable conductive ultra-light weight polymer sponges for use as Joule heaters, light weight constructions, pressure sensors, tissue engineering etc. Therefore, in this study we wanted to explore the preparation of thermally stable and highly conductive polymer sponges. For the thermal and chemical stability, we selected polyimide (PI), which is well-known to have excellent thermal and chemical stability, and excellent electrospinnability from its precursor,[29-30] can be processed to nanocomposites,[31] and could be even electrospun from water.[32] PI is insoluble and therefore obtained by annealing from its soluble precursor poly (amic acid) (PAA) by polymer analogous conversion. As PI is inherently electrically insulating like most other polymers we have selected silver nanowires (AgNWs) as conductive filler which combines metallic electrical conductive and shape anisotropy. The shape anisotropy will provide high conductivity by percolation even at low filler content.[33] Moreover, sponges with dual pore size distribution (large and small pores (< 10 μm)) are expected to provide a 3D network of AgNWs on infiltration with inter- and intra-coverage of pores with AgNWs. With this concept, we show here, light weight PI/AgNWs nanocomposite sponges with stress responsivity, high thermal and mechanical stability, and excellent flexibility. The very high conductivity of 166.6 S/cm

was achievable depending upon the compressive strain. We also show that the sponges can be applied as Joule heaters, which makes them of particular interest for applications as they combine the features of thermal insulation and heating on demand depending on applied voltage. We strongly believe that these new concepts for the preparation of conductive and stable polymer nanofiber sponges will foster the preparation of many new type of nanocomposite ultralight sponges.

8.4 EXPERIMENTAL SECTION

Materials

Electrospun polyamic acid (PAA) and polyimide (PI) fibrous mats made from monomers of pyromellitic dianhydride and 4,4'-oxydianiline are kindly provided by Jiangxi Xian Cai Nanofibers Technology Co., Ltd. 10 g of PI mats (10 g) were cut into small pieces and mixed with 1 L of solvents (dioxane/water, 50/50, v/v). The mixture was cooled with liquid nitrogen until it is pasty. Then the paste was cut by a mixer (Robot Coupe Blixer 4, Rudolf Lange GmbH & Co. KG) at 3500 rpm for 2 min. After that, the powder of short fibers were obtained by freeze-drying for 24 h. Ethylene glycol (EG**,** 99.5%, Fluka), $FeCl_3$ (99.9%, Sigma-Aldrich), poly (vinyl pyrrolidone) (PVP, K40, Sigma-Aldrich) $AgNO_3$ (>99%, Sigma-Aldrich), and polyethyleneimine (PEI**,** M_n ~ 1200 g/mol, 50 wt% solution, Sigma-Aldrich) were used as received.

Preparation of PI sponge (PIS)

120 mg of PI short fibers were mixed with 29 mL of dioxane and 1 mL of PAA solutions (50 mg of PAA in DMSO). The short fiber dispersion was freeze-dried into sponges. Then the obtained sponges were thermally imidized using the following protocol: 1) heating to 150 °C (3 °C/min) and annealing for 1 h; 2) heating to 350 °C (1.5 °C/min) and annealing for 1 h; 3) cooling down to room temperature. The obtained PIS possessed a density of 10.1 mg/cm^3.

Preparation of AgNWs

AgNWs were synthesized using the polyol process according to a previous report.[34] 160 mL EG was preheated at 130 °C for 1 hour under 500 rpm magnetic stirring. 0.2 mL NaCl (0.01985 g/mL), 0.1 mL $FeCl_3$ (0.0054 g/mL), 20.76 mL PVP (0.042 g/mL) and 20.76 mL $AgNO_3$ (0.042 g/mL) in EG were added to the above hot EG under nitrogen atmosphere. After reaction at 130 °C for 6 h, the solution was cooled down to room temperature and acetone was added to flocculate the AgNWs. After three times purification with acetone, AgNWs were centrifuged at 1000 rpm for 10 min and then the AgNWs were dispersed in water to obtain a dispersion with AgNWs concentration of 8 mg/mL.

PIS/AgNWs composite sponges

The PIS (diameter: 2.5 cm, height: 2.5 cm) was coated with a thin layer of branched PEI by squeezing the sponge in PEI water solution (10 mg/L). The excessive PEI was removed by washing with Milli Q water for 10 times. After that, the sponge was put into 40 mL of AgNWs dispersion (8 mg/mL) and shaking for 2 days at 37 °C. Then another 15 mL of AgNWs dispersion was added and the mixture was shaken for another 12 h at 37 °C. The obtained grey coloured PIS/AgNWs composite sponges were washed by Milli Q water for ten times and freeze-dried overnight. The amount of the AgNWs in the composite sponges was calculated from the weight of the sponges before and after AgNWs coating.

Characterizations

The morphology of the samples was observed by scanning electron microscope (SEM, Zeiss Leo 1530) equipped with energy dispersive X-ray spectroscopy (EDS). A 3 nm layer of platinum was coated on the sponges before SEM measurement and a carbon coating was applied to the sample for EDX. Transmission electron microscopy (TEM, Zeiss LEO 922 OMEGA) were used to observe the morphology of AgNWs. The compression test and cyclic compression

test were performed on a Zwick Z2.5 machine equipped with a 200 N sensor at compression rate of 10 mm/min. 10000 compression cycles were measured and the curves for first and 500n (n=1, 2, ……, 20) cycles were recorded. The sample for cyclic compression tests possess diameter of 2.1 cm and height of 2.1 cm. The current source heating was performed on a self-assembly set-up including a DF-3010 DC power supply, a multimeter, a TrueIR Thermal Imager 650C (IR camera, Keysight Technologies), a LED lamp as power on-off indicator and a windows phone as video maker (**Figure 8.1**). Different electrical currents of 1.10, 1.48, 2.10, 2.43, 2.68 and 3.05 A were applied to heat the PI/AgNWs sponges with 20% and 50% mechanical compression rate. The heating and cooling process by the electrical currents were recorded by the videos and the time-dependent temperature changes were depicted by Origin software. The sample for electrical heating has an original size with height of 1.0 cm and diameter of 0.6 cm. The current was recorded by the DC power supply while the voltage applied to the sponge was recorded by the multimeter. The LED lamp and the PI/AgNWs sponge were connected in series circuit.

Electric conductivity (σ) was calculated from the electric resistivity (R) of the PI/AgNWs sponges according to the following equations.

$R=\rho L/S$ (1)

$\rho=RS/L$ (2)

$\sigma=1/\rho=L/RS$ (3)

where L and S are the height and the cross-section area of the sample, respectively. For the measurement, the sponge samples were pressed between two parallel copper plates (1 mm thickness), which were connected to a Keithley 2420 High-Current Source Meter. The electric resistivity of the samples was obtained to subtract the electric resistivity of the wires and the copper plates from the values of the whole system including the sponges. Three samples were used for measurement and the average value was calculated.

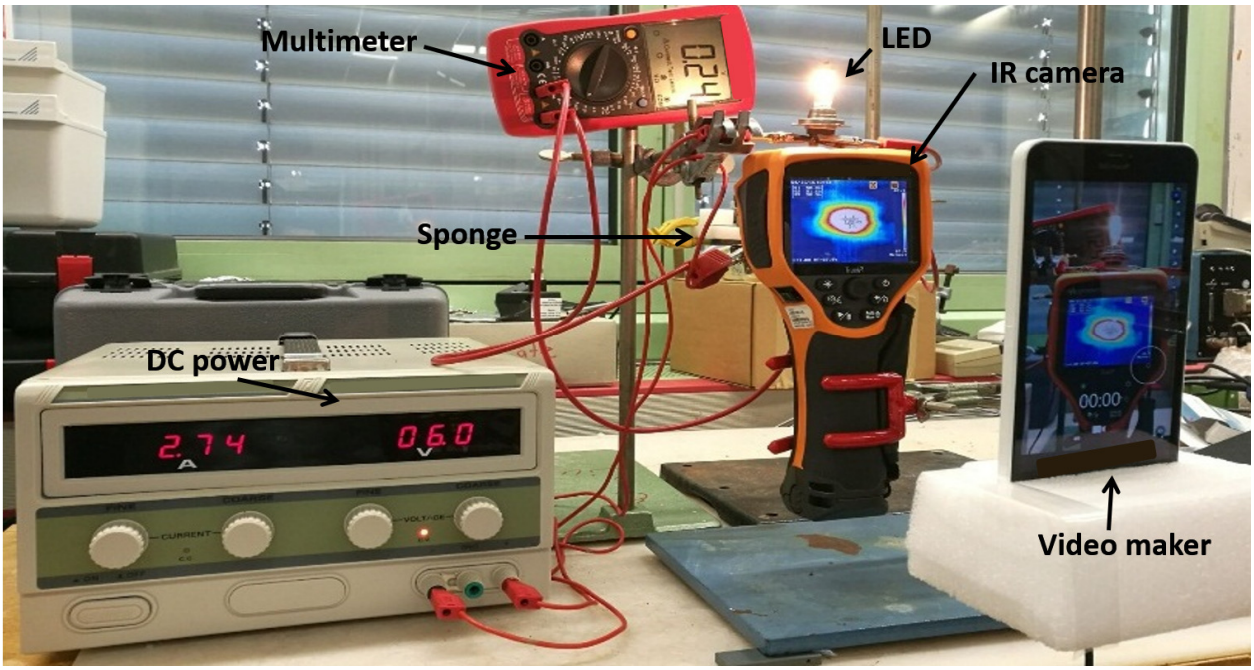

Figure 8.1. Lab-made set-up for lighting LED (12 W) and Joule heating.

8.5 RESULTS AND DISCUSSION

The PIS made by self-assembly of self-glued short fibers during freeze-drying had a density of 10.1 mg/cm^3 with bimodal pore-size distribution (large pores 121 ± 72 µm and small pores < 10 µm) as shown in **Figure 8.2a**. The soaking of the PIS with a solution of polyethylene imine (PEI) followed by shaking with the dispersion of AgNWs (average diameter: 75 ± 28 nm; average length: 14 ± 6 µm, **Figure 8.2b-e**) resulted in PIS/AgNWs nanocomposite sponges.

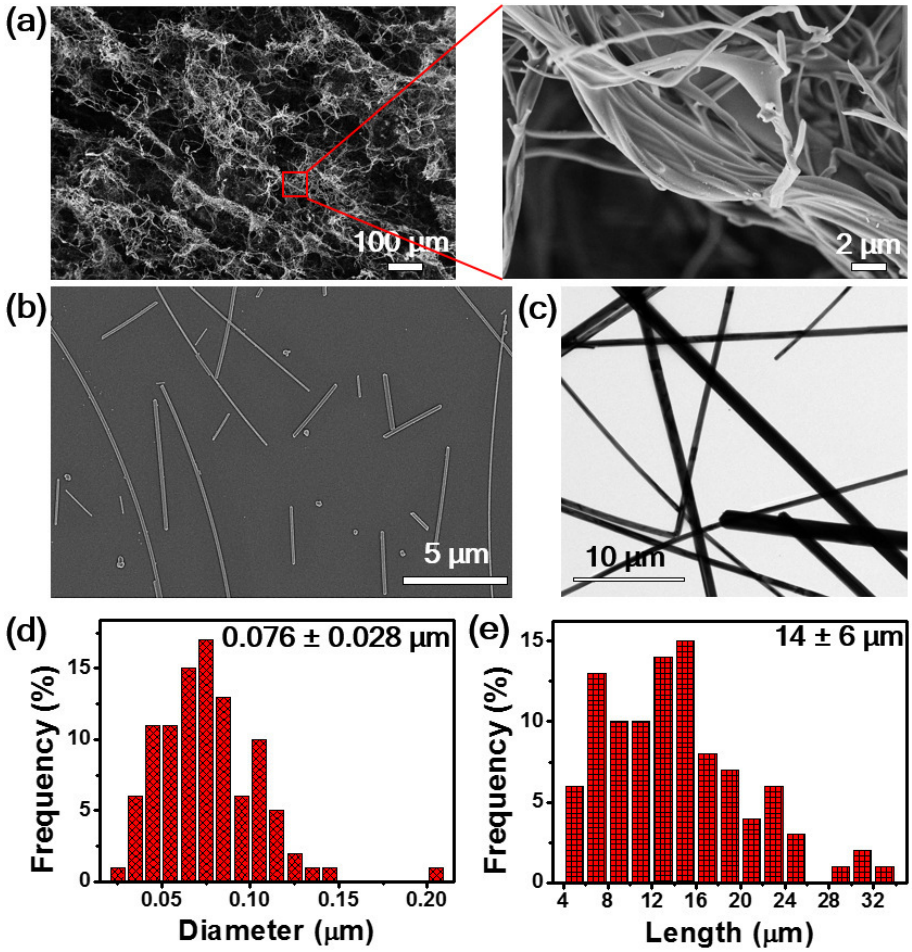

Figure 8.2. Morphology of PIS (SEM, a) and AgNWs (SEM b, and TEM c), and the corresponding diameter (d) and length (e) distributions of AgNWs.

The PIS took up 113 wt.% of AgNWs and the PIS/AgNWs composite sponge showed a density of 40.6 mg/cm^3 (**Figure 8.2**a). The composite sponge possessed a very high porosity of 98%. The PIS/AgNW sponge retained the form and shape of the original PIS sponge but some change in dimensions. SEM showed presence of ultrafine wires mostly wrapped around and some interconnected between the PI fibers. Further investigation by EDS measurement confirmed that the ultrafine filaments were AgNWs (**Figure 8.3**i, j) while the elements mapping of C, O, and N confirmed that the larger filaments were PI fibers (**Figure 8.3**f-h). The distribution of AgNWs was checked on the outer surfaces and in the bulk by SEM images. It is well-known that the sponges with large pore size could filter particles with much smaller size due to the 3D

porous structure of sponges.[35-37] In our work, the longer AgNWs made a 3D-net-work on and around the big pores of the PIS and could not penetrate through the small pores and remained homogenously distributed on the surface while the smaller AgNWs were infiltrated through the small pores. A double 3D network of PI fibers and AgNWs was obvious.

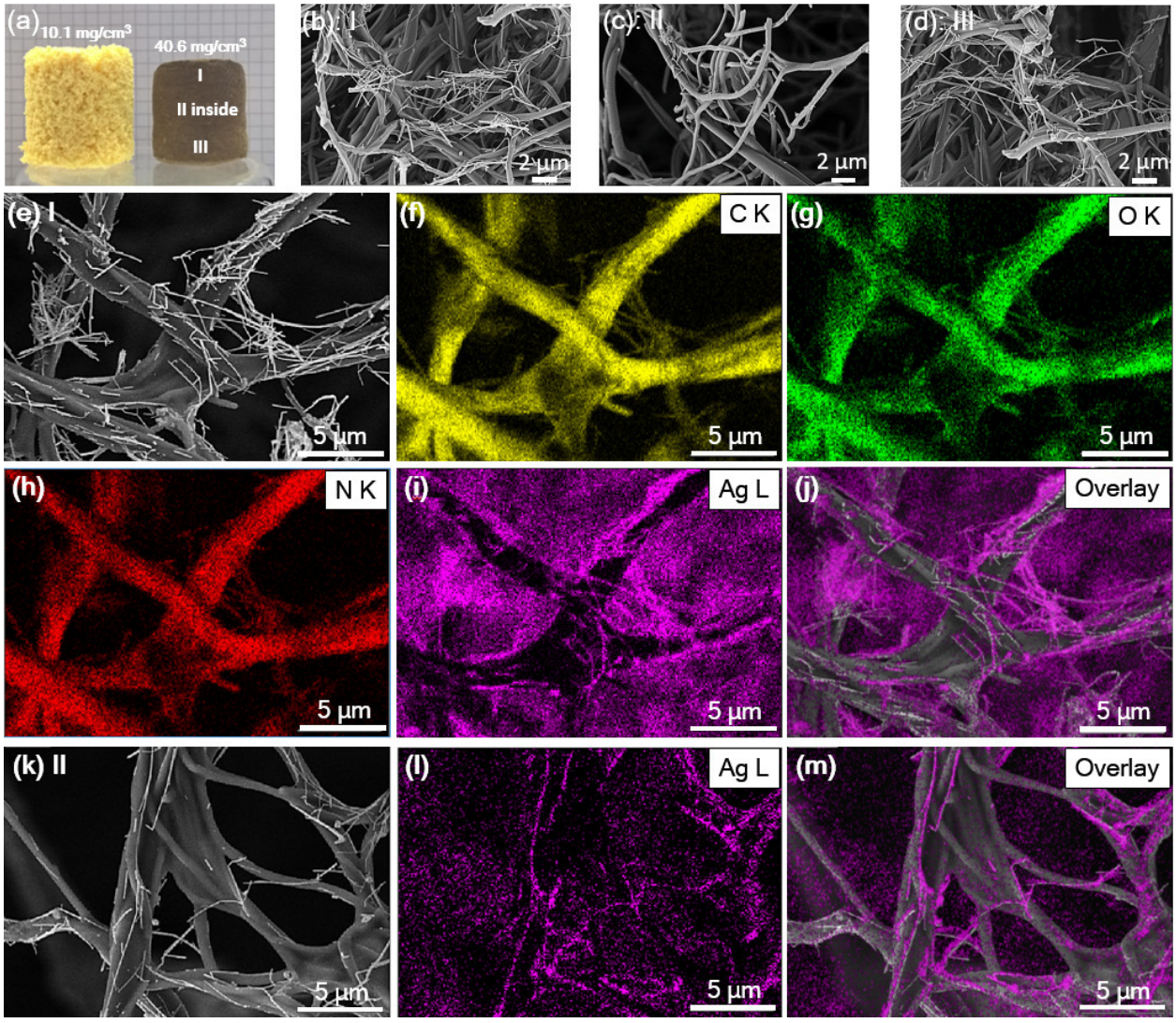

Figure 8.3. Photo of PIS before and after AgNWs coating (a), SEM images (b-d) of PIS/AgNWs sponge on top surface (position I, b), middle inside (position II, c) and bottom (position II, d), back scattering SEM image (e, k) of PIS/AgNWs and the corresponding elements mapping (f-j, l-m).

Further quantitative analysis on the amount of silver element in position I (surface) and II (bulk) was shown in **Figure 8.4**. It is clear that the sample in position I and II both possessed elements of N, O, C and Ag. The amount of silver in position I is much higher than in position II (75% vs 34%), which confirmed the gradient distribution of AgNWs on the surface (position I) and inside (position II) the composite sponge.

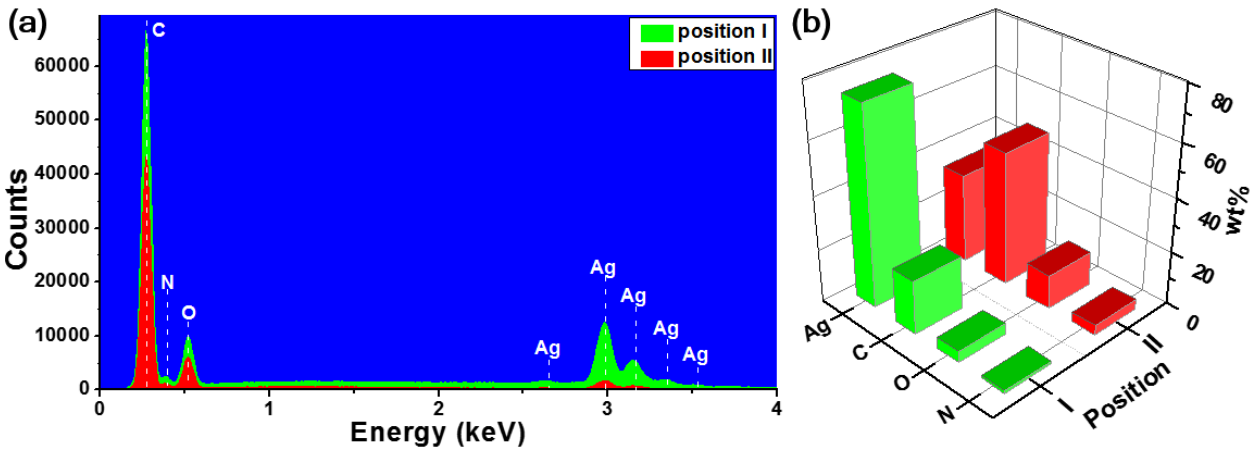

Figure 8.4. (a) EDS spectra for position I and II of PIS/AgNWs in Figure 3 and (b) the quantitative amounts (wt%) of the elements N, O, C and Ag from the corresponding EDS spectra.

The PIS/AgNWs composite sponge also presents excellent elasticity and improved compression properties (**Figure 8.5**). PIS/AgNWs exhibited a compression strength of 3.6 kPa (50% compressive strain), which was 64% larger than that of PIS (2.2 kPa, **Figure 8.5a**). The PIS/AgNWs also possessed excellent elasticity, which could be compressed and released for 10 000 cycles (**Figure 8.5b, SI-video 8.01, SI-video 8.02**). During the 10 000 cycling compression, the compressive strength still remained in the range of 3.45-3.61 kPa and the compressive strength is only <5% smaller than that in the first cycle (**Figure 8.5c**). By monitoring the work done during the whole cycling test, the work did not change significantly after first cycle (remained in the range of 3.1-4.0 mJ, **Figure 8.5d**), thereby signifying the mechanical stability of the composite sponge.

After the first cycle, the energy loss and loss coefficient were also kept in a nearly constant value of 0.72-0.81 mJ and ~ 0.2, respectively (**Figure 8.5e, f**).

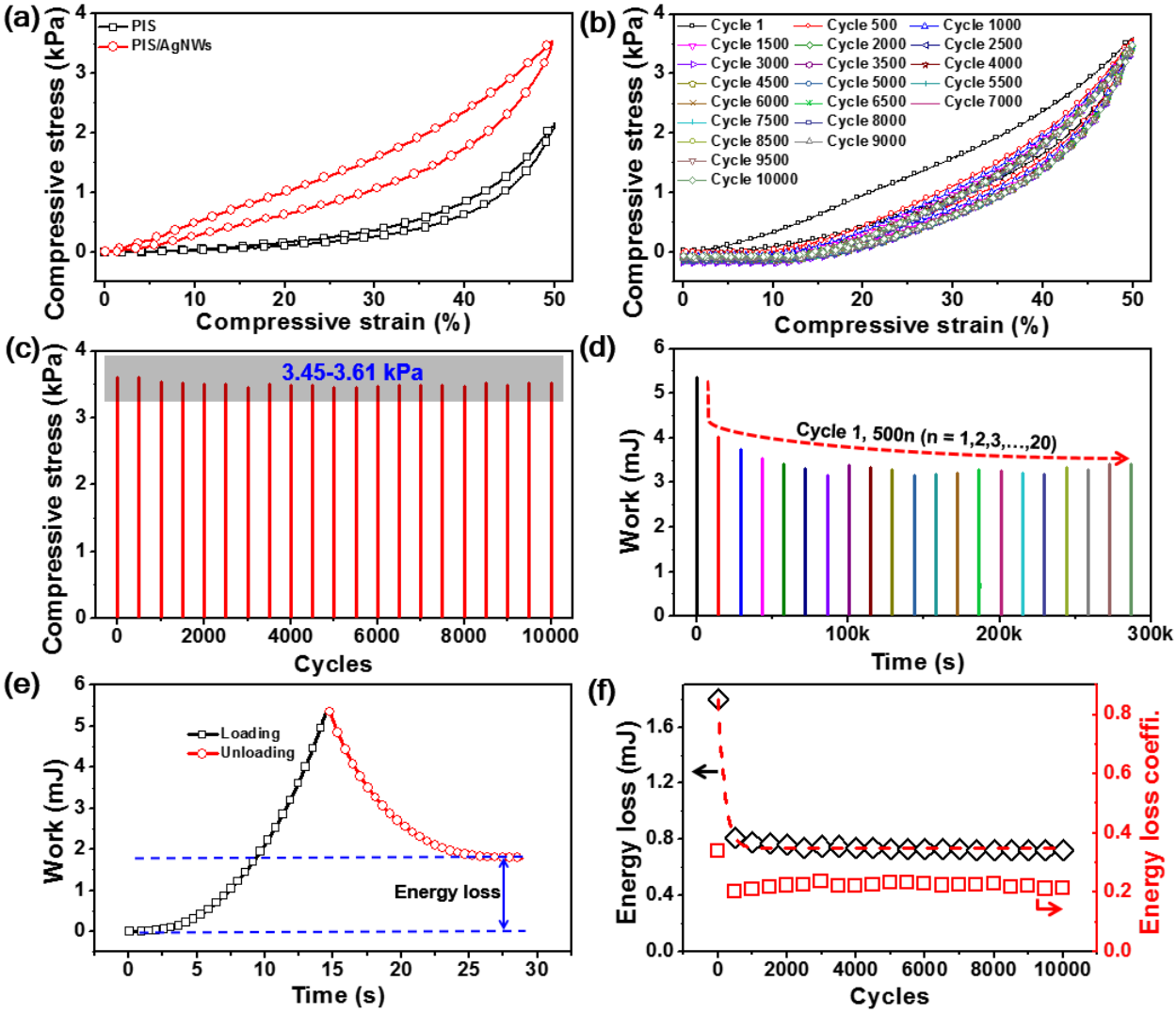

Figure 8.5. Compressive properties of PIS/AgNWs. (a) Typical compressive stress-strain curves of PIS and PIS/AgNWs; (b) cyclic compressive curves, (c) cycle-dependent compressive stress, and (d) time dependent work done during cyclic compression, (e) typical work done in first cycle and (f) cycle-dependent energy loss and energy loss coefficient for PIS/AgNWs.

Although 113 wt% of AgNWs was coated, the PIS/AgNWs composite sponge still exhibited low thermal conductivity, which was comparable to the value of cork (0.07 W/mK). Comparison on the thermal conductivities and thermal diffusivities of PIS/AgNWs at different

compression rate were shown in **Figure 8.6**. The composite sponge showed high thermal insulation even at high compression (0.1036 W/mK at 60% compression). This value was slightly higher than that of thermal insulation material made from cotton stalk fibers (0.0585 to 0.0815 W/m K), but its density even under 60% compression (100 mg/cm^3)was much lower than the reported cotton stalk fibrous materials (150 ~ 450 mg/cm^3).[38] As increasing the compressive strain, the thermal diffusivity of PIS/AgNWs increased slightly from 1.244 mm^2/s to 1.373 mm^2/s, but still much smaller than the value of air (19 mm^2/s) and comparable to that of sandstone.[39]

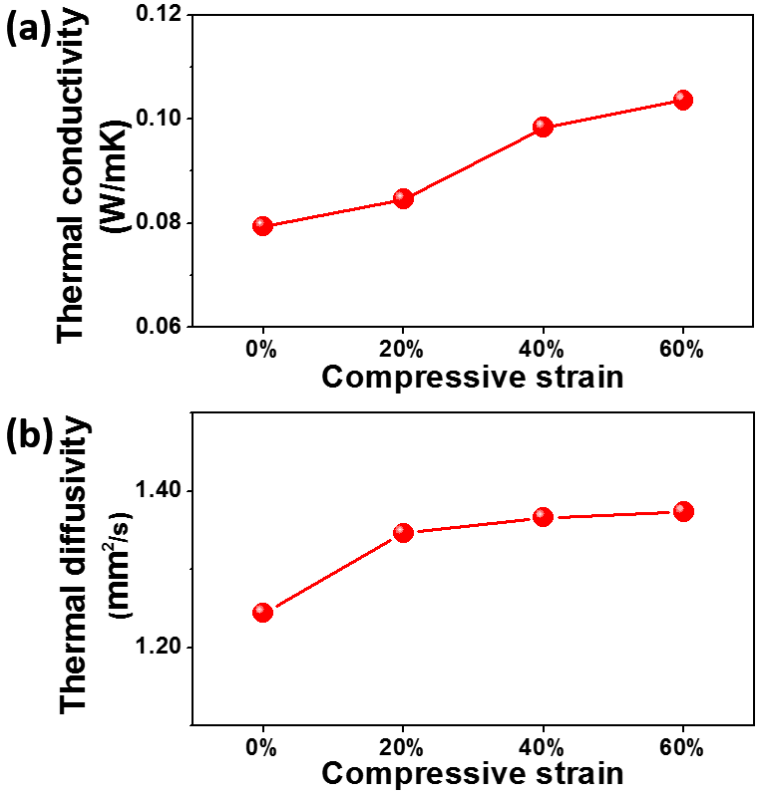

Figure 8.6. Compressive strain-dependent thermal conductivity (a) and thermal diffusivity (b) of PIS/AgNWs.

The PIS/AgNW sponge showed very high electronic conductivity of 166.6 S/cm at 50% compressive strain. The conductivity of PIS/AgNWs sponge was controlled by the compression status. The electrical conductivity of PIS/AgNWs sponge at zero

compression is 1.70 S/cm (**Figure 8.7**), which is in the range or higher than carbon nanotube (CNT) sponges (1.32 S/cm),[40] physically cross-linked graphene sponge/aerogel (< 0.025 S/cm),[41-42] and chemically cross-linked graphene aerogel (0.87 S/cm).[43] As increasing the compressive strain to 10, 20, 30, 40, 50%, the electrical conductivity increased to 7.69, 20.02, 26.21, 45.77, 166.6 S/cm, respectively. The increased electrical conductivity could be due to the enhanced contacts between AgNWs on compression (insert of **Figure 8.7**).

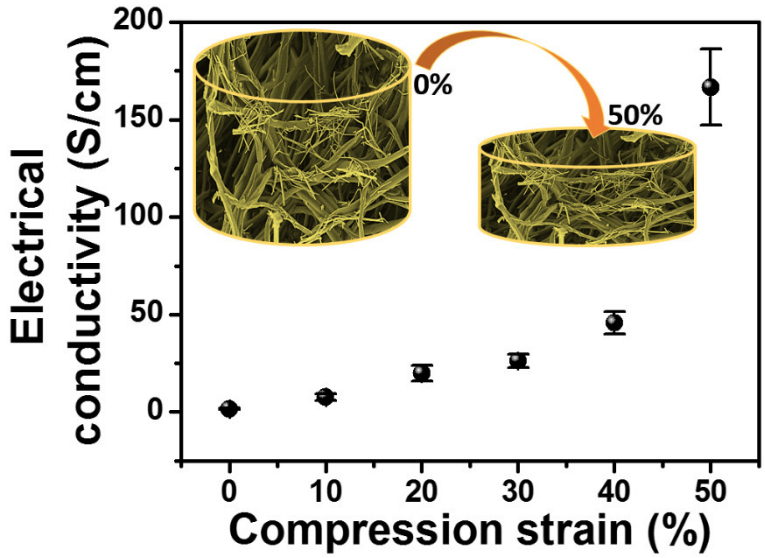

Figure 8.7. Electrical conductivity of PIS/AgNWs at different compressive strain.

The conductivity of sponge enabled the operation of LED (an automobile 12 W LED) (**Figure 8.1**, **SI-video 8.03 and SI-video 8.04**). Further, the passage of current led to very fast heating of the sponge which cooled also extremely fast on switching off the current. The heating (current on) and cooling times (current off) provide an additional feature for a well-controlled Joule heater. The increase in temperature could also be controlled by the compression strain besides the current. The increased electrical currents from 1.10 A to 3.05 A led to an increase in temperature from 32 to 108 °C for

sample with 20% compressive strain, and from 28 to 66 °C for sample with 50% compressive strain, respectively (**Figure 8.8**).

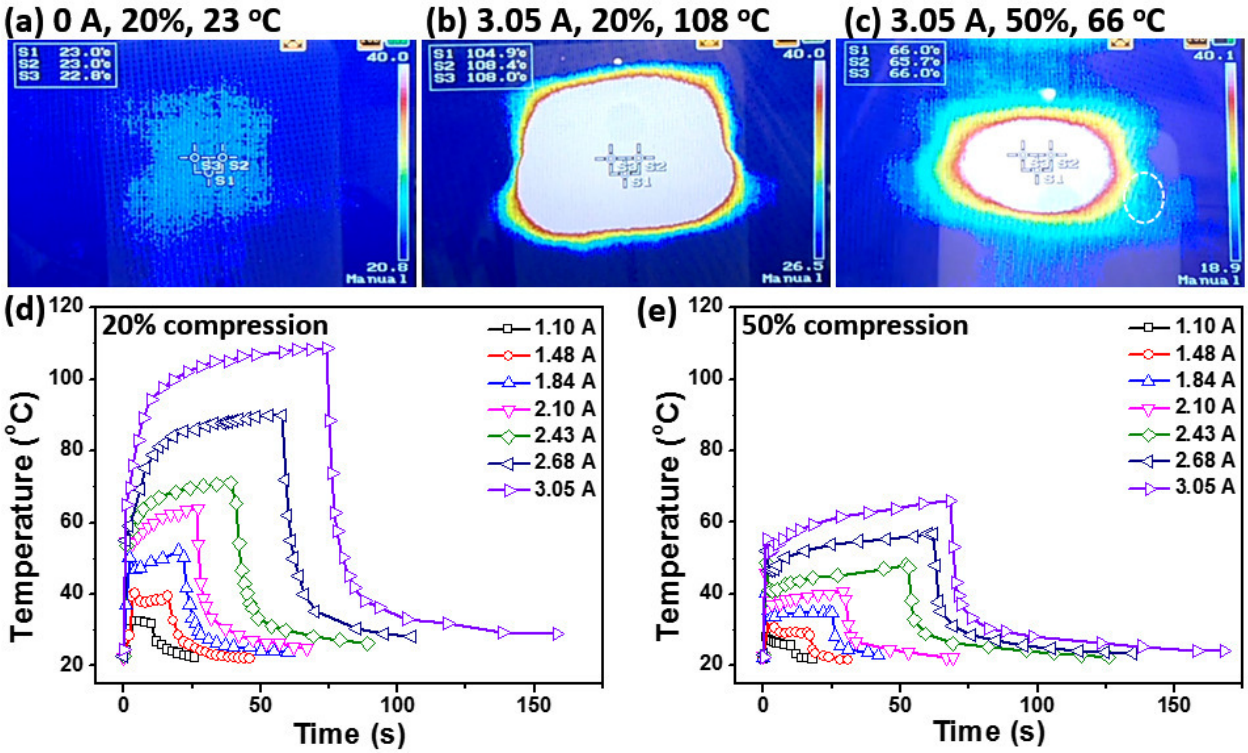

Figure 8.8. Thermal IR Images of PIS/AgNWs at 20 and 50% compressive strain by applying electrical current of 0 and 3.05 A (a-c), Joule heating from PIS/AgNWs by applying different electrical current when the samples were compressed by 20% (d) and 50% (e), respectively.

Interestingly, when the same electrical current was applied, the sponge with 20% compression could be heated to higher temperature than that with 50% compression (**Figure 8.8d, e**). The different final heating temperature is due to the Joule heating. Unlike to the conventional heating system, which was controlled by the thermal conductivity of the samples, Joule heating result from the electrical resistance when the conductive sample was passed through electrical current. According to Joule's law (8.1) and equation (8.2) for electrical conductivity (σ) and the electrical resistance (R),

$Q = I^2Rt$ (8.1)

$R = L/\sigma S$ (8.2)

the relationship between the Q and σ could be calculated by equation (8.3):

$Q = I^2Lt/\sigma S$ (8.3)

Where Q is the heat generated, I is the applied electrical current, t is the time, L is the height of the sample, and S is the cross-section area of the sample. Larger electrical conductivity generates less Joule heating and therefore leads to smaller temperature change. In this work, the PIS/AgNWs with 50% compression possessed much higher electrical conductivity than that with 20% compression (166.60 S/cm vs 20.02 S/cm). Therefore, The PIS/AgNWs with 50% compression could facilitate the pass of electrical current and therefore produced less heat than the sample with 20% compression and exhibited smaller heating temperatures with the same electric currents. Another key factor to evaluate the performance of the heating device is the responding time. By passing electrical current through the PIS/AgNWs composite sponge at 20% and 50% compression, it could be heated rapidly from room temperature to a steady final temperature within 10-74 s, depending on the input electrical current.

Moreover, PIS and PIS/AgNWs also presented excellent gas permeability which was proved by a specially designed experiment in which a piece of sponge was tightly inserted in a syringe and a gas was passed through it (**SI-video 8.05**). These properties make PIS/AgNWs promising for several applications putting different demands such as gas permeable heat insulator, heater by electric current, pressure sensor, light weight thermally stable conductive sponge etc.

8.6 CONCLUSIONS

In conclusion we show stress responsive, electrically conductive, flexible, and breathable nanocomposite sponges made of short electrospun PI nanofiber and AgNWs. The sponges provided excellent mechanical stability in combination with compressibility due to the choice of PI as polymer component and the additional treatment by PAA followed by annealing. The high electric conductivity was possible due to the excellent metallic conductivity of AgNWs as sponge component. The escalation of the electric conductivity of the sponge with increased stress, could be understood by the increase of the percolation of AgNWs upon sponge compression which is of interest for the mechanically-responsive controlled operation of electric devices.

The sponges could be applied directly as electrodes as well as very efficient Joule heaters. Naturally, the operation of these devices could be controlled by the compression status of the sponges. It is very interesting to note that heating and cooling rates are very fast and that the maximum temperature reached by electric heating depends on the compression state. We believe strongly that these sponges will open a new area for novel sponge-based conductive devices with relevant real world applications as the applied preparation methods could be upscaled.

8.7 Supporting Information.

SI-Video 01: Cyclic compression of PIS/AgNWs for 100 times (2X).
SI-Video 02: Cyclic compression measurement of PIS/AgNWs (64X).
SI-Video 03: Joule heating of PIS/AgNWs at 20% compression (32X).
SI-Video 04: Joule heating of PIS/AgNWs at 50% compression (32X)..
SI-Video 05: Breathability of PIS/AgNWs.

8.8 ACKNOWLEDGMENT

Authors would like to thank German Science Foundation (SFB 840, projects A12 and B8) for financial support.

8.9 REFERENCES

1. Jiang, S.; Agarwal, S.; Greiner, A., Low-Density Open Cellular Sponges as Functional Materials. *Angew. Chem. Int. Ed.* **2017,** *DOI: 10.1002/anie.201700684*.

2. Lai, F.; Huang, Y.; Zuo, L.; Gu, H.; Miao, Y.-E.; Liu, T., Electrospun Nanofiber-Supported Carbon Aerogel as a Versatile Platform toward Asymmetric Supercapacitors. *J. Mater. Chem. A* **2016,** *4* (41), 15861-15869.

3. Li, L.; Wang, K.; Huang, Z.; Zhang, C.; Liu, T., Highly Ordered Graphene Architectures by Duplicating Melamine Sponges as a Three-dimensional Deformation-tolerant Electrode. *Nano Research* **2016,** *9* (10), 2938-2949.

4. Si, Y.; Wang, X.; Yan, C.; Yang, L.; Yu, J.; Ding, B., Ultralight Biomass-Derived Carbonaceous Nanofibrous Aerogels with Superelasticity and High Pressure-Sensitivity. *Adv. Mater.* **2016,** *28* (43), 9512-9518.

5. Duan, G.; Koehn-Serrano, M.; Greiner, A., Highly Efficient Reusable Sponge-Type Catalyst Carriers Based on Short Electrospun Fibers. *Macromol. Rapid Commun.* **2017,** *38* (3), 1600511.

6. Jiang, S.; Duan, G.; Kuhn, U.; Mörl, M.; Altstädt, V.; Yarin, A. L.; Greiner, A., Spongy Gels by a Top-Down Approach from Polymer Fibrous Sponges. *Angew. Chem. Int. Ed.* **2017,** *56* (12), 3285-3288.

7. Jiang S.; Uch, B.; Agarwal, S.; Greiner, A., Ultralight, Thermally Insulating, Compressible Polyimide Fiber Assembled Sponges. *ACS Appl. Mat. Interfaces* **2017,** *DOI: 10.1021/acsami.7b11045*.

8. Yao, Q.; Cosme, J. G. L.; Xu, T.; Miszuk, J. M.; Picciani, P. H. S.; Fong, H.; Sun, H., Three Dimensional Electrospun PCL/PLA Blend Nanofibrous Scaffolds with Significantly Improved Stem Cells Osteogenic Differentiation and Cranial Bone Formation. *Biomaterials* **2017,** *115*, 115-127.

9. Yang, L.; Zou, M.; Wu, S.; Xu, W.; Wu, H.; Cao, A., Graphene Oxide Glue-Electrode for Fabrication of Vertical, Elastic, Conductive Columns. *ACS Nano* **2017,** *11* (3), 2944-2951.

10. Wu, Z.-Y.; Li, C.; Liang, H.-W.; Chen, J.-F.; Yu, S.-H., Ultralight, Flexible, and Fire-Resistant Carbon Nanofiber Aerogels from Bacterial Cellulose. *Angew. Chem. Int. Ed.* **2013,** *52* (10), 2925-2929.

11. Xie, X.; Ye, M.; Hu, L.; Liu, N.; McDonough, J. R.; Chen, W.; Alshareef, H. N.; Criddle, C. S.; Cui, Y., Carbon Nanotube-Coated Macroporous Sponge for Microbial Fuel Cell Electrodes. *Energy Environ. Sci.* **2012,** *5* (1), 5265-5270.

12. Gui, X.; Wei, J.; Wang, K.; Cao, A.; Zhu, H.; Jia, Y.; Shu, Q.; Wu, D., Carbon Nanotube Sponges. *Adv. Mater.* **2010,** *22* (5), 617-621.

13. Zhao, J.; Ren, W.; Cheng, H.-M., Graphene Sponge for Efficient and Repeatable Adsorption and Desorption of Water Contaminations. *J. Mater. Chem.* **2012,** *22* (38), 20197-20202.

14. Pu, X.; Yang, G.; Yu, C., Liquid-Type Cathode Enabled by 3D Sponge-Like Carbon Nanotubes for High Energy Density and Long Cycling Life of Li-S Batteries. *Adv. Mater.* **2014,** *26* (44), 7456-7461.

15. Chabot, V.; Higgins, D.; Yu, A.; Xiao, X.; Chen, Z.; Zhang, J., A Review of Graphene and Graphene Oxide Sponge: Material Synthesis and Applications to Energy and the Environment. *Energy Environ. Sci.* **2014,** *7* (5), 1564-1596.

16. Sun, H.; Xu, Z.; Gao, C., Multifunctional, Ultra-Flyweight, Synergistically Assembled Carbon Aerogels. *Adv. Mater.* **2013,** *25* (18), 2554-2560.

17. Chen, Z.; Ren, W.; Gao, L.; Liu, B.; Pei, S.; Cheng, H.-M., Three-Dimensional Flexible and Conductive Interconnected Graphene Networks Grown by Chemical Vapour Deposition. *Nat. Mater.* **2011,** *10* (6), 424-428.

18. Chen, Z.; Xu, C.; Ma, C.; Ren, W.; Cheng, H.-M., Lightweight and Flexible Graphene Foam Composites for High-Performance Electromagnetic Interference Shielding. *Adv. Mater.* **2013,** *25* (9), 1296-1300.

19. Kim, K. H.; Vural, M.; Islam, M. F., Single-Walled Carbon Nanotube Aerogel-Based Elastic Conductors. *Adv. Mater.* **2011,** *23* (25), 2865-2869.

20. Wu, C.; Huang, X.; Wang, G.; Lv, L.; Chen, G.; Li, G.; Jiang, P., Highly Conductive Nanocomposites with Three-Dimensional, Compactly Interconnected Graphene Networks via a Self-Assembly Process. *Adv. Funct. Mater.* **2013,** *23* (4), 506-513.

21. Wu, C.; Fang, L.; Huang, X.; Jiang, P., Three-Dimensional Highly Conductive Graphene–Silver Nanowire Hybrid Foams for Flexible and Stretchable Conductors. *ACS Appl. Mat. Interfaces* **2014,** *6* (23), 21026-21034.

22. Ge, J.; Yao, H.-B.; Wang, X.; Ye, Y.-D.; Wang, J.-L.; Wu, Z.-Y.; Liu, J.-W.; Fan, F.-J.; Gao, H.-L.; Zhang, C.-L.; Yu, S.-H., Stretchable Conductors Based on Silver Nanowires: Improved Performance through a Binary Network Design. *Angew. Chem.* **2013,** *125* (6), 1698-1703.

23. Langner, M.; Agarwal, S.; Baudler, A.; Schröder, U.; Greiner, A., Large Multipurpose Exceptionally Conductive Polymer Sponges Obtained by Efficient Wet-Chemical Metallization. *Adv. Funct. Mater.* **2015,** *25* (39), 6182-6188.

24. Liang, S.; Li, Y.; Yang, J.; Zhang, J.; He, C.; Liu, Y.; Zhou, X., 3D Stretchable, Compressible, and Highly Conductive Metal-Coated Polydimethylsiloxane Sponges. *Adv. Mater. Technol.* **2016,** *1* (7), 1600117.

25. Duan, G.; Jiang, S.; Jérôme, V.; Wendorff, J. H.; Fathi, A.; Uhm, J.; Altstädt, V.; Herling, M.; Breu, J.; Freitag, R.; Agarwal, S.; Greiner, A., Ultralight, Soft Polymer Sponges by Self-Assembly of Short Electrospun Fibers in Colloidal Dispersions. *Adv. Funct. Mater.* **2015,** *25* (19), 2850-2856.

26. Si, Y.; Yu, J.; Tang, X.; Ge, J.; Ding, B., Ultralight Nanofibre-Assembled Cellular Aerogels with Superelasticity and Multifunctionality. *Nat. Commun.* **2014,** *5*, 5802.

27. Chen, W.; Chen, S.; Morsi, Y.; El-Hamshary, H.; El-Newhy, M.; Fan, C.; Mo, X., Superabsorbent 3D Scaffold Based on Electrospun Nanofibers for Cartilage Tissue Engineering. *ACS Appl. Mat. Interfaces* **2016,** *8* (37), 24415-24425.

28. Xu, T.; Miszuk, J. M.; Zhao, Y.; Sun, H.; Fong, H., Electrospun Polycaprolactone 3D Nanofibrous Scaffold with Interconnected and Hierarchically Structured Pores for Bone Tissue Engineering. *Adv. Healthcare Mater.* **2015,** *4* (15), 2238-2246.

29. Ding, Y.; Hou, H.; Zhao, Y.; Zhu, Z.; Fong, H., Electrospun Polyimide Nanofibers and Their Applications. *Prog. Polym. Sci.* **2016,** *61*, 67-103.

30. Ding, M., Isomeric Polyimides. *Prog. Polym. Sci.* **2007,** *32* (6), 623-668.

31. Jiang, S.; Duan, G.; Schöbel, J.; Agarwal, S.; Greiner, A., Short Electrospun Polymeric Nanofibers Reinforced Polyimide Nanocomposites. *Compos. Sci. Technol.* **2013,** *88* (0), 57-61.

32. Jiang, S.; Hou, H.; Agarwal, S.; Greiner, A., Polyimide Nanofibers by "Green" Electrospinning via Aqueous Solution for Filtration Applications. *ACS Sustain. Chem. Eng.* **2016,** *4* (9), 4797-4804.

33. Park, J. S.; Kim, T.; Kim W. S., Conductive Cellulose Composites with Low Percolation Threshold for 3D Printed Electronics. *Sci. Rep.* **2017,** *7*, 3246.

34. Bergin, S. M.; Chen, Y.-H.; Rathmell, A. R.; Charbonneau, P.; Li, Z.-Y.; Wiley, B. J., The Effect of Nanowire Length and Diameter on the Properties of Transparent, Conducting Nanowire Films. *Nanoscale* **2012,** *4* (6), 1996-2004.

35. Li, H.; Gui, X.; Zhang, L.; Wang, S.; Ji, C.; Wei, J.; Wang, K.; Zhu, H.; Wu, D.; Cao, A., Carbon Nanotube Sponge Filters for Trapping Nanoparticles and Dye Molecules from Water. *Chem. Commun.* **2010,** *46* (42), 7966-7968.

36. Yahel, G.; Eerkes-Medrano, D. I.; Leys, S. P., Size Independent Selective Filtration of Ultraplankton by Hexactinellid Glass Sponges. *Aquat. Microb. Ecol.* **2006,** *45* (2), 181-194.

37. Ledda, F. D.; Pronzato, R.; Manconi, R., Mariculture for Bacterial and Organic Waste Removal: a Field Study of Sponge Filtering Activity in Experimental Farming. *Aquacult. Res.* **2014,** *45* (8), 1389-1401.

38. Zhou, X.-y.; Zheng, F.; Li, H.-g.; Lu, C.-l., An Environment-Friendly Thermal Insulation Material from Cotton Stalk Fibers. *Energy Build.* **2010,** *42* (7), 1070-1074.

39. Vosteen, H.-D.; Schellschmidt, R., Influence of Temperature on Thermal Conductivity, Thermal Capacity and Thermal Diffusivity for Different Types of Rock. *Phys. Chem. Earth, Parts A/B/C* **2003,** *28* (9), 499-509.

40. Zhou, G.; Zhang, H.; Xu, S.; Gui, X.; Wei, H.; Leng, J.; Koratkar, N.; Zhong, J., Fast Triggering of Shape Memory Polymers using an Embedded Carbon Nanotube Sponge Network. *Sci. Rep.* **2016,** *6*, 24148.

41. Li, Y.; Chen, J.; Huang, L.; Li, C.; Hong, J.-D.; Shi, G., Highly Compressible Macroporous Graphene Monoliths via an Improved Hydrothermal Process. *Adv. Mater.* **2014,** *26* (28), 4789-4793.

42. Li, Y.; Samad, Y. A.; Polychronopoulou, K.; Alhassan, S. M.; Liao, K., Highly Electrically Conductive Nanocomposites Based on PolymerInfused Graphene Sponges. *Sci. Rep.* **2014,** *4*, 4652.

43. Worsley, M. A.; Pauzauskie, P. J.; Olson, T. Y.; Biener, J.; Satcher, J. H.; Baumann, T. F., Synthesis of Graphene Aerogel with High Electrical Conductivity. *J. Am. Chem. Soc.* **2010,** *132* (40), 14067-14069.

Supporting Information

SI-Video 01. Cyclic compression of PIS/AgNWs for 100 times (2X).
SI-Video 02. Cyclic compression measurement of PIS/AgNWs (64X).
SI-Video 03. Joule heating of PIS/AgNWs at 20% compression (32X).
SI-Video 04. Joule heating of PIS/AgNWs at 50% compression (32X)..
SI-Video 05. Breathability of PIS/AgNWs.

9. Liste der Publikationen

In dieser Arbeit gezeigte und diskutierte Publikationen

[1] S. Reich, A. Greiner, *Angwandte Chemie*, zur Einreichung (non final version)

[2] P. Kaiser, S. Reich, D. Leykam, M. Willert-Porada, A. Greiner, R. Freitag, *Macromolecular Bioscience*, **2017**, 17, 1600442.

[3] S. Reich, P. Kaiser, D. Rhinow, H. Schmalz, R. Freitag, A. Greiner, *Part. Part. Syst. Charact.*, zur Einreichung (non final version)

[4] S. Reich, M. Burgard, M. Langner, S. Jiang, X. Wang, S. Agarwal, B. Ding, J. Yu, A. Greiner, *npj Flex. Electron.*, **2018,** 2, 1417.

[5] S. Jiang, S. Reich, B. Uch, P. Hu, S. Agarwal, A. Greiner, *ACS Applied Materials & Interfaces*, **2017**, 9(39), 34286-34293.

Themenfremde Publikationen

[6] V. Buchholz, M. Molnar, H. Wang, S. Reich, S. Agarwal, M. Fischer, A. Greiner, *Macromolecular Bioscience*, **2016**, 16(9), 1391-1397.

10. Danksagung

Die vorliegende Dissertation entstand am Lehrstuhl für Makromolekulare Chemie II der Universität Bayreuth unter der Leitung von Herrn Prof. Dr. Andreas Geiner. Hiermit möchte ich mich für die intensive Betreuung ihrerseits bedanken.

Frau Prof. Dr. Seema Agarwal, Prof. Dr. Ruth Freitag, Prof. Dr. Charles Greenblatt, Prof. Dr. Eyal Zussman danke ich für die angenehmen und konstruktiven Diskussionen und Hilfestellungen bei Seminaren im In- und Ausland.

Ich danke Prof. Dr. Andreas Greiner, Prof. Dr. Ruth Freitag und Prof. Dr. Peter Strohriegl für die Übernahme des Mentorats in BayNAT.

Für die finanziellen Hilfen, danke ich der Deutschen Forschungsgemeinschaft, der Graduiertenschule der Universität Bayreuth und dem Bayrischen Ministerium für Umwelt- und Verbraucherschutz.

Herrn Dr. Holger Schmalz danke ich ebenfalls für die konstruktiven Hilfestellungen bei der Bearbeitung schwieriger experimenteller Problemstellungen.

Bei meinem Kooperationspartner, Patrick Kaiser, bedanke ich mich für die angenehme Zusammenarbeit bei der Bearbeitung des BayBiotech-Projektes, bei dem ein Austausch zwischen Polymerchemie und Bioverfahrenstechnik unumgänglich war.

Bei meinen Laborkollegen Markus Langner, Florian Käfer, Tobias Moss, Matthias Burgard, Judith Schöbel, Paul Pineda, Amanda Pineda, Rika Schneider bedanke ich mich für die zahlreichen Diskussionen, Hilfestellungen und Problemlösungen während meiner Promotionszeit.

Zum Schluss danke ich meinen Eltern und meinen Geschwistern, die mich während meiner Ausbildung, meines Studiums und meiner Promotionszeit unterstützt haben. Ihr habt mich immer wieder aufgebaut, wenn es mal nicht nach Plan lief.

Vielen Dank!

11. (Eidesstattliche) Versicherung und Erklärungen

(§ 9 Satz 2 Nr. 3 PromO BayNAT)

Hiermit versichere ich eidesstattlich, dass ich die Arbeit selbständig verfasst und keine anderen als die von mir angegebenen Quellen und Hilfsmittel benutzt habe (vgl. Art. 64 Abs. 1 Satz 6 BayHSchG).

(§ 9 Satz 2 Nr. 3 PromO BayNAT)

Hiermit erkläre ich, dass ich die Dissertation nicht bereits zur Erlangung eines akademischen Grades eingereicht habe und dass ich nicht bereits diese oder eine gleichartige Doktorprüfung endgültig nicht bestanden habe.

(§ 9 Satz 2 Nr. 4 PromO BayNAT)

Hiermit erkläre ich, dass ich Hilfe von gewerblichen Promotionsberatern bzw. -vermittlern oder ähnlichen Dienstleistern weder bisher in Anspruch genommen habe noch künftig in Anspruch nehmen werde.

(§ 9 Satz 2 Nr. 7 PromO BayNAT)

Hiermit erkläre ich mein Einverständnis, dass die elektronische Fassung meiner Dissertation unter Wahrung meiner Urheberrechte und des Datenschutzes einer gesonderten Überprüfung unterzogen werden kann.

(§ 9 Satz 2 Nr. 8 PromO BayNAT)

Hiermit erkläre ich mein Einverständnis, dass bei Verdacht wissenschaftlichen Fehlverhaltens Ermittlungen durch universitätsinterne Organe der wissenschaftlichen Selbstkontrolle stattfinden können.

Bayreuth, den

Steffen Reich